2001

Elucidation of the physiological and pathophysiological role of thiols and S-nitrosothiols with the aid of novel probes.

Niroshan. Ramachandran
University of Windsor

ELUCIDATION OF THE PHYSIOLOGICAL AND PATHOPHYSIOLOGICAL ROLE OF THIOLS AND S-NITROSOTHIOLS WITH THE AID OF NOVEL PROBES

BY

Niroshan Ramachandran

A Dissertation
Submitted to the Faculty of Graduate Studies and Research
through the Department of Chemistry and Biochemistry
in Partial Fulfillment of the Requirements for
the Doctor of Philosophy at the
University of Windsor

Windsor, Ontario, Canada
2001

Abstract

By

Niroshan Ramachandran

The role of nitric oxide (NO) in the physiological system is complex. It functions as a signaling molecule in the neuronal, vascular and immunological systems. To date information regarding NO and its metabolites are plentiful offering various mechanisms of actions, regulation, transport and storage. One such important aspect is the discovery of S-nitrosothiols (RSNO). These thiol bound NO compounds act as storage and transport forms for NO while eliciting similar responses as NO.

We developed a novel probe, N,N-didansylhomocystine, for the detection of RSNO influx into live cells. Utilizing the short range excited state energy transfer properties observed in N-dansyl-S-nitrosohomocysteine, we were able to monitor influx of S-nitroso-albumin (BSA-NO) and S-nitrosoglutathione in endothelial cells and fibroblasts. The K_M values for RSNO uptake were 20-30μM. Furthermore, cell surface PDI (csPDI) was implicated in catalyzing denitrosation reactions at the cell surface and the subsequent transfer of NO into the cell. The reaction of NO and O_2 was accelerated in the cell membrane producing N_2O_3 which was shown as the nitrosating agent of the intracellular thiols.

Continued studies revealed the pathogenic effect of oxidized and reduced homocyst(e)ine (HCys, $HCys_2$) in the vascular system was attributed to its effects on NO and RSNO metabolism. HCys and $HCys_2$ inhibited L-Arg uptake and reduced the production of NO in endothelial cells. HCys/$HCys_2$ also inhibited uptake of RSNO in a csPDI dependant manner. *In vitro* studies revealed that the denitrosation activity was sensitive to $HCys_2$ concentrations while isomerization activity was not affected. Therefore the pathophysiological role of HCys/$HCys_2$ affects NO/RSNO metabolism. Decreasing endogenous levels of NO and decreasing denitrosation of extracellular RSNO, tend to promote cell-cell aggregation and cell-matrix aggregation. Leaving the isomerization activity intact promotes the csPDI-catalyzed binding of integrins to cell adhesion molecules. Its pro-aggregatory effects may explain the thrombotic and atherogenic behaviour observed in hyperhomocysteinaemia.

An innovative study was designed to use Raman spectroscopy to probe biological samples. We were able to detect glutathione and S-nitrosoglutathione levels in solution with detection limits of 200mM. By derivatizing thiols with 5,5'-dithio-*bis*-3-nitrobenzoate we were able to achieve sensitivities in the low mM range. Final attempts to observe thiols in live cells and model systems such as liposomes and red blood cells were not successful. This study has shown the possibilities and limitations of Raman spectroscopy with respect to its use in biological samples.

Dedicated to my parents Chellappah & Kirupaimalar Ramachandran

And to my family Narissa Seenath, Suganthy Ganesh

& Umeshan Ramachandran

Acknowledgements

First and foremost I would like to thank Dr. Bulent Mutus for this opportunity and for his trust and confidence over the years. My gratitude is also extended to my committee members Dr. Gilbert C. Walker, Dr. Cotter, Dr. Keith E. Taylor, and Dr. Siyaram Pandey for their contributions.

I am grateful for all the helping hands of Sanjay Jacob, Patrick Cervini, Paul Root, Nidhi Sood, Shane Miersch, and Tom Quach all who have contributed immensely towards my thesis. I would also like to thank my group members Arianna Vignini, Shirin Akhter, and Okechuku Ukairo for their companionship. I appreciate and value the many intellectual conversations I have had with Gregory John Earl Davidson and Liam Patrick Spencer. My thanks to Monique Verhaegen and Dr. Sirinart Ananvoranich for their critical reading of my dissertation and for the many scientific discussions.

Finally I would like to thank my parents, Chellappah & Kirupaimalar Ramachandran, whose strength and courage have been truly inspirational and my family Suganthy, Umesh, & Narissa for all their love, and support throughout the years.

Thank you.

Table of Contents

Part III

Chapter 1

Chapter 2

Chapter 3

Chapter 4

Chapter 5

List of Figures

List of Abbreviations

Alb	Albumin
Alb-NO	S-nitroso-albumin
L-Arg	L-arginine
BSA	Bovine serum Albumin
BSA-NO	S-nitroso-BSA
CAM	Calmodulin
cGMP	Cyclic guanosine monophosphate
csPDI	Cell surface protein disulphide isomerase
Cys	Cysteine
Cys_2	Cystine
Cyst(e)ine	Cystine/Cysteine
DCF	Dichlorofluorescein
DnsHCys	N-dansylhomocysteine
$DnsHCys_2$	N,N-didansylhomocystiine
DnsHCysNO	N-dansyl-S-nitrosohomocysteine
DnsCMHCys	*N*-dansyl-*S*-carboxymethylhomocysteine
DMEM	Dulbecco's modified Eagle's medium
DTNB	5,5'-dithio-*bis*-3-nitrobenzoate
DTT	Dithiothreitol
ECGS	Endothelial cell growth supplement
EDRF	Endothelial Derived Relaxation Factor
eNOS	Endothelial NOS
E.coli	Escherichia Coli
FBS	Fetal bovine serum
FB	Fibroblasts
GSAO	4-(N-(S-glutathionylacetyl)amino)- phenylarsenoxide
GSCA	4-(N-(S-glutathionylacetyl)amino)benzoic acid
GSH	Glutathione
GSNO	S-nitrosoglutathione
GSSG	Oxidized glutathione
GST	Glutathione-S-Transferase
H_4B	Tetrahydrobiopterin
HCys	Homocysteine
$HCys_2$	Homocystine
Homocyst(e)ine	Homocysteine/Homocystine
HPLC	High performance liquid chromatography
HUVECs	Human umbilical vein endothelial cells
iNOS	Inducible NOS
LDL	Lipoproteins
LOOH	Lipid peroxides
mBB	Monobromobimane
mCB	Monochlorobimane
Me-THF	N-5-methytetrahydrofolate
NADPH	Nicotinamide adenine dinucleotide phosphate

NO	Nitric Oxide
NOHArg	N-hydroxyarginine
NOS	Nitric oxide Synthase
nNOS	Neuronal NOS
OxLDL	Oxidized lipoproteins
PBS	Phosphate buffered Saline
PDI	Protein disulphide isomerase
RNase A	Scrambled Ribonuclease A
ROS	Reactive oxygen species
RSH	Thiols
RSSR	Oxidized thiols
RSNO	S-nitrosothiols
$TRX(SH)_2$	Thioredoxin (red)
$TRX(S)_2$	Thioredoxin (ox)
TNB^-	Thionitrobenzoic anion
THF	tetrahydrofolate
UV	Ultraviolet

Part I

Development of S-nitrosothiol probes and the role of Cell Surface Protein Disulphide Isomerase in S-nitrosothiol transport

1.0 Abstract

We developed a novel dynamic assay to monitor S-nitrosothiol (RSNO) influx in live cells. The assay is based on the finding that the fluorescence emission of N-dansyl-S-nitrosohomocysteine (DnsHCysNO) was enhanced ~8-fold upon removal of the NO group. Short range excited state energy transfer between the SNO and dansyl moieties resulted in quenching of the dansyl fluorescence. Further exploitation of this compound revealed its ability to undergo transnitrosation/reverse nitrosation reactions and serve as a sensitive thiol/S-nitrosothiol probe in solution.

The findings led to the development of an intracellular RSNO probe, N,N-didansylhomocystine ($DnsHcys_2$). $DnsHcys_2$ was easily taken up by the cell and reduced to DnsHCys which is readily nitrosatable. Importantly, the fluorescence emission of DnsHCys is quenched upon the addition of low molecular weight (S-nitrosoglutathione, GSNO) and high molecular weight (S-nitroso-albumin, BSA-NO). We therefore used $DnsHCys_2$ as the probe to detect the transport of NO. A recent study suggested a cell surface mechanism where protein disulfide isomerase (csPDI) might catalyze the transfer the S-nitrosothiol bound NO (Zai, A., Rudd, A., Scribner, A.W., Loscalzo, J., (1999) *J. Clin. Invest.* **103**(3), 393-399). Our initial attempts involved the use of common PDI inhibitors, 5,5'-dithio-*bis*-3-nitrobenzoate (DTNB) and bacitracin, to implicate PDI in RSNO transport. PDI inhibitors caused acceptable inhibition (~50%) of RSNO transport without conclusively implicating PDI. The use of 4-(N-(S-glutathionylacetyl)amino)-phenylarsenoxide (GSAO), which contains a crucial trivalent arsenic that is capable of

binding to vicinal cell-surface dithiols, completely inhibited RSNO transport. More conclusive evidence arose with the use of a PDI over- and under-expressing cell line, HT1080. Overexpression of PDI increased intracellular nitrosation by 3-fold while underexpressed cells decreased intracellular nitrosation by 85%.

The reaction of NO and O_2 to produce N_2O_3 is accelerated in the hydrophobic core of the cell membrane. To identify whether NO or N_2O_3 is the nitrosating species that transverses the membrane, a quencher of N_2O_3, α-tocopherol, was used. Cells treated with α-tocopherol completely inhibited intracellular nitrosation.

In conclusion, the novel probe was successful in implicating the role of csPDI in the transport of RSNO-bound NO. Furthermore, the proposed mechanism suggests that NO is oxidized to N_2O_3, a potent nitrosator, that is capable of nitrosating thiols at the membrane cytosol interface.

1.1.1 Nitric Oxide

A general misconception in modern molecular biology is to believe that large and complex molecules regulate many bodily functions. Therefore, emergence of a small molecule, nitric oxide (NO), as an endothelium relaxation factor (EDRF) and effector of various biological responses was unexpected (Bredt *et al.*, 1999). NO is a heterodiatomic, free radical and a toxic gas. Its small size and neutrality allows it to freely diffuse through cellular membranes. This simple chemical has been shown to be a crucial mediator in neuronal communication, blood vessel modulation and immune responses (Bredt *et al.*, 1999).

1.1.1.1 Nitric Oxide Synthase

Endogenous NO is produced from L-Arg by various isoforms of Nitric oxide synthase (NOS). NOS from endothelial (eNOS) and neuronal (nNOS) cells are constitutively expressed and their activities are dependant on intracellular calcium levels. On the other hand, immune responses are dependent on the calcium independent inducible NOS (iNOS) (Brune *et al.*, 1996). Expression of iNOS protein is mediated via transcriptional activation by various cytokines (Hobbs *et al.*, 1999). All three enzymes utilize the co-substrates NADPH as an electron donor, and O_2 as an electron acceptor. The enzyme catalyzes the 5 step sequential oxidation of the guanidino group of L-Arg to yield citrilluline and NO. The production of NO and the modulation of NO as a signaling agent is tightly regulated at the level of NO biosynthesis (Hobbs *et al.*, 1999). Activity of

NOS is mediated by allosteric enzyme regulation, posttranslational modification and subcellular targeting (Brune *et al.*, 1996).

NO synthesis maybe triggered by chemical agonists (Bradykinin, ATP, acetylcholine) or by physical agonists (shearing, mechanical compression, light, electric shock) (Harris *et al.*, 2001; Paolocci *et al.*, 2001; Vetri *et al.*, 2000). Most agonists generate NO by Ca^{+2} influx, with a threshold of > 100nM stimulating NO production for a period of 1min. In the vasculature NO production is usually stimulated by hemodynamic force generated by flow of blood over the endothelial cells (Malinski *et al.*, 1998). Reversible phosphorylation of the serine residues of membrane bound NOS will inactivate the enzyme.

1.1.1.2 NOS Structure & Function

NOS is composed of a C-terminal reductase domain and a N-terminal oxygenase domain. The catalytic core is comprised of the oxygenase domain (500 aa) and the calmodulin (CaM) binding domain (30 aa) (Masters *et al.*, 1996). Synthesis of NO occurs at the core, which binds L-Arg, tetrahydrobiopterin (H_4B) and heme. The C-terminal reductase domain binds FMN, FAD, and NADPH, Fig 1.1.1. During NO synthesis, electrons are transferred from NADPH through the flavins to the heme iron, which allows binding of the heme. This activates oxygen and NO synthesis (Hemmens *et al.*, 1998). The binding of CaM is critical for constitutively expressed NOS, which activates the reductase domain independent of the oxygenase domain and increases the rate of electron transfer (Abu-Soud *et al.*, 1994). In the case of iNOS, CaM is

irreversibly bound and therefore active at basal concentrations of calcium (Cho *et al.*, 1992). Using bacterial systems, only eNOS and nNOS were shown to fold into the active conformation in the absence of CaM. Since iNOS did not show the same pattern, it implies that CaM binding is crucial in the folding of iNOS (Fossetta *et al.*, 1996; Rodriguez-Crespo *et al.*, 1996). The active form of NOS exists as a homodimer involving the interaction of the oxygenase domain, while the reductase domains help regulate their interaction (Chen *et al.*, 1996). For dimerization to occur, formation of the reductase domain is required followed by the incorporation of heme and H_4B (Stuehr, 1997). Incorporation of the heme occurs via the formation of a metal thiolate bond, critical for conformational changes (Hemmens *et al.*, 1998). The metal-thiolate bond is formed with one of the eight cysteinyl thiols found in the core oxygenase domains. A different cysteinyl thiol is known to form a disulphide with an adjacent subunit resulting in dimerization. The remaining thiols present in the core oxygenase domains are predicted to be redox sensors (Crane *et al.*, 1998).

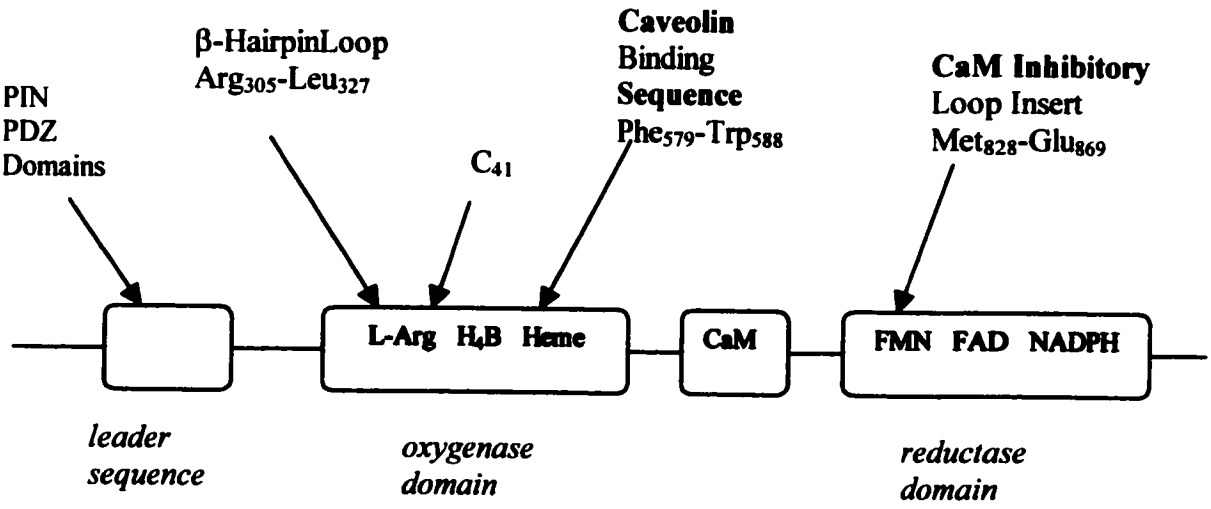

Figure 1.1.1:- Single Domain of Nitric Oxide Synthase (Stuehr, 1999)

1.1.1.3 NO synthesis by NOS

The hydroxylation of L-Arg leading to NO production proceeds via the activation of oxygen, Fig 1.1.2. Iron–oxygen species hydroxylate L-Arg to form N-hydroxyarginine (NOHarg) enzyme bound complex. Incorporation of another O_2 forms an iron-dioxy species, which can pose as an antioxidant to abstract an electron from NOHarg. This produces an iron-peroxy species and NOHarg radical. The final phase is speculated to proceed by a tetrahedral intermediate whereby the reaction of the iron-peroxy species with the NOHarg radical yields NO and citrulline (Kerwin *et al.*, 1995; Griffith *et al.*, 1995).

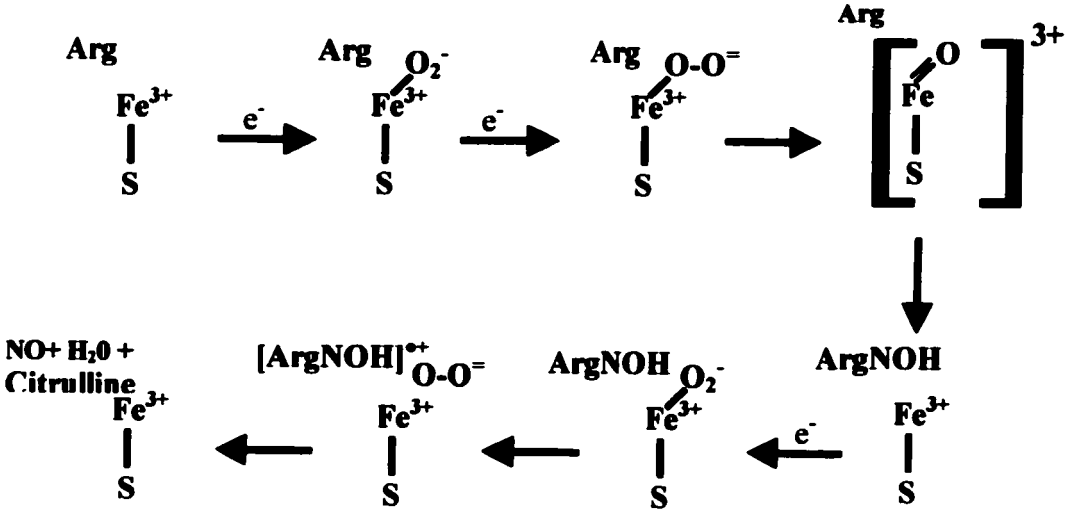

Figure 1.1.2:- Generation of NO from L-Arg.

1.1.1.4 Regulation of NOS

There are a number of ways in which the catalytic activity of NOS is regulated. Most commonly observed, is the feedback mechanism by NO. NO binds both ferric and ferrous forms of the heme iron in a reversible manner (Wang *et al.*, 1994). NOS regains activity upon the dissociation of NO. Dissociation of NO is considered to be substantially low with only 10-30% of the enzymes found in the active form (Hurshman *et al.*, 1995). Inhibition by NO may cause breakage of the cysteine thiolate-iron bond resulting in decoupling of the enzyme. This mode of regulation occurs when substrates such as H_4B and L-Arg are limiting (Abu-Soud *et al.*, 1998). NOS activity is sensitive to NO levels as well as the presence of NO scavengers and donors.

H_4B is crucial in the coupling of iron reduction to NO synthesis (Stuehr *et al.*, 1997). H_4B binding to NOS is anti-cooperative, where binding of the first H_4B reduces the binding of the second (Gorren *et al.*, 1996). Therefore, most dimers bind to only one H_4B. Lack of H_4B binding results in decoupling and generation of partially reduced oxygen, superoxide (Mayer *et al.*, 1995). In some instance NO synthesis has been limited by the availability of H_4B (Harrison *et al.*, 1997).

1.1.1.5 Physiological Effects

NO is produced in large amounts in neuronal cells where NO functions as a messenger molecule. NO is regarded as a major non adrenergic non-cholinergic (NANC)

neurotransmitter. It is involved in the release of glutamate from the presynaptic neuron to the postsynaptic neuron. Glutatmate binds to the N-methyl-D-aspartate receptor (NMDA), which activates the receptor complex and stimulates the influx of Ca^{+2}. This increase in Ca^{+2} activates the Ca^{+2} dependent neuronal NOS. NO as a diffusible secondary messenger is capable of triggering cGMP in the neurons to propagate the signal. It also plays a key role in smooth muscle relaxation in cerebral circulation, and as well as the gastrointestinal, urogenital and in the respiratory tract. Various pathophysiological conditions arise upon deregulation of NOS activity, such as migraines, hypertrophy and male impotency. More importantly, its function as a neuronal modulator affects various aspects of learning and memory (Bredt *et al.*, 1999).

The more renowned role of NO is its regulation of smooth muscle relaxation. NO production by endothelial cells is the major endogenous vasodilator. This system is counteracted by the vasoconstriction induced by the sympathetic nervous system and renin-angiotensin system (Huige *et al.*, 2000). NO as a secondary messenger induces smooth muscle relaxation by stimulating soluble guanylate cyclase, Fig 1.1.3 (Huige *et al.*, 2000). Activation of guanylate cyclase follows the interaction of NO with the iron bound heme complex of the enzyme. The interaction alters the position of the iron causing a conformational change thus exposing the active site. Activation of the enzyme and exposure of the active site to GTP results in an increase in cGMP levels (Ignarro *et al.*, 1984). This increase results in the activation of cGMP dependant kinases, which in turn phosphorylates proteins, initiating smooth muscle relaxation and vasodilation.

NO is also implicated in immune responses since T cells and macrophages induce NOS expression in the presence of pathogenic organisms. The strong binding of calmodulin to iNOS allows higher activity of the enzyme at lower calcium concentrations. These immune responsive cells bind pathogens and produce large amounts of NO. The presence of the localized effect of NO destroys the cell (Brune *et al.*, 1996).

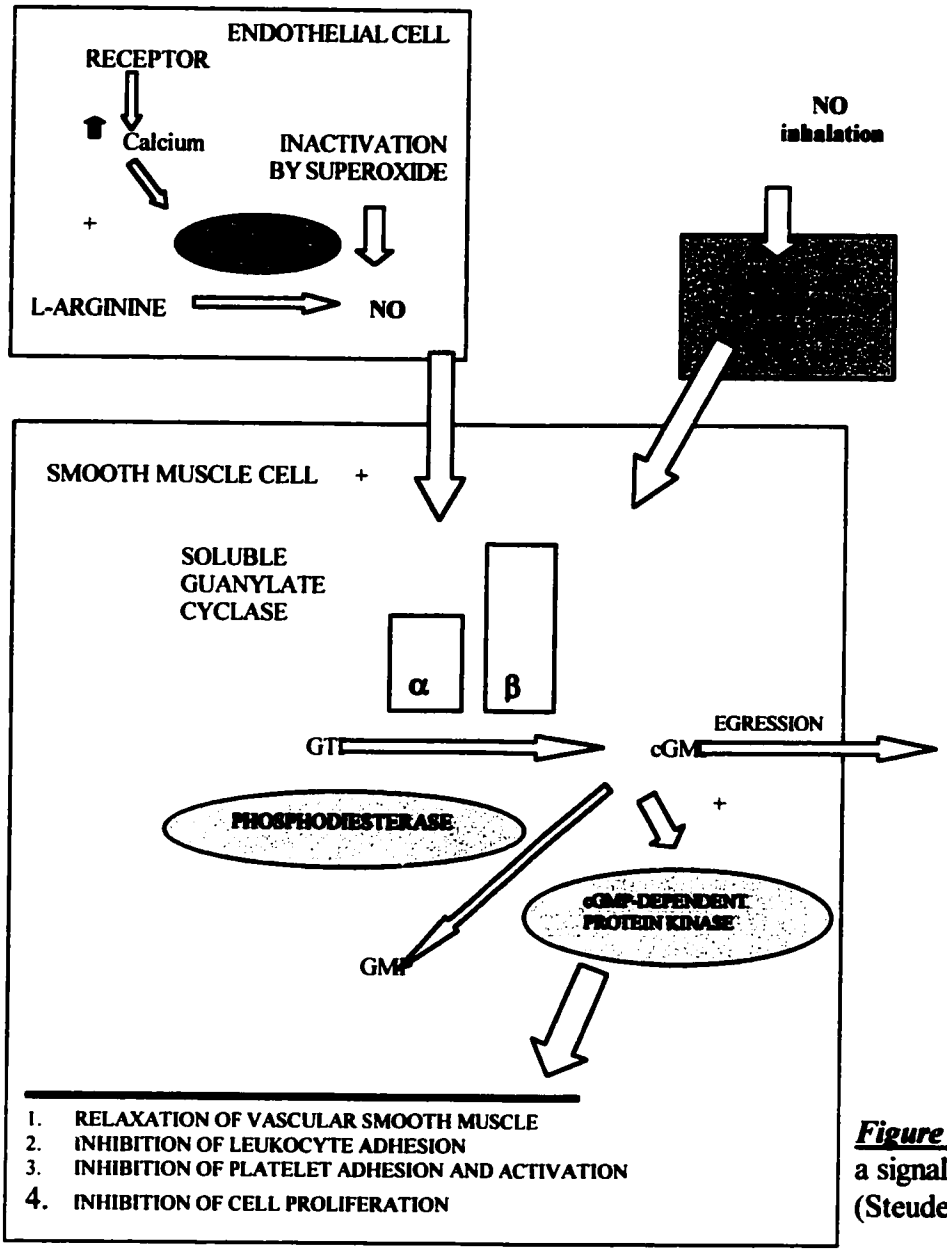

Figure 1.1.3:- NO as a signaling molecule (Steudel *et al.*, 1999)

1.1.1.6 NO Chemistry

Nitrogen reacts with molecular oxygen to form various oxides. Of these oxides, NO is paramagnetic and contains an odd number of electrons making it a highly reactive radical. The half-life of NO is inversely proportional to its concentration. At physiological concentrations of NO (1μM-10nM), the half-life may vary from 9-900 min (Kelm, 1999). Its solubility in water under standard temperature and pressure conditions is less than 2mM, whereas solubility under cellular conditions has been reported to concentrate 300 fold greater in the hydrophobic core of the membrane.

Steady state levels of NO are usually maintained in the cell by the rate of formation and the rate of decomposition. Additionally the mode and rate of NO metabolism is derived from its concentration, diffusibility and presence of other bioreactants (Kelm, 1999). NO is thought to be a freely diffusible molecule due to its charge neutrality. The reported diffusion constant in aqueous medium is $3300\mu m^2 s^{-1}$, which is approximately 1.4-fold larger than oxygen (Kelm, 1999). The presence of bioreactants such as oxygen, thiols, and reduced hemeproteins may also reduce the effective concentration of NO.

1.1.1.7 $NO_{(x)}$

Determinations of NO levels within cells have been difficult and controversial due to its high reactivity with a variety of bioreactants. The resonant NO, Fig 1.1.4.A, exists in 3 redox forms, nitrosonium ion(NO^+), nitric oxide(NO) and nitrosyl anion(NO^-). NO can readily form NO^+ or NO^- by reacting with transition metals to donate or accept electrons into their outer shell (Bentz *et al.*, 2000). NO reacts with molecular oxygen to produce a brown gas, NO_2. These two compounds are in dynamic equilibrium with each other. NO_2 readily reacts with NO in the presence oxygen to form N_2O_3, Fig 1.1.4B. In the absence of oxygen, NO_2 dimerizes to form N_2O_4. NO_2 can further be oxidized to nitrate (NO_3^-). Stability of NO ($t_{1/2}$=~1s) is lower than its oxidized counterparts NO_2 ($t_{1/2}$=~110s) and NO_3^- ($t_{1/2}$=~6hr). Therefore, NO_2 and NO_3^- are targeted for assays as possible indicators of NO levels.

There are also several reactive oxygen species (ROS) other than molecular oxygen that also react with NO. Some of these reactive oxygen species involved in the oxidation of NO are superoxide (O_2^-), hydroxyl radical (OH^-), and hydrogen peroxide (H_2O_2). Upon reacting with O_2^-, NO forms peroxynitrite ($ONOO^-$) at diffusion controlled rates (Goss *et al.*, 1999). Peroxynitrite anion ($ONOO^-$) and its conjugate acid peroxynitrous acid (ONOOH) can traverse cell membranes at comparable rates, however protonation of $ONOO^-$ decreases stability, which decomposes into NO_3^-, Fig 1.1.4C. In hydrophobic environments, $ONOO^-$ primarily catalyzes nitration of phenolic groups and tyrosines, while in aqueous environments, hydroxylation and nitration are predominant reactions (Goss *et al.*, 1999).

A) Resonance forms of NO

$$^{\bullet}N^{+}\text{-}O^{-} \leftrightarrow {}^{\bullet}N{=}O \leftrightarrow {}^{+}N{=}O^{-\bullet} \leftrightarrow N{\equiv}O^{\bullet}$$

B) Oxidation of NO

$$2NO + O_2 \longrightarrow 2NO_2$$

$$NO_2 + NO \longrightarrow N_2O_3$$

$$N_2O_3 + H_2O \longrightarrow 2HNO_2 \longrightarrow 2NO_2^- + 2H^+$$

C) Formation of Peroxynitrite

$$^{\bullet}NO + O_2^{-\bullet} \longrightarrow ONOO^- \ (k = 6x10^9\ M^{-1}s^{-1})$$

$$ONOO^- + H^+ \longrightarrow ONOOH \ (pKa = 6.5)$$

Isomerization of peroxynitrite upon protonation from *cis* to *trans*.

$$ONOOH \longrightarrow HNO_3$$

Figure 1.1.4:- Reactions of $NO_{(x)}$

1.1.1.8 Role as an Antioxidant/Oxidant

Studies in NO chemistry have shown that NO plays a multifaceted role in the biological system. The production of NO can lead to the production of various reactive nitrogen oxide species (RNOS) (Violi *et al.*, 1999). These species have pro-oxidant properties, which augment toxicity mediated by oxidative stress. Conversely, studies have also shown that NO can protect against oxidative stress and exert a positive effect on oxidative tissue injury (Wink *et al*, 1999, Kelly *et al.*, 1999).

NO itself is a poor oxidant however NO reacts with superoxide anion at diffusion controlled rates to yield peroxynitrite ($ONOO^-$) (Beckman *et al.*, 1990). $ONOO^-$ is a potent oxidant, which causes oxidation of low density lipoproteins (LDL). NO donors inhibit antioxidant enzymes such as glutathione peroxidase causing increases in peroxide levels and lipid peroxidation (Asahi *et al.*, 1995). Polyunsaturated fatty acids (PUFA) are susceptible to hydrogen abstraction by oxygen radicals resulting in oxidation to alkanes, aldehydes, alcohols or hydroperoxides (Hogg *et al.*, 1998). Oxidation of the cellular or mitochondrial lipid bilayer results in loss of membrane integrity. This change in permeability leads to loss of metabolite and electrolyte gradients, compromising cell function (Hogg *et al.*, 1998). The cell expresses a repair mechanism to reprocess damaged lipids, however lipid oxidation is a chain reaction and essentially unstoppable (Halliwell *et al*, 1984).

On the other hand NO can act as a antioxidant due to its ability to quench hydroxyl radical. The hydroxyl radical is considered the most reactive ROS making it relatively an unselective oxidant. Hydroxyl radicals are generated from hydrogen peroxide and Fe^{+2} or Cu^{+1} by the Fenton reaction. Due to its high reactivity, successful hydroxyl radical scavenger should exist in high (mM) concentrations. Since NO is not found in such high concentrations (nM-μM), the reaction with hydroxyl radicals to produce nitrites ($k > 10^{10} M^{-1}s^{-1}$), may not be physiologically relevant (Hogg *et al.*, 1998). NO can also react with ferrous iron to form metal-nitrosyls which inhibit the iron mediated production of the hydroxyl radical (Kanner *et al.*, 1991). More significantly, NO has a role in the chain termination reaction with lipid peroxide radicals (Goss *et al.*, 1999, Kelly *et al.*, 1999). The profound effects of NO, either oxidatively or antioxidatively, depend on the concentrations of NO, ROS and other competing reactants (Violi *et al.*, 1999).

$$LH + oxidant^{\bullet} \longrightarrow L^{\bullet} + oxidant\text{-}H \quad \textit{(initiation)}$$

$$L^{\bullet} + O_2 \longrightarrow LOO^{\bullet} \quad \textit{(propagation cycle)}$$

$$LOO^{\bullet} + LH \longrightarrow L^{\bullet} + LOOH \quad \textit{(propagation cycle)}$$

$$L^{\bullet} + L^{\bullet} \longrightarrow \text{non-radical products} \quad \textit{(termination)}$$

$$L^{\bullet} + LOO^{\bullet} \longrightarrow \text{non-radical products} \quad \textit{(termination)}$$

$$LOO^{\bullet} + \text{Antioxidant-H} \longrightarrow LOOH + \text{Antioxidant}^{\bullet} \quad \textit{(chain-termination)}$$

NO and chain-termination reactions:

$$\mathbf{LOO^{\bullet} + {}^{\bullet}NO \longrightarrow LOON{=}O} \quad \textbf{\textit{(chain-termination)}}$$

$$\mathbf{LO^{\bullet} + {}^{\bullet}NO \longrightarrow LON{=}O} \quad \textbf{\textit{(chain-termination)}}$$

Figure 1.1.5:- Role of NO in Lipid Peroxidation

1.1.2 S-Nitrosothiols

S-nitrosothiols are classified as signaling molecules and bioreactants of nitrogen oxides. Biologically relevant molecules containing reactive sulfhydryl groups can be nitrosated to form S-nitrosothiols. S-nitrosothiols act as a sink for NO and prolong its half life. The ability of SNO compounds to elicit NO dependent responses has given rise to its newfound interest.

1.1.2.1 Physiological effects

When considering NO as an EDRF, questions arise concerning their respective half lives. As stated earlier, $t_{1/2}$ of NO is ~1sec, however $t_{1/2}$ of EDRF has been reported to be ~10sec. Therefore, it has been speculated that S-nitrosothiols may play a key role in the effects of EDRF. Moreover, the physiological effects of RSNOs span into regulation of protein bioactivity via S-nitrosylation. Nitrosylation of protein thiols may lead to conformational changes or even oxidation of vicinal thiols (Arnelle and Stamler 1995). A number of nucleophilic protein side groups containing hydroxyls, amines, or aromatic carbons are susceptible to nitrosation. Stamler *et al.*, (1994) has studied the reactivity of RSNO towards these nucleophilic centers as well as the functional consequence.

Thiol groups are shown to be more sensitive to nitrosation than oxygen, nitrogen or aromatic carbons. One of the important modifications associated with nitrosation is

the formation of nitrotyrosine. Presence of nitrotyrosine has been commonly used as a marker for nitrosative stress induced by NO^+ donors (Gaston, 1999). Questions have also been raised regarding the impact of tyrosine nitrosation on phosphorylation activity. Proteins containing the motif Cys-Asp-Glu have been proposed to undergo conformational changes upon nitrosylation of the cysteine residue (Gaston, 1999). Nitrosation has been known to affect the bioactivity of various proteins such as tissue plasminogen activator, phosphotyrosine phosphatase, N-methyl-D-aspartate (NMDA) receptors, as well as the oxygen affinity of haemoglobin and various transcriptional regulatory proteins in *E.Coli* (Stamler *et al.*, 1994; Mayer *et al.*, 1998). Additionally, families of enzymes that catalyze thiol reactions namely the enzymes involved in the glutathione pathway are inhibited by the SNO mechanism.

1.1.2.2 S-NO formation

In aqueous samples the nitrosation of thiols is carried out in the presence of acidified nitrite. Under physiological conditions, nitrosation has been proposed to occur by NO^+, N_2O_3 or $ONOO^-$. Preliminary reports have suggested that nitrosation of thiols by NO occurs at neutral pH, however recent reports by Kharitonov *et al.* have been contradictory. Nitrosation of thiols occurs only in the presence of oxygen where rates of reaction are first order with respect to oxygen and second order with respect to NO (Kharitonov *et al.*, 1995). Under aerobic conditions, NO is oxidized to N_2O_3, a powerful nitrosating species. In aqueous conditions N_2O_3 is rapidly hydrolyzed, therefore nitrosation reactions are always in competition with hydrolysis by water. Under cellular

conditions the concentration of thiols (glutathione) is sufficiently high, ~10mM, allowing S-nitrosation of glutathione to out-compete hydrolysis by water. Therefore, rates of nitrosation are independent of thiol concentration due to the high concentration of intracellular thiols. Rates for nitrosation of small molecular weight thiols range from 1.5 to 3 x 10^5 $M^{-1}s^{-1}$ while larger proteins such as albumin attain slower rates of 0.03 to 0.06$M^{-1}s^{-1}$ (Kharitonov *et al.*, 1995).

The question arises whether the formation of N_2O_3 is physiologically pertinent. As reported by Liu *et al.*, (1998a) the reaction of NO and O_2 in a hydrophobic environment is 300 times faster and able to out compete its reaction with water. Due to its short life span and localized area of synthesis, nitrosylation of target proteins would be limited. In view of this, Nedospasov *et al.*, (2000) has recently reported the formation of N_2O_3 to occur by micellar catalysis. Oxidation of NO occurs in the hydrophobic cores of the protein, thus allowing the target proteins to catalyze their own nitrosylation (Nedospasov *et al.* 2000).

Stamler, (1994) has reported that S-nitroso albumin (Alb-NO) is the primary S-nitroso adduct in mammalian plasma. Albumin, a 585 aa containing single polypeptide chain, is the most abundant plasma protein thiol, 0.50mM, and hence serves as a reservoir for NO generated by endothelial cells. There are other proteins like albumin, but albumin binds to many ligands reversibly with high affinity. A 3 domain model (I, II, III) has been proposed, with each consisting of two sub-domains (A,B). Various regions of binding have been identified with varying affinities for different substrates (Kragh-

Hansen, 1990). The binding of most ligands occur at the principal binding site located in domains IIA and IIIA. Albumin possesses a Cys-34, which is situated in a hydrophobic crevice of depth 9.5A° between helices 1 and 2 of domain I and can undergo nitrosation (He *et al.*, 1992). The low pKa of Cys-34 makes it highly reactive towards NO species (specifically NO^+). Unlike CysNO and GSNO, Alb-NO undergoes conformational changes with decreasing pH. Therefore the degree of conformational freedom of the nitrosated Cys-34 residue is dependant on the degree of protein folding (Mohney *et al.*, 1997).

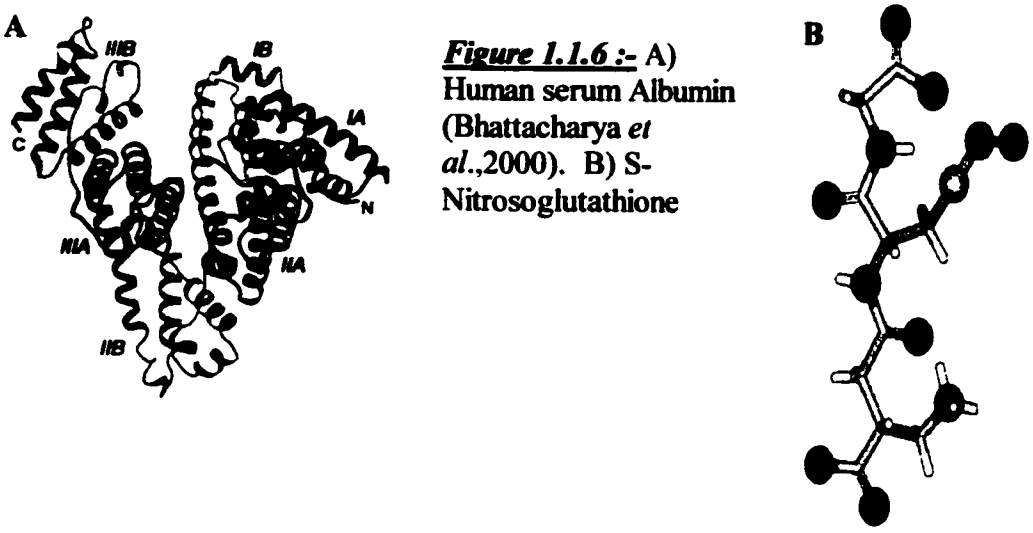

Figure 1.1.6 :- A) Human serum Albumin (Bhattacharya *et al.*,2000). B) S-Nitrosoglutathione

Recent reports by Mayer *et al.*, (1998) have shown that NOS produces GSNO as opposed to NO in the presence of GSH. Previous notions regarding S-nitrosothiol formation *in vivo* was thought to occur via peroxynitirite formation. Peroxynitrite or its product upon reacting with NO could also nitrosate free thiols. However inhibition of

peroxynitrite formation continued to yield SNO formation illustrating the natural tendency of NOS to produce GSNO in the presence of GSH.

1.1.2.3 S-NO Decomposition

To date, many mechanisms of SNO decomposition have been proposed, however the actual process is still unclear. Furthermore, the release of NO *in vivo* has been poorly addressed due to lack of assays for SNO. This is partially attributed to the unstable nature of these compounds. RSNOs can decompose in a number of different manners.

1.1.2.3.1 Copper :- Since, Cu^{+2} is reduced by thiol groups to form Cu^{+}, decomposition of RSNOs is thought to occur via Cu^{+} involving a six-membered ring structure. Cu^{+} binds to the nitrogen of NO and also an electron rich atom such as carbon or nitrogen. The net product of this decomposition is Cu^{+2} and RS^{-}, which dimerizes to RSSR (Williams, 1996).

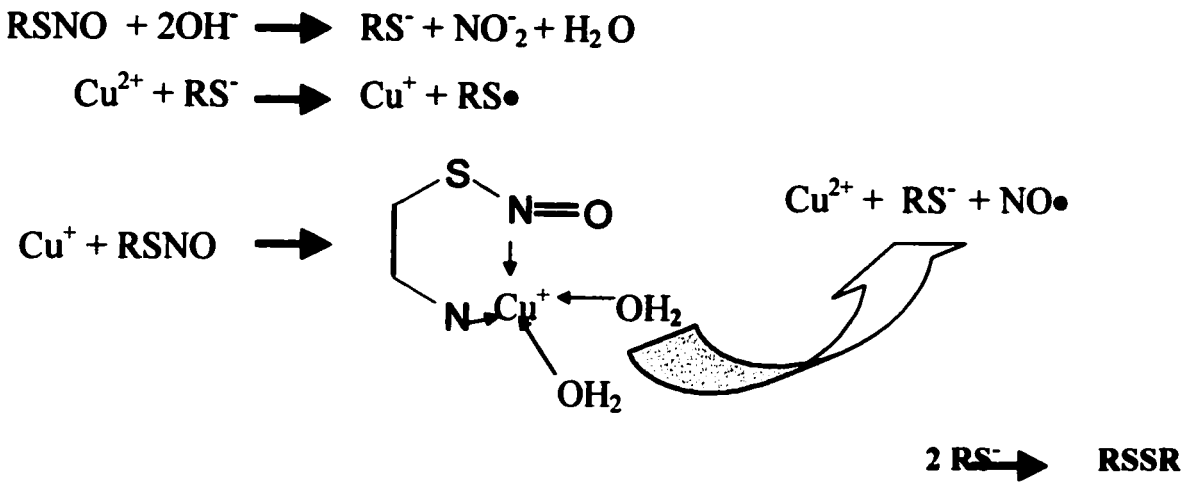

Figure 1.1.7:- Copper Catalyzed Denitrosation

1.1.2.3.2 Transnitrosation:- Transnitrosation occurs when RSNO in the presence of free thiols, allows for the rapid transfer of the NO moiety (Butler *et al.*, 1998; Askew *et al.*, 1995; Barnett *et al.*, 1995). Free thiols can perform a nucleophillic attack on the SNO bond resulting in the formation of a disulphide bond and NO.

Transnitrosation

$$2RSNO + 2R'S^- \longrightarrow 2RS^- + 2R'SNO$$

$$2R'SNO \xrightarrow{Cu^+} 2R'SSR' + 2NO$$

Nitrosation

$$N_2O_3 + RSH \longrightarrow RSNO + NO^-_2 + H^+$$

Figure 1.1.8:- Transnitrosation and nitrosation reactions

1.1.2.3.3 Enzymatic Decomposition:- Various enzymes in the glutathione cycle have been speculated to catalyze denitrosation of RSNO compounds. With regards to intracellular S-nitrosothiols, GSNO can be degraded by γ-glutamyl transpeptidase. Removal of one or more of the peptides drastically reduces the stability of the SNO complex. This is also evident from the differences in half lives of various SNO compounds. However, the mechanism of degradation is still poorly understood (Askew et al., 1995). Other enzymes implicated in GSNO decomposition are thioredoxin, glutathione reductase, and xanthine oxidase.

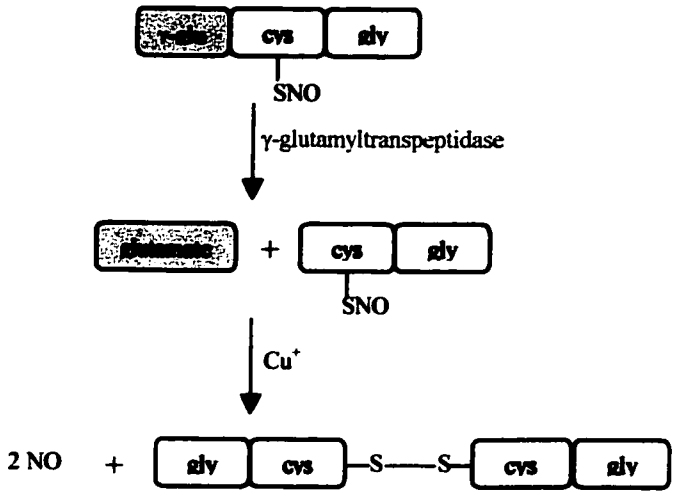

Figure 1.1.9:- Enzyme catalyzed RSNO decomposition

Recently Liu *et al.*, (2001) have isolated a metabolic enzyme with GSNO reductase activity. The role of this enzyme is to maintain homeostatic levels of GSNO and S-nitrosylated proteins. The presence of this enzyme has been shown in bacteria, yeast and humans. The suppression of its activity increases intracellular levels of GSNO and S-nitrosylated proteins. The enzyme with GSNO reductase activity is thought to be the glutathione dependant formaldehyde dehydrogenase (GS-FDH). The reaction occurs at diffusion controlled rates in a NADH dependant manner. GS-FDH protects cells from nitrosative stress rather than oxidative stress (Liu *et al.*, 2001).

$$GSNO + NADH + H^+ \longrightarrow GSNHOH + NAD^+$$

$$GSNHOH + NADH + H^+ \longrightarrow GSNH_2 + NAD + H_2O$$

$$GSNH_2 + GSH \longrightarrow GSSG + NH_3$$

Figure 1.1.10:- Reaction Catalyzed by GSNO reductase

1.1.2.3.4 Photochemical Decomposition:- Two models have been proposed for the photochemical degradation of RSNOs. S-nitrosothiols absorb radiation in the range of 345-370nm. The study outlined by Barrett *et al.*, (1995) has shown that S-nitrosotoluene absorbs radiation at 365nm, which excites the molecule to 330kJ.Mol^{-1} resulting in the fission of the SNO bond and release of NO. These free thiols will then oxidize to form a disulphide. However, Josephy *et al.*, (1984) have reported that irradiation of RSNO compounds causes homolytic cleavage resulting in thiol radicals. In a chain termination reaction the two thiol radicals will then readily form a disulphide. RSNOs appear to undergo thermal decomposition via a similar mechanism yielding the same products as by photochemical decomposition.

$$RSNO \longrightarrow RS^{\bullet} + NO^{\bullet}$$
$$RS^{\bullet} + RSNO \longrightarrow RSSR + NO^{\bullet}$$
$$RS^{\bullet} + O_2 \longrightarrow RSOO^{\bullet}$$
$$RSOO^{\bullet} + RSNO \longrightarrow RSSR + NO^{\bullet} + O_2$$

Figure 1.1.11:- Photolytic Release of NO from RSNO

1.1.2.4 Physiological relevance of SNO decomposition

Ascorbate has been implicated in the accelerated decompositon of S-nitrosothiols under physiological pH. Additionally, ascorbate enhances smooth muscle relaxation and platelet aggregation in response to RSNOs. Two plausible mechanisms exist for ascorbate based denitrosation. The Cu^{+2}/Cu^{+} dependant pathway, section 1.1.2.3.1, occurs at low concentrations of ascorbate, while at higher concentrations, ascorbate is capable of

performing a nucleophilic attack on the SNO group releasing of NO (Al-Sa'Doni *et al*, 2000).

The predominant pathways for SNO decomposition *in vivo* are mediated by Cu^{+}, transnitrosation with thiols and various enzymic pathways.

1.1.3 Intracellular Thiol buffer

Extensive mechanisms are employed to ensure the maintenance of the intracellular reducing environment. This reducing environment is regulated by the thiol buffer system and a number of antioxidative enzymes such as glutathione reductase, superoxide dismutase, thioredoxin and various other enzymes involved in the glutathione cycle. The thiol buffer system is largely composed of reduced glutathione and is considered to be a measure of the cellular redox environment.

1.1.3.1 Glutathione

The tripeptide GSH is the most abundant non protein thiol found in the cell with concentrations ranging from 5-10mM (Till *et al.*, 1998). GSH is usually synthesized in the cell and provides the cell with a reducing milieu. This protects thiols of proteins and antioxidants, as well as preventing oxidative and free radical damage (Meister *et al.*, 1981). GSH prevents tissue damage from exposure to oxidizing environments like hyperoxia, hyberbaric oxygen, and ozone (Deneke *et al.*, 1983,1985,1987, & 1989).

Furthermore, tissues are also protected from radiation, UV light and photodynamic effects (Connor *et al.*, 1987).

1.1.3.2 Glutathione cycle

The biosynthetic pathway of GSH involves a number of key enzymes such as γ-glutamyl-cysteine synthetase (γ-GCS), glutathione synthetase (GSHase), γ-glutamyl cyclotransferase, oxoprolinase, γ-glutamyl transpeptidase (γ-GT) and peptidase. These enzymes are involved in intracellular synthesis of GSH as well as uptake of extracellular GSH. In an organism, various organs such as the liver are considered to be synthesizers, users and primary exporters of GSH, while organs such as the kidneys heavily depend on the uptake of plasma GSH (Meister *et al.*, 1981).

1.1.3.3 Enzyme mediated uptake

Substrates for GSH synthesis are made available by active transport of amino acids into the cell or by the activity of γ-GT. γ-GT is an membrane bound enzyme which catalyses the hydrolysis of any γ-glutamyl peptide allowing the enzyme very broad substrate specificity. After hydrolysis, the γ-glutamyl moiety is transferred to another amino acid, most likely cysteine, and transported into the cell. If the product is γ-glutamylcysteine, it is directly utilized in the cycle while other γ-glutamyl conjugates will be subject to γ-glutamyl cyclotransferase activity for generation of glutamate (Meister *et al.*, 1981).

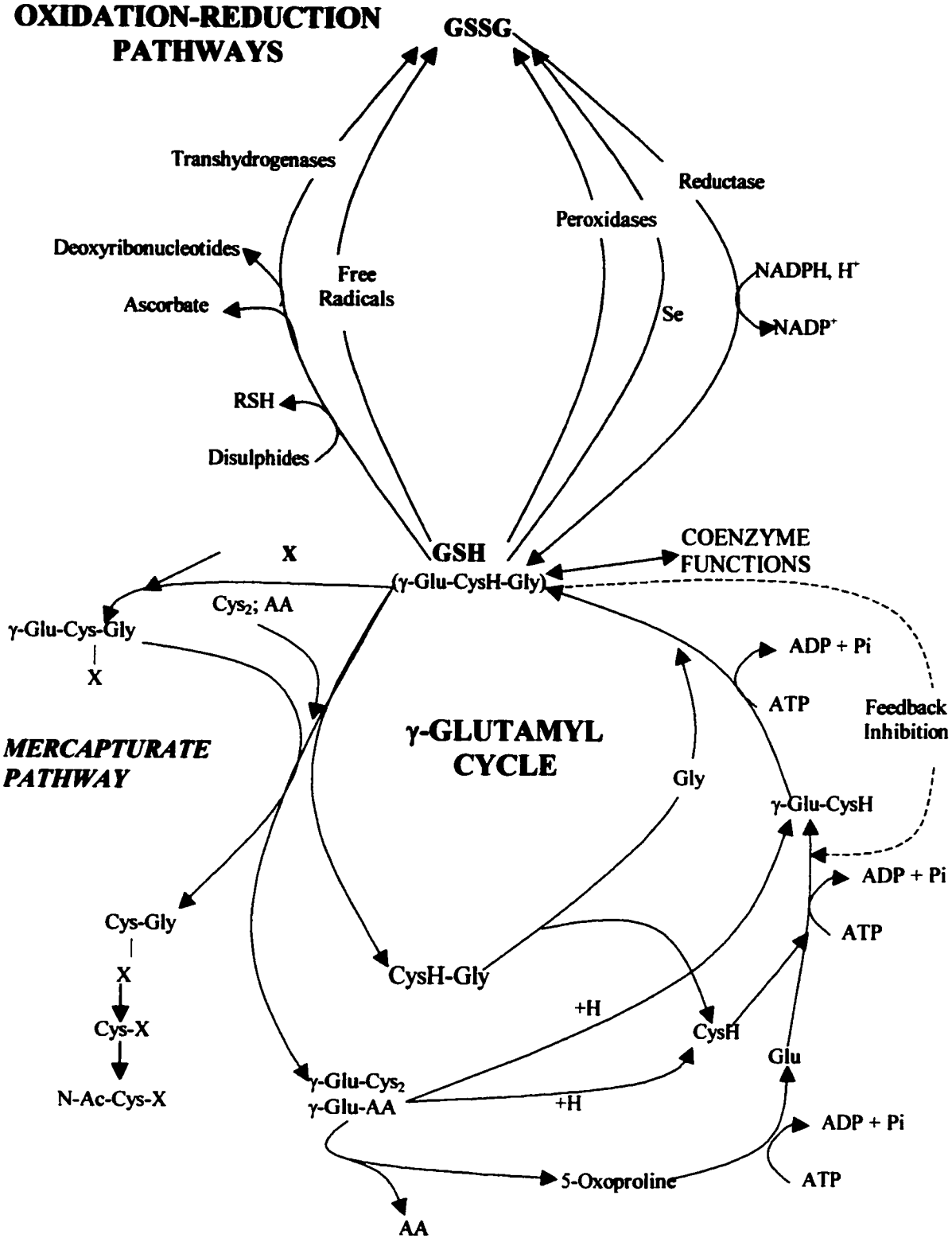

Figure 1.1.12 :- Glutathione Cycle (Red) and the Redox Cycle (Blue) (Meister *et al.*, 1981).

1.1.3.4 Transporter Mediated Uptake

Individual components of GSH (glutamate, cysteine, glycine) are taken up by various membrane bound transporters with overlapping substrate specificities. Glutamate is primarily transported by the System X^- family, which is composed of sodium dependent, anionic specific transporters and sodium independent transporters. Cysteine is primarily transported via the System A/ASC family of transporters which are sodium dependent and specific for neutral amino acids. Uptake of glycine is mediated by System Gly which is another sodium dependant transporter (Christensen, 1984; Deneke *et al.*, 1989).

Uptake of intact GSH is not considered to be the predominant source of GSH in most tissues with the exception of the kidney and the intestinal brush border. Most GSH transporters in cells exhibit low affinity for the substrate considering the plasma concentration of GSH is only 2-10μM (Flagg *et al.*, 1993; Svardal *et al.*, 1990).

1.1.3.5 Regulation of GSH Cycle

Two key control points of GSH metabolism depend on the activity of γ-GCS and GSHase. Activity of γ-GCS is inhibited by GSH via a feedback mechanism. However, an increase in glutamate blocks the regulatory site decreasing inhibition by GSH. Activity of GSHase may also be inhibited by GSH resulting in the accumulation of γ-glutamyl cysteine, which is decomposed into cysteine and oxoproline by γ-glutamyl cyclotransferase. As indicated by the outlined pathway, oxoproline is converted to

glutatmic acid. Any genetic defects in the oxoprolinase reaction results in the accumulation of oxoproline leading to acidosis.

1.1.3.6 Protective Role of Glutathione

The protective role of GSH is dependant on the activity of glutathione peroxidase (GPX), glutathione reductase (GSR), and glutathione transferase (GST). GPX is a selenoprotein that utilizes the reducing potential of GSH to reduce H_2O_2 and various lipid peroxides. Activity of GPX is specific to the presence of GSH and not the presence of other biological thiols. Continued activity of GPX results in the accumulation of GSSG. The accumulation of GSSG is prevented by the subsequent reduction of GSSG to GSH by glutathione reductase (GSR). GSR is a flavoprotein which is dependant on the reducing potential of NADPH. The resultant $NADP^+$ is regenerated via the pentose-phosphate pathway. The K_m of GSR for GSSG is 30-100μM, therefore GSR activity maintains GSSG levels below its K_m (Schrimer *et al.*, 1989). Any malfunction in GSR activity results in the accumulation of GSSG. Increase in GSSG levels may potentially lead to the formation of mixed disulphides, resulting in impaired protein function (Deneke *et al.*, 1989).

GST are cytosolic enzymes which catalyze the conjugation of GSH to various compounds with electrophillic centers as a detoxification mechanism. Nucleophilic attack of the thiolate moiety onto its substrate may also occur non-enzymatically. GST activity is considered to be most important in the liver but is also present in the lung,

intestine and erythrocytes. In addition to detoxification mechanisms, GSH conjugation is critical in the metabolism of steroids, and leukotrienes.

1.1.4 Protein Disulphide Isomerase

The formation of disulphide bonds has significant importance in protein folding and overall stability. Many proteins are able to spontaneously oxidize and refold in air or in the presence of thiol buffers. However, the attainment of correct structure and biological activity is often slow. *In vitro* studies have shown that disulphide formation occurs at a slower rate (minutes to hours) when compared to *in vivo* conditions where disulphide formation occurs in seconds to minutes. Early work by Goldberg *et al.*, (1994) alluded to an enzyme system that was capable of catalyzing thiol exchange reactions accurately and efficiently in protein folding. This enzyme system is part of the thioredoxin family of proteins and is currently referred to as protein disulphide isomerase.

PDI is a 56 800 Da, ~510 residue, protein commonly found in the lumen of the endoplasmic reticulum of eukaryotic cells (Freedman, 1984). This enzyme catalyses thiol exchange reactions during posttranslational modification of proteins. As far as catalytic efficiency of PDI is concerned, it is rather poor, due to the high concentrations required to observe any activity. This may be attributed to its lack of substrate specificity. In addition to catalyzing thiol exchange reactions several other novel functions of PDI have been recently proposed. Subunits of larger proteins have now been shown to contain PDI

such as the β subunit of prolyl hydroxylase, the N-linked glycosylation apparatus of the golgi bodies and thyroid hormone binding protein (Cheng *et al.*, 1987; Obata *et al.*, 1988; Koivu *et al.*, 1987; Geetha-Habib *et al.*, 1988). However the isomerization activity of PDI has not been observed in some of these parent proteins.

1.1.4.1 Thioredoxin Family

PDI is part of the thioredoxin superfamily. Generally, proteins catalyzing thiol exchange reactions belong to the thioredoxin family. Most proteins in this superfamily contain one or more thioredoxin folds (β–α–β–α–β–α–β–β–α) which encompass the active site motif Cys-Xaa-Xaa-Cys. The active site of PDI contains two catalytically active cysteine residues as stated above and shows high sequence homology to thioredoxin. The PDI enzyme complex is made up of four thioredoxin related domains. Therefore, from an evolutionary perspective, it is believed that PDI has been derived from thioredoxin.

1.1.4.1.1 Thioredoxin:- Thioredoxin is a small ubiquitous protein of 12kDa. This enzyme in conjunction with thioredoxin reductase is able to catalyze similar reactions as PDI in the presence of NADPH. Thioredoxin is found in several enzymes such as ribonucleotide reductase, T7 DNA polymerase and subunits of various proteins. In some cases, the parent protein does not require the redox activity of thioredoxin. Similar to PDI, thioredoxin also has the two cysteine motif in the active site with the sequence, Cys-Gly-Pro-Cys. Thioredoxin has a hydrophobic site at close proximity to the active site,

Gly 33 Pro 34 Ile 75 Pro 76 and Ala 93, responsible for substrate binding (Holmgren, 1995). There exists a great variation in the sequence of thioredoxin from various species, approximately less than 25% homology, however they all contain the same tetrapeptide in the active site (Hoog *et al.*, 1984; Eklund *et al.*, 1991).

1.1.4.1.2 ***Thioredoxin Structure:-*** The crystal structure of thioredoxin indicates an exposed Cys 32 residue which is part of the catalytic site. The pKa of the Cys 32 is 7.1 which is less than the pKa of free cysteine (pKa 8.5) (Martin , 1995; Dyson *et al.*, 1997). Cys 32 is thought to share a hydrogen bond with Cys 35 at physiological pH (Jeng *et al.*, 1995). The difference in pKa is attributed to the close proximity of a buried Asp 26 residue with a partial charge (Chivers *et al.*, 1996) . Asp 26 might have a role as a general acid/base in thioredoxin reactions (Chivers *et al.*, 1997). During catalysis, the exposed Cys 32 is poised to perform a nucleophilic attack on its substrate (disulphide). The resulting mixed disulphide serves as a substrate for Cys 35. The activity of Cys 35 is triggered upon donating its hydrogen to the nearby Asp 26. The final product being the reduced substrate and the oxidized cysteine residues in the thioredoxin active site. Regeneration of the active site is carried out by thioredoxin reductase and NADPH.

1.1.4.1.3 ***Thioredoxin Reductase:-*** Thioredoxin reductase has 40-50% sequence homology with that of glutathione reductase. In fact, both systems, glutathione/glutathione reductase and $TRX(SH)_2$/ $TRX(S)_2$, perform similar functions by harnessing the reducing power of NADPH. Both enzyme systems are members of the pyridine nucleotide –disulphide oxidoreductase family, and possess the ability to undergo

disulphide exchange reactions (Williams *et al.*, 1995). Their main differences lie in the limited substrate specificity of glutathione reductase, which only reduces glutathione. The catalytic site of $TRX(SH)_2$ has a binding site for FAD, & NADPH and contains a redox sensitive disulphide. Electrons are transferred from the NADPH to FAD and then to the disulphide.

1.1.4.2 PDI Structure

PDI is composed of 4 thioredoxin domains (**a,a',b,b'**) and a **c** domain (Ferrari *et al.*, 1999). The **a** and **a'** domains have high homology to thioredoxin domains with the active site sequence Cys-Gly-His-Cys (Kemmink *et al.*, 1997). Experimental data has shown that neighbouring **b** and **b'** domains do not have catalytically active residues and hence lack activity. This may be due to point mutations in the active site, since both **b** and **b'** domains contain the other residues that contribute to the catalytic activity (Ferrari *et al.*, 1998). The **c** domain is located near the C terminus, functionally it has a low affinity, high capacity, and highly acidic Ca^{+2} binding site. This is characteristic of many endoplasmic reticulum lumenal proteins where metabolic regulation is mediated by Ca^{+2} levels, ~50mM (Freedman *et al*, 1995). The overall secondary structure and protein folding topology are very similar (Kemmink *et al.*, 1997). Based on the secondary and tertiary structures of these subunits, each subunit was categorized in three boxes, A, B and C. Box A expresses a $\beta-\alpha-\beta$ element in both **a** and **b** domains however they are the least conserved among the superfamily. The C box among all subunits is the most highly conserved region, $\beta-\beta-\alpha$ (Ferrari *et al.*, 1999).

Crosslinking studies using a homobifunctional crosslinking reagent, N,N,-methylene (bis) iodoacetamide, was aimed at determining the approximate distance between the two active sites localized in subunits **a** and **a'**. Crosslinkers with a variable number of methylene groups revealed the interactive distance between the two active sites to be ~16A°.

Figure 1.1.13- (A) The active **a** domain of PDI. (B) The inactive **b** domain of PDI (Kemmink *et al*, 1993).

1.1.4.2.1 Peptide Binding:- The ability of PDI to catalyze thiol exchange reactions with various substrates depends on its ability to bind to polypeptides. Reports by Darby and Crieghton (1994) have alluded to the importance of the silent **b** and **b'** domains. Activity of **a** and **a'** domains alone showed drastically reduced isomerase activity while retaining their redox activity. The activity of PDI was determined using a model substrate, Bovine Pancreatic Trypsin Inhibitor (BPTI) that requires both the redox and isomerization activity of PDI (Darby *et al.*, 1998). Mutational analysis of PDI using BPTI as its substrate showed that **b** and **b'** were necessary for its isomerization activity. Furthermore, **b'** may act as a peptide binding site resulting in the stabilization of the transition state. The **b** and **b'** subunits may also be a target for phosphorylation and possibly catalyze ATP hydrolysis (Quemeneur *et al.*, 1994; Guthapfel *et al.*, 1996). However, to date there has been no conclusive evidence that ATP affects PDI activity. Furthermore, the c subunit, proximal to the **a'** domain and responsible for Ca^{+2} binding is also believed to be involved in substrate binding. Deletion of the C- terminal residues thought to be responsible for substrate binding resulted in reduced refolding of various disulphide containing proteins. These findings indicate the presence of a distinct binding site and its relation to the redox activity of PDI (Dai *et al.* 1997).

PDI exhibits low affinity for most peptides (K_d>100μM) (Morjana *et al.*, 1991). The affinity does increase with increasing length and Cys content. Comparing polypetides of the same length, polypeptides containing Cys residues have been shown to bind 4-8 fold more strongly (Klappa *et al.*, 1997). Polypeptides lacking Cys residues were able to reversibly bind native PDI and were sensitive to treatment with Triton X-

100. Based on these findings by Klappa *et al.*, (1997) hydrophobic interactions have been introduced as a significant parameter in the efficiency of binding Performing inhibition studies with small peptides, the apparent peptide binding site appears to be the same or juxtaposed with that of the polypeptide binding site. The binding site was located near the active site whereby binding of the peptides inhibited redox activity of PDI (Ferrari *et al.*, 1999).

1.1.4.2.2 ***PDI activity:-*** PDI catalyzes three types of reactions, isomerization, reduction, and oxidation. As described earlier, the catalytic activity of PDI is similar to that of its ancestery protein, thioredoxin. The N-terminal Cys residue of both **a** and **a'** is capable of independently performing nucleophillic attack on its substrate (Chivers *et al.*, 1996). Unlike thioredoxin the pKa of the N-terminal Cys is much lower, pKa=4.5, possibly due to the presence of a histidine imidazole group within the catalytic site, Cys-Gly-His-Cys. The close proximity of a partially positive N-terminus of an α helix may also contribute to the low pKa. The side chain of Glu 30 located proximal to the active site has been implicated in catalytic activity of PDI, possibly analogous to Asp 26 of thioredoxin, however studies have not been conclusive. The difference in pKa values of the Cys residues in PDI and thioredoxin is reflected by their relative activities. The disulphide form of the PDI enzyme is less stable than that of thioredoxin. This is evident in the oxidative role of PDI in contrast to the reductive role of thioredoxin (Kortemme *et al.*, 1996; Freedman *et al.*, 1995).

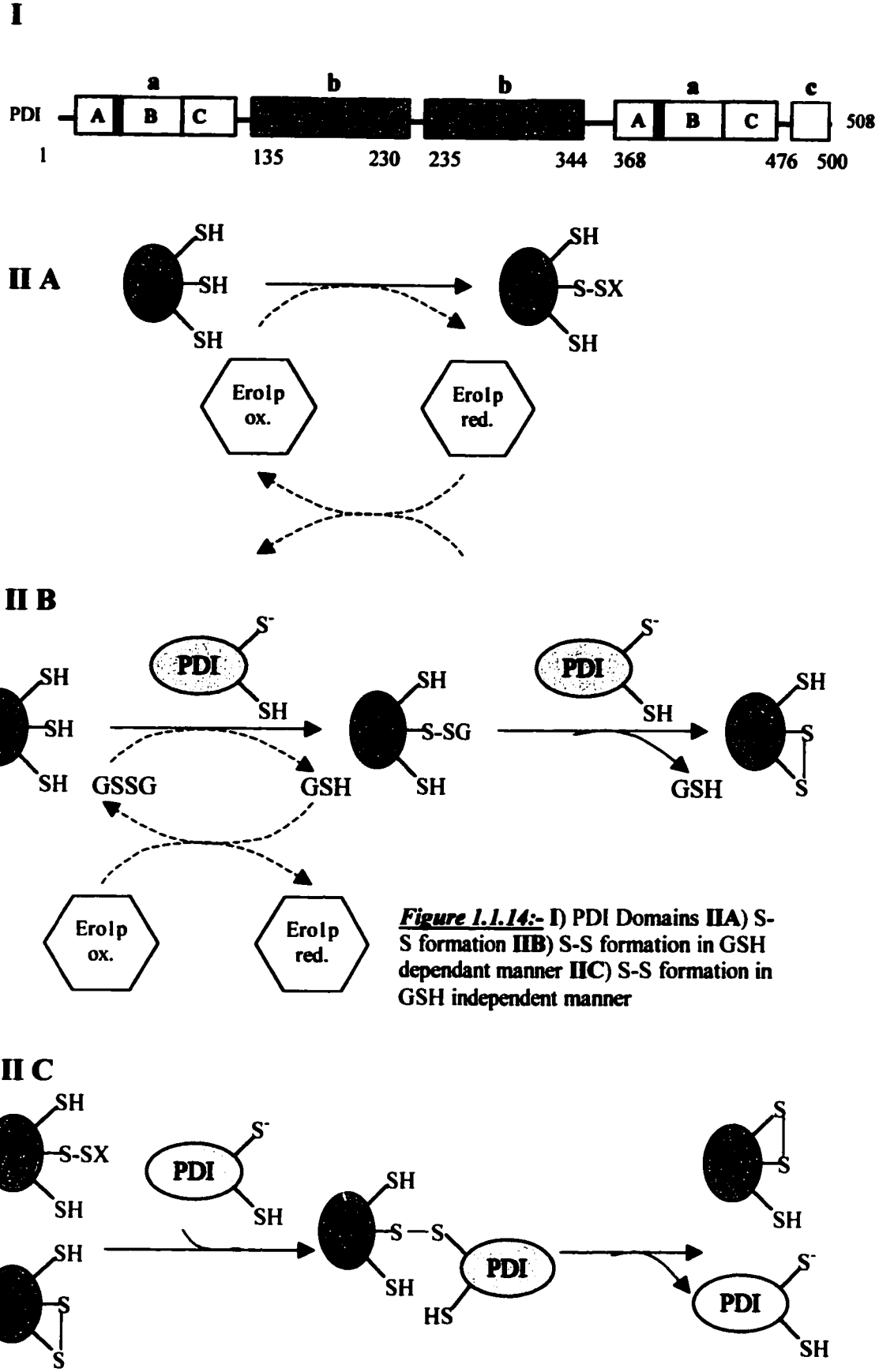

Figure 1.1.14:- **I) PDI Domains IIA) S-S formation IIB) S-S formation in GSH dependant manner IIC) S-S formation in GSH independent manner**

1.1.4.2.3 ***Redox Modulation of PDI activity:-*** Activity of PDI is dependant upon redox potential of the environment. The redox environment of the endoplasmic reticulum is highly oxidizing in comparison to that of the cystosol. The ratio of GSH to GSSG in the endoplasmic reticulum is 2:1 whereas in the cytosol it is 100:1 (Hwang *et al.*, 1992). This allows the PDI active site to be in equilibrium between the reduced and oxidized forms, the predominant being the reduced isomer. Under these conditions, the active site of thioredoxin is fully oxidized rendering the enzyme inactive. As stated earlier, PDI catalyzes oxidation, reduction and isomerization reactions (Pollard *et al.*, 1998). The proposed mechanism has shown that isomerization reactions are independent of reoxidation by GSSG. However, PDI primarily catalyses oxidation of proteins via a glutathione intermediate resulting in the formation of a mixed disulphide (Darby *et al.*, 1994; Ruoppolo *et al.*, 1996).

The ability of PDI to efficiently catalyze redox reactions depends on the standard redox potential. The redox potential of PDI is -180mV, while that of thioredoxin is –260mV (Hawkins *et al.*, 1991). These potentials can be stated with respect to small thiol analogues such as oxidized and reduced glutathione. The redox potentials of PDI and thioredoxin are equivalent to equilibrium constants of GSH/GSSG of ~50μM and ~1mM respectively (Freedman *et al.*, 1994). Difference in redox potential allows PDI to catalyze isomerization reactions 50 fold higher than thioredoxin (Hawkins *et al.* 1991). The difference in activity and redox potential is soley attributed to the active site sequence. Studies by Huber-Wunderlich *et al.*, have clearly shown that mutation of the thioredoxin box, Cys-Gly-Pro-Cys, to that of the PDI active site, Cys-Gly-His-Cys,

increased oxidation and isomerization reactions by 10 fold (Lundstrom *et al.*, 1992; Freedman 1994).

1.1.4.2.3 Chaperone Activity:- PDI is a well known chaperone molecule. Chaperone molecules assist in the folding of nascent proteins or refolding of incorrectly folded proteins. A chaperone molecule is able to create a microenvironment whereby it is able to outcompete aggregation reactions. PDI is a chaperone to a variety of proteins that contain disulphide linkages such as acidic phospholipase A2, glyceraldehyde-3-phosphate dehydrogenase (GAPDH).

Since disulphide formation in proteins may occur co-translationally, PDI is able to catalyze isomerization reactions to produce functional proteins at 1000 fold higher rate than uncatalyzed reactions (Weissman *et al.*, 1993). This is due to the fact that *in vivo*, PDI is able to facilitate disruption of disulphide bonds, scan various disulphide isomers and prevent trapping of PDI in mixed disulphide complexes (Walker *et al.*, 1997).

1.1.4.2.4 Cell Surface PDI:- PDI has traditionally been found in the lumen of the endoplasmic reticulum and is known to catalyze thiol exchange reactions. Recent reports have provided evidence to the existence of PDI on the plasma membrane of various cell types, such as membranes of platelets, megakaryocytes and endothelial cells (Chen *et al.*, 1992; Kroning *et al.*, 1994). In some instances PDI is secreted from cells, as in the case of rat exocrine pancreatic cells and activated platelets (Akagi *et al.*, 1988; Chen *et al*, 1992). PDI contains a C-terminal tetrapeptide sequence known as the endoplasmic

retention signal, KDEL (Munro *et al.*, 1987). This anchor mediates the interaction between PDI and membranes of the golgi apparatus via a KDEL receptor. The PDI-KDEL receptor complex is "recycled" back into the endoplasmic reticulum (Griffiths *et al*, 1994). A saturation of the retention mechanism results in the secretion of PDI. The PDI is exported with the KDEL signal and deposited on the cell membrane and stabilized by electrostatic interactions (Yoshimoro *et al.*, 1990; Terada *et al.*, 1995).

The change in localization of the enzyme implies a change in function of the enzyme. Cell surface PDI (csPDI) is responsible for controlling the redox state of many exofacial protein thiols. A change in PDI levels on the plasma membrane affects the expression of thiol containing proteins on the membrane surface (Jiang *et al.*, 1999). More specific functions of PDI have been characterized in platelets, HIV, cell adhesion, and thryrotropin receptor function.

1.1.4.2.5 ***Role of CsPDI in TSH receptor shedding:-*** The metabolic hormone thyrotrophin (TSH) regulates the growth and function of the thyroid gland via a thyroid receptor. This receptor is expressed as a pro-receptor on the surface of human thyroid cell membranes (thyrocytes). Extracellular portions of the membrane consist of an α subunit (~53kDa) and a membrane spanning β subunit (~38kDa) both containing disulphide linkages. Transition from a pre-receptor to a receptor involves the "shedding" of the α subunit. PDI catalyzes the reduction of the TSH receptor disulphide bond resulting in the shedding of the TSH receptor ectodomain.

1.1.4.2.6 ***Role of CsPDI in Platelets:-*** The redox state of platelet surface thiols have been shown to influence their function. Reduction of surface thiols will expose the fibrinogen receptor and activate glycoprotein receptors. PDI on resting platelets is found mainly in the oxidized form (26% dithiol) whereas in activated platelets most PDI active site residues are reduced (81% dithiol). Furthermore, in activated platelets, the glycoprotein receptor exposes more free thiols than in resting platelets. Studies by Hogg *et al.*, (2000) and Essex *et al.*, (1999) have shown that reduction of PDI active sites lead to conformational changes in glycoprotein receptor exposing free thiols and activating platelets. The redox state of surface thiols also affects integrin mediated platelet adhesion. A receptor-ligand mediated interaction causes conformational changes in the receptor resulting in platelet adhesion. Platelet adhesion is an important step in blood clotting and occurs via binding of fibrinogen, fibronectin, or collagen to the activated integrin receptor complex. The role of PDI is to catalyze disulphide formation between the ligand and the receptor. This has been shown in the irreversible binding of collagen to the integrin adhesion receptor (Lahav *et al.*, 2000).

1.4.2.7 ***Role of CsPDI in HIV:-*** The ability of HIV to penetrate cellular membranes relies on the reductive strength of the membrane. Treatment of human lymphoid cells with membrane impermeant sulfhydryl reagents inhibits HIV infection. This suggests that infection by HIV must be mediated via a thiol exchange reaction. Infection of cells by HIV was markedly reduced by the use of PDI antibodies and inhibitors. Fenouillet *et al.*, (2001) have reported that PDI mediates the reduction of crucial disulphides in the

viral membrane glycoprotein gp 124 and its CD4 receptor. The reduction of these disulphides and subsequent binding are key modulators for the penetration of HIV.

1.1.4.2.8 PDI Catalyzed Transnitrosation reactions:- Pioneering work by Zai *et al.*, (1999) was successful in implicating the csPDI as having a role in the transport of S-nitrosothiols. It was hypothesized that the presence of cell surface thiols able to undergo transnitrosation reactions with RSNOs may play a role in its transport. This novel study utilizing inhibitors of PDI and antisense mediated expression of PDI suggested that CsPDI was crucial in transporting RSNO bound NO from the extracellular matrix to the intracellular. This was observed by monitoring its intracellular bioactivity, activation of guanyl cyclase. However, the actual mechanism by which NO was transported into the cell was unclear. One plausible mechanism was the reductive denitrosation of RSNO resulting in disulphide formation. This may have also occurred through a disulphide radical formation. A commonly believed mechanism includes the transfer of NO to surface thiols or transmembrane thiols. Current studies have not clearly shown if PDI directly transfers NO into the cell or by nitrosation of surface thiols (Zai *et al.*, 1999).

1. $RSNO + RSH \longrightarrow RS^{\bullet}\text{-}SR + NO^{\bullet} + H^{+}$

2. $2RSNO + 2R'SH \longrightarrow 2NO^{\bullet} + 2RSH + R'SSR'$

Figure 1.1.15:- PDI Catalyzed Transnitrosation

1.1.4.2.9 PDI Kinetics:- Studies by Gilbert, (1989), have been successful in characterizing the kinetic parameters of PDI. In his preliminary attempts to probe the mechanism of PDI, Gilbert (1989), used a disulphide-containing hexapeptide (CYIQNC) and the most abundant non-protein thiol, GSH. Prior to kinetic analysis, thiol content in PDI was determined by titration with 5,5'-dithio-*bis*-3-nitrobenzoate (DTNB). Surprisingly, a slow reaction with DTNB was observed, yielding 0.8 equivalent of thiol per PDI subunit. However, following treatment with DTT, 7.1 equivalents of thiol per PDI subunit were obtained. It was therefore concluded that the PDI subunit contains one free thiol and three disulphide bonds. Initial kinetic studies entailed the reduction of PDI by GSH, which generates GSSG. The reaction is then coupled to glutathione reductase activity with excess NADPH to monitor PDI-dependant production of GSSG. The reduction of the PDI disulphide occurred in sequential phases, slow (k_{slow}=0.0019min^{-1}), medium (k_{med}=0.025min^{-1}), and fast (k_{fast}=0.21min^{-1}). The fast reduced disulphide was considered to be catalytically relevant. The proposed mechanism (below) for the reduction of PDI by GSH shows that low GSH concentrations k_3 becomes the rate-limiting step. With increasing concentrations of GSH, the reaction will favour reduction of PDI disulphide (k_3) as opposed to the intramolecular catalyzed expulsion of the mixed disulphide (k_2).

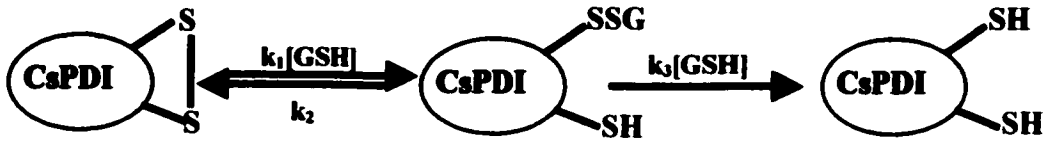

Figure 1.1.16:- Mechanism for PDI catalyzed disulphide reduction which proceeds through mixed disulphide formation (Gilbert H.F., 1989).

Attempts to determine the Michaelis-Menten parameters of PDI for its substrates GSH and the hexapeptide proved to be cumbersome. Increasing the concentrations of GSH and the hexapeptide was limited due to non-enzymatic reaction between the two substrates at a rate higher than that of PDI. K_M values obtained for GSH (>>14mM) and hexapeptide (>>1mM) were substantially high. Initial velocity kinetic experiments revealed a sequential addition of substrates. Realizing the nature of the reactions catalyzed by PDI, a ping-pong mechanism might be plausible whereby GSH reduces PDI prior to PDI mediated reduction of the hexapeptide. Taking into account all factors, Gilbert, (1989), proposed the following hybrid mechanism based on their findings and that of Crieghton *et al.*, (1980) and Lambert and Freedman *et al.*, (1983).

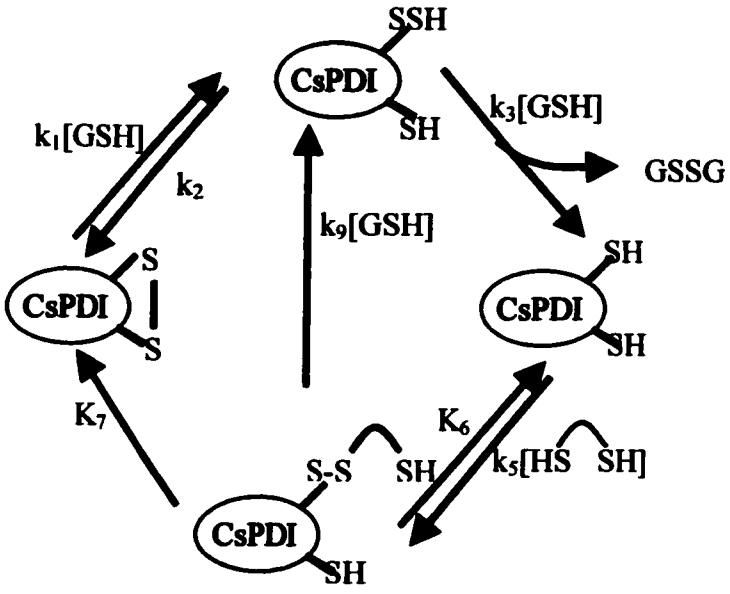

Figure 1.1.17. :- Proposed mechanism for PDI catalyzed reactions with small peptides (Gilbert H.F., 1989).

PDI is initially reduced by GSH upon which it forms a mixed disulphide with the peptide. At this cross road, two separate mechanisms may occur. Under high GSH concentrations the reaction follows a sequential mechanism resulting in a ternary complex formation. The complex is broken down to yield a reduced peptide and an enzyme-GSH mixed disulphide (k_9). Under low GSH concentrations, a ping pong mechanism prevails where intramolecular cleavage of the enzyme-peptide mixed disulphide yields a reduced peptide and oxidized enzyme (k_7). The finding that increasing the concentrations of GSH or the hexapeptide did not show saturation or a true V_{max} supports this mechanism. Since, GSH and the hexapeptide react in a bimolecular fashion the rate of the reaction depends on the rate limiting substrate. Therefore, the sequential mechanism proceeds by the steps k_3, k_5, and k_9 while ping-pong mechanism proceeds by k_3, k_5, and k_7. To date there is no evidence suggesting the presence of a ping-pong mechanism.

1.1.4.2.10 Inhibitors of PDI:- Kinetic studies involving PDI have been attempted using a number of inhibitors. Common inhibitors employed in these studies have varied from membrane impermeant sulfhydryl reagents such as DTNB and parachloromercuribenzinesulphonate (PCMBS), non-sulfhydryl reagents (bacitracin, antibodies) and peptides. Studies by Mandel *et al.*, (1993) have shown that *in vitro*, bacitracin is a poor inhibitor of PDI since large concentrations (~3mM) are required under long incubation times (~4-6hrs), to achieve a ~90% inhibition of PDI disulphide reduction activity. Results *in vivo* showed an inhibition rate of 70%.

Sulfhydryl reagents proved to be better inhibitors of PDI , with almost 100% inhibition observed using 1mM DTNB and pCMB. Use of PDI monoclonal antibodies showed only 50% activity after increasing concentrations to 200μg/mL. Reports by Kaetzel *et al.*, (1987) suggest that these antibodies may bind only near or at one active site resulting in poor inhibition. In this study we use 4-(N-(S-glutathionylacetyl)amino)-phenylarsenoxide (GSAO) as an inhibitor of csPDI. GSAO has been used to bind to surface dithiols for the purposes of isolation and identification of membrane dithiol containing proteins (Donoghue *et al.*, 2000). A number of factors affect the inhibitory effect of these compounds. Under *in vitro* conditions, inhibitor strength can be easily characterized, however factors *in vivo* such as cell type, requirements for substrate binding, substrate affinity, effect of inhibitor on cell metabolism and viability become key components.

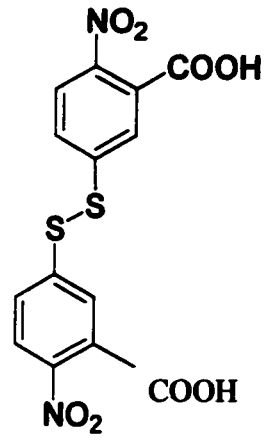

Ellman's Reagent (DTNB)
2,7-dithionitrobenzoic acid

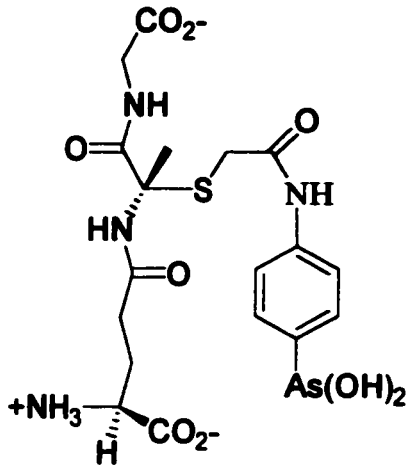

GSAO
(4-(N-(S-glutathionylacetyl)amino) phenylarsenoxide)

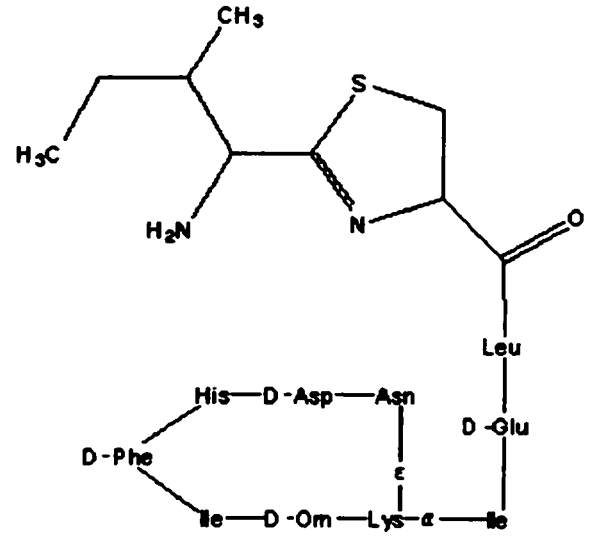

Bacitracin A

Fig 1.1.18:- Inhibitors of cell surface PDI employed in this study

1.2.1 Materials

Sigma-Aldrich (Oakville):- Glutathione (GSH, GSSG), Homocyst(e)ine, dansyl chloride, bacitracin, 5,5'-dithio-*bis*-3-nitrobenzoate (DTNB), α-tocopherol, dithiothreitol, aprotinin, bovine serum albumin, iodoacetate, α-tocopherol, Sephadex G-10 & G-25,

Hogg's Lab (University of New South Wales, Australia):- HT1080 Cell line, 4-(N-(S-glutathionylacetyl)amino)- phenylarsenoxide (GSAO), 4-(N-(S-glutathionylacetyl)amino)benzoic acid (GSCA)

Gibco-BRL (Burlington, ON):- DMEM media, F12K, Fetal bovine serum, Antibiotic antimycotic, Heparin, Endothelial Cell Growth Factor, Trypsin/EDTA, Trypan Blue

Panvera (Madison, WI):- Protein disulfide isomerase

American Type Cell Culture (Manassas, VA):- Hamster Lung fibroblast (CCL-93), HUVECs(HUVEC-CRL 1730)

Sarsdedt (Newton, NC):- 75cm^2 Cell culture flask, 35mm^2 petri dishes 25mm syringes and filters (0.2μm), 10mL pipettes

1.2.2 Equipment

Centrifuge - Hettich Zentrifugen EBA 12, Rose Scientific, (Mississauga, ON)

UV/Vis Spectrometer - Agilent 8453, Agilent Technologies, (Mississauga, ON)

pH Meter -Orion 420A, Orion Research Inc. (Boston, MA)

Microcentrifuge tube centrifuge - Eppendorf Mixer 5423, VWR Scientific (Mississauga, ON)

Ultrasonicator – Transonic T420, Mandel Scientific (Toronto, ON)

Lyophilizer - Labconco Model 4451F, Labequip Limited (Markham, ON)

Weigh balance - Mettler AJ100, Mettler Instrumetn Corp. (Hightstown, NJ)

Brightline Hemocytometer, Reichter-Jung, Hausser Scientific (Horsham, PA)

Stirrer – Stirrer 360, VWR Scientific (Mississauga, ON)

BioRad HPLC System (Hercules, CA)

BioRad Econo System (Hercules, CA)

Binomic Controller BC 100(20/20 Technology Inc)

Zeiss Axiovert 200 microscope, Empix (Mississauga, ON)

Laminar Flow Hood, Nuare (Plymouth, MN)

Nuare Autoflow 5% CO2 regulated Incubator (Plymouth, MN)

1.3 Methods

1.3.1 Synthesis of GSNO: Glutathione is dissolved in ice cold 0.5M HCl. Equimolar sodium nitrite is added and the reaction was carried out in the dark at 4°C for 40min. The reaction mixture was adjusted to pH 7.0, and crystallized by the slow addition of cold acetone. Similar protocol was used in the synthesis of BSANO.

1.3.2 Synthesis of Aprotinin:- Aprotinin (0.95mg) was reacted with Dansyl chloride (10mg in 1mL of acetonitrile) for 24 h in $LiCO_3$ buffer (pH 9.5). The product was purified on a Sephadex G-25 column. Fluorescence of dansylated aprotinin was determined using a Shimadzu RF 551 fluorometer and the concentration was standardized with dansyl chloride absorbance at 320nm (ε=3,980$M^{-1}cm^{-1}$). GSNO (83μM) was added to the dansylated aprotinin. The resulting product was separated on the Sephadex G25 column. The fluorescence of the separated dansyl aprotinin was obtained with respect to its absorbance at 320nm.

1.3.3 Synthesis of N-Dansyl-S-nitrosohomocysteine: S-nitrosohomocysteine (HCysNO) was prepared by treating homocysteine (HCys) with acidified nitrite. Dansylation was carried out in 0.1M phosphate buffer (pH 8.5) at stoichiometric amounts. The product was purified on a G-10 Sephadex column.

1.3.4 Synthesis of N,N-Didansylhomocystine: Homocystine was dissolved in water (80 mL) and saturated $NaHCO_3$ (25mL). Once the solution was clear 30mL of acetone was

added. Dansyl chloride (1.608g/80mL of acetone) was then added drop wise over a 5h period. The acetone was removed under reduced pressure and the aqueous solution was acidified to pH 2-3 with 4M HCl. The solution was extracted with ethyl acetate and washed with water; dried over Na_2SO_4 and evaporated to dryness. The residue was subject to chromatography on a silica gel column using the following solvent system: 1- methylene chloride; 2- 50% methyl chloride/ethyl acetate; 3- 80% methylene chloride/ 20% methanol. The purity of the product was confirmed using NMR.

1.3.5 Detection of free thiols in S-nitrosothiol stock:- To determine contamination of S-nitrosothiol sample by free thiols, 100μM s-nitrosothiol sample was incubated with 1mM DTNB. Absorbance at 412nm (ε 13 600 $M^{-1}cm^{-1}$) was used to determine the concentration. Two controls necessary to obtain accurate readings, first is the absorbance of 100μM S-nitrosothiols at 412nm and the second is the residual absorbance of DTNB at 412nm. Less than 0.5% contamination of free thiols was considered acceptable.

1.3.6 NO solution:- NO solution was prepared in PBS (200mM, pH 7.4) in 20mL vials sealed with septa seal and parafilm. The vial and buffer were degassed by purging solution with nitrogen for 1hr. NO gas was passed through 10% KOH before passing through the buffer. The KOH acts as a scrubber to remove other oxides of NO. Concentration of NO in solution was found to be ~1-1.5mM.

1.3.7 Fluorescence of N-dansyl-S-nitrosohomocysteine:- Initial fluorescence of DnsHCysNO was obtained using a HPLC Shimadzu fluorometer. The DnsHCys sample was exposed to 350nm light for 30mins prior to obtaining photolysed spectra.

1.3.8 Time dependant increase in Fluorescence:- DnsHCysNO was exposed to excitation light (λ_{Ex} 350nm), and the increase in fluorescence (λ_{Em} 520nm) was monitored by data acquisition software, Duo 18.

1.3.9 Photolytic Release of NO:- An NO selective electrode, ISO NOII, was placed in a fluorescence cuvette containing DnsHCysNO. Fluorescence upon exciting at 350nm was monitored by the Shimadzu fluorometer. Simultaneous changes in NO levels were monitored using the NO electrode. Both measurements were obtained by the data acquisition system, Duo 18.

1.3.10 Transnitrosation (Soln Studies):- DnsHCysNO (36μM) was exposed to varying concentrations of GSH(0-4μM). Change in fluorescence was monitored by a Shimadzu fluorometer. Equal volumes were added in varying concentrations to avoid dilution effects.

1.3.11 Reverse Nitrosation (Soln Studies):- DnsHCys(100μM) was exposed to 350nm light to allow photolytic degradation to DnsHCys. The saturable fluorescence of DnsHCys was exposed to varying concentrations of GSNO (0-18μM). Additionally, dynamic transnitrosation reactions were monitored by adding 100μM GSNO to

photolysed to DnsHCys. The resulting change in fluorescence was monitored using Shimadzu fluorometer and Duo 18.

1.3.12 HPLC analysis of Cell Lysate: The DnsHCys and its derivatives were chromatographed on a C18 reverse phase column attached onto a Bio-Logic HPLC with a Shimadzu RF 551 fluorescence detector. The solvents employed were 0.1% trifluoroacetic acid and 60% acetonitrile with 0.1% trifluoroacetic acid. The S-carboxymethyl-DnsHCys standards were prepared by reducing $DnsHCys_2$, (200μM) with 1mM dithiothreitol and reacting the mixture with 10 mM iodoacetate for 30 min (0.1 M Tris-HCl, pH 8.5). Appropriate amounts of this mixture were injected into the HPLC to obtain a standard curve. Hamster lung fibroblasts ($1x10^6$ cells) were incubated in 200μM $DnsHCys_2$ for 2 min. The cells were lysed by ultrasonication in buffer (0.1 M Tris-HCl, pH 8.5) containing 20mM iodoacetate. The cell lysate was filtered using a 0.45 μm syringe filter prior to HPLC analysis. Concentration of the lysate was interpolated from a standard curve and the intracellular concentration was determined based on the assumption the average cell volume is ~1pL.

1.3.13 Protein Disulphide Isomerase Assay: PDI activity was determined by using DnsHCysNO as substrate. PDI inhibition studies were performed in triplicates with PDI (0.25μM) and DnsHCysNO (0.5 μM -20 μM) co-incubated with BSANO (0.1 μM, 1μM, 10μM). The reaction was performed in PBS supplemented with 50μM GSH and the data were obtained over 60secs at 100msec interval via a Cary Eclipse fluorometer.

1.3.14 ***α-tocopherol treatment:-*** Cell media enriched with 10μM α-tocopherol was added to cells. Cells were incubated for 17h prior to fluorescence studies.

1.3.15 ***Cell Culture:*** Chinese hamster lung fibroblasts were cultured in Dulbecco's modified Eagle's medium supplemented with 4mM glutamine, 1.5g/L sodium bicarbonate, 4.5g/L glucose, 1.0mM sodium pyruvate, and 10% fetal bovine serum. Cells were grown to confluence on slides at 37°C with 10% atmospheric CO_2. Human umbilical vein endothelial cells were grown in Gibco's Ham F12K with 2mM L-glutamine, 1.5g/L sodium carbonate, 100ug/mL heparin , 50μg of endothelial cell growth supplement and 10% fetal bovine serum. The HUVECs were grown to confluence on slides at 37°C with 10% atmospheric CO_2. HT1080 cells were grown in Dulbecco's modified Eagle's medium supplemented with 4mM glutamine, 1.5g/L sodium bicarbonate, 4.5g/L glucose, 1.0mM sodium pyruvate, 600ug/mL G14 and 10% fetal bovine serum. Cells were grown to confluence on slides at 37°C with 10% atmospheric CO_2.

1.3.16 ***Subculturing:-*** Cells grown to confluence were trypsinized to detach cells by using 0.25% trypsin, 0.03% EDTA for 5-10mins at 37°C. The cells were washed with media and resuspended in freezing media, 95% culture media and 5% DMSO. The cell density must be ensured to be above 1 x 10^6/mL. The sample was aliquoted into 1mL freezing vials and stored at –80°C.

1.3.17 csPDI Inhibition studies: For PDI inhibition studies, hamster lung fibroblasts and HUVECs were incubated with 3mM bacitracin for 4h prior to the fluorescence microscopy experiments. Effects of DTNB on hamster lung fibroblast and HUVECs were carried out in the presence of 100μM DTNB for 30min prior to fluorescence studies. GSAO (100μM) incubation was carried out similar to DTNB with 30min incubations prior to transport studies. Additionally a control used for GSAO was GSCA, where the active arsenic group was replaced with carboxylic acid.

1.3.18 Fluorescence Microscopy: Cells were incubated in PBS containing 0.2 mM $DnsHCys_2$ for 2 min. The incubation was followed by 4 x 30 sec washes with PBS. The fluorescent cells were incubated in 1mL of PBS; cell images were acquired at 0.5sec intervals for 60sec upon the addition of 100μL of varying GSNO concentrations (1.0mM to 10μM). The ambient temperature was maintained at 37°C by Binomic Controller BC 100 (20/20 Technology Inc.). Cell images were captured upon the addition of GSNO using a real time image acquisition system (Northern Eclipse 6.0). The change in fluorescence intensity was determined by computer assisted image analysis (Northern Eclipse 6.0). Fluorescence of cells was observed via a Zeiss Axiovert 200 microscope by phase and fluorescence microscopy using a 40x fluor objective. Similar protocol was used to observe BSA-NO (200μM - 1μM) uptake in hamster lung fibroblast and HUVECs.

1.3.19 Trypan Blue Exclusion Assay:- Cells were scraped and diluted with equal volume of Trypan blue dye. 10μL of sample was loaded on to a hematocytometer. If the cell number in the center square was >50, the cell count at that location was obtained as an average of all four corners as well as the center. If the center was <50 cells, then all four corners were counted in addition to the center square and averaged. The number was multiplied by volume of square (1mm x 1mm x 0.1mm =1x 10^{-4}mL and multiplied by dilution factor (x2) to give number of cells/mL.

1.4 Results

1.4.1 Development of S-Nitrosothiol Probe

1.4.1.1 ***Fluorescence of DnsHCysNO:-*** Freshly synthesized DnsHCysNO (Fig 1) exhibited very low fluorescence. In fact, the fluorescence of this compound could not be detected visually using a hand held UV lamp. It is conceivable that the observed fluorescence quenching could result from a short range energy transfer of the dansyl group (λ_{Ex} 320, λ_{Em} 520nm) to the 543nm (ε_M= $18M^{-1}cm^{-1}$) forbidden n to π^* absorption of the S-NO moiety. In order to test this, a sample of DnsHCysNO was exposed to light in order to induce photolytic denitrosation. As can be observed in Fig 2, the fluorescence of the sample gradually increased and reached a maximum in 30mins. The maximum intensity was ~8 fold larger than the sample kept in the dark. Following the same parameters, the sample was excited at 350nm and its fluorescence at 520nm was monitored dynamically. There was an increase in fluorescence upon exposure to light over ~7min period (Fig 3).

1.4.1.2 ***Role of NO:-*** This hypothesis was further strengthened by molecular modeling studies (simulated annealing Triposyl Sybyl), Fig 4, which revealed several minimum energy structures where the S-NO is 3.5 to 4.2A° from the dansyl ring. Over a 10fs period, the minima was observed ~5 times. The close proximity and the frequency at which it is achieved provide ideal energy transfer conditions. Therefore, removal of the NO moiety from DnsHCysNO should result in fluorescent enhancement as observed

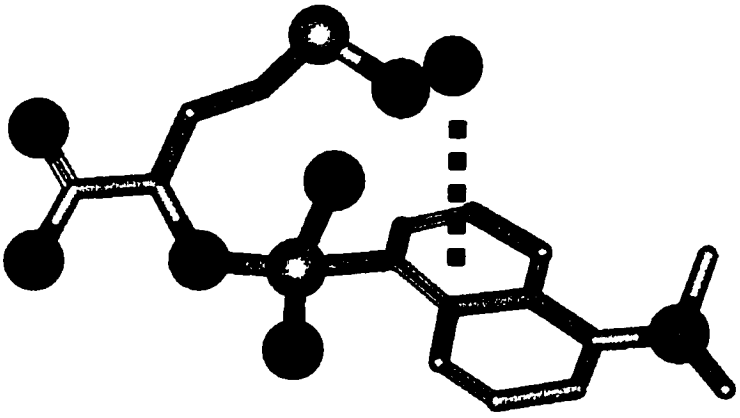

Fig 1.4.1:- Structure of N-Dansyl-S-Nitrosohomocysteine. The structure was obtained using Triposyl Alchemy. This conformation was chosen to illustrate the close proximity of the Dansyl moiety to that of SNO. The distance was determined to be ~4A°.

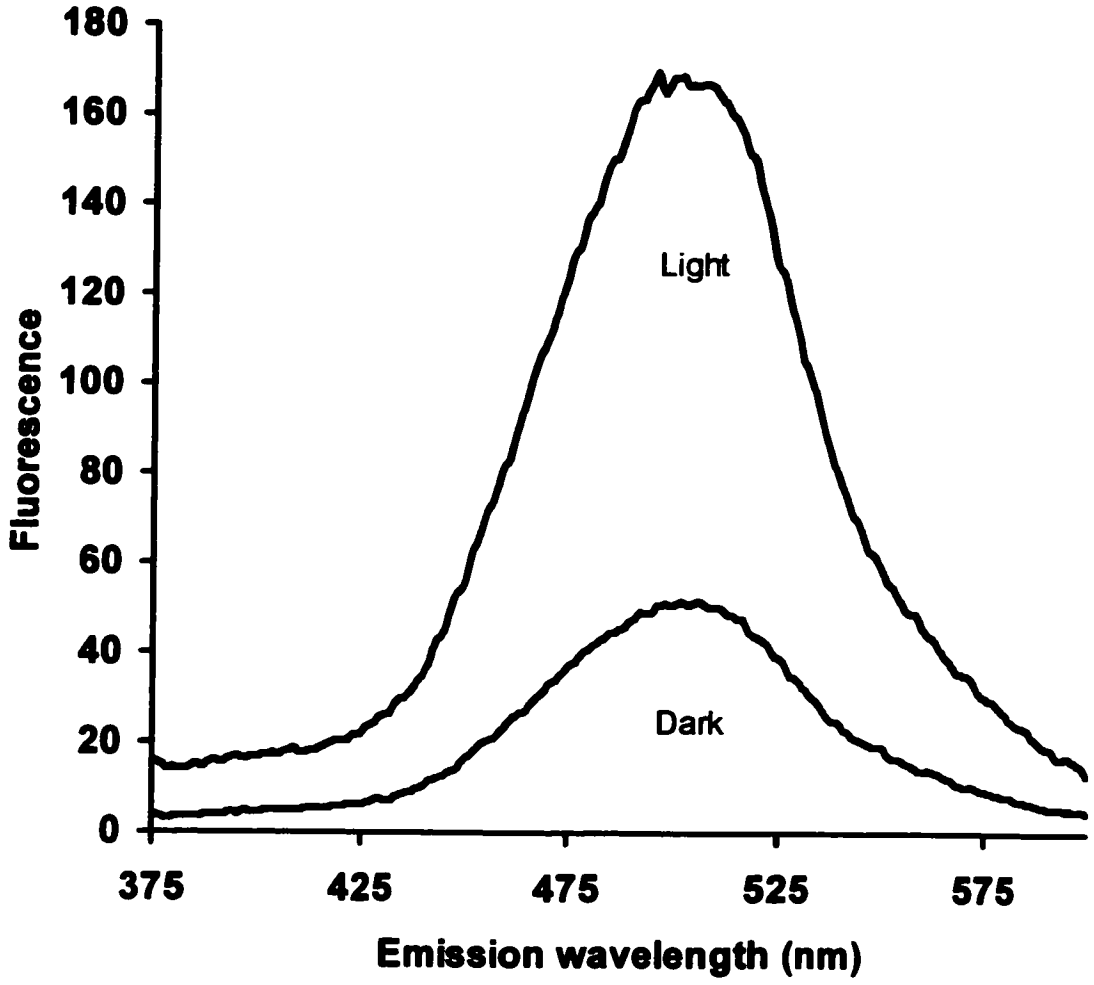

Fig 1.4.2:- DnsHCysNO (100μM) exposed to light or kept in the dark for 30 minutes at room temperature. Fluorescent samples were excited at 350nm using a Shimadzu RF 551 Fluorescence monitor with Duo.18 (WPI) data acquisition.

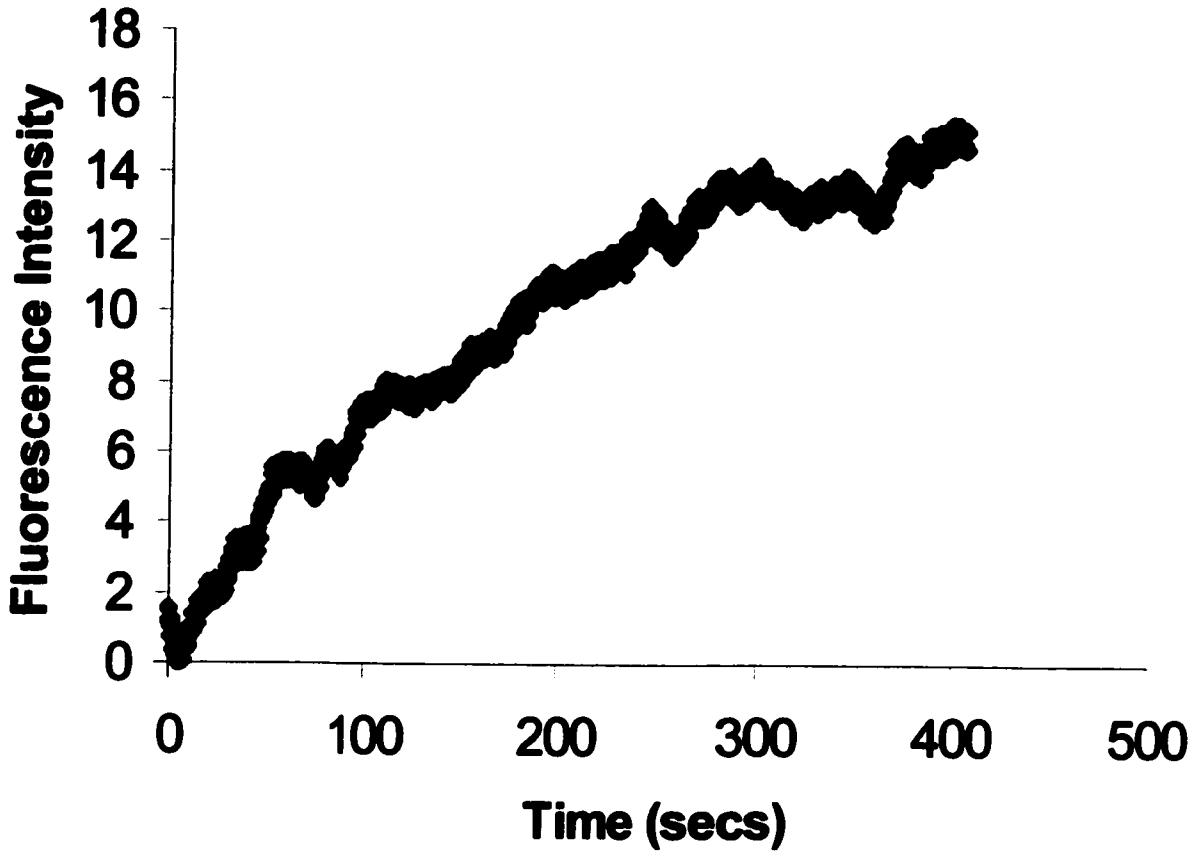

Fig 1.4.3:- Increase in DnsHCysNO fluorescence upon exposure to 350nm light. Increase in fluorescence was monitored using a Shimadzu fluorometer and data acquisition system Duo 18, over ~7min

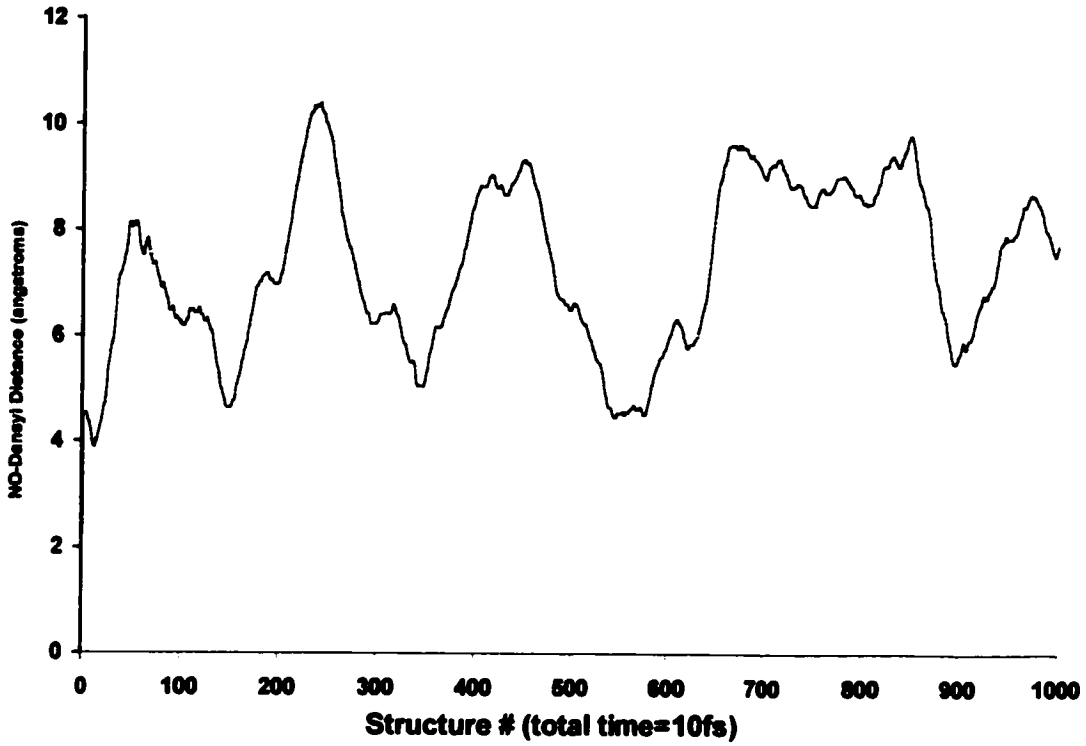

Fig 1.4.4 :- Molecular modeling of DnsHCysNO using Triposyl Alchemy. The conformational changes undergone by DnsHCysNO was simulated under increasing temperature (°C). During the tumbling motion the distance between NO and Dansyl moiety were monitored over a 10fs period.

earlier. In order to show the increase in fluorescence was due to NO loss, [NO] and the fluorescence were measured simultaneously during the photolysis experiment. As predicted NO release paralleled the fluorescence increase over a 50 min period, Fig 5.

1.4.1.3 Effects of NO on Dansyl:- Another question pertained to whether the observed quenching was reversible or due to the chemical modification of the dansyl ring in the energy transfer process. This was tested by dansylating the protein, aprotitin (molecular weight 6.5K) that contains 5 Lys residues. When excess GSNO (83 μM) was added to dansyl-aprotinin (0.7 μM) the fluorescence (Fig 6 circles) was quenched by ~38% (Fig 6 squares). The dansyl-aprotinin was separated from the GSNO by chromatography on Sephadex G-25. Upon removal of the GSNO, the dansyl-aprotinin fluorescence was restored to ~90% (Fig 6 triangles) of the original suggesting that the dansyl moiety is not chemically altered during the quenching.

1.4.1.4 Thiol probe:- Realizing the NO moiety does not modify the dansyl ring, then the removal of NO by thiols, transnitrosation reactions, should also cause an increase in fluorescence. DnsHCysNO (36μM) was exposed to increasing concentrations of GSH (0-3.5μM). GSH was increased incrementally by 3μM. The fluorescence intensity increased with increasing GSH concentrations in a saturable manner, Fig 7. This supports our notion that DnsHCysNO can undergo transnitrosation reactions with free thiols. If DnsHCysNO can be denitrosated to yield to highly fluorescent compound then it is equally feasible to expect nitrosation of DnsHCys to quench the fluorescence. A solution of DnsHCysNO (100μM) was photolysed to ensure maximum fluorescence, at

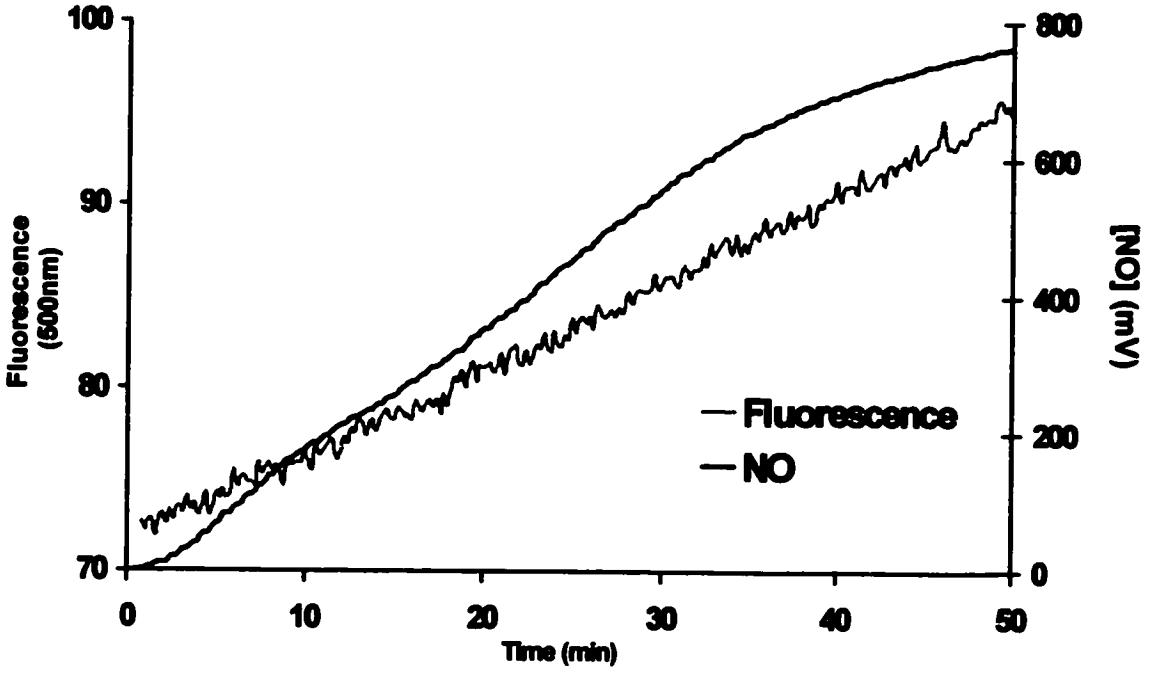

Fig 1.4.5:- Monitoring of $[NO]_{aq}$ and fluorescence during the exposure of DnsHCysNO to 350nm light. NO measurements were made using an ISO-NO Mark II NO electrode with Duo.18 (WPI) data acquisition. Fluorescence measurements were made on a Shimadzu RF 551 Fluorescence HPLC monitor with Duo.18 (WPI) data acquisition.

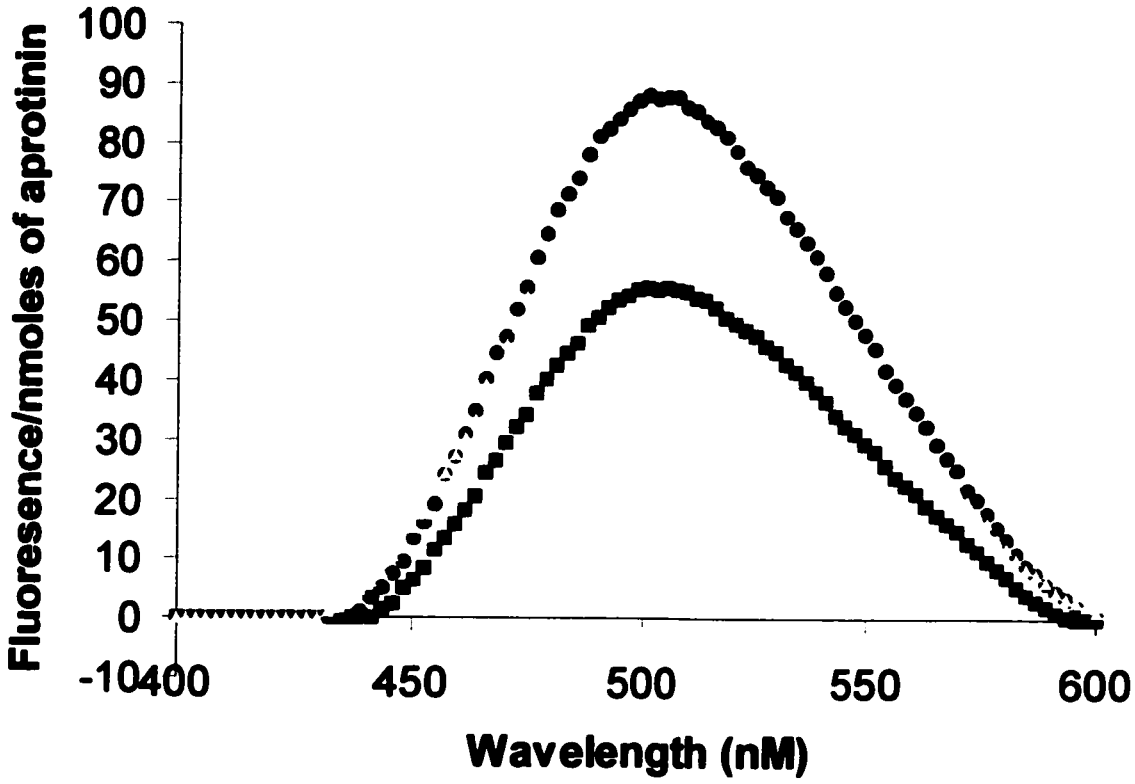

Fig 1.4.6:- (A) Fluorescence of Dansylated Aprotinin (Circles). (B) Fluorescence of Dansyl Aprotinin in the presence of 200μM GSNO (Triangles). (C) Fluorescence of Dansyl aprotinin after separation of dansyl aprotinin-GSNO complex on a sephadex G-25 column (Diamonds). The compounds were excited at 320nm and the emission spectra was obtained from 400-600nm. Emission spectra were standardized against dansyl aprotinin concentration.

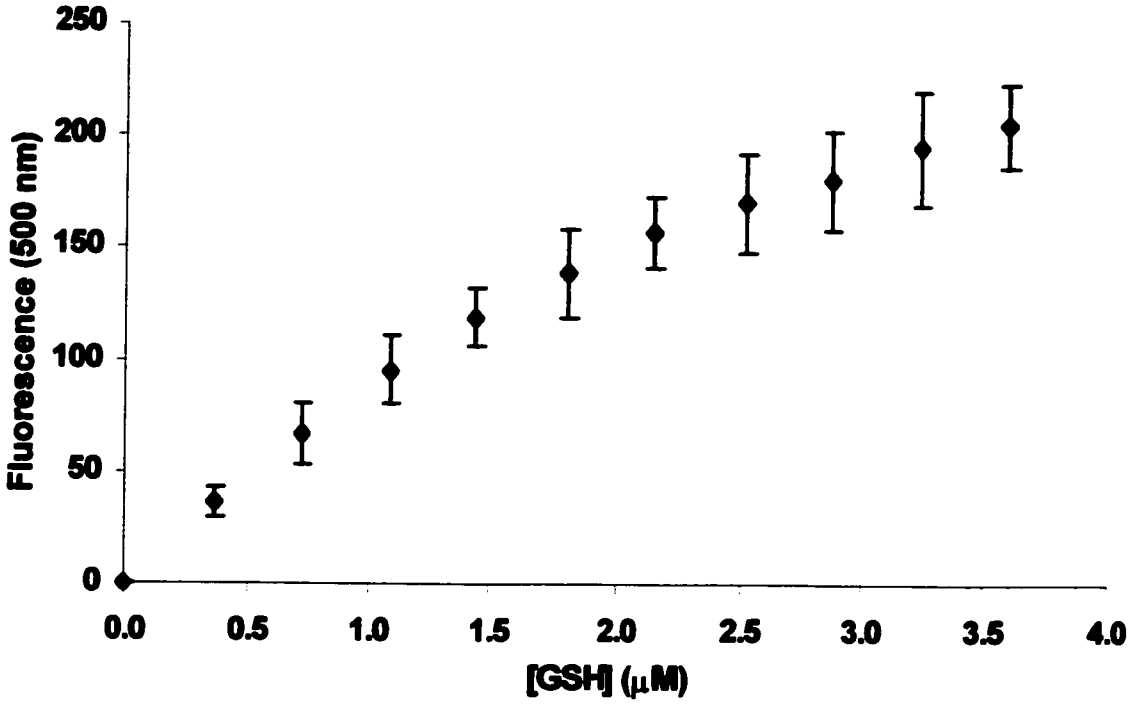

Fig 1.4.7:-Results of transnitrosation between DnsHCysNO (36μM) and GSH. Fluorescent measurements were made using a Shimadzu RF 551 fluorescence HPLC monitor. Error bars represent standard deviation (n=6).

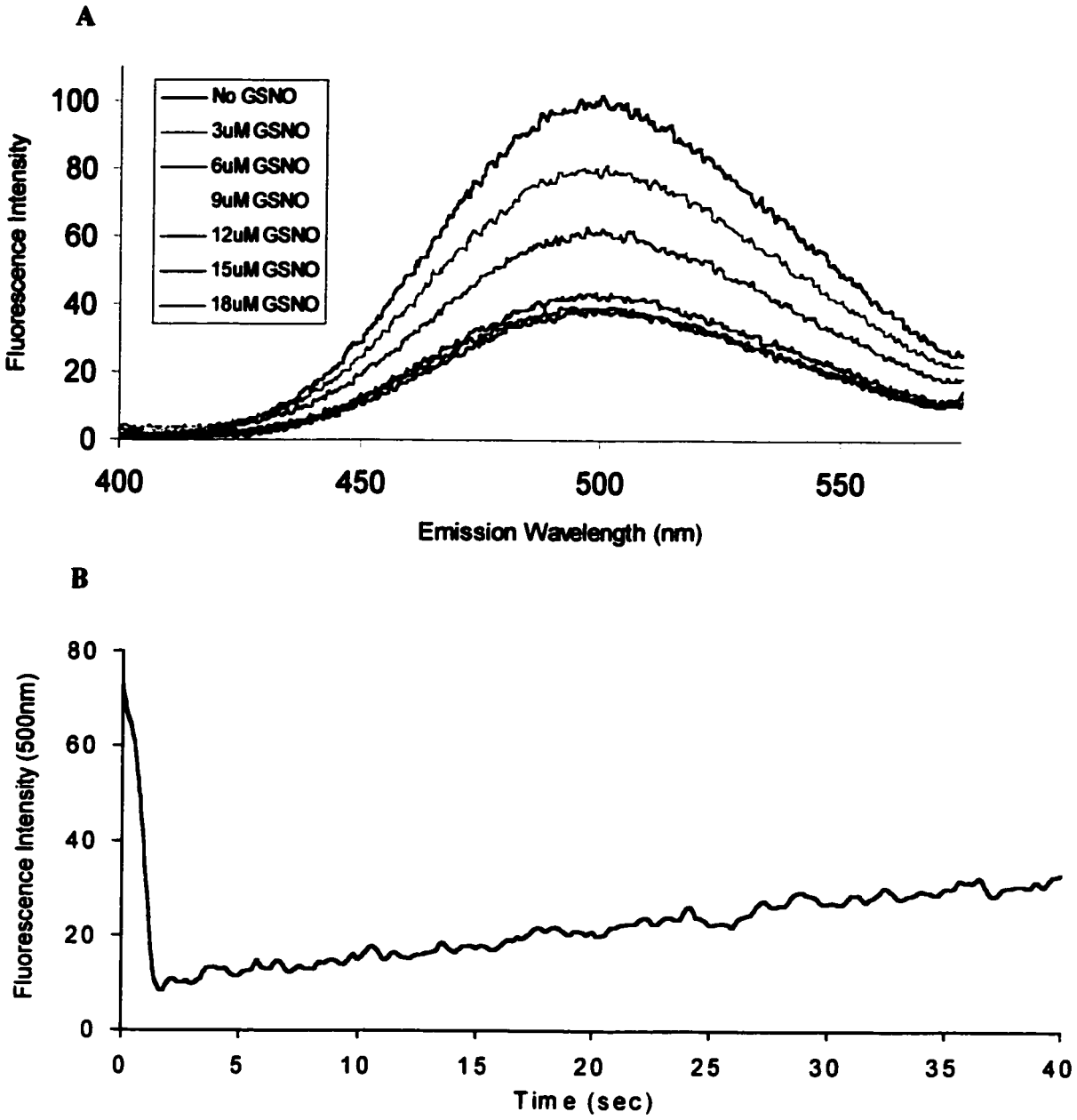

Fig 1.4.8:- (A) Results of reverse nitrosation between DnsHCys and GSNO. GSNO was added to achieve an equal increase in concentration upon each addition. (B) GSNO (100μM) added to a solution of DnsHCysNO (100 μM) that had previously photolysed to remove NO. Fluorescence measurements were taken using a Shimadzu RF 551 Fluorescence HPLC monitor with Duo.18 (WPI) data acquisition.

which point increments of GSNO (0-18μM) were introduced into the solution. The sample was excited at 320nm and the emission spectra, 400-600nm, was obtained with maximum emission at ~500nm, Fig 8A. The decrease in fluorescence occurred in a GSNO concentration dependant manner. Furthermore, the quenching was found to be saturable. DnsHCys is then capable of undergoing nitrosation by GSNO. Fig 8B, provides evidence relating to the rate of nitrosation. The same photolysed sample of DnsHCysNO (100μM), DnsHCys, was exposed to GSNO (100μM) and the change in emission at 500nm was monitored with respect to time. Addition of GSNO resulted in dramatic decrease in fluorescence over a few seconds, following a transient increase in fluorescence over the next ~40sec was observed. The sudden decline in fluorescence is attributed to nitrosation of DnsHCys as noted above. The subsequent increase in fluorescence is attributed to either photolysis by the excitation light or denitrosation by neighbouring free thiols.

1.4.2 Role of Cell Surface Protein Disulfide Isomerase in RSNO uptake

1.4.2.1 Solution studies with DnsHCys$_2$:- In the above study, we have shown that the S-nitrosation of DnsHCys resulted in ~90 % quenching of the dansyl fluorescence. In search of a more stable probe that can utilize this system yet can transverse the cell membrane with ease, we developed N,N-didansylhomocystine (Fig 9). In converse to its counter part, this compound is highly fluorescent. We hypothesized that this compound will be internalized due to its non-polar nature and subsequently be reduced to DnsHCys which may readily undergo nitrosation by S-nitrosothiols. In an attempt to mimic cellular

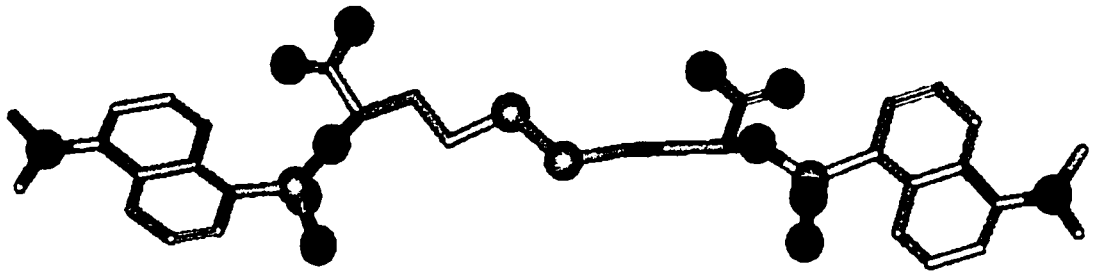

Fig 1.4.9:- Structure of N,N-Didansyl-S-Nitrosohomocystine. The structure was obtained using Triposyl Alchemy.

conditions, $DnsHCys_2$ (10μM) was incubated with excess GSH (100μM) prior to adding increasing concentrations of GSNO, Fig 10. As $DnsHCys_2$ was reduced by the thiol pool, it then was susceptible to nitrosation and in effect decrease fluorescence.

1.4.2.2 HPLC analysis:- Intracellular GSH concentrations are in the 1-10mM range (Till *et al.*, 1998). Therefore, the first question was, whether this is sufficient reducing potential for the amount of $DnsHCys_2$ accumulated intracellularly upon incubation of the cells with this compound. In order to test this, fibroblasts ($0.5x10^6$ cells) were incubated with 200μM of $DnsHCys_2$ for 2min. The cells were washed and lysed in the presence of 1 μM iodoacetic acid (IA). In this manner all the reduced thiols would be alkylated thus preventing their re-oxidation. The cell extracts were centrifuged and chromatographed on an HPLC with a fluorescence detector, Fig 11. Authentic $DnsHCys_2$ and *N*-dansyl-*S*-carboxymethylhomocysteine (DnsCMHCys) had retention times under the conditions employed of 17.8min and 28.9min respectively. The cell extract had one major fluorescent peak corresponding to the retention time of DnsCMHCys indicating that there is sufficient intracellular GSH to reduce the accumulated $DnsHCys_2$. In addition, the peak area of DnsCMHCys corresponded to ~ 50 pmol/10^6cell. If it is assumed that the volume of a fibroblast is ~1 pL, ~50 μM of DnsHCys must have accumulated in the cells after 2 min (Freshney, 2000).

1.4.2.3 BSA-NO uptake:- The transport of S-nitrosothiols has been speculated upon but has been difficult to study due to lack of S-nitrosothiol assays. We attempted to use our

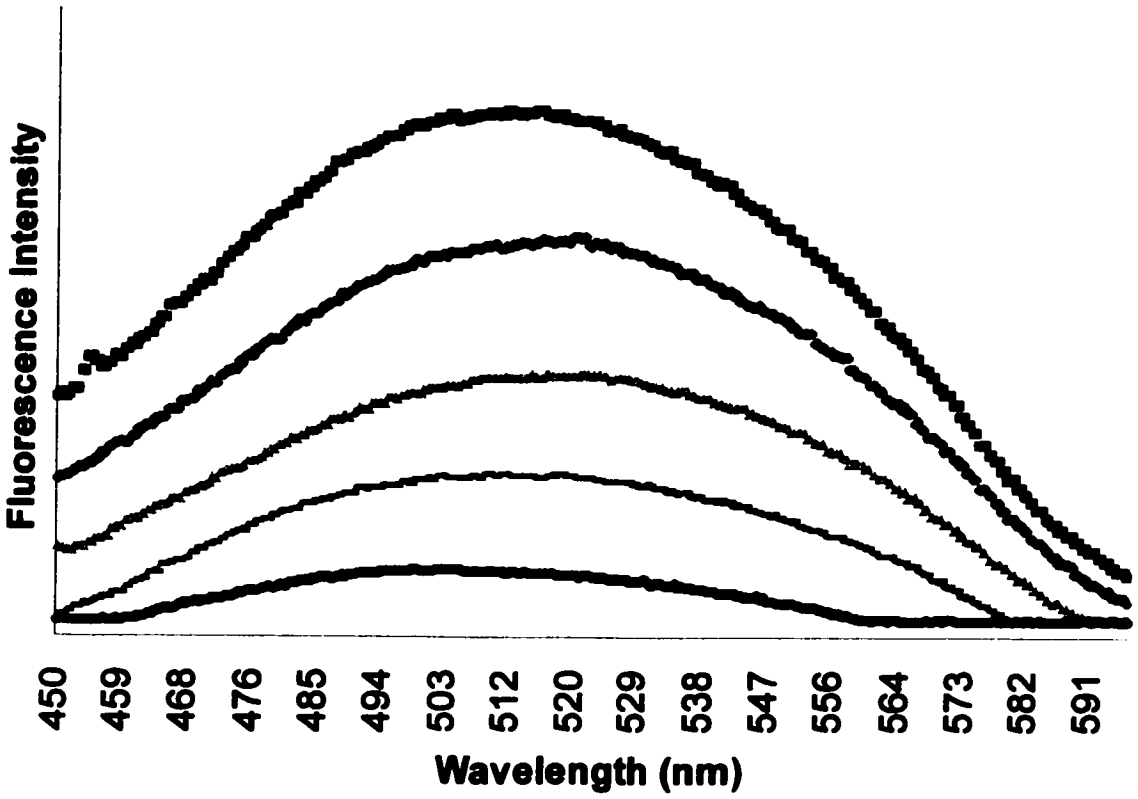

Fig 1.4.10:- Nitrosation of reduced $DnsHCys_2$ by GSNO. $DnsHCys_2$ (1μM) was reduced in the presence of 10-fold excess GSH (10μM). GSNO (Control, blue square; 10μM, red diamond; 25μM, orange triangle; 50μM, green dash; 100μM, purple circle) was added in increasing concentrations. Decrease in fluorescence was monitored using Shimadzu fluorometer.

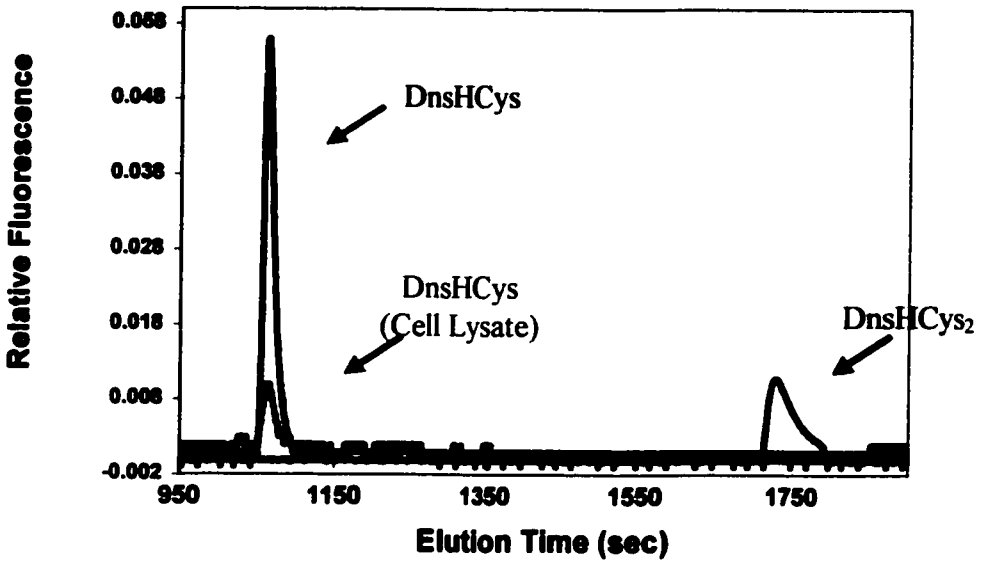

Fig 1.4.11:- Elution of Reduced and oxidized DnsHCys. HUVECs were washed and lysed in the presence of 200mM iodoacetic acid (IA). In this manner all the reduced thiols would be alkylated thus preventing their re-oxidation. The cell extracts were centrifuged and chromatographed on an HPLC with a fluorescence detector. Authentic $DnsHCys_2$ and *N*-dansyl-*S*-carboxymethylhomocysteine (DnsCMHCys) were also eluted as standards.

fluorescent compound to detect S-nitrosothiol influx. Using a low molecular weight S-nitrosothiol, GSNO, we were able to successfully observe quenching of intracellular DnsHCys. Transport of GSNO may occur through various amino acid transporters and may not provide insight into the involvement of membrane associated factors that affect RSNO transport as speculated by Zai *et al.*, (1999), and Marks *et al.*, (1995). A clear and concise method to observe effects of membrane phenomenon is to construct a membrane impermeable RSNO. BSA-NO was chosen, as a substrate for our assay since it lacks membrane transporter systems yet possesses physiological relevance. HUVECs preloaded with $DnsHCys_2$ were exposed to BSA-NO (200μM) and the change in fluorescence was monitored via fluorescence microscopy, Fig 12. Two observations were made in this study; firstly incubation with BSA-NO reduced the intracellular fluorescence suggesting an extracellular mechanism that aids the transport of BSA-NO bound NO. Secondly, the saturable uptake of BSA-NO occurred on a millisecond scale.

1.4.2.4 PDI Assay:- To date there are no direct assays for the RSNO denitrosation activity of PDI. In order to test whether DnsHCysNO could be used as a direct fluorogenic substrate for PDI, DnsHCysNO, 100μM was added to a stirred cuvette in a fluorometer. The slit widths were adjusted to yield minimal photolysis of the S-NO bond. Upon addition of 0.25μM PDI the fluorescence increased in a time dependent manner (Fig. 13). The increase in fluorescence in Fig 13 shows the initial, linear part of trace from which the initial rates were estimated. This arises from the conversion of the less-fluorescent DnsHCysNO to the fluorescent DnsHCys by the action of PDI.

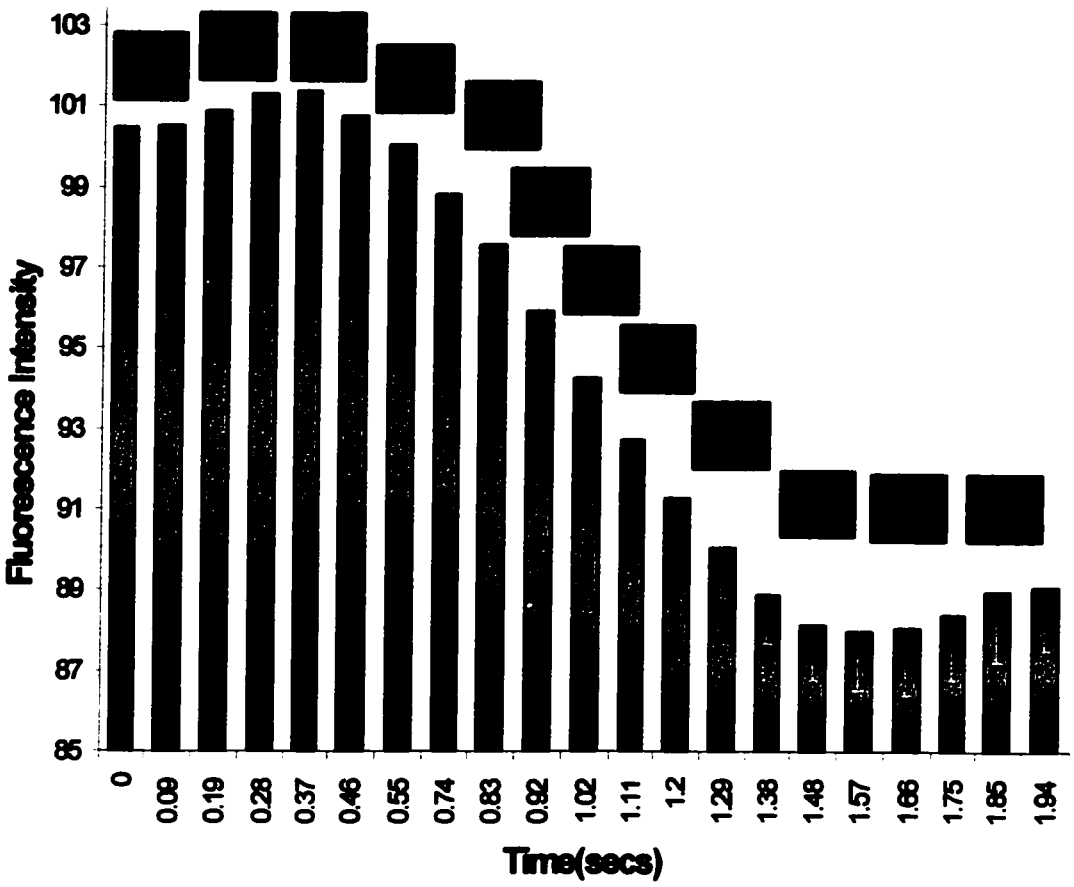

Fig 1.4.12:- Transport of BSA-NO bound NO in HUVECs. HUVECs, preloaded with DnsHCys$_2$, were exposed to 200μM BSA-NO. The quenching of the intracellular fluorescence was monitored over msec time period by data acquisition software, Northern Eclipse 6.0.

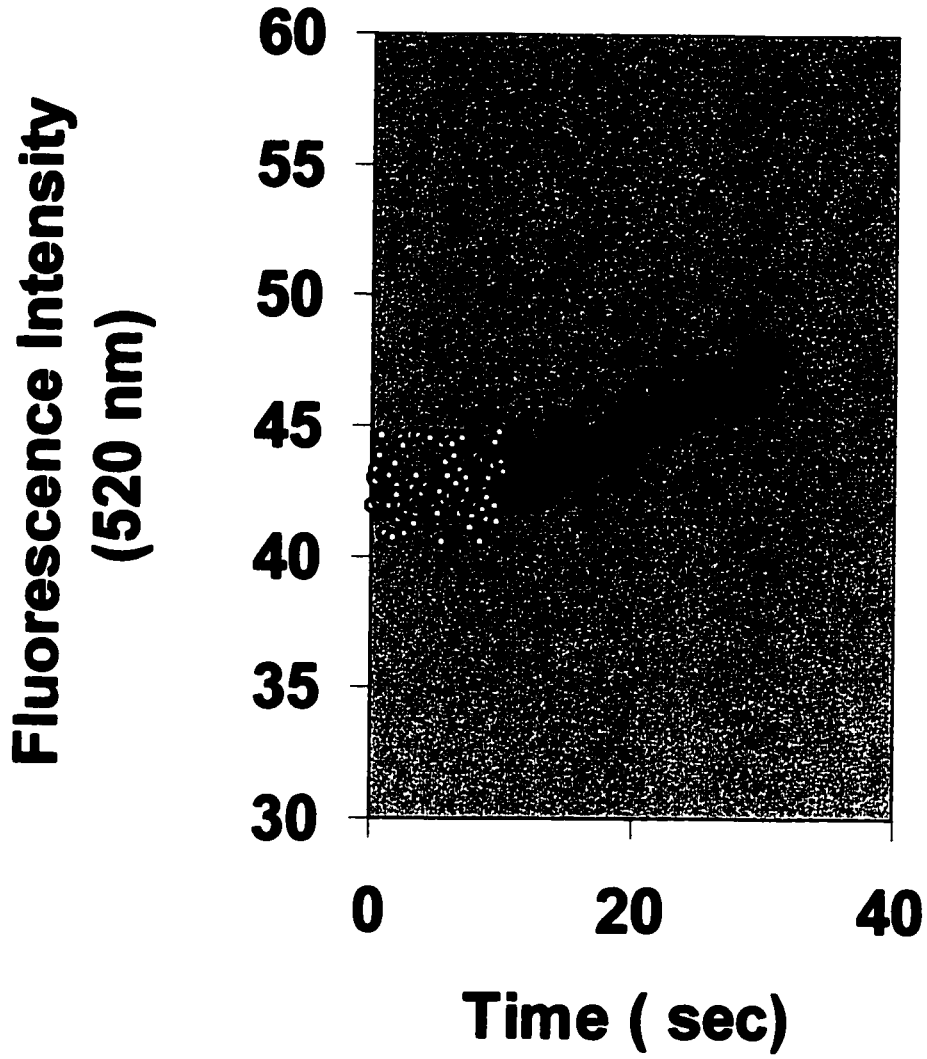

Fig 1.4.13:- Demonstration of PDI catalyzed DnsHCysNO fluorescence increase as a function of time. The fluorescence of 25 μM DnsHCysNO before (yellow circles) and after the addition of 0.25 μM PDI (green circles). The rate of fluorescence increase upon addition of PDI, 0.34 ± 0.02/sec, was significant in comparison to the blank rate, 0.02 ± 0.01/sec (n=4).

When these experiments were repeated with varying [DnsHCysNO], the initial rates of fluorescence increase were well accommodated by the Michaelis-Menten equation, yielding an apparent K_M for DnsHCysNO of ~2 ± 0.5 μM (Fig 14). In order to estimate the affinity of PDI for the physiologically relevant RSNO, Serum albumin-NO, the [DnsHCysNO] steady-state kinetics was performed in the presence of constant [BSA-NO]. As can be observed from Fig 14, BSA-NO was a potent competitive inhibitor of PDI-catalyzed DnsHCysNO denitrosation with an estimated K_I of 1 ± 0.7 μM.

1.4.2.5 Uptake of DnsHCys$_2$:- It is clear from the above studies that DnsHCysNO can be used to monitor PDI activity by the increase in the fluorescence signal. Therefore, if DnsHCys is placed in the cytosol, its fluorescence-quenching rate should represent the intracellular S-nitrosation flux. DnsHCys should compete with GSH as a nitrosation target and because of its hydrophobic dansyl moiety should have an advantage over GSH in the cytosol/membrane interface. To this end, the more hydrophobic, oxidized form of DnsHCys, $DnsHCys_2$ was prepared. It was observed that $DnsHCys_2$ rapidly accumulated in cells as the intracellular fluorescence reached a maximum within 2 min and remained constant for up to 20 min.

1.4.2.6 Rates for Nitrosation Reactions in Solutions:- The DnsHCys fluorescence-quench kinetics was then performed in solution and with fibroblasts. In the solution studies, the $DnsHCys_2$, 25 μM was reduced with GSH, 100 μM and was treated with either NO (aq), 200 μM or GSNO, 200 μM. Under these conditions, [DnsHCys] in solution would be close to the value (50 μM) estimated to be accumulated in cells from

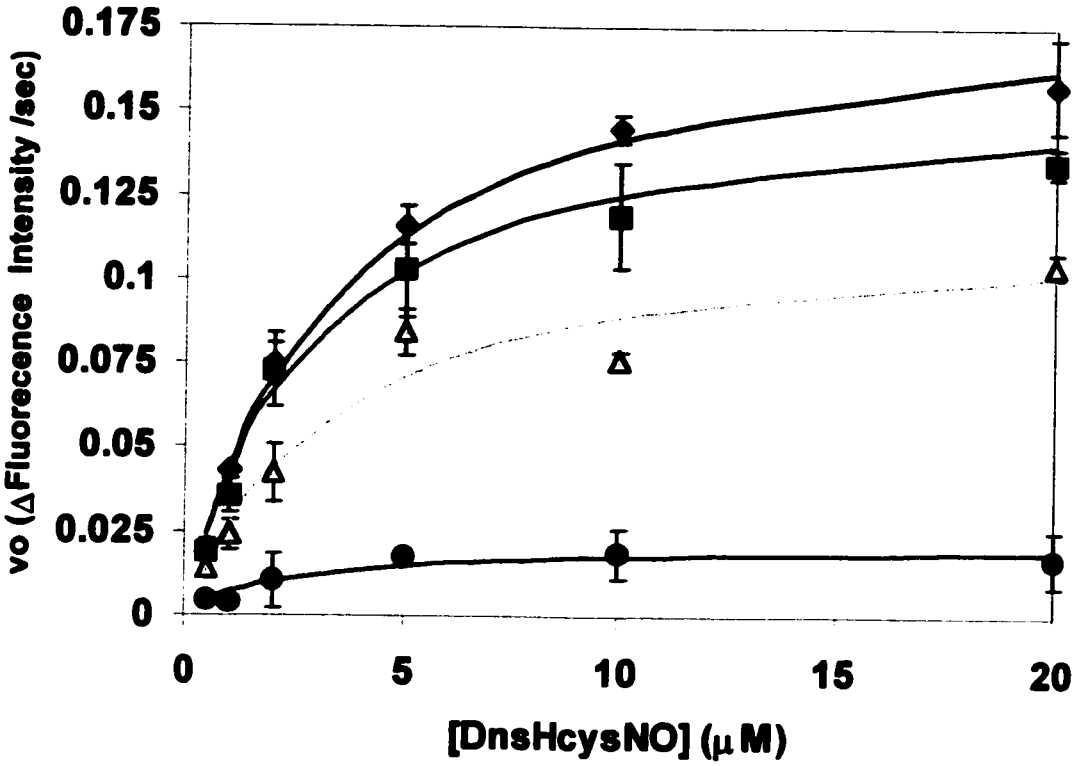

Fig 1.4.14:- Plots of the initial rates of fluorescence increase, as a function of DnsHCysNO concentration in the presence of 0.25 μM PDI: no inhibitor (diamonds); or in the presence of BSA-NO 0.1 μM (squares), 1.0 μM (triangles), 10 μM (circles) Error bars represent standard deviation (n=6). The solid line represents the best fit of the data to the Michaelis-Menten equation.

the HPLC studies. Under the present experimental conditions NO (aq) when exposed to oxygenated buffer is expected to be rapidly converted to N_2O_3, a very efficient nitrosating agent. As expected, the fluorescence of DnsHCys was quenched upon exposure to NO (aq) with k_{obs} of 1.21 ±0.067 sec^{-1} (Fig 15A). When GSNO was introduced to DnsHCys in solution the k_{obs} was 2.14 ±0.094 sec^{-1} (Fig 15B).

1.4.2.7 Rates for Nitrosation Reactions in Cells:- The quenching rates for intracellular DnsHCys by extra cellular RSNOs or NO were calculated from the change in the intracellular fluorescence intensity/μm^2 of images collected at 100 msec to 250 msec intervals. A sample, time-dependent image series, where GSNO, 200 μM was added to the culture media (at t=0), is presented in Fig. 3C. The k_{obs} for extracellular-NO (aq) (Fig 16A) and GSNO (Fig 16B) were 0.78 ± 0.022 sec^{-1} and 0.74 ± 0.078 sec^{-1} respectively. Although the k_{obs} were the same within experimental error, extracellular NO (N_2O_3) yielded nearly 80 % more intracellular nitrosation, in comparison to GSNO (~18 μM vs. 10 μM as determined from the degree of DnsHCys quenching).

In the solution studies, the k_{obs} for transnitrosation by GSNO was ~2-fold larger than that for S-nitrosation by NO (N_2O_3). The fact that the rate of quenching of intracellular DnsHCys occurred with the same rate with NO or with GSNO and that this rate was closer to that observed with NO in solution, suggests that the S-nitrosation of intracellular DnsHCys is mediated through N_2O_3 rather than by transnitrosation.

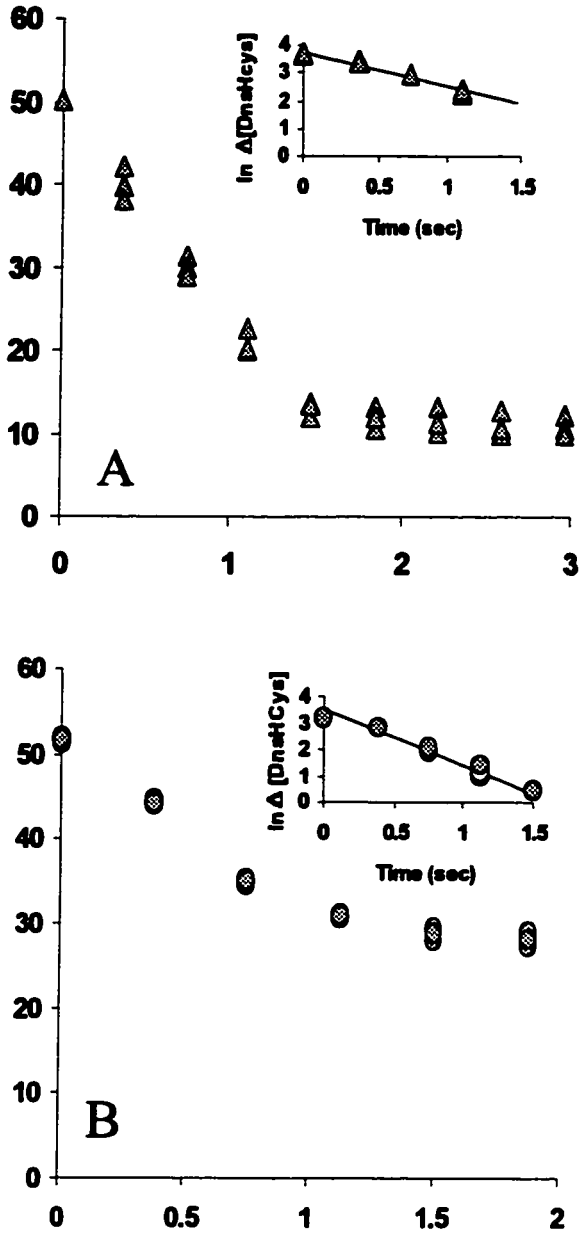

Fig 1.4.15:- DnsHCys fluorescence-quench kinetics. Fluorescence decrease was monitored as a function of time. Insets show the semi-ln plots from which the k_{obs} was estimated. The solid line represents the best fit of the data to a first order process (n=3).

A $DnsHCys_2$, 25 μM was reduced with GSH, 100 μM and was treated with $NO_{(aq)}$, 200 μM, (triangles) in a 3.0 mL stirred fluorescence cuvette (n=3).

B $DnsHCys_2$, 25 μM was reduced with GSH, 100 μM and was treated with $GSNO_{(aq)}$, 200 μM (circles), in a 3.0 mL stirred fluorescence cuvette (n=3).

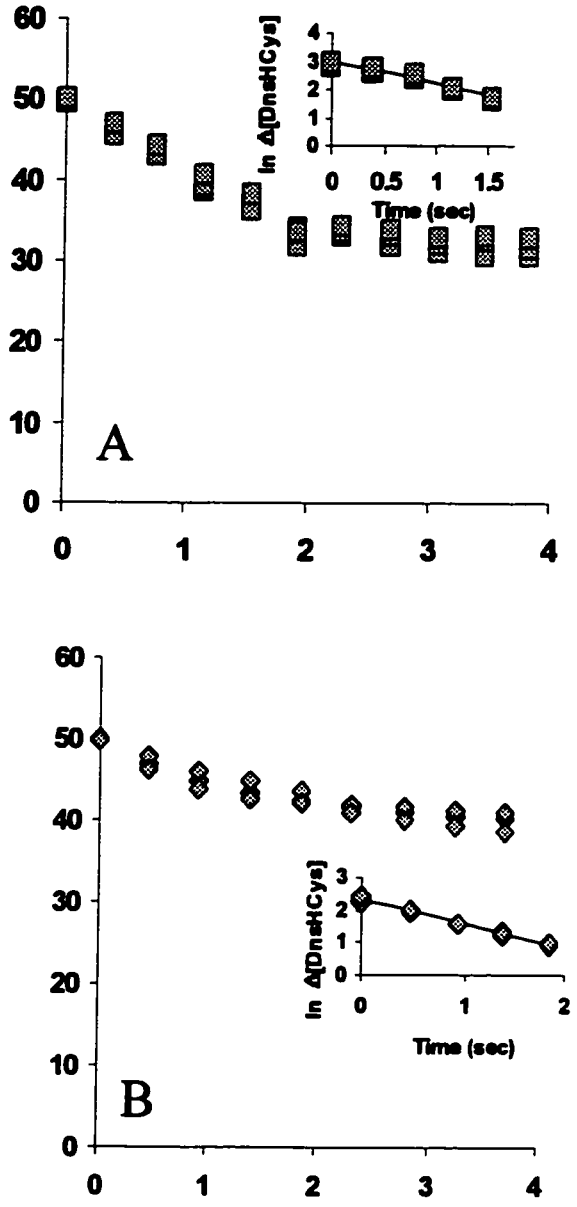

Fig 1.4.16:- DnsHCys fluorescence-quench kinetics. Fluorescence decrease was monitored as a function of time. Insets show the semi-ln plots from which the k_{obs} was estimated. The solid line represents the best fit of the data to a first order process (n=3).

A The quenching rates for intracellular DnsHCys by extra cellular $NO_{(aq)}$, 200 μM (squares) were extracted with the aid of Northern Exposure image processing software from the change in the intracellular fluorescence intensity/μm^2 of microscope images of cells grown on cover slips; collected at ~250 msec intervals (n=3).

B The quenching rates for intracellular DnsHCys by extra cellular GSNO, 200 μM (diamonds), were extracted with the aid of Northern Exposure image processing software from the change in the intracellular fluorescence intensity/μm^2 of microscope images of cells grown on cover slips; collected at ~250 msec intervals (n=3).

1.4.2.8 Expression of csPDI:- Up to this point it is clear that DnsHCys in the cytosol can be S-nitrosated by extracellular RSNO but is this process dependent on cell surface PDI? In order to obtain a clear answer to this question, these experiments were repeated with HT1080 fibrosarcoma cells in which PDI was either under expressed by antisense mediation, or over expressed. When compared to control H1080, the over-expression and antisense mediated under-expression of PDI resulted in 70 ± 20 % increase and 50 ± 25 % decrease, respectively, in the surface-bound dithiol form of PDI as determined by labeling with the biotin-linked maleimide, MPB which only reacts with free thiols. Jiang *et al.*, (2000) have established that under the conditions employed here, 2/3 of the free thiols of csPDI are oxidized thus underestimating csPDI levels by as much as 3-fold. This would appear to be the case as the total secreted PDI levels, as determined by Western blotting of the media indicated that over- or under-expression of PDI resulted in 3.7-fold increase and 47% decrease, respectively, in secretion of PDI as compared to controls.

1.4.2.9 BSA-NO transport in csPDI Over/Under expressed Cells:- These cells were preloaded with DnsHCys and BSA-NO, 200μM, was introduced to the medium. In the cells in which the enzyme was under expressed there was a small amount of intracellular fluorescence quenching (~15% of control) (Fig 17, triangles). On the other hand in cells where the PDI was over-expressed (Fig 17, circles), the total intracellular fluorescence quenching was ~3-fold larger than those of controls (Fig 17, squares). These experiments clearly demonstrate the requirement for csPDI in the transfer of NO from extracellular RSNOs to those in the cytosol.

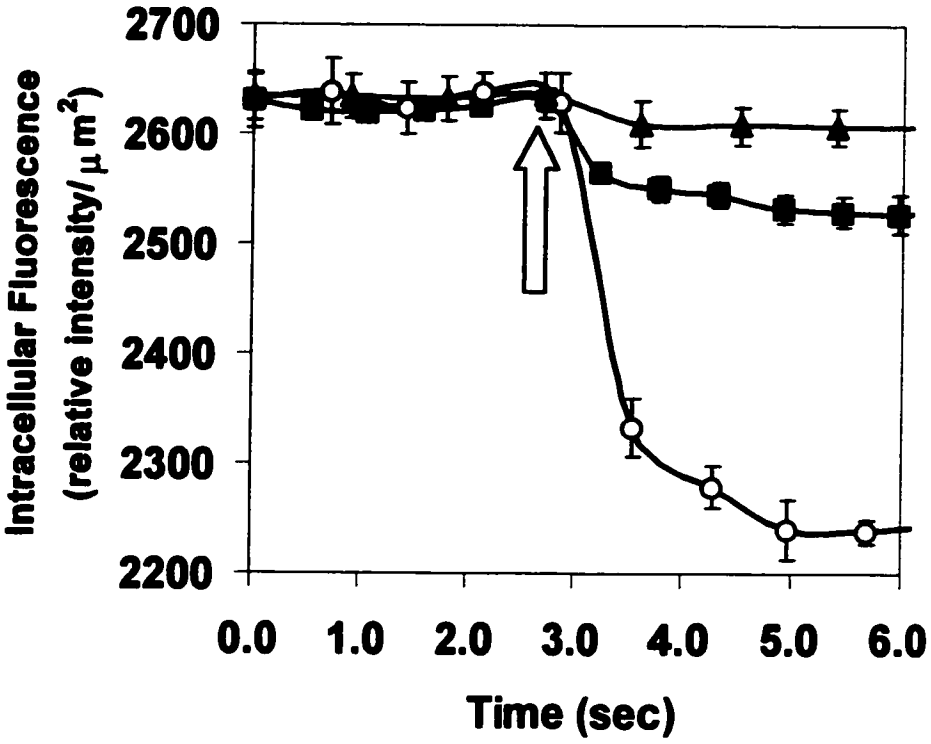

Fig 1.4.17:- Intracellular fluorescence intensity of $DnsHCys_2$ treated HT1080 fibroblastoma cells upon introduction of 100 μM BSA-NO (indicated by up arrow) to cells in which csPDI was underexpressed (triangles) or overexpressed (circles). Control cells transfected with vector alone are shown by the squares. Intracellular (fluorescence/ μm^2) was calculated from digitized images of the observation field taken every 250 msec with the aid of Northern Eclipse 5.0 imaging software (Empix, Mississauga, ON).

In an effort to kinetically characterize csPDI in HT1080s, the cells were preincubated with $DnsHCys_2$, 200 μM for 2 min and then exposed to varying concentrations of BSA-NO, 1 μM to 200 μM. The fluorescence images were captured ~ every 250 msec. The initial rates of fluorescence quenching/ μm^2 were calculated with the aid of Northern Eclipse image acquisition system (Empix, Mississauga, ON). The plots of the initial rates as a function of [RSNO] were hyperbolic. The steady state treatment of HT1080 cell kinetic data resulted in estimated apparent K_M values for BSA-NO of 35 ± 2 μM and 35 ± 4 μM for control and csPDI over-expressing cells respectively. In addition, the estimated V_{max} for the csPDI over-expressing cell line was ~ 2-fold larger than controls (Fig 18).

1.4.2.10 Use of csPDI inhibitors:- Next, kinetic studies were performed on HUVECS (Fig 19,20) and hamster lung fibroblasts (Fig 21,22) in culture, yielding apparent K_M values for BSA-NO of 17 ± 2 μM and 12 ± 3 μM respectively and K_M values for GSNO 55 ± 4 μM and 80 ± 2 μM respectively. Another piece of evidence that intracellular DnsHCys is measuring csPDI activity came from the fact that the initial rates of fluorescence quenching were inhibited by DTNB (Fig 19 -22, triangles), and bacitracin (Figs 19 -22, squares). DTNB is a membrane impermeable sulfhydryl reagent and hence expected to react with cell surface thiols on the other hand bacitracin is known to inhibit PDI but contains no active thiol group. Mechanism of inhibition by bacitracin is poorly understood nonetheless provides insight into the involvement of csPDI in RSNO transport.

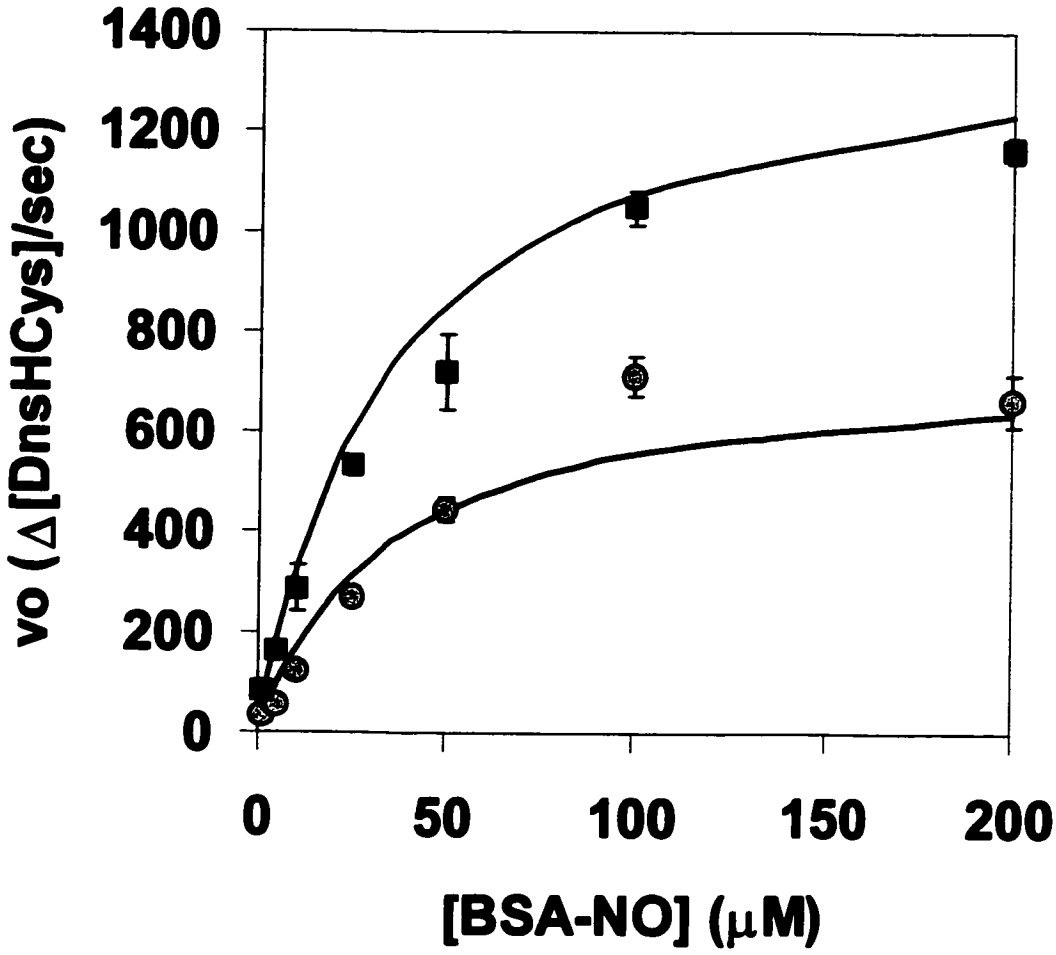

Fig 1.4.18:- Initial rates of intracellular DnsHCys fluorescence quenching as a function of BSA-NO concentration. Control HT1080 cells are indicated by the circles, while HT1080 cells over-expressing csPDI are indicated by the squares. The error bars represent standard deviation (n=6). The solid line represents the best fit of the data to the Michaelis-Menten equation.

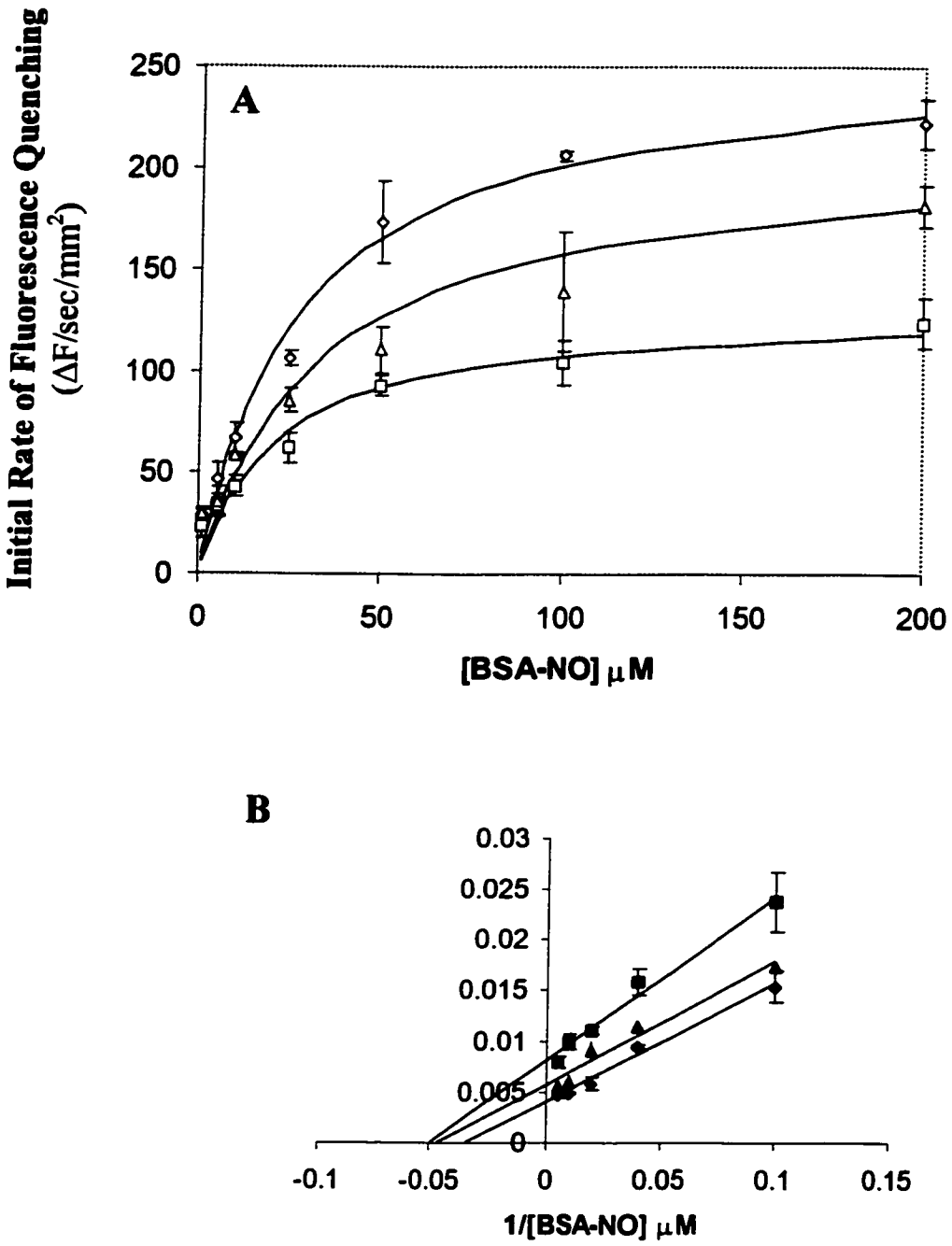

Figure 1.4.19:- Inhibition of BSA-NO transport in Huvecs. Cells were incubated with 100μM DTNB for 30min prior to determining transport kinetics (Squares). Cells were treated with bacitracin (3mM) for 4hrs prior to determining transport kinetics (Triangles). The Michaelis-Menton (A) and the double reciprocal (B) plots are with respect to control (Diamonds).

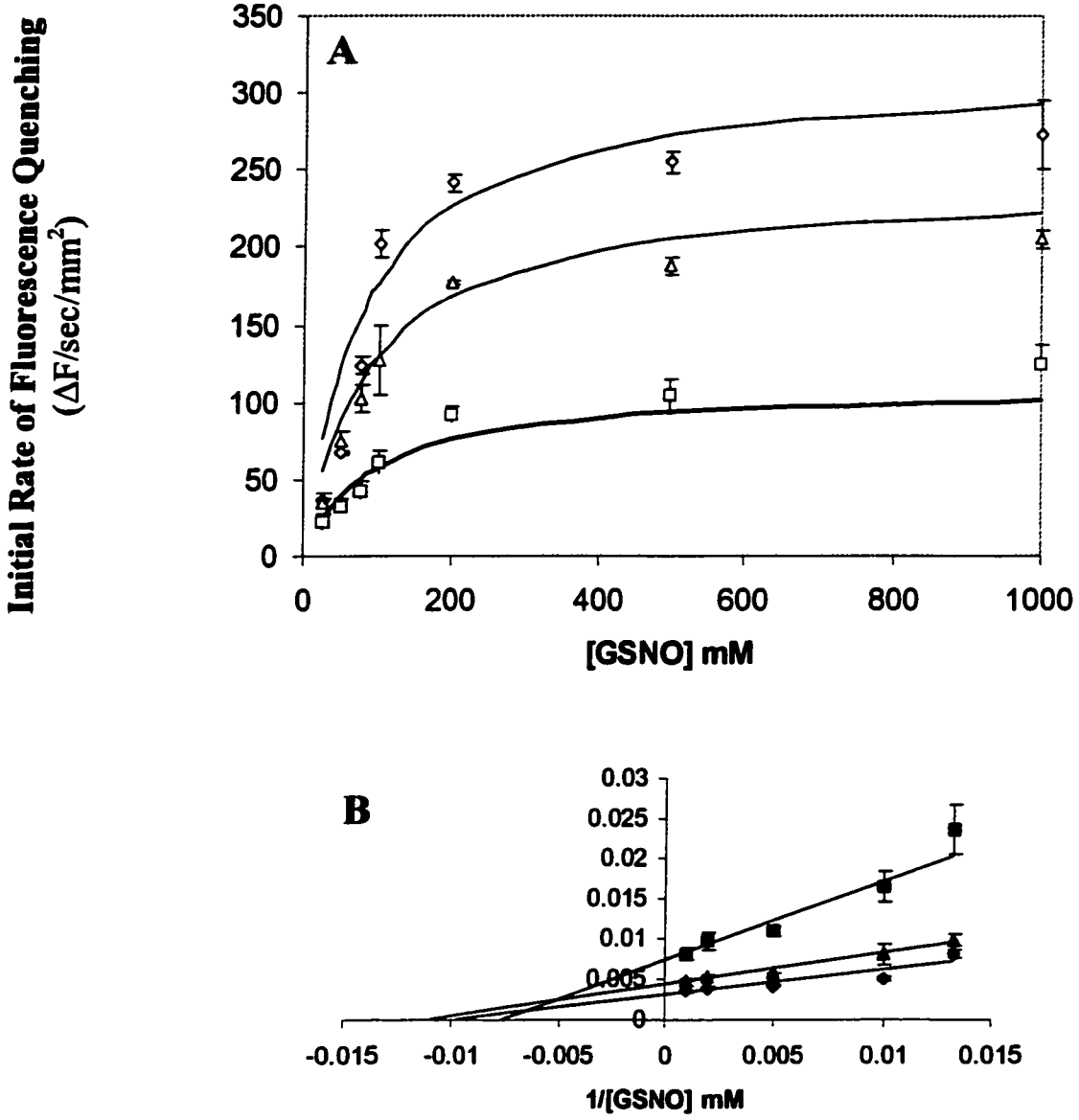

Fig 1.4.20:- Inhibition of GSNO transport in HUVECs. Cells were incubated with 100μM DTNB for 30min prior to determining transport kinetics (Squares). Cells were treated with bacitracin (3mM) for 4hrs prior to determining transport kinetics (Triangles). The Michaelis-Menton (A) and the double reciprocal (B) plots are with respect to control (Diamonds).

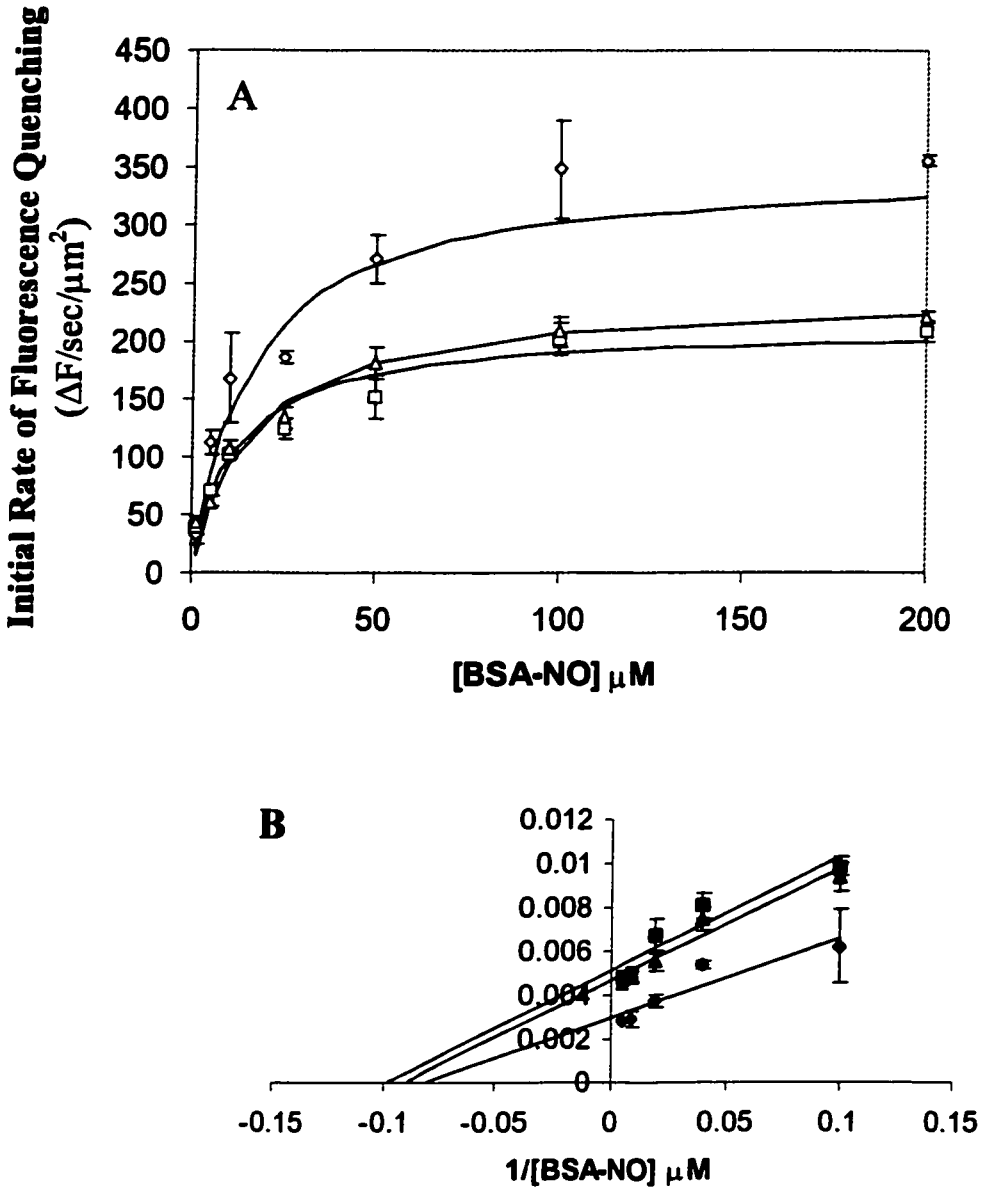

Fig 1.4.21:- Inhibition of BSA-NO transport in Hamster lung fibroblasts. Cells were incubated with 100μM DTNB for 30min prior to determining transport kinetics (Squares). Cells were treated with bacitracin (3mM) for 4hrs prior to determining transport kinetics (Triangles). The Michaelis-Menten (A) and the double reciprocal (B) plots are with respect to control (Diamonds).

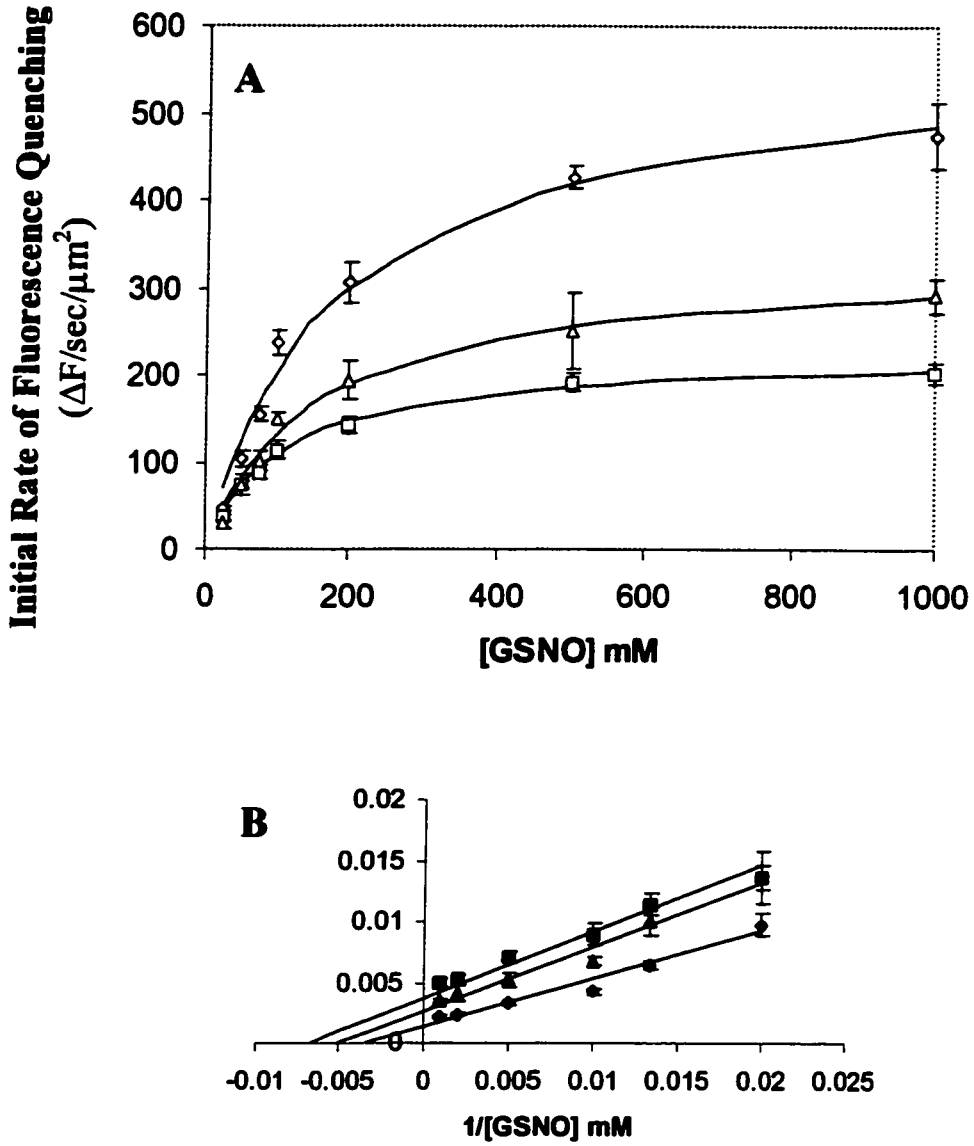

Fig 1.4.22:- Inhibition of GSNO transport in Hamster lung fibroblasts. Cells were incubated with 100μM DTNB for 30min prior to determining transport kinetics (Squares). Cells were treated with bacitracin (3mM) for 4hrs prior to determining transport kinetics (Triangles). The Michaelis-Menten (A) and the double reciprocal (B) plots are with respect to control (Diamonds).

Fig 19, describes the degree of inhibition by bacitracin (3mM) and DTNB (100μM) on the transport of BSA-NO by HUVECs. No significant changes in K_M were observed however the V_{max} was reduced by ~50% with DTNB while only a 20% reduction was observed with bacitracin. In the uptake of GSNO, Fig 20, no significant changes in K_M were observed as well. Reduction in V_{max} was greater with DTNB, ~60%, than with bacitracin, ~25%. Furthermore, GSNO uptake showed slightly more sensitivity to the use of inhibitors.

As with HUVECs, inhibition of RSNO uptake in fibroblasts showed no significant changes in K_M values. Incubation with DTNB reduced the uptake of BSA-NO by ~40% and reduced the uptake of GSNO by ~50%. Effects of bacitracin were less profound with ~40% reduction in uptake of BSA-NO and GSNO in fibroblasts, Figs 21, 22.

Time dependent intracellular fluorescence quenching with GSCA, where the arsenic was replaced with a carboxylic group (Fig 23, diamonds) was indistinguishable from controls (Fig 23, triangles). HUVECs treated with GSAO (Fig 23, circles) showed no noticeable changes in fluorescence upon the addition of BSA-NO. DTNB is a non-specific thiol reagent that will block free thiols on the cell surface. GSAO on the other hand is a trivalent arsenical with one of its sites occupied by the thiol group of GSH. The remaining two thiol sites specifically blocks proteins that, like PDI, contain vicinal dithiols. GSAO does not react with monothiol containing peptides.

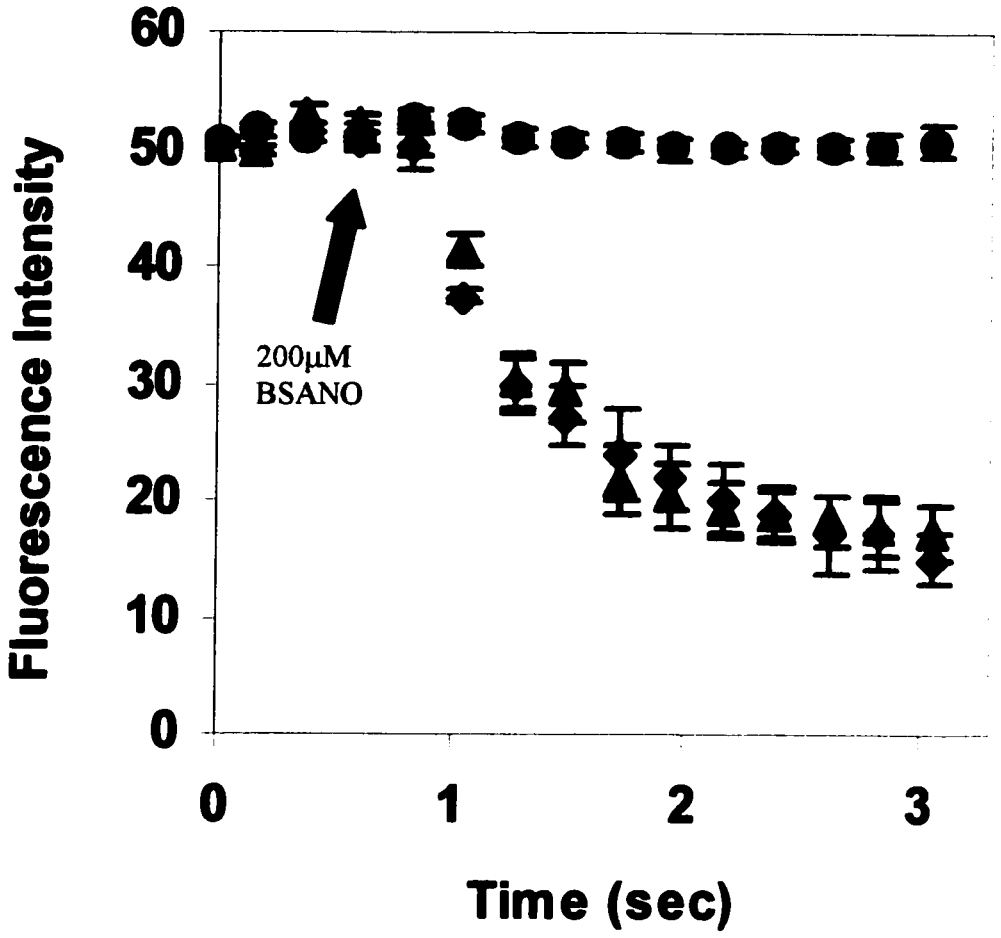

Fig 1.4.23:- Dynamic fluorescence quenching of intracellular DnsHCys fluorescence upon the addition of 200 μM BSA-NO (indicated by arrow). HUVEC, no inhibitor (triangles); 100 μM GSAO (circles); 100 μM GSCA (diamonds). The error bars represent standard deviation (n=6).

1.4.2.11 ***α-tocopherol treatment:-*** In an effort to determine the effects of membrane soluble N_2O_3 quenchers on the csPDI-dependent RSNO influx, HUVEC were grown in the presence of 10 μM α-tocopherol for 14 h. Jiang *et al.*, (2000) have reported that under these conditions epithelial cells were able to accumulate ~0.9 nmol of α-tocopherol/10^6 cells. This translates to a membrane concentration of ~5 mM. The rates of intracellular DnsHCys quenching by the extracellular introduction of BSA-NO, 25 μM were then compared in α-tocopherol treated and control cells (Fig. 24). As can been seen, the initial rates of intracellular nitrosation was inhibited by ~70% in the α-tocopherol treated cells. In addition, α-tocopherol had a very large effect on the K_m and V_{max} estimated for csPDI-catalyzed BSA-NO denitrosation as determined from the intracellular DnsHCys quenching rates (Fig. 25). The K_m increased from 17 μM in controls to 45 μM in α-tocopherol treated cells, whereas the V_{max} decreased by nearly 4-fold (control, 26 μM/sec, α-tocopherol-treated, 7 μM/sec).

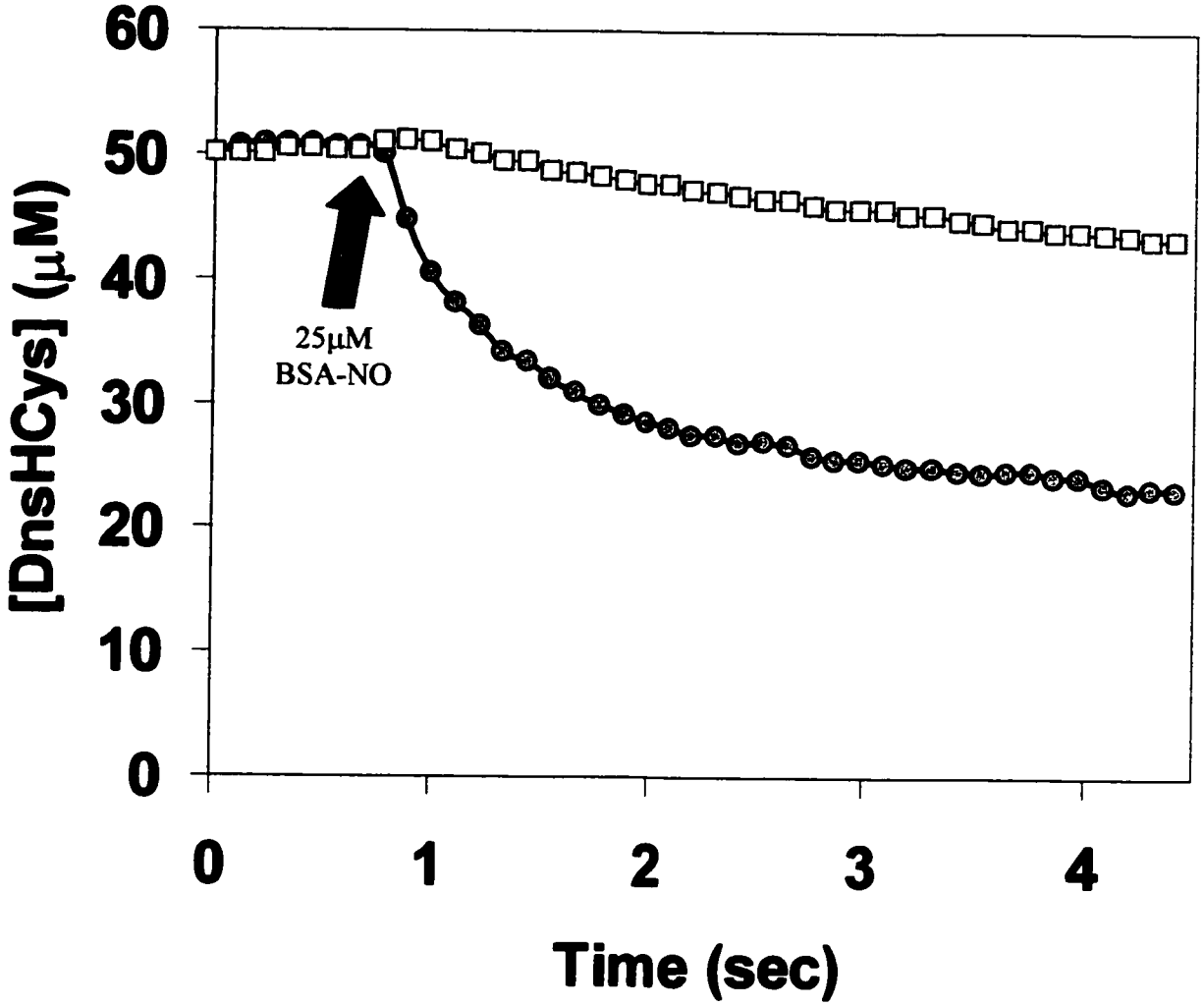

Fig 1.4.24:- The intracellular fluorescence of $DnsHCys_2$-pretreated HUVEC, controls (circles); or grown in the presence of 10 μM α-tocopherol for 14 h (squares), monitored subsequent to the extracellular addition of BSA-NO, 25 μM (indicated by down arrow).

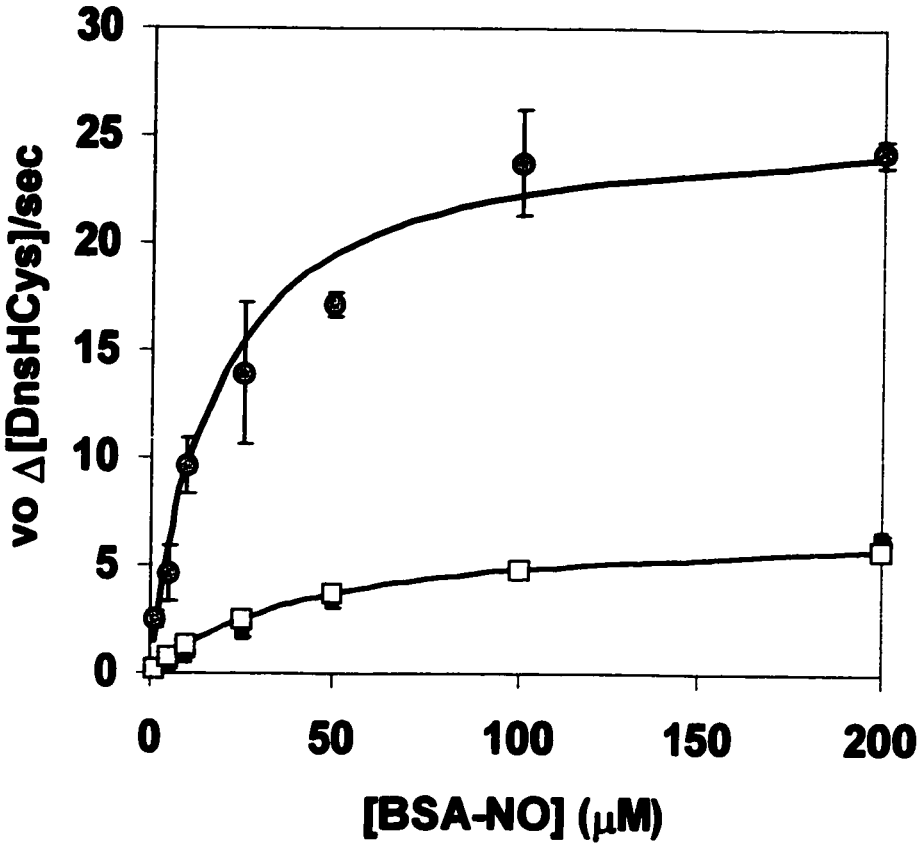

Fig 1.4.25:- Initial rates of intracellular DnsHCys fluorescence quenching as a function of BSA-NO concentration. HUVEC, controls (circles); or grown in the presence of 10 μM α-tocopherol for 14 h (squares). The error bars represent standard deviation (n=6). The solid line represents the best fit of the data to the Michaelis-Menten equation.

1.5 Discussion

1.5.1 Development of S-nitrosothiol probe

S-nitrosothiols are formed by the reaction of thiols and NO^+ or by transnitrosation with other S-nitrosothiols. Intra and extracellular S-nitrosothiols like GSNO and BSA-NO are carriers of NO in the cytosol and serum, respectively (Marks *et al.*, 1995; Liu *et al.*, 1998). S-nitrosothiols have been shown to elicit similar responses, as NO therefore the detection of RSNO/NO transport is important in the regulation of numerous aforementioned physiological effects.

In this study, we synthesized a S-nitrosothiol derivative of N-dansylhomocysteine, N-dansyl-S-nitrosohomocysteine and characterized its fluorescence properties. This potential probe upon synthesis exhibited low fluorescence. Subsequent exposure to light resulted in increased fluorescence by ~8 fold. We developed a hypothesis to explain the difference in fluorescence intensity between DnsHCys and its nitrosated counterpart, DnsHCysNO. The fluorescence quenching could be attributed to the close proximity of the NO moiety to the dansyl moiety. This hypothesis was supported by the molecular modeling study that showed the close proximity of the NO and dansyl group. The distance between the two groups allow for efficient energy transfer. The short range fluorescence energy transfer disenables the ability of dansyl to fluorescence. If this is true simply removing the NO could disrupt the energy transfer. The parallels observed in the release of NO and the increase in fluorescence thereafter,

also supports the notion that NO is a quencher.

The SNO group absorbs strongly in the UV/Vis at 340nm (ε 1000M^{-1} cm^{-1}) and weakly at 545nm (ε 18$M^{-1}cm^{-1}$) which closely overlaps with the excitation/emission spectra (λ_{Ex} 320nm, λ_{Em} 520nm) of dansyl. The quenching effect of SNO is two-fold, in which excitation light and the dansyl emission are both absorbed by close proximity of the SNO compound. These findings provided the foundation for the recent unpublished work by Chen *et al.*, (in press) who developed 12 compounds, based on excited state energy transfer between SNO and dansyl. Chen *et al.* chose to use alkyl linkers of varying lengths, in our study the linker was the side chain of homocysteine. Their detailed study suggested that favourable energy transfer depends on factors such as length of linker, and rigidity of sulfonamide unit, which should allow for overlap of SNO and dansyl groups. The stabilization energy that arises from this overlap contributes to efficient energy transfer.

Transnitrosation reactions are rapid and reversible reactions. This holds great physiological significance since the transfer of the nitroso group is regarded as a pathway of NO transport and a plausible mechanism for modification of protein activity (Scharfstein *et al.*, 1994; Park *et al.*, 1993). The transfer of the NO moiety from one thiol to another occurs via a nucleophilic attack of the free thiol. Since the reaction depends on the generation of a thiolate anion, other factors such as stereoelectronic effects (charge, steric hindrance), acidity of the sulfhydryl group and the reaction medium affect transnitrosation reactions. To date, these reactions have been monitored via changes in

UV/vis absorption of RSNOs (Singh *et al.*, 1996). In this study we showed that DnsHCysNO could undergo transnitrosation reactions with free thiols. DnsHCysNO nitrosated GSH in a concentration dependant manner, which was monitored by the increase in fluorescence of DnsHCys. We expect that varying thiol groups will yield varying sensitivities and rates of reaction due to the parameters discussed earlier. For instance albumin would have larger rate constants than low molecular weight thiols, based on the high acidity of the single sulfhydryl group, Cys 34.

If DnsHCysNO is capable of nitrosating free thiols, in reverse it should be nitrosatable. As expected DnsHCys was nitrosated by GSNO in a concentration dependant manner. Increasing concentrations of GSNO translates into the production of DnsHCysNO. The decrease in fluorescence due to this transition was used to monitor the nitrosation process.

In conclusion, DnsHCysNO exhibits low fluorescence in comparison to its highly fluorescent counterpart, DnsHCys. This has been attributed to the short range energy transfer that occurs between the NO and dansyl group situated in close proximity. DnsHCysNO is capable of undergoing transnitrosation and reverse nitrosation with low molecular thiols/S-nitrosothiols. Therefore, DnsHCysNO has been successfully developed as a probe for thiols/S-nitrosothiols. It provides a novel method for monitoring transnitrosation reactions with increased sensitivity.

1.5.2 Role of PDI in S-nitrosothiol transport

There is increasing evidence that S-nitrosylation plays a large role in the regulation of key metabolic enzymes. And unlike NO, whose effects are localized, NO derivatives of serum proteins like albumin can carry NO far from its point of synthesis to regulate vascular tone and platelet function. The other advantage of RSNOs over NO is that the delivery of RSNO-bound NO to the cytosol can be regulated (Zai *et al.*, 1999). In addition, Mayer *et al.* have suggested GSNO as an intermediate in the NO/cGMP signaling pathway (Mayer *et al.*, 1998). Transport mechanisms for RSNO bound NO into live cells have been speculated upon (Zai *et al.*, 1999; Hogg *et al.*, 1997). However, studies of this process have been hampered by the inability to directly measure the kinetics of uptake in living cells.

If RSNOs are central players in signal transduction, there must be an efficient process by which their bound NO is transferred from the extracellular environment to the cytosol. Recent work by Zai *et al.* (1999) suggested a central role for csPDI in this process. This membrane bound enzyme is capable of catalyzing thiol-disulphide exchange as well as transnitrosation reactions (Ferrari *et al.*, 1999).

In this study, we have demonstrated that DnsHCysNO can be employed as a fluorogenic substrate for PDI with an apparent K_M of 2 μM. Using this kinetic assay, we were also able to demonstrate that BSA-NO competitively inhibited this reaction with an

apparent K_I of ~ 1 μM. We also demonstrated that DnsHCys could act as an intracellular kinetic probe for csPDI in live cells *in vitro*. The initial rates of fluorescence quenching as a function of extracellular RSNO was hyperbolic indicating that a saturation phenomenon was being monitored. Furthermore, this saturable RSNO-dependent process was inhibitable by compounds commonly employed as inhibitors of PDI (Essex *et al.*, 1999; Mandel *et al.*, 1993).

Our attempt to elucidate the role of csPDI in the transport of S-nitrosothiol bound NO involved the use commonly employed PDI inhibitors such as bacitracin and DTNB. DTNB is membrane impermeant sulphydryl reagent that reacts with any surface thiols and hence is not specific to PDI. To target inhibition of PDI, bacitracin was used which does not possess any reactive thiols. Bacitracin is transported poorly in the mamalian system and thus expected to inhibit csPDI, largely. Reports by Couet *et al.*, (1996) utilized the two inhibitors to observe the role of csPDI in the shedding of human thyrotropin receptor ectodomain. The TSH receptor expressed by the cell is composed of an α and β domain joined by a disulphide linkage. CsPDI is expected to cleave the S-S bond releasing the α domain into the extracellular, "shedding". The use of DTNB and bacitracin inhibited this process by 70% and 80% respectively (Couet *et al.*, 1996). Another report by Mandel *et al.*, (1993) implicated the role of csPDI in the cytotoxic activation of diptheria toxin. Diptheria toxin is a heterodimer that is linked together by a disulfide linkage and binds to a receptor on the cell membrane. Activation of the toxin occurs upon reductive cleavage of the disulfide linkage resulting in chain separation. In this study, bacitracin and DTNB were able to inhibit this process by approximately 85%

and 50% (Mandel *et al.*, 1993). The use of these similar inhibitors resulted in about 50-60% inhibition with DTNB and lower inhibitions with bacitracin, 40-50%. This experiment does not clearly identify PDI as a sole responsible element in RSNO transport over enzymes such as thioredoxin and glutaredoxin that are also present on the mammalian cell surface. Generally bacitracin is used to distinguish the activity of PDI from that of other cell surface reducing mechanisms. The large concentrations and the unknown mechanism of bacitracin makes this a very unattractive inhibitor of PDI.

Perhaps the most convincing piece of evidence that we were monitoring csPDI activity, was obtained in the studies where the fluorescence quenching by extracellular BSA-NO was tested with HT1080 cells under-expressing or over-expressing PDI. The results of these experiments showed that over-expression increases csPDI levels by ~1.7 ± 0.2-fold whereas under-expression decreased csPDI levels by ~75 ± 25%. Once these values are adjusted for the fact that MPB-labeling underestimates csPDI by as much as 3-fold (Jiang *et al.*, 1999), they closely mirror the ~3-fold increase and ~85 % decrease in intracellular nitrosation upon PDI over- and under-expression respectively (Fig. 4). In addition, the fact that intracellular nitrosation was totally abolished with the cell-impermeant, vicinal-dithiol-specific reagent GSAO (Donoghue *et al.*, 2000) indicates the absolute requirement for csPDI and other vicinal dithiol containing proteins in the transport of RSNO bound NO to the cytosol. We reach this conclusion since GSAO does not react with single protein thiols or with Cu- or Zn-containing proteins.

We then determined the physiological significance of the kinetic constants. The K_I for BSA-NO was ~1 μM (Fig. 2). The HSANO level in serum of healthy individuals has recently been estimated by a combination of gas chromatography and mass spectrometry to be 181 ± 150 nM (n=22) (Tsikas *et al.*, 1999). This means that with the kinetic constants estimated here, the enzyme would be operating at ~17% of V_{max}. However, the serum albumin-NO concentration on the cell surface may be many fold larger as many cells contain surface receptors for HSA (Pietraforte *et al.*, 1995). In addition Pietraforte *et al.*, (1995) suggested that HSA-NO might concentrate on cell surface via electrostatic interactions.

The K_M estimated from the intracellular DnsHCys quenching rates was ~ 10 to 30 fold larger depending on the cell types studied here. This observation might be related to the manner and the form in which NO released by csPDI, nitrosates thiols in the cytosol. The mechanism(s) by which PDI catalyzes the release of NO (or NO^+ or NO^-) from extracellular RSNOs is unknown, however Zai *et al.*, (1999) have demonstrated that OxyMyoglobin is converted to MetMyoglobin in the presence of PDI and RSNOs indicating that NO is released during catalysis. Therefore, a proposed plausible mechanism was (Zai *et al.*, 1999):

$$2RSNO + PDI\text{-}2SH \rightarrow 2NO + 2RSH + PDI\ (S\text{-}S).$$

For csPDI to catalyze further denitrosation a mechanism is required to reduce the oxidized form of the protein. This may be accomplished by the plasma membrane

NADH-oxidoreductase system which has been implicated in reduction of extracellular protein disulfide bonds (Wolvetang *et al.*, 1996). Another possibility is thioredoxin reductase (Lundstrom *et al*, 1990), which is secreted by peripheral blood cells and is in plasma at a concentration of 18 ng per mL (Soderberg *et al.*, 2000).

Another unknown is how the NO released by PDI nitrosates intracellular thiols. A potential clue to this comes from the work of Lancaster and coworkers (Liu *et al.*, 1998) who demonstrated that the reaction of NO and O_2, both hydrophobic molecules, is ~300-fold more rapid in cell membranes than in aqueous media. The product of this reaction is the powerful nitrosating agent N_2O_3. More recently, Nudler and coworkers (Nedospasov *et al.*, 2000) have demonstrated that under physiological concentrations of NO, N_2O_3 forms inside protein-hydrophobic cores and causes autonitrosylation within the protein interior.

We propose, therefore, that csPDI catalyzed NO released from RSNOs accumulates in the membrane where it reacts with O_2, to produce N_2O_3. Intracellular thiols then get nitrosated by N_2O_3 at the membrane-cytosol interface (Figure 26). If this hypothesis is correct, depletion of membrane N_2O_3 with membrane soluble quenchers such as vitamin E (α-tocopherol) should inhibit intracellular nitrosation by csPDI (Hogg *et al.*, 1996). This is indeed what was observed when HUVEC were preincubated with α-tocopherol. The rate of intracellular DnsHCys fluorescence quenching decreased by ~70 % in cells where membrane vitamin E levels were elevated. In addition, vitamin E increased the K_M by ~3-fold and decreased V_{max} by ~ 4-fold. Furthermore, this

hypothesis can account for the ~10-30-fold difference in the K_I estimated for BSA-NO in the direct PDI assay and the K_M estimated from intracellular quenching of DnsHCysNO. When the S-nitrosation probe is in the cytosol, the amount of NO produced by csPDI at low BSA-NO will likely yield smaller amounts of N_2O_3, which will be quenched by the normal levels of vitamin E present in the membrane. Only at high BSA-NO levels would there be enough N_2O_3 buildup to permit the detection of intracellular nitrosation via DnsHCys-fluorescence quenching. This can explain why the apparent K_M in the α-tocopherol treated cells was ~3-fold larger than in controls.

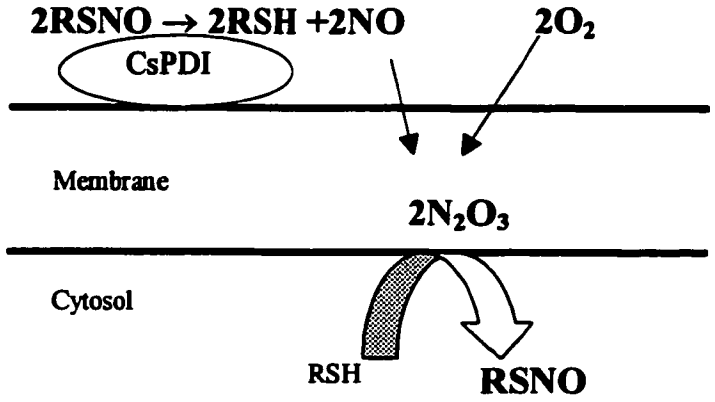

Figure 26:- Proposed mechanism for the transport of S-nitrosothiol bound NO

In this study we have introduced DnsHCysNO as a direct fluorogenic substrate for PDI and using this compound have estimated the affinity of PDI for BSA-NO. We have also used DnsHCys in the cytosol as an S-nitrosation probe to demonstrate the absolute requirement for csPDI for the transfer of extracellular RSNO in to the cytosol. In addition, we have proposed and tested a mechanism by which the NO released by csPDI from RSNOs can nitrosate intracellular thiols at the membrane-cytosol interface. The fact that this process is affected by membrane-antioxidant levels, raises the possibility that cells can regulate the bi-directional movement of RSNO bound NO by csPDI activity/expression as well as by controlling the membrane redox status.

Part II

Effects of Homocyst(e)ine on NO/RSNO metabolism

2.0 Abstract

Homocysteine (HCys) is an independent marker for cardiovascular diseases. Its role in NO/RSNO metabolism is complex yet important in the progression of vascular diseases. It has been shown that HCys decreases the bioavailability of NO via oxidative inactivation (Upchurch *et al.*, 1997). In this study, we show that the L-Arg transporter and cell surface protein disulfide isomerase are modulators in NO/RSNO metabolism and both modulators are targets for homocysteine (HCys) and homocystine ($HCys_2$). Long-term treatment of endothelial cells with HCys inhibited L-Arg uptake and decreased NO secretion by endothelial cells. Incubation of endothelial cells with 100μM HCys (6h) resulted in a ~2 fold increase in K_m (150μM) for L-Arg transport and ~1.4-fold decrease in V_{max} (110pmoles/10^6 cells/min) as compared to control. Oxidized and reduced forms of glutathione and cyste(i)ne did not show significant changes in L-Arg uptake. The use of a NO specific electrode revealed 34% reduction in endothelial secreted NO levels. Our evidence suggests that HCys plays a multifaceted role in NO/RSNO metabolism possibly leading to vascular damage.

In the realm of NO metabolism, cell surface protein disulfide isomerase (CsPDI) has been recently implicated in the rapid transport of extracellular RSNO bound NO (Zai *et al.*, 1999). Using the novel probe, N,N-didansylhomocystine assay ($DnsHcys_2$) for PDI catalyzed RSNO influx, $HCys_2$ was found to decrease the uptake of BSA-NO bound NO in HUVECs. In solution, $HCys_2$ had no effect on the isomerization activity of csPDI, while a ~20% reduction in its denitrosation activity was observed. The cellular redox

state of endothelial cells treated with HCys was probed using the fluorescence of monocholorobimane (mCB) and 2,7-dichloroflourescein diacetate (DCF). The use of glutathione specific mCB revealed a 55% increase in intracellular glutathione levels while DCF fluorescence showed a 53% increase in reactive oxygen species for HCys treated cells. Our results clearly show a reduction in NO secretion and inhibition of csPDI denitrosation activity without any significant effects to its isomerization activity. NO is a known inhibitor of platelet aggregation and cell adhesion while the isomerization activity of csPDI has been implicated in the aggregation of activated platelets and endothelial cell adhesion. Therefore our results reveal a plausible mechanism for the vasoconstrictive and pro-aggregatory pathophysiology observed in patients with hyperhomocysteinaemia.

2.1 Introduction

2.1.1 Homocysteine

Homocysteine (HCys) is a non-protein sulfhydryl amino acid, similar to glutathione and cysteine. Cysteine and HCys differ by the presence of a methylene group in the side chain. This small difference in molecular structure has accounted for their vast differences in physiological effects. HCys is involved in the metabolism of dietary methionine (Niittynen *et al.*, 1999), undergoing remethylation to form methionine or transulfuration to form cysteine. Increased concentrations of plasma HCys have been implicated in patients with coronary, pheripheral and cerebral atherosclerosis (Olszewski *et al.*, 1993). It is considered an independent risk factor for cardiovascular diseases (Niittynen *et al.*, 1999). Currently there are many controversies surrounding the effects of HCys on the cardiovascular system, NO metabolism, and HCys transport.

2.1.1.1 ***Homocysteine uptake:-*** Determining the transport kinetics of HCys would provide crucial insight into its pathophysiological mechanism. However to date, very few studies have been conducted regarding its mode of transport with respect to cell line and the factors influencing its uptake.

Given the molecular similarities between glutathione, cysteine and HCys, one would expect a similar transport mechanism. Ewadh *et al.*, (1990) have reported HCys uptake occurs in both a Na^+ dependant and independent manner. The use of a well

known inhibitor of the Na^+ independent System L, β-2-aminobicyclo(2,2,1)heptane-2carboxylic acid (BCH), inhibits HCys uptake. Depleting the Na^+ in the growth media in addition to treatment with BCH resulted in the complete inhibition of HCys uptake. From these results, it was concluded that System L is responsible for the Na^+ independent uptake of HCys. The K_M of HCys for System L was determined to be ~160μM (Ewadh *et al.*, 1990).

In order to distinguish between two Na^+ dependant transports, System A and System ASC, further inhibition studies were performed. The use of System A inhibitors showed no inhibition of HCys uptake, indicating that most likely System ASC was responsible for the Na^+ dependant uptake of HCys. The K_M of HCys for System ASC was calculated to be ~73μM (Ewadh *et al.*, 1990).

The HCys uptake was competitively inhibited by cysteine. Surprisingly, HCys uptake was also inhibited by cystine. This was unexpected since cystine uptake occurs via a glutamate co-transporter. Furthermore, HCys imposes no inhibitory effect on glutamate uptake and conversely glutamate has no effects on HCys transport (Ewadh *et al.*, 1990).

Reports by Hutlberg *et al.*, (1998) have suggested that endothelial cells are equipped with a robust HCys export System to compliment the uptake System. In comparison to various human cell lines, endothelial cells maintained the lowest intracellular HCys concentration. These cells were shown to export most of the

endogenously generated HCys and furthermore did not metabolize the extracellular HCys. Therefore, the chronic exposure to large concentrations of HCys might increase the sensitivity of the endothelial cells to HCys, explaining the development of hyperhomocysteinemia and vascular disease (Hultberg *et al.*, 1998).

2.1.1.2 Metabolism:- The major pathway of HCys metabolism is remethylation to methionine, Fig 2.1.1. This step involves a crucial enzyme methionine synthase, which requires vitamin B12 as a cofactor and methyl donor. The methyl donor, N-5-methyltetrahydrofolate (Me-THF), is reduced from methylenetetrahydrofolate, (methylene-THF), by a reductase (MTHFR). Activity of methionine synthase demethylates Me-THF to tetrahydrofolate (THF). The remethylation cycle of methionine and Me-THF are closely associated to yield methionine. However, HCys could also be derived from a methionine via the precursor adenosyl-methionine. Adenosyl-methionine is a principal methyl donor in mammals and can undergo transmethylation (methyl transfer reaction) to generate S-adenosyl- homocysteine (Mudd *et al.*, 1989). S-adenosyl-homocystiene is hydrolyzed by a hydrolase to yield homocysteine and adenosine (Olszewski *et al.*, 1993; Hultberg *et al.*, 1998).

HCys may also enter a transsulfuration pathway to produce cysteine. The enzyme, cystathionine synthase, which catalyzes the formation of the intermediate cystathionine, is considered to be a key step in HCys metabolism (Welch *et al.*, 1998; Moghadasian *et al.*1997). Cystathionine is eventually broken down to yield homoserine and cysteine.

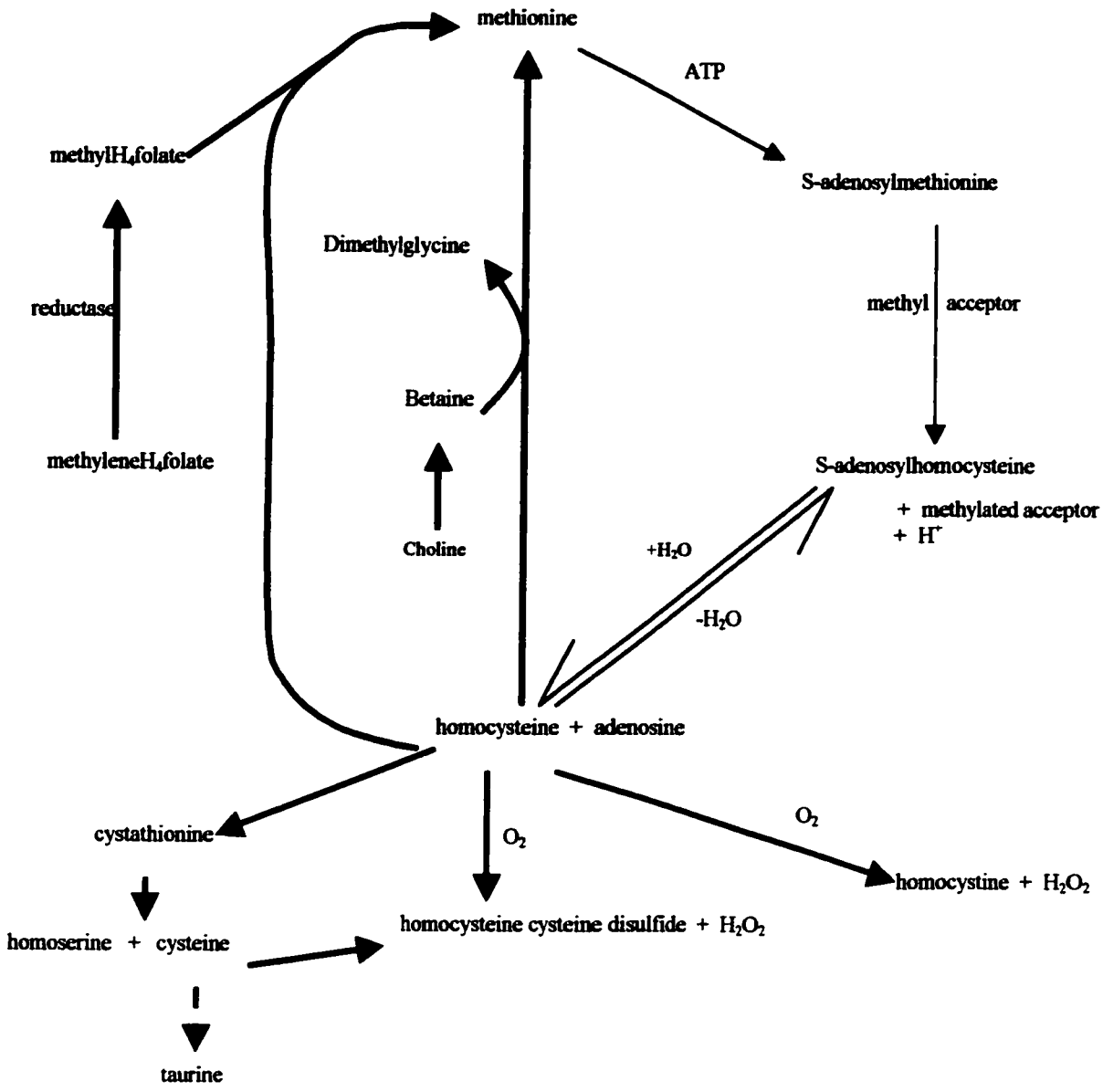

Fig 2.1.1:- Metabolic pathway of Homocysteine (Olszewski *et al.*, 1993)

Cysteine serves as a substrate for the biosynthesis of taurine after undergoing a series of decarboxylation reactions. Unlike HCys, taurine has several positive effects in the cardiovascular system. It is known to possess antioxidant activity, lower blood pressure, reduce blood cholesterol and depress platelet aggregation (Canas, P.E., 1992; Azuma *et al.*, 1992; Mizushima *et al.*, 1996; Hayes *et al.*, 1989). Taurine is found in high concentrations in animals and almost entirely absent in plants (Huxtable, R.J., 1992).

The third fate of HCys as commonly seen in plasma samples is the oxidation of HCys to form homocystine ($HCys_2$) or other protein thiols resulting in mixed disulfides. In plasma, HCys is predominantly found, 70-80%, in disulfide links with other proteins. Therefore clinical assays are based on the determination of total homocyst(e)ine levels. The normal plasma concentration is approximately 5-15μM (Welch *et al.*, 1998).

2.1.1.3 Chemistry of Homocysteine:- HCys is a sulfhydryl compound and therefore an electron donor. These compounds are able to take part in redox reactions with transition metals, such as Fe^{3+} and Cu^{2+}. In cultured endothelial cells, the oxidation of HCys to $HCys_2$ in the presence of oxygen produces hydrogen peroxide (Starkebaum *et al.*, 1986). Hydrogen peroxide is capable of oxidizing Fe^{+2} to produce a hydroxyl radical and a hydroxyl anion via the Fenton reaction. The hydroxyl radical has a very short half-life and is considered to be the more potent reactive oxygen species (ROS). Additionally, Fe^{+3} and Cu^{+2} can mediate the production of the homocysteinyl radical, the homocystine radical anion, and homocysteine-cysteine mixed disulfide radical anion and peroxysulfur anions, Fig 2.1.2. The formation of these homocysteine radicals enhances the oxidative

damage already induced by hydrogen peroxide. Specifically, the oxidation of catalytic sites on various enzymes leads to the loss of activity. Hydrogen peroxide, Fe^{+3} and Cu^{+2} are known to inhibit glutamine synthase by binding transition metals to the divalent cation binding site of the enzyme. The presence of hydrogen peroxide will then oxidize the transition metals while producing hydroxyl radicals, as mentioned above, rendering the enzyme inactive (Olszewski *et al.*, 1993; Wall *et al.*, 1980).

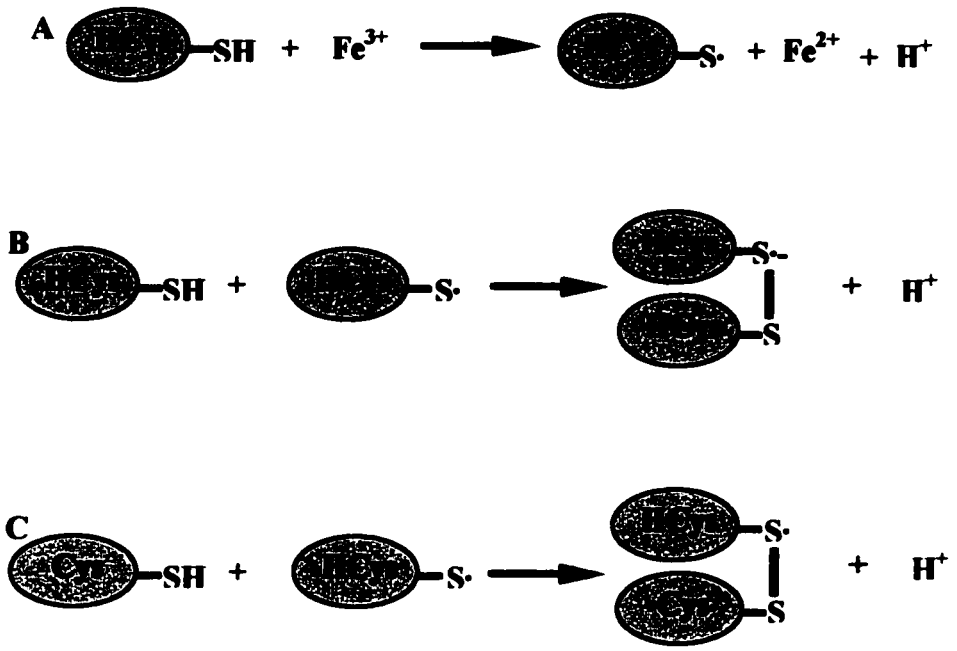

Fig 2.1.2 : Proposed mechanisms for HCys radical formation (Olszewksi *et al.*, 1993).

HCys can also be oxidized to HCys thiolactone by ROS. HCys thiolactone is capable of dimerizing to form diketopiperazine. Polymerization occurs by the oxidation of the sulfhydryl in HCys diketopiperazine. The solubility of this polymer is very low and requires highly acidic conditions. It is known that this polymer could cause damage to the surface of arterial walls and is suspected to be in atherosclerotic plaques . HCys thiolactone is also known to react with retinoic acid to produce thioretinamide, Fig 2.1.3. Thioretinamide could also react with cobalamin to form a complex known as thioretinaco. Thioretinaco is commonly found in the F1 complex in the mitochondria. The complex is highly electrophilic and is capable of reducing reactive oxygen species to water in the presence of ascorbate. Therefore depletion of thioretinaco or any perturbations in its production will result in higher levels of ROS causing premature aging, atherosclerosis, and possibly cancer (McCully *et al.*, 1993; Olszewski *et al.*, 1993).

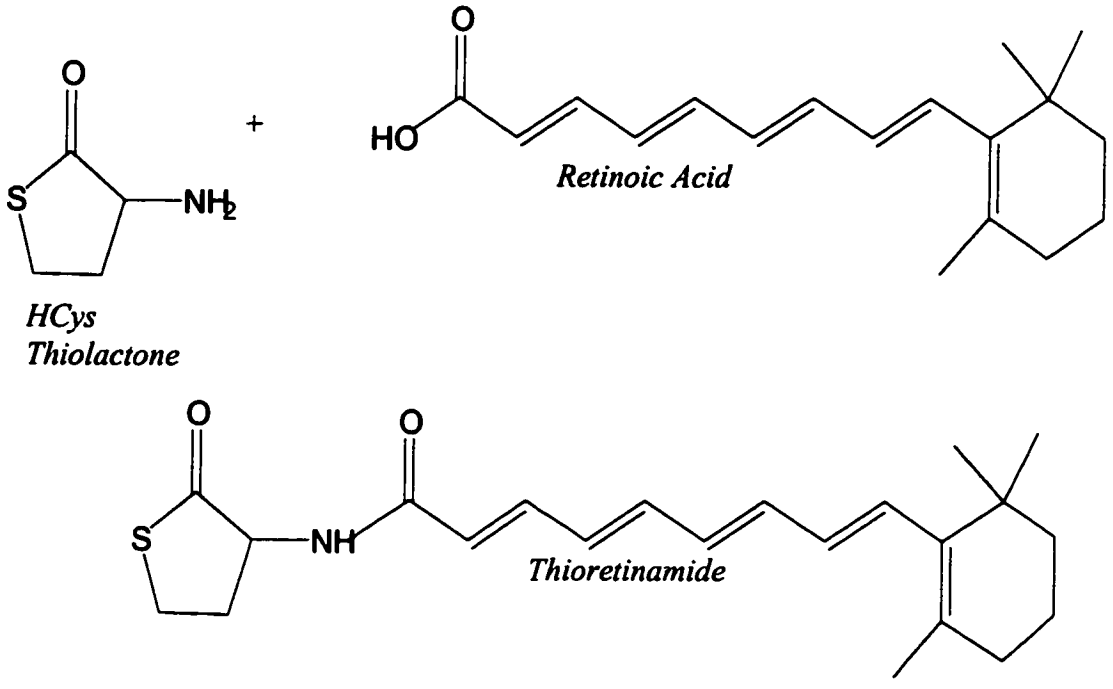

Fig 2.1.3:- Formation of Thioretinamide

The effects of HCys and homocysteine thiolactone on lipids are thought to be the underlying cause of vascular damage. HCys, cysteine, and glutathione have been shown to oxidatively modify low-density lipoproteins *in vitro,* through peroxidation reactions. However, in plasma, cysteine is predominantly found in its oxidized cystine form, while glutathione is largely present intracellularly in the reduced state. The secretion of excess glutathione may cause modifications of LDL, but no such effect have been reported (Parthasarathy *et al.*, 1987). HCys has been shown as the principle thiol compound responsible for oxidizing lipoproteins. HCys thiolactone causes thiolation of lipoproteins, which introduces sulfhydryl groups into lipoproteins causing their susceptibility to oxidation. HCys thiolactone is considered to be prothrombotic due to various aggregatory effects observed in platelets, and between fibrin and lipoproteins leading to atherogenesis (Scanu *et al.*, 1990).

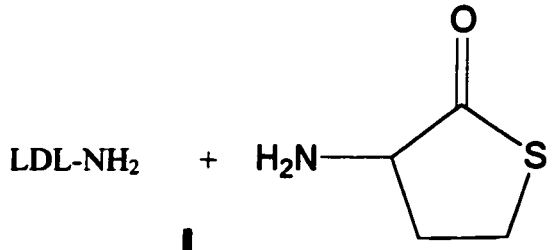

LDL-NHCOCH(NH_2)CH_2CH_2**SH** + **HS**-apo(a)

Homocysteinyl LDL

LDL-NHCOCH(NH_2)CH_2CH_2**SS**-apo(a)

Lipoprotein (a)

Fig 2.1.4 : Oxidation of Lipoproteins by homocysteine thiolactone (Olszewski *et al.*, 1993)

2.1.1.4 ***Hyperhomocysteinaemia:-*** Hyperhomocysteinaemia, caused by elevated plasma concentrations of HCys, is a risk factor for coronary heart disease, atherosclerotic vascular disease, thromboembolic diseases and various other cardiovascular diseases. Increases in HCys may be attributed to a deficiency or abnormality in the enzymes cystathionine β-synthetase or methylene tetrahydrofolate reductase, or the absence of cofactors (folate,vitamin B_{12} or vitamin B_6). A deficiency in cystathionine β-synthetase is the major cause of hyperhomocysteinemia, leading to dramatic increases in HCys and vascular damage as well as increases in plasma methionine and HCys containing disulfides. Absent or deficient enzymes are not able to execute the catabolic pathway of homocysteine and therefore cannot deal with HCys produced at normal levels without pharmaceutical assistance (Dudman *et al.*, 1996).

Deficiency in methylene tetrahdrofolate reductase also gives rise to hyperhomocysteinaemia. The folate dependant re-methylation of homocysteine is not a major metabolic pathway and any suppression of the enzyme should not greatly effect the HCys concentration. A plausible explanation for the observed increase in HCys suggests that the activity of cystathionine β -synthetase is regulated by S-adenosylhomocystiene. Therefore, any defect in the generation of S-adenosylhomocystiene by the reductase will in turn affect the activity of cystathionine β-synthetase. The reduced rate of cystathionine β-synthetase may then be the cause of hyperhomocysteinaemia.

As fore-mentioned, homocysteine is considered to be a graded risk factor independent of other risk factors. It has been shown that homocysteine is a much more

sensitive marker for cardiovascular diseases than cholesterol (Nittynen *et al.*, 1999). The plasma HCys concentrations of a healthy individual ranges from 5-10μM. An increase in HCys levels by 5μM increases the risk of coronary heart disease to the same extent as an increase in cholesterol by 0.5mM. A HCys plasma concentration of 20μM increases the risk factor of heart disease by seven fold (Boushey *et al.*, 1999). Treatment of hyperhomocysteinaemia is usually conducted by administration of cofactors such as folic acid, vitamin B12 and Vitamin B6. Folic acid supplementation resulted in 25% decrease in HCys plasma concentration, whereas treatment with vitamin B6 showed no effect (Nittynen *et al.*, 1999). No conclusive evidence has been presented to date to suggest that lowering HCys plasma concentration by dietary supplementation reduces cardiovascular diseases.

2.1.2 Effects of Homocysteine

As mentioned earlier, HCys is known to have adverse effects on the cardiovascular system. Two major hypotheses regarding the harmful effects of HCys have been proposed. The first suggests HCys damages endothelial cells that line the vasculature, and the second proposes that HCys interferes with the vasodilatory effects of NO. Both of these hypotheses ultimately lead to the same result that is the formation of vessel occlusions.

2.1.2.1 ***Effects of Homocysteine on NO production:-*** The correlation between the concentration of HCys and vascular damage, in respect to epithelial cell function, has

directed the focus of our research. In particular the NO metabolism of the endothelial cells were observed. Upchurch *et al.*, (1997) proposed that treatment of endothelial cells with HCys results in the decrease of NO levels. However their studies showed that a decrease in NO levels may not infer a low production of NO but rather the decrease in bio-availability of NO (Upchurch *et al.*, 1997). Exposure to HCys resulted in increasing levels of RSNO, while intracellular thiols such as glutathione and cysteine showed no effect. Therefore, increases in NO levels were attributed to the formation of S-nitrosohomocysteine (HCysNO). To date, the S-nitroso adduct has not been shown in cardiovascular diseases. Therefore, HCysNO might participate in a detoxification mechanism since it is unable to induce hydrogen peroxide and thiolactone formation. HCysNO may actually play a beneficial role in the vasculature by serving as a vasodilator and inhibitor of platelet function (Upchurch *et al.*, 1996).

The adverse effects of HCys on NO metabolism are more prevalent upon longer incubations of epithelial cells with high concentrations of HCys. High concentrations of HCys (~5mM) decreased the production of NO and RSNO (Upchurch *et al.*, 1996). These damaging effects are due to the endothelial cells being unable to sustain elaborate production of NO (Stamler *et al.*, 1993). High concentrations of HCys detected in hyperhomocysteinaemic patients might therefore interfere with NO production and continue to induce oxidative damage.

2.1.2.2 Effects of Homocysteine on NOS activity:- Realizing the effects of HCys on NO and RSNO production in endothelial cells, the next relevant question pertains to its effect on NOS activity. Studies by Zhang *et al.*, (2000) did not show any change in the expression of either eNOS or iNOS in the presence of HCys. Treating endothelial cells with Bradykinin, an agonist of NO production, increases mRNA levels of eNOS. Upchurch *et al.*, (1997) observed a synergistic behaviour of HCys where mRNA levels of eNOS were increased to a greater extent upon co-incubation with HCys and Bradykinin. Conversely, when Upchurch *et al.*, (1996) treated endothelial cells with abnormally high concentrations of HCys (5mM), and detected a decrease in the basal NO production in the absence of the agonist, Bradykinin. These observations were specific to HCys, but not to the other two biologically relevant thiols, GSH and Cys (Upchurch *et al.*, 1996; Zhang *et al.*, 2000).

Zhang *et al.*, (2000) also probed the activity of recombinant NOS to potentially differentiate the effect of HCys on enzyme activity as opposed to enzyme expression. Generally, damaging effects of HCys depend on the length of incubation and concentration of HCys. However, long term incubations with HCys and recombinant eNOS did not affect its activity. *In vitro* studies using recombinant eNOS have shown susceptibility to oxidation by diamide decreasing its activity, however, no effect was observed with HCys. This is not to say that HCys cannot modify eNOS, since HCys induces oxidative stress, which in turn may indirectly modify the sulfhydryl groups of NOS (Zhang *et al.*, 2000). Studies have shown that ROS generated by the oxidation of HCys inhibits eNOS. Therefore, NO-generating activity of NOS may not be directly

affected by HCys but by the increased levels of ROS in HCys treated cells (Zhang *et al.*, 2000).

2.1.2.3 Effects of Homocysteine on Glutathione Peroxidase activity:- HCys induces oxidative stress via the increase in H_2O_2 levels (Brattstrom *et al.*, 1984). These changes could be a direct result of HCys oxidation. More recently, it has been shown that the effects of HCys to be far beyond simple oxidation to its effects on glutathione peroxidase (GPx) activity. Endothelial cells treated with 250μM HCys exhibited a 81% decrease in cytosolic GPx activity (Upchurch *et al.*, 1997). In addition, HCys also decreased the steady state expression of GPx. In comparison, Cys is capable of ROS generation upon oxidation but has no effect on the bio-availability of NO or activity of GPx (Heinecke *et al.*, 1987). Decrease in GPx activity does not only increase H_2O_2 levels but also leads to inactivation of NO by peroxides. GPx catalyses the reduction of H_2O_2 as well as lipid peroxides utilizing GSH as a co-substrate. These inhibitory effects of HCys were not consequences of limiting substrates or enzyme activity, suggesting that HCys is able to inhibit the dual role of GPx by retarding its ability to reduce peroxides and prevent inactivation of NO. A pathological mechanism derived from these findings suggest that primary injury to the endothelial cells leads to platelet activation and smooth muscle cell proliferation caused by decreased bioactive NO leading to thrombosis (Upchurch *et al.*, 1997).

2.1.3 L-Arg

The cationic, dibasic, amino acid L-Arg is considered to be "semi-essential" in the mammalian diet (Casey *et al.*, 2000; Barbul *et al.*, 1986). Cellular L-Arg is involved in various metabolic pathways. In addition to its requirements in protein synthesis, L-Arg also serves as a precursor for urea, creatine and polyamine biosynthesis. Our interests lie in the use of L-Arg as a precursor for the synthesis of the bioregulatory nitric oxide, as well as its cellular uptake as part of its role in cellular function.

Similar to most large polar molecules, their transport requires specialized carrier proteins. The presence of these carrier proteins has been demonstrated on cell membranes by using radiolabelled substrates. Competitive studies with other amino acids have confirmed that one carrier would regulate the transport of more than one amino acid (Christensen, 1990). Due to the negative membrane potential, L-Arg and other cationic amino acids can be concentrated within the cell without direct coupling to energy consumption process. Different types of transporters have been identified in various cell lines such as System Y^+, Y^+L and $B^{0,+}$. These Systems are members of the cationic transporter (CAT) family (Casey *et al.*, 2000). The use of these transporters and their relative efficiencies have been found to correlate their functions to the need for plasma L-Arg. The plasma concentration of L-Arg varies from 23μM to 100μM (Dickenson *et al.*, 1965). Most active transporters of L-Arg have K_M values around 100μM, while transporters that utilize facilitated diffusion express higher K_M values in the millimolar range (2-5mM).

2.1.3.1 L-Arg and NO:- As previously stated, L-Arg is a substrate for NOS and therefore an important regulator of NO production. An interesting controversy is the dependence of NOS activity on L-Arg concentration. L-Arg transporters actively maintain a higher intracellular concentration, 10-20 fold, with respect to the extracellular concentration. Ideally, cellular concentrations of L-Arg should be sufficient for NO production to occur without the influence of L-Arg transport. Baydoun *et al.*, (1990) reported that following a 24hr L-Arg depletion, the intracellular concentration of L-Arg was greater than the EC_{50} for that of NOS, indicating that NOS should be saturated with L-Arg even under L-Arg depleted conditions. The controversy arises when cells were treated with NO agonists, such as Bradykinin, ATP or various cytokines, and the increase in NO release was accompanied by an increase in L-Arg uptake. This observation tends to show correlation between L-Arg influx and NOS activity. A plausible explanation might include the (1) compartmentalization of L-Arg in the cell, localization of NOS in the (2) membrane and the (3) caveolae of the cell, lowers the effective concentration of L-Arg. Furthermore, the stimulation of NO production would increase the transport of L-Arg to NOS (Bogle *et al.*, 1991). The immunofluorescence of porcine endothelial cells showed co-localization of NOS, caveolin and the L-Arg transporter (Closs *et al.*, 1999).

Chronic and acute administration of L-Arg improved endothelial function such as vasodilation, reduced platelet adhesion and aggregation, and regression of atherosclerotic lesions; this has been attributed to enhance NO formation (Preik-Steinhoff *et al.*, 1995).

2.1.3.2 Urea cycle:- The role of urea cycle, an integral part of L-Arg metabolism, is two fold. First it converts excess dietary nitrogen from net biosynthesis into urea, thus preventing the accumulation of ammonium and glutamine, which may cause encephalopathy. Secondly, it is a regulator of *de novo* biosynthesis and degradation of L-Arg. The urea cycle includes five enzymes catalyzing the formation of urea and intermediate substrates. Five well-described diseases (each with genetic and phenotypic variability) are resulted from the disorders of the urea cycle enzymes: deficiencies of carbamyl phosphate synthetase (CPSD), ornithine transcarbamylase (OTCD), argininosuccinic acid synthetase (ASD), argininosuccinase (ALD) and arginase (ARD).

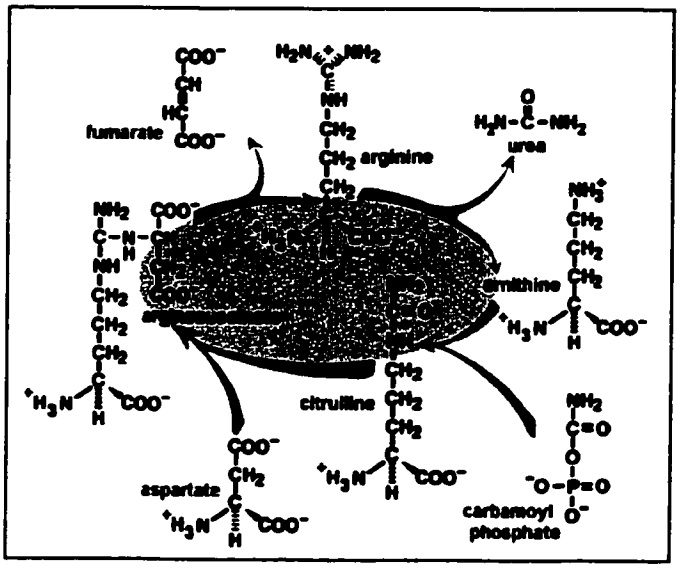

Fig 2.1.5 :- Urea Cycle

Diseases related to low L-Arg synthesis, ALD or ASD, are treated by supplementing the diet with L-Arg and reducing protein intake. Diseases derived from ARD are treated with a protein restricted diet. The pathophysiology of defective urea cycle enzymes results in hyperammonia causing an increase in intracranial pressure and cerebral edema leading to brain damage (Burton *et al.*, 2000).

2.1.4 L-Arg Transport

The transport of L-Arg and other cationic amino acids into the cell occurs primarily via System y^+, a member of the Cationic Transport (CAT) family. Other transporters of L-Arg include $B^{0,+}$ and y^+L , members of the Broad-scope transporter (BAT) family. The latter family also accepts neutral amino acids. These transporters are classified by the group of crossing amino acids through the membrane, and mode of transport.

Some of the other transporters on the cell membrane not directly involved in L-Arg transport are Systems A, ASC, and L. System A is a sodium-coupled transporter of neutral amino acids with lower affinity for branched or cyclic amino acids. System ASC is a sodium dependant transporter, which prefers linear amino acids such as alanine, serine and cysteine. Amino acids with an N-methyl group tend to serve as poor substrates for System ASC. An isoform of System ASC, System asc, exhibits the same amino acid preferences but is sodium independent. Finally, System L is a sodium independent transporter of bulky amino acids, such as leucine, and is in fact regulated by the availability of this amino acid (Reviewed Deves *et al.*, 1998; Christensen *et al.*, 1982; Chillaron *et al*, 2000; Kanai *et al.*, 1996).

2.1.4.1 System y^+:- System y^+ is a transmembrane protein comprised of 622 amino acids with 14 transmembrane domains. Initial controversy on the number of transmembrane

domains present in the transporter (12 or 14) was settled by immunohistochemical staining. The staining indicated that third and forth loops were present on the extracellular domain. This was in contrast to the 12 transmembrane model where the corresponding loops were located intracellularly. The total molecular weight was estimated to be 67kDa (Albritton *et al.*, 1989; Deves *et al.*, 1998; Woodward *et al.*, 1994). Two N-glycosylation sites were identified in the third loop of the 14 transmembrane model at Asn 223 and Asn 229 (Deves *et al.*, 1998). System y^+ is kinetically distinguishable from other transporters responsible for acidic and neutral amino acids. It catalyzes the flow of ω-guanidino amino acids such as L-Arg, lysine and ornithine. This transporter is sodium independent, pH insensitive, stereoselective and inhibitable by neutral acids (White *et al.*, 1982). L-Arg uptake is sensitive to membrane polarization and is found to be an indicator of membrane potential in human fibroblasts (Bussolati *et al.*, 1989). The hyperpolarization of the membrane results in increased activity of System y^+ and L-Arg uptake (Bussolati *et al.*, 1989).

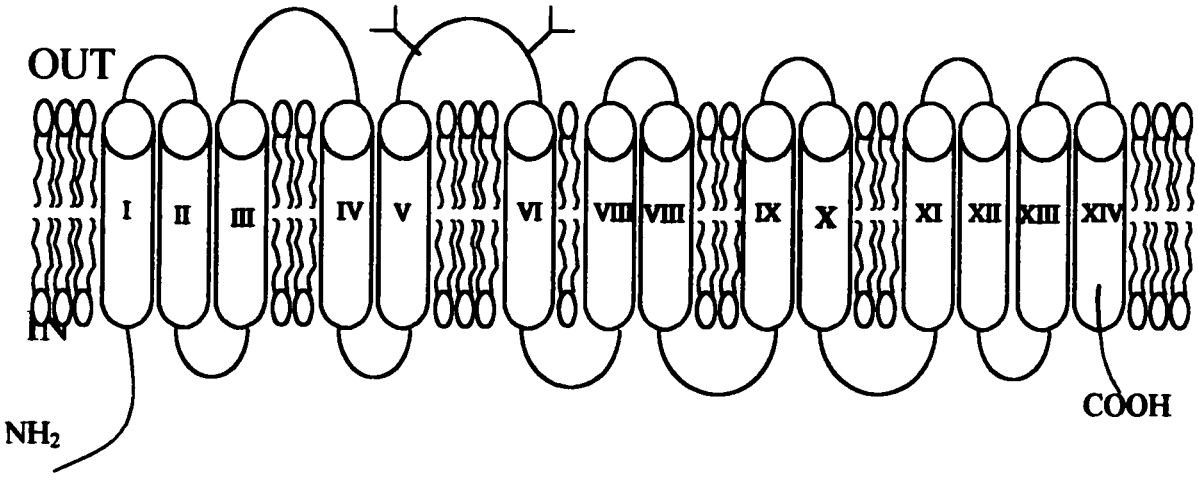

Fig 2.1.6 : Cationic Amino transporter (System y^+) (Deves *et al.*, 1998)

Christensen *et al.*, (1982) successfully demonstrated the importance of System y^+ and its kinetic mechanism. As previously stated, L-Arg is concentrated 10-20 fold within the cytosol by System y^+. Its affinity (K_M) for L-Arg, lysine, and ornithine is approximately 30-100μM. A positive correlation was demonstrated between the increasing number of methylene groups between the α carbon and the terminal cationic group and its strength of attraction to System y^+ (Wileman *et al.*, 1995). Although, α-N methylation reduces the interaction with System y^+, L-Arg analogs methylated at the guanido group are still transported. One such example is the NOS inhibitor N^G-monomethyl-L-Arg. Studies in fibroblasts and endothelial cells have shown that under physiological conditions, System y^+ is the primary transporter of L-Arg. As plasma concentrations increase and saturate System y^+, transport by other non-saturable transporters becomes more pronounced.

The mode of action by which System y^+ transports L-Arg involves a mobile carrier (White *et al.*, 1982). This transport has been best described as a iso uni uni reaction where the membrane component is able to interact with the substrates in the cytosol as well as in the extracellular environment. Upon binding to the substrate, the membrane protein undergoes isomerization. Consequently the substrate is translocated from one face to another. System y^+ exhibits a cycle of efflux and a cycle of influx. Fig 2.1.7, depicts the iso uni uni reaction where S1 & S2 are extracellular and intracellular substrates and Y1&Y2 are extracellular and intracellular transporters, respectively.

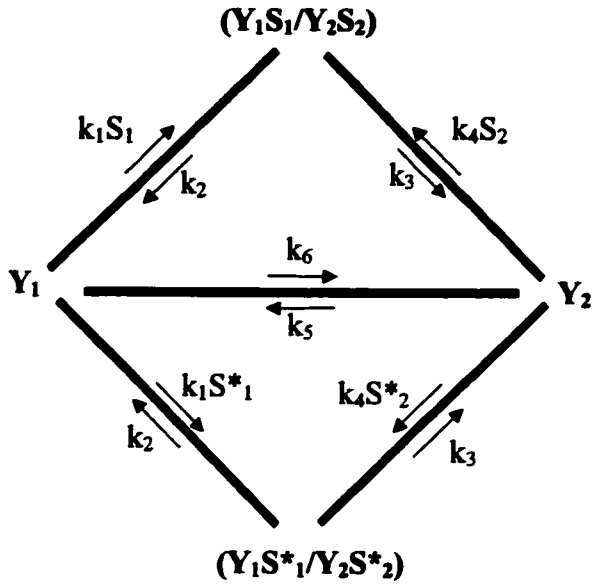

Fig 2.1.7: Transport of L-Arg by System y+ occurs in a Iso Uni Uni fashion (White *et al.*, 1982)

2.1.4.2 System y^+L:- System y^+ L is primarily found in human erythrocytes, intestine, and placenta and is derived from System L which transports neutral amino acids. Christensen *et al.*,(1982) observed that System L in addition to neutral amino acids also transports lysine. Hence it was coined as the lysine accepting system, System L^+, to express its positive charge tolerance. Further studies lead to the discovery of System y^+ L , referred to as the lysine-preferring agency, and by definition selective for cationic amino acids. The K_M of System y^+L for lysine is 10μM, much lower than System y^+. In the presence of Na^+ and Li^+, similar K_M values of neutral and cationic amino acids were also observed. Moreover, treatment with N-ethylmaleimide (NEM) inhibited System y^+ but not System y^+ L. This difference in reactivity has been used in transport studies to distinguish between System y^+ and System y^+ L. In comparison to System y^+, System y^+

L exhibits low maximal rates, indicating the low capacity or low expression of the carrier protein (Ribeiro *et al.*, 1999; Chillaron *et al.*, 1996; Deves *et al.*, 1992).

2.1.4.3 System $B^{0,+}$/ $b^{0,+}$:- This System is primarily found in the epithelia of the small intestine and renal tubules. Its function is to catalyze the uptake of cationic amino acids, and neutral amino acids in a sodium dependant manner. It transports the small neutral amino acids, alanine, serine, and any amino acids that are branched at the α and β C atoms. On the other hand, System $b^{0,+}$ catalyses similar uptake in a sodium independent manner. Preferred substrates for System $b^{0,+}$ are cationic amino acids and large α and β unbranched C atoms (Chillaron *et al.*, 1996).

At low concentrations ~1μM, System $B^{0,+}$ and $b^{0,+}$ account for most of the uptake of amino acids such as leucine, and lysine.

2.1.5 Cell-Cell Adhesion

The adhesive behaviour of cells to one another or to the matrix is important to their function and their localization. The binding of cells is mediated by a number of different metabolites. The biochemistry of these molecules provides information on the role of adhesion in cell migration and development. The regulation of these molecules are also targets for developing treatment for thrombosis, inflammation and cancer (Kries et al., 1993).

The adhesion of cells to other cells as well as the extracellular matrix occurs by an important family of transmembrane glycoproteins known as integrins. They are composed of various isoforms of α and β subunits to form dimers, which catalyze the binding of various ligands. Some integrins may bind various aggregatory factors while some dimers are specific to their ligand. It has been shown that integrins bind to fibronectin, vitronectin, collagen, von Willebrand factor, laminin and thrombospondin (Plow et al., 1985). Integrin (β1 and β3) binding of these proteins are important cell-matrix interactions where the cell adheres to the proteins of connective tissue.

On the other hand the binding of integrins to cell adhesion molecules (CAM) is import in cell-cell adhesion (Humphries et al., 1990). The following proteins are considered to be superfamilies of CAM required for cell-cell adhesion, immunoglobulins, cadherins, selectin and H-CAM. Immunglobulins and cadherins are an important family of proteins involved in tissue formation during embryonic development. They are found in various cell lines such as neuronal, epithelial and muscle cells. Cadherin molecules play a significant role in tumorogenesis, where the loss of cadherin molecules promotes the dissociation of tumour cells from parent cell. The inhibition of cadherin mediated cell-cell adhesion promotes the invasion of surrounding tissue and the formation of metastases (Frixen et al., 1991; Vleminckx et al., 1991). Selectin is primarily found in leukocytes, endothelial cells and platelets. In the presence of inflammatory agents, P selectin is expressed in the endothelial cells; consequently P-selectin mediates the aggregation of leukocytes on to the endothelium. Subsequently, the flow of leukocytes in the blood stream is slowed down. This process is known as rolling, following which the

leukocyte leaves the blood stream and migrates into tissue, known as extravasation. Continued inflammation in conjunction with the involvement of other selectin and immunoglobulin molecules will enhance aggregation of leukocytes to the endothelium (Butcher et al., 1991; Hynes et al., 1992).

2.1.5.1 Effect of NO on Cell Adhesion:- NO as a signaling molecule is discussed in section 1.1. In this section we discuss the role of NO as an anti-atherogenic molecule. NO inhibits the expression of the vascular cell adhesion molecule-1 (VCAM-1). VCAM-1 is expressed by endothelial cells in the presence of pro-inflammatory agents (Khan et al., 1996). The integrins of the leukocytes bind to VCAM-1 of endothelial to target inflammatory sites. The expression of VCAM-1 is modulated by the redox sensitive transcription factor NF-κB. NO and NO donors induce the expression of NF-κB inhibitor (IκB) and prevent the IκB degradation in the presence of cytokines. NO also inhibits the activation of the NF-κB by the cytokine (TNF-α). Specifically this inhibition occurs upon nitrosation of Cys-62 of NF-κB (Khan et al., 1996; Chen et al., 1999).

Increase in reactive oxygen species also promotes atherogenic behaviour. It has been reported that the expression of VCAM-1 is increased in the presence of oxidized lipoproteins (oxLDL), while no effects were detected with LDL and glycated LDL (Khan et al., 1995). Similar to NO, oxLDL also targets the redox sensitive transcription factor NF-kB. Depending on the amount of NO produced, NO may act as an anti-oxidant. The role of NO as an anti-oxidant is discussed in detail in section 1.1.8. NO inhibits Fe and Cu mediated oxidation of LDL and is involved in the chain termination step of lipid

peroxidation (Hogg et al., 1993). NO also reduces superoxide levels by reacting with endothelium derived superoxide to produce peroxynitrite. Therefore the effects of NO are two fold, it is capable of regulation of the expression of VCAM-1 as well as reduce the generation of oxygen derived free radicals.

The atherogenic effects are enhanced in hypercholesteremia while L-Arg treatment augments these effects. The role of NO on VCAM-1 expression and its reactivity with reactive oxygen species confirms its role as an anti-atherogenic molecule.

2.1.5.2 Effects of Homocysteine on Cell Adhesion:- HCys has been implicated in many aspects of the cell adhesion mechanism. Treating of endothelial cells with HCys and Cys have been shown to promote its detachment from the substratum. These observations were only noted with the use of amino acids containing sulfhydryl moieties. Since cystine has not been implicated in atherogenesis, it is believed that these findings might be relevant in defining the effects of HCys on the vascular System (Dudman *et al.*, 1991). Recently, HCys and oxidized low density lipoproteins (oxLDL) have been reported to be involved in a thrombogenic mechanism that enhanced the adhesion of platelets to endothelial cells. Incubating endothelial cells with HCys for 16hrs resulted in 2-3-fold increase in platelet adhesion and cell surface tissue factor activity. These aggregatory effects of HCys occur through fibrin formation (Dardik *et al.*, 2000). Pruefer *et al.*, (1999) have been able to successfully link the effects of HCys on NO metabolism to its aggregatory behaviour. Exposing the vascular wall for prolonged periods to high HCys concentrations increased the interaction between leukocytes and endothelial cells.

The down regulation of NO production by HCys is responsible for leukocyte rolling, adherence and transmigration. This finding was supported by the treatment of endothelial cells with NO donors, which inhibited the aggregatory effects of HCys (Pruefer *et al.*, 1999). Dudman and co-workers observed similar phenomena, where neutrophils were shown to interact with the endothelium in HCys treated cells. Neutrophils were also thought to bind to the endothelium and migrate, resulting in endothelium dysfunction leading to vascular damage (Dudman *et al.*, 1999).

With the relevant information available, Wang *et al.*, (1999) has proposed a hypothesis for vascular pathogenesis derived from the effects of HCys on cell adhesion. The effects of HCys on the vascular system that causes detachment and departure of endothelial cells are restored by repair mechanisms. However, prolonged exposures to HCys in conjunction with blood pressure, shear force, and phospholipids/cholesterol negatively affect the repair mechanism leading to enhanced inflammation. Its aggregatory behaviour promotes membrane-cytoskeleton association resulting in a rigid network enhancing the formation of vascular occlusions (Wang *et al.*, 1999).

2.1.5.3 Role of csPDI in Cell-Cell Adhesion:- The role of protein disulfide isomerase (PDI) and cell surface protein disulfide isomerase (csPDI) has been extensively discussed in section 1.1.4. In this section the role of csPDI as a modulator of cell-cell adhesion is discussed. The isomerization activity of PDI has been implicated in the adhesion of activated platelets and promotes binding of adhesion molecules in endothelial cells. CsPDI promotes aggregation by activation of the platelet glycoprotein GP IIaIIIb. The latter binds to the endothelial vitronectin receptors resulting in adhesion of the platelets to

the endothelium (Pearson *et al.*, 1999). Similar to endothelial cells, csPDI is also secreted by activated platelets. Its role in platelets is to catalyze thiol exchange reactions to expose fibrinogen and as mentioned above to activate the GP IIaIIIb receptor. The use of PDI inhibitors such as sulfhydryl reagents, bacitracin, and PDI antibody attenuated platelet aggregation and secretion. More importantly platelet aggregation and secretion were blocked by the presence of scrambled RNase A. This demonstrates the importance of the isomerization reaction catalyzed by csPDI for platelet aggregation (Essex *et al.*, 1999). Even though the promotion of platelet adhesion to endothelium results in vascular pathogenesis, it is a critical step in blood coagulation. To mediate adhesion, platelets express the following integrin receptors $\alpha_2\beta_1$, $\alpha_5\beta_1$, and $\alpha_{IIb}\beta_3$ to bind collagen, fibronectin, and fibrinogen. The binding was thought to occur by electrostatic interactions but the use of EDTA and weak ionic detergents did not interfere in the integrin mediated adhesion of platelet. The use of reducing agents did however disrupt collagen binding to integrin $\alpha_2\beta_1$. It has been shown that ecto-sulfhydryls are important in platelet adhesion and csPDI plays an important role in increasing the availability of free sulfhydryl during platelet adhesion (Lahav *et al.*, 2000).

2.2.1 Materials

Sigma-Aldrich (Oakville):- Glutathione (GSH, GSSG), Homocysti(e)ne, Cyst(e)ine, L-arginine, dansyl chloride, bovine serum albumin, Sephadex G-10 & G-25, scintillation fluid

Molecular Probes: - Monochlorobimane, monobromobimane, 2,7-dichlorofluorescein

Gibco-BRL (Burlington, ON):- DMEM media, F12K, Fetal bovine serum, Antibiotic antimycotic, Heparin, Endothelial Cell Growth Factor, Trypsin/EDTA, Trypan Blue

Panvera (Madison, WI):- Protein disulfide isomerase

American Type Cell Culture (Manassas, VA):- Hamster Lung fibroblast (CCL-93), HUVECs(HUVEC-CRL 1730)

Sarsdedt (Newton, NC):- 75cm^2 Cell culture flask, 35mm^2 petri dishes 25mm syringes and filters (0.2μm), 10mL pipettes, scintillation vials

2.2.2 Equipment

Beckman LS 6500 Multipurpose scintillation counter – Beckman Intruments Inc. (Mississauga, ON)

Centrifuge - Hettich Zentrifugen EBA 12, Rose Scientific, (Mississauga, ON)

UV/Vis Spectrometer - Agilent 8453, Agilent Technologies, (Mississauga, ON)

Fluorometer – Cary Eclipse, Varian (Mississauga, ON)

pH Meter -Orion 420A, Orion Research Inc. (Boston, MA)

Microcentrifuge tube centrifuge - Eppendorf Mixer 5423, VWR Scientific (Mississauga, ON)

Ultrasonicator – Transonic T420, Mandel Scientific (Toronto, ON)

Lyophilizer - Labconco Model 4451F, Labequip Limited (Markham, ON)

Weigh balance - Mettler AJ100, Mettler Instrumetn Corp. (Hightstown, NJ)

Brightline Hemocytometer, Reichter-Jung, Hausser Scientific (Horsham, PA)

Stirrer – Stirrer 360, VWR Scientific (Mississauga, ON)

BioRad HPLC System (Hercules, CA)

BioRad Econo System (Hercules, CA)

Binomic Controller BC 100(20/20 Technology Inc)

Zeiss Axiovert 200 microscope, Empix (Mississauga, ON)

Laminar Flow Hood, Nuare (Plymouth, MN)

Nuare Autoflow 5% CO2 regulated Incubator (Plymouth, MN)

2.3 Methods

2.3.1 Treatment with HCys:- HUVECs were grown to confluence in 35mm^2 petri dishes for NO measurements and fluorometric glutathione analysis. For total thiol determination, dichlorofluorescein assay and S-nitrosothiol assay cells were grown on cover slips. Cells were incubated for 6hrs with HCys (100μM) dissolved in complete F12K media. Following incubation cells were washed with PBS (pH 7.4).

2.3.2 L-Arg Transport:- HCys treated and control cells grown to confluence on coverslips were incubated in PBS for 1hour. Cells were incubated with varying concentrations of L-Arg (0-1mM), supplemented with 1.0μCi/mL ^{3}H-arginine (ICN), for 1min. Cells were washed with 4x1mL for 2mins. Non-specific counts were determined by incubating cells with 2.5M ^{3}H-arginine. The radioactive counts (cpms) of the cover slip in 10 mL of scintillation fluid, was obtained using a Beckman scintillation counter. Cell count was obtained using Trypan blue exclusion assay and L-Arg uptake was measured in pmol/min/10^6 cells. Rate of L-Arg uptake was also monitored in the presence of oxidized and reduced homocysti(e)ne, glutathione and cysti(e)ne. Cells were incubated with 100μM of each compound for 6hrs. Following 1hr L-Arg deprivation, cells were incubated for 1min with 100μM ^{3}H-arginine. Cells were washed and cpms were determined.

2.3.3 Total thiols:- HCys treated and control cells were incubated with PBS for 1hour. Cells were then incubated in 100μM monobromobimane (mBB) for 10mins. Time lapsed

study showed intracellular fluorescence of mBB attained saturation within 2min. Fluorescence intensity was determined using Zeiss Axiovert 200 fluorescent microscope and image analysis software, Nothern Eclipse 6.0. Fluorescence was also determined via a fluorescence microtiter plate reader, Gemini XS, Molecular devices and data was acquired by SOFT max Pro 3.1.2.

2.3.4 Glutathione Level:- HCys treated and control cells were incubated with PBS for 1h. Cells were scraped in 100μM monochlorobimane (mCB) in H_2O. Cell lysis was performed by ultra sonication for 5min and verified by Trypan blue exclusion assay. Glutathione-S-transferase (GST) (1U/mL) was added to cell homogenate and incubated for 30min on shaker. The fluorescence was determined using an Eclipse fluorescence microtiter plate reader from Varian. The amount of glutathione was determined by accounting for non-specific fluorescence obtained without the GST. Results are displayed with respect to control as 100%. Fluorescence of the cell lysate was determined via a fluorescence microtiter plate reader, Gemini XS, Molecular devices and data was acquired by SOFT max Pro 3.1.2. Additionally, fluorescence microscopy was utilized to capture intracellular mCB fluorescence.

2.3.5 Dichlorofluorescein:- HCys treated and control cells were incubated in PBS for 1h. Huvecs were incubated with varying L-Arg concentrations (0mM, 1mM, and 10mM) for 10min. Cells were then incubated in 10μM dichlorofluorescein diacetate for 1min. DCF fluorescence saturation was observed after 30sec of incubation. The cellular fluorescence was obtained using Zeiss Axiovert 200 fluorescent microscope and image

analysis software, Nothern Eclipse 6.0. Fluorescence (λ_{Ex} 390nm, λ_{Em} 478nm) was also determined via a fluorescence microtiter plate reader, Gemini XS, Molecular devices and data was acquired by SOFT max Pro 3.1.2.

2.3.6 NO Measurement:- After HCys treatment, cellular L-Arg was depleted by incubating in PBS for 1h prior to incubation with serum free media for 1h. The supernatant was added to 10mM ascorbic acid with final pH of 3.5. Evolution of NO was monitored by NO sensitive electrode, ISO-NOII. The data was obtained using Duo18, data acquisition system. Total amount of NO production was determined by integrating the area under curve using Origin 4.1. A standard curve was constructed to obtain μmoles of NO produced.

2.3.7 Preparation of Scrambled Rnase A:- Ribonuclease (30mg/mL) was incubated in 50mM Tris-HCl buffer, pH 8.6. 9M urea and 130mM DTT were added and reaction mixture was incubated for 1hr at 35^0C. The reaction was acidified with glacial acetic acid to pH 4 followed by an immediate elution from a G25 column. The sample was eluted using degassed sample of 0.1M acetic acid. The eluants were analyzed using a UV spectrometer, at 280nm. Concentration was determined using native ribonuclease as standard (0-20mg/mL). To the protein pool, urea (10mM) and sarcosine phosphate (0.1mM) were added. The pH was adjusted to 8.5 with 1M Tris. The protein samples were pooled and exposed to atmospheric O_2 at ambient temperature. Free thiol level in the sample was monitored via the DTNB assay over timed intervals for two days, where less than 1% was in the reduced form. The reaction mixture was acidified with glacial

acetic acid to pH 4 and eluted from Sephadex G-25 with 0.1M acetic acid. The protein pool was adjusted to pH 8 with 1M Tris and stored at 4°C.

2.3.8 PDI Assay with Scrambled RNase A:- PDI (1μM) was added to the reaction mixture containing GSH (2mM), GSSG(0.2mM) and scrambled RNase A (0.20mg/mL) in 0.1mM sodium phosphate buffer, pH 7.5. The reaction was incubated at 25°C for 15min. Cyclic GMP (0.28mg) was added and the incubation was further continued for 3mins. Absorbance at 285nm was measured as activity of PDI. Activity of PDI is measured by the activity of RNase A, and RNase A activity is defined as the amount required to hydrolysis cGMP to cause an increase in absorbance by $1x10^{-3}$. The readings were corrected for activity of reduced RNase A and absorbance of PDI.

2.3.9 Protein Disulphide Isomerase Transnitrosation Assay: PDI activity was determined by using DnsHcysNO as substrate. PDI inhibition studies were performed in triplicates with PDI (1μM) and DnsHCysNO (100 μM). The reaction was performed in PBS supplemented with 2mM GSH and 0.2mM GSSG. The data was obtained over 60secs at 100msec interval via a Cary Eclipse fluorometer.

2.4 Results

2.4.1 Effects of HCys on L-Arg uptake:- HUVECs and fibroblasts were treated with HCys to determine its effect on L-Arg transport. Uptake of [^{3}H]-L-Arg was saturable upon 2-5min incubation as determined from the time dependant kinetics (data not shown). Initial studies involved co-incubation of HCys and L-Arg in HUVECs and fibroblasts for 1min. Using varing L-Arg concentrations (25μM-1mM), the K_M for endothelial cells and fibroblasts were ~80μM. Co-incubation of L-Arg with varying concentrations of HCys (0-200μM) increased the K_M in both cell lines, (Fig 1, 2). The degree of inhibition of L-Arg uptake by HCys was determined using the K_I values obtained for HUVECs, 168± 3μM, and fibroblasts, 139± 4μM. The double reciprocal plots show competitive inhibition of L-Arg uptake by HCys upon co-incubation (inset Fig 1, 2).

HCys has been shown to affect various aspects of NO metabolism upon longer incubation periods. Here we incubated HUVECs and fibroblasts for 6h in media supplemented with varying concentrations of HCys (0-200μM). Longer incubation periods with HCys also inhibited L-Arg uptake in both cell lines with respect to control (Fig 3,4). The K_I values of HCys treated HUVECs was 101± 2μM, and fibroblasts was 90 ±1μM. The degree of inhibition increased upon longer incubations with HCys by 35-40% for HUVECs and fibroblasts in comparison to co-incubation studies. The double reciprocal plots indicate a mixed inhibition of L-Arg uptake in HCys treated cells as opposed to the competitive inhibition observed with co-incubation of HCys (inset Fig 3,4).

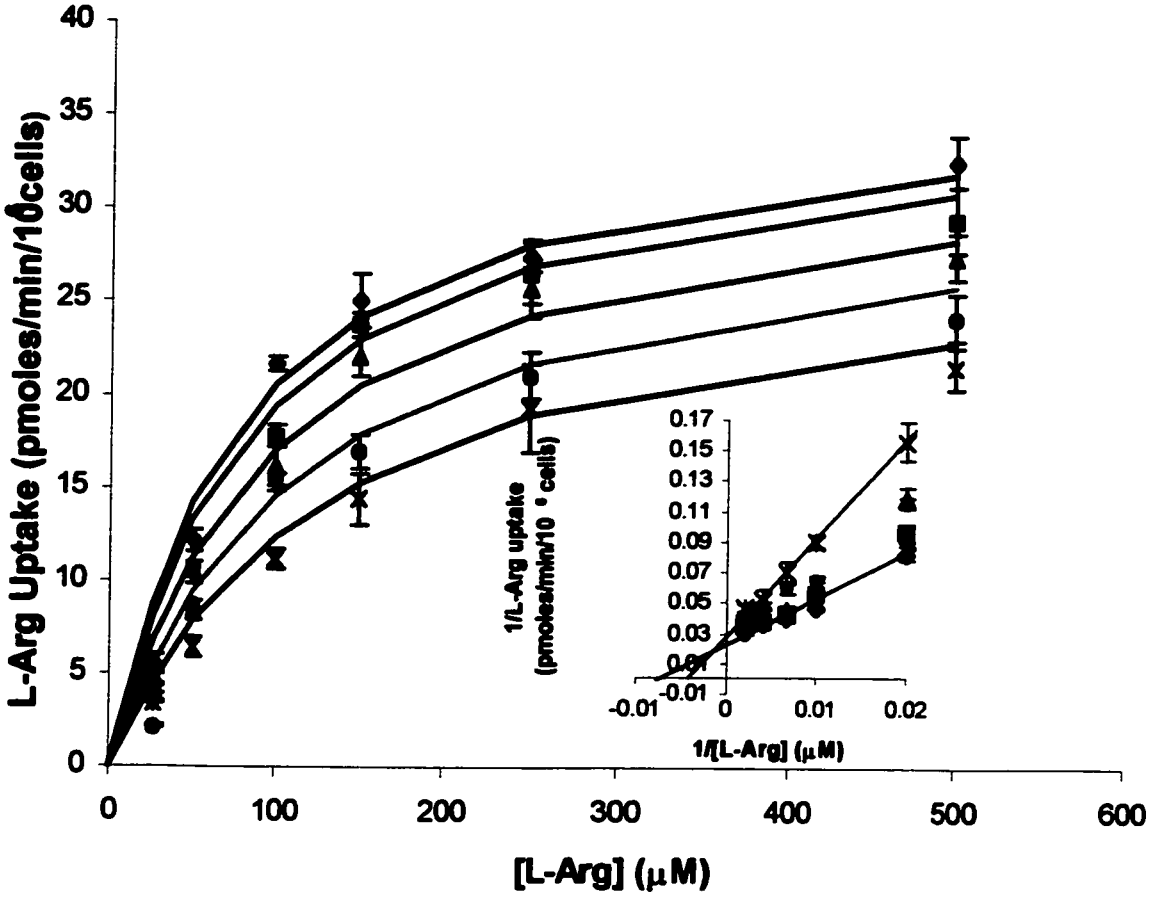

Fig 2.4.1:- Uptake of L-Arg in the presence of HCys in Hamster lung fibroblasts. Following a 1hr Arg depletion, labeled ^{3}H-Arg (0-0.5mM) was co-incubated with HCys (control, diamonds; 10μM, squares; 50μM, triangles; 100μM, circles; 200μM, asterisks) for 1min. The cells were washed 3 times with 1mL PBS for 1min, and the counts were obtained using a Beckman Scintillation counter. The counts were corrected for background and non-specific binding. The error bars represent standard deviation (n=6). The inset represents the double reciprocal plot of the saturation plot.

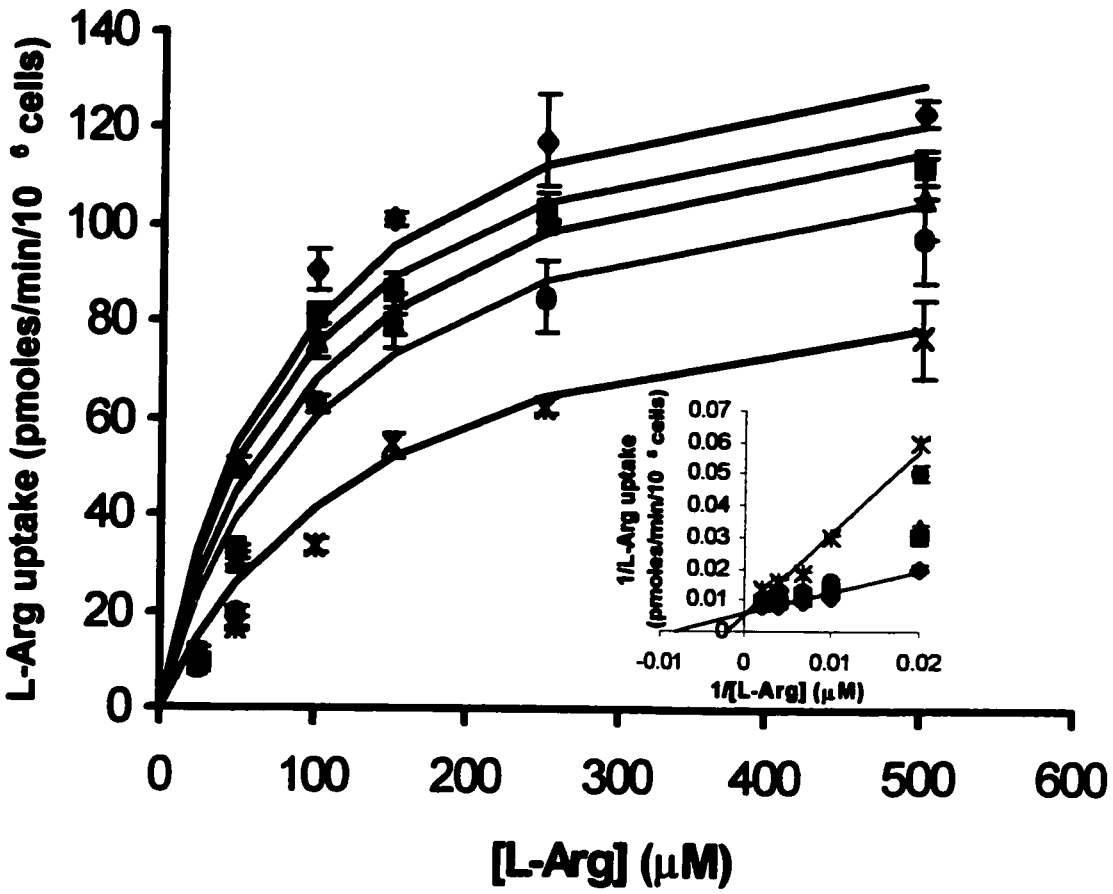

Fig 2.4.2:- Uptake of L-Arg in the presence of HCys in HUVECs. Following a 1h Arg depletion, labeled ^{3}H-Arg (0-0.5mM) was co-incubated with HCys (control, diamonds; 10μM, squares; 50μM, triangles; 100μM, circles; 200μM, asterisks) for 1min. The cells were washed 3 times with 1mL PBS for 1min, and the counts were obtained using a Beckman Scintillation counter. The counts were corrected for background and non-specific binding. The error bars represent standard deviation (n=6). The inset represents the double reciprocal plot of the saturation plot.

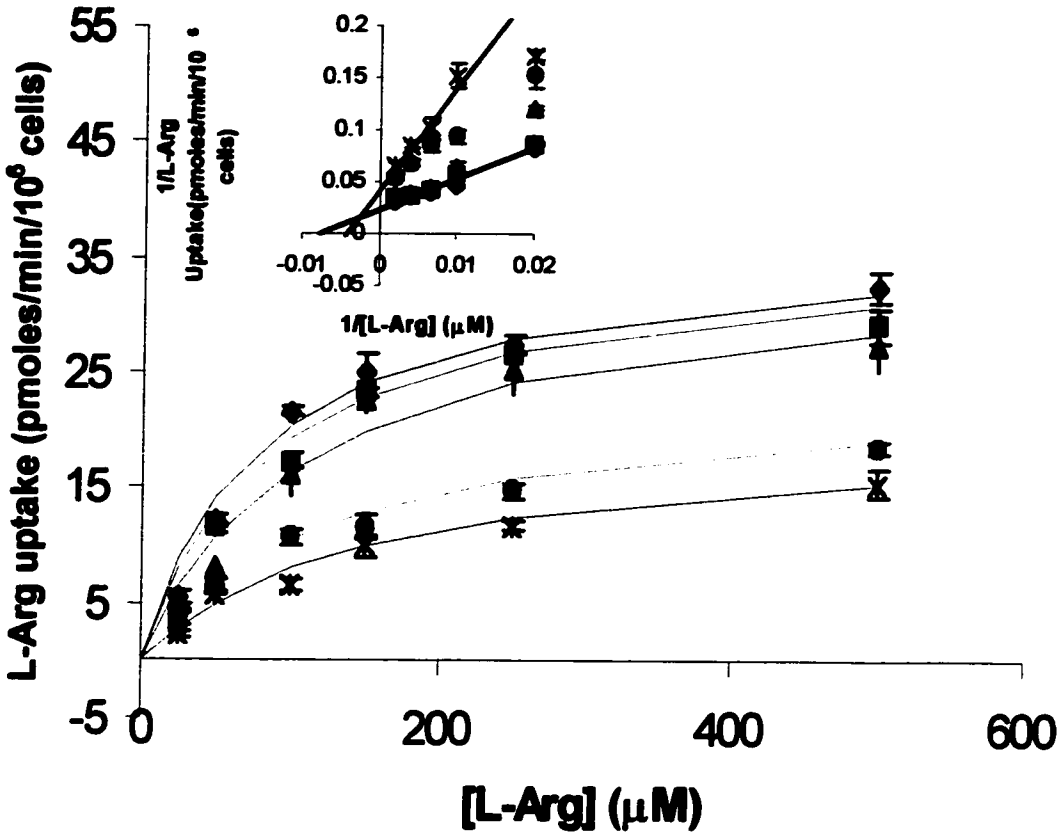

Fig 2.4.3:- Uptake of L-Arg in Hamster lung fibroblasts pretreated with HCys. Cells were incubated with HCys(control, diamonds; 10μM, squares; 50μM, triangles; 100μM, circles; 200μM, asterisks) for 6hrs prior to Arg transport study. Following a 1hr Arg depletion, transport study was conducted with Labeled ^{3}H-Arg (0-0.5mM). The cells were washed 3 times with 1mL PBS for 1min, and the counts were obtained using a Beckman Scintillation counter. The counts were corrected for background and non-specific binding. The error bars represent standard deviation (n=6). The inset represents the double reciprocal plot of the saturation curve.

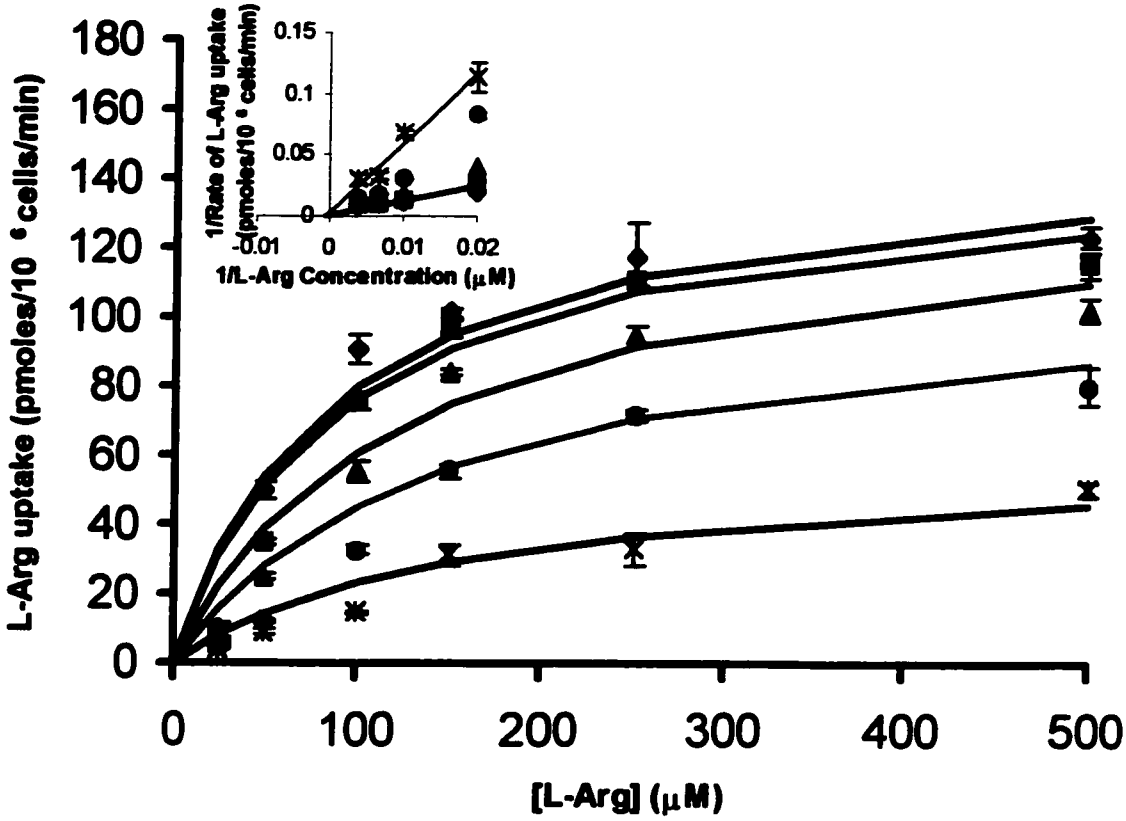

Fig 2.4.4:- Uptake of L-Arg in HUVECs pretreated with homocysteine. Cells were incubated with HCys (control, diamonds; 10μM, squares; 50μM, triangles; 100μM, circles; 200μM, asterisks) for 6hrs prior to Arg transport study. Following 1h Arg depletion, transport study was conducted with Labeled ^{3}H-Arg (0-0.5mM). The cells were washed 3 times with 1mL PBS for 1min, and the counts were obtained using a Beckman Scintillation counter. The counts were corrected for background and non-specific binding. The error bars represent n=6. The inset represents the double reciprocal plot of the saturation curve.

In most studies, cells are treated with HCys to determine its effects on cell metabolism, however HCys in the plasma is found predominantly in the oxidized form ($HCys_2$) or in mixed disulfides (80%) (Welch *et al.*, 1998). Our study showed that upon long-term incubations the complete oxidation of HCys in media and buffer occurs within 2-3h, Fig 5. Therefore, we observed L-Arg uptake in HUVECs upon longer incubations (6h) with HCys and $HCys_2$. The uptake of L-Arg (100μM) in HCys (100μM) treated cells was reduced by 38±2% while a 52±3 % reduction was observed in $HCys_2$ (100μM) treated cells. Control study involving both redox forms of glutathione and cysteine did not show significant changes in L-Arg uptake.

2.4.2 NO production:- To this end, it is conceivable that the effects of HCys may also affect NO production. To this, HUVECs were pre-incubated with HCys as previously described for 6h. NO production in HCys treated cells was stimulated by 1mM L-Arg. The level of NO secretion was determined after the addition of ascorbic acid which accelerates the reduction of NO_2 to NO. The generation of NO was monitored over time, (Fig 7A). The total amount of NO evolved from the supernatant was calculated from the area under the curve, (Fig 7B). HCys treated HUVECs produced lower levels of nitrite, 3.44 μmoles/10^6cells, than the control, 5.23μmoles /10^6 cells. Since nitrite levels are indicative of NO production, a 34% reduction in NO production was observed in HCys treated cells.

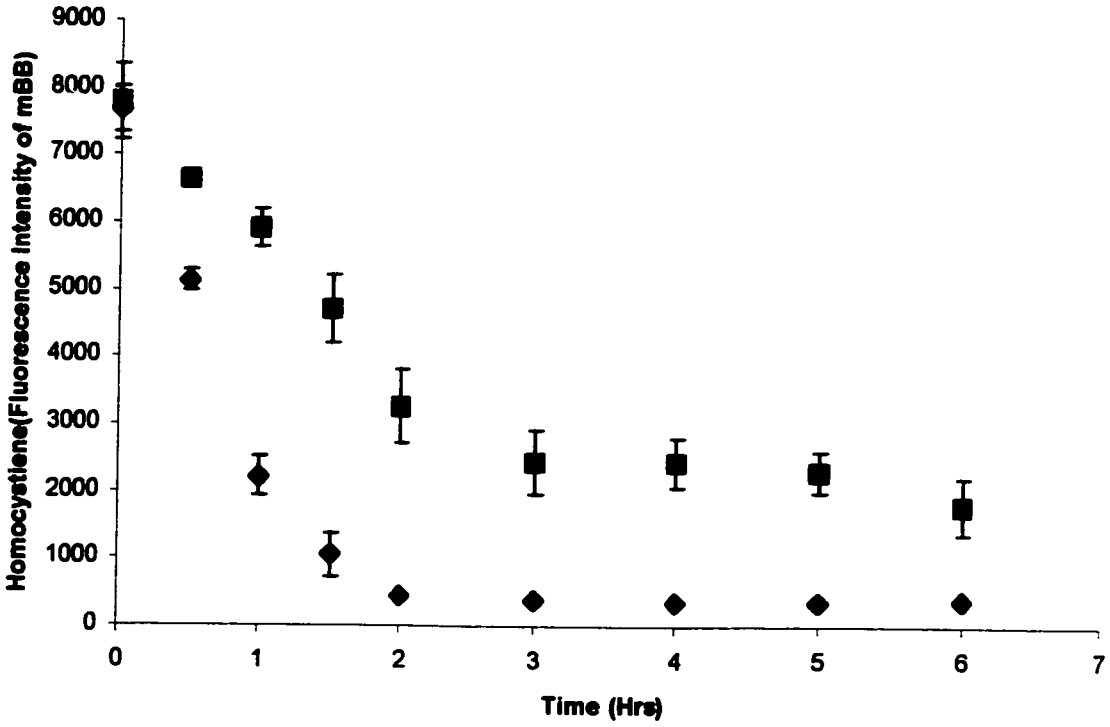

Fig 2.4.5:- Oxidation of HCys in media + HUVECs (squares) and in PBS (diamonds). HCys (200μM) was incubated in cell culture oven (37°C, 10% CO_2) for 6h. Oxidation of thiols was monitored at specified intervals by the fluorescence of monobromobimane (mBB). Both assays were performed in microtiter wells, however a microtiter with confluent HUVECs were used for the assay in media. The data was corrected for background and nonspecific and the error bars represent standard deviation (n=5).

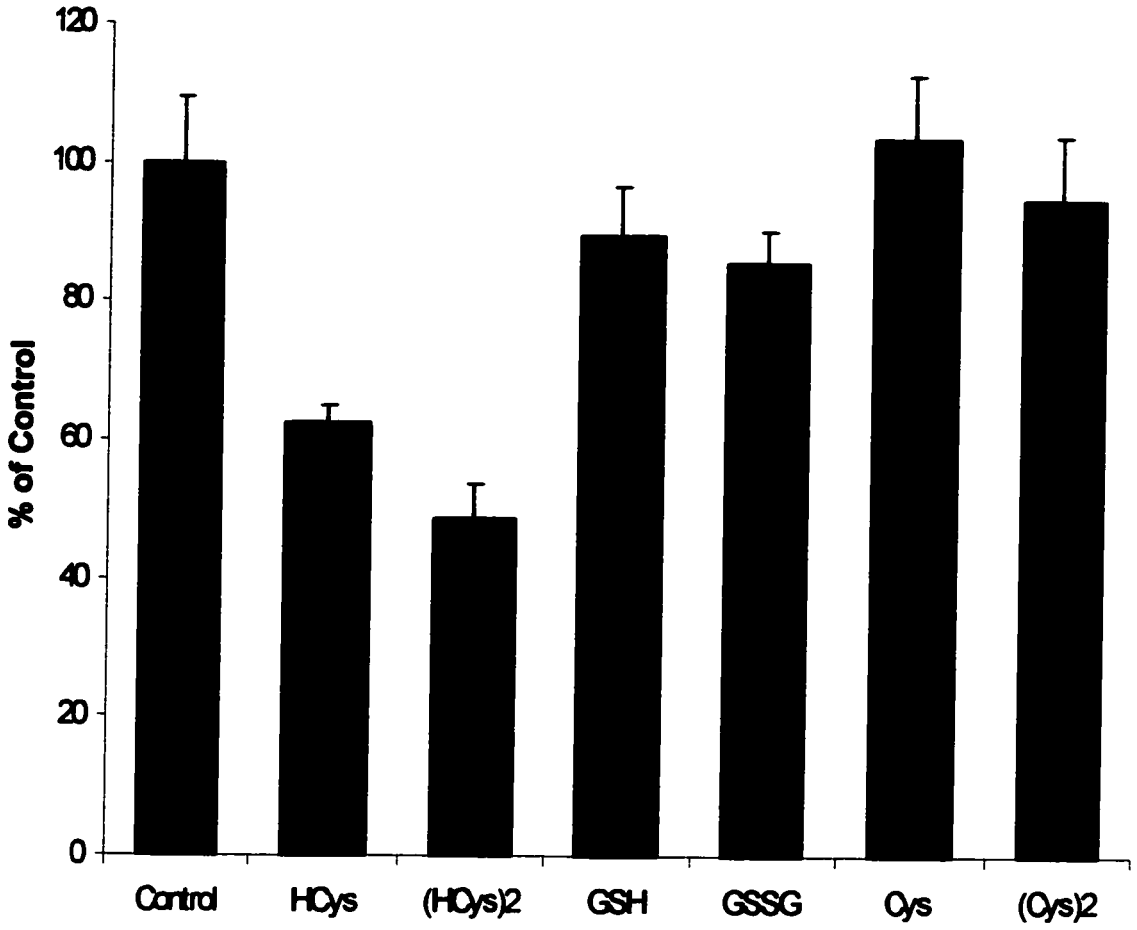

Fig 2.4.6:- Effects of various oxidized and reduced thiols on the Uptake of L-Arg in Huvecs. Cells were incubated with 100μM amounts of homocysti(e)ne, cysti(e)ne and oxidized and reduced glutathione for 6h. Following Arg depletion, rate of uptake was determined by 1min incubation with 100μM ^{3}H-Arg. The cells were washed and the counts were determined by a Beckman scintillation counter. The error bars represent standard deviation (n=5) and the data is represented as percent change with respect to control.

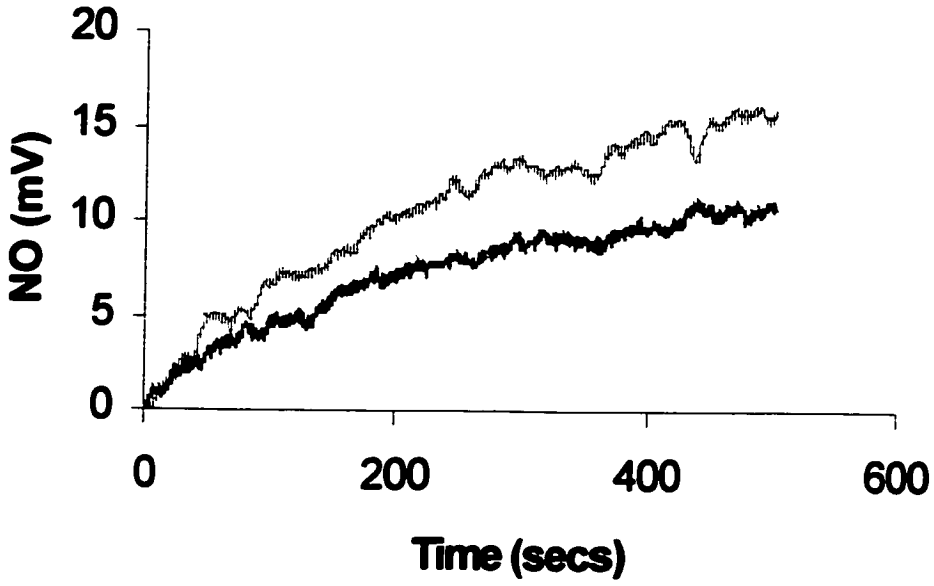

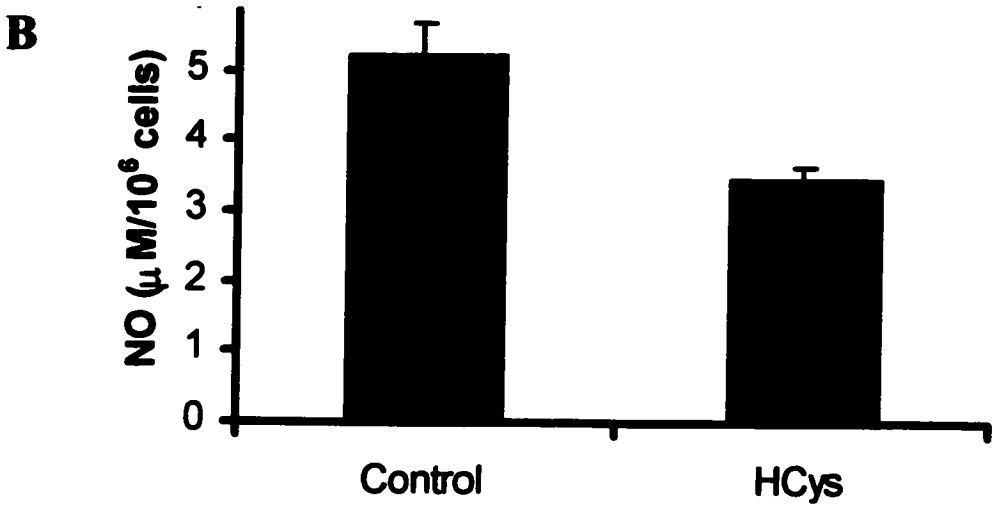

Fig 2.4.7:- NO levels in HCys treated HUVECs. Cells were treated with 100μM HCys for 6hrs. Following 1hr Arg depletion, cells were incubated with 1mM Arg for 2hrs. The NO levels were detected using the NO specific electrode and the media supplemented with 100mM ascorbic acid. Fig A, represents detection of NO by electrode. Fig B, represents area under the curve (Fig A), and error bars correspond to standard deviation (n=6).

2.4.3 Oxidative Stress:- The role of HCys on NO production may influence the intracellular redox status. In this study a membrane permeable fluorescent probe, dichlorofluorescein diacetate (DCF), was used as a measure oxidative stress. The probe is oxidized in the presence of ROS, specifically by superoxide, yielding a highly fluorescent product. The intracellular fluorescence of the oxidized DCF is a indicative of ROS levels. Common DCF assays are performed in cell lysate, however we attempted to utilize fluorescence microscopy to probe the redox status of the cell. The uptake of DCF in cells was monitored over 3min, (Fig 8B). DCF uptake was saturable within 30sec of incubation. HCys treated cells (100μM, 6h) and controls were then incubated with varying concentrations of L-Arg (0,1mM, 10mM) for 10mins at which point DCF was added for 30sec. The change in fluorescence was corrected for respective controls at various L-Arg concentrations, (Fig 8). An ~80% increase in superoxide production was observed in HCys treated cells in the absence of L-Arg. HCys treated cells in the presence of 1mM L-Arg reduced ROS production by 30±1% in comparison to HCys treated cells in the absence of L-Arg. While treatment with 10mM L-Arg further decreased cellular ROS levels by 40± 2% from HCys treated cells in the absence of L-Arg.

2.4.4 Thiol levels:- Perturbations in the intracellular redox environment are expected to affect the cellular reducing pool, which is predominantly maintained by glutathione. In this study we measured the total cellular thiol concentration using monobromobimane (mBB), a thiol specific fluorescent dye. While cellular glutathione levels were determined using monochlorobimane (mCB), glutathione specific fluorescent dye. HCys

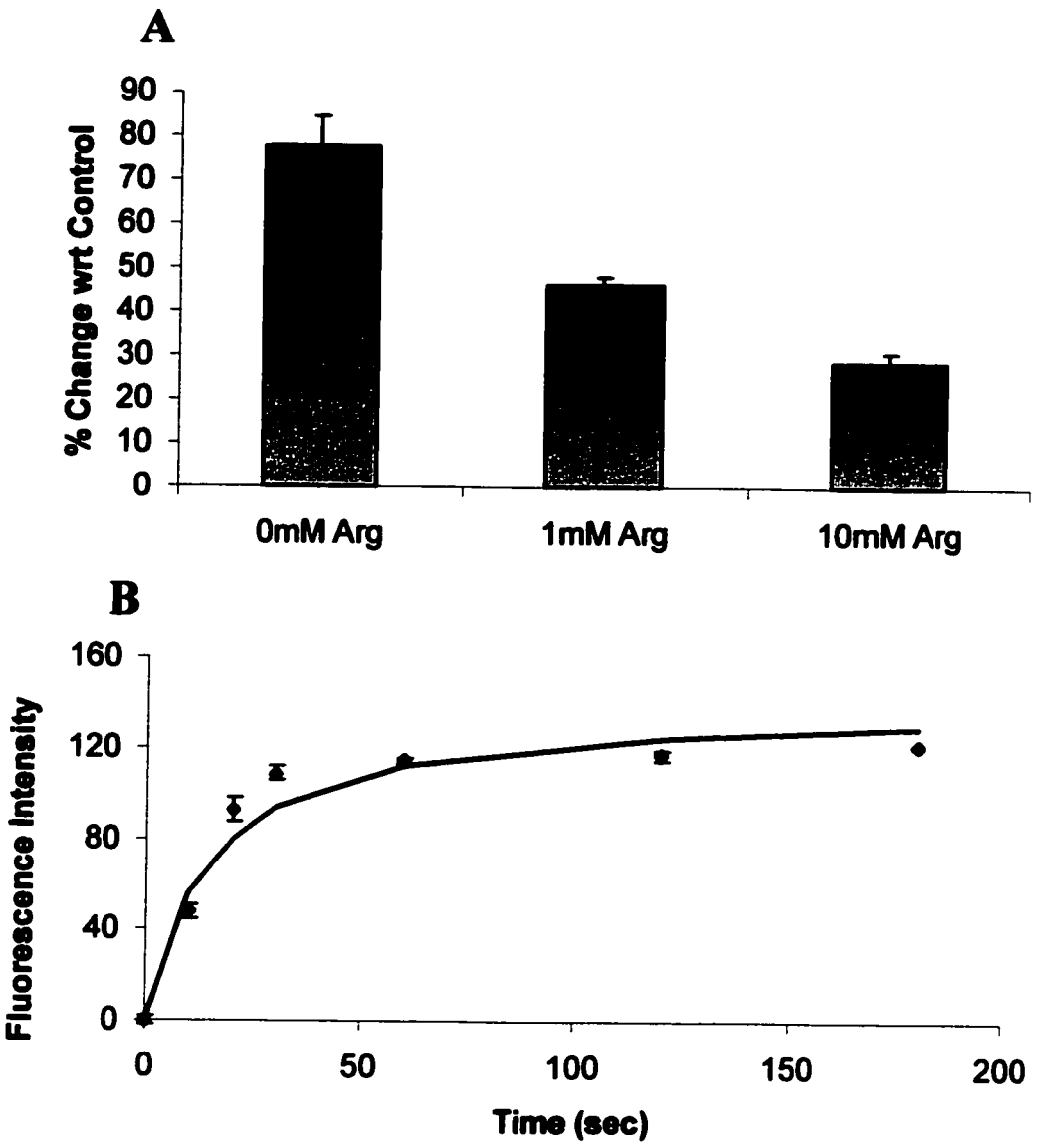

Fig 2.4.8:- (A) Oxidative stress in HUVECs treated with HCys. HUVECs incubated with HCys (100μM) for 6hrs were then incubated for 10min with varying concentrations of L-Arg (1-10mM). The intracellular ROS levels were detected by incubating the cells for 1min with DCF (10μM). The readings were corrected for by the control performed with varying concentrations of L-Arg (0-10mM). The fluorescence intensity was determined by fluorescence microscopy using Leica Axiovert 200 and image analysis software, Northern Eclipse 6.0. (B) Time dependant saturation of DCF fluorescence. Incubation with DCF (10μM) was carried out at varying time intervals upto 3mins. Error bars represent standard deviation (n=6).

treated (100μM, 6h) and control cells were incubated with both dyes for 10mins prior to fluorescence imaging. Using mBB, total thiol levels of HCys treated cells increased by 34% over control cells, (Fig 9). Fluorescence imaging with mCB showed ~50% increase in glutathione levels, (Fig 10 images). To support the data obtained from fluorescence imaging with mCB, the conventional assay of the cell lysate was performed. Incubating the cell lysate with mCB in the presence of γ-GST increases the sensitivity and specificity of the glutathione assay. Using this protocol, the cellular glutathione concentration increased by 54±3% in HCys treated cells, Fig 10.

2.4.5 RSNO Transport:- This study has shown that HCys reduces the uptake of extracellular L-Arg and NO secretion. The effects of HCys/$HCys_2$ on RSNO uptake were then determined. The novel probe, N,N-didansylhomocystine, was utilized to study the effects of HCys/$HCys_2$ on S-nitrosothiol transport.

HUVECs were treated with both redox forms of HCys/$HCys_2$ (100μM) for 6h. Pre-treatment with HCys inhibited BSA-NO uptake, where a ~55% increase in K_M was observed in HCys treated cells, (Fig 11A). $HCys_2$ was also found to inhibit BSA-NO uptake. The K_M of the $HCys_2$ treated cells, 30±2μM, was ~75% higher with respect to control cells, 17±2μM, (Fig 11B). These inhibitory effects of HCys/$HCys_2$ are only evident upon 6h pre-treatment, when studies involving short treatments (10min) of HCys showed no significant inhibition, (Fig11C). Our control study involved the uptake of BSA-NO in oxidized glutathione (GSSG) treated cells, also resulting in no significant effects, (Fig 11D).

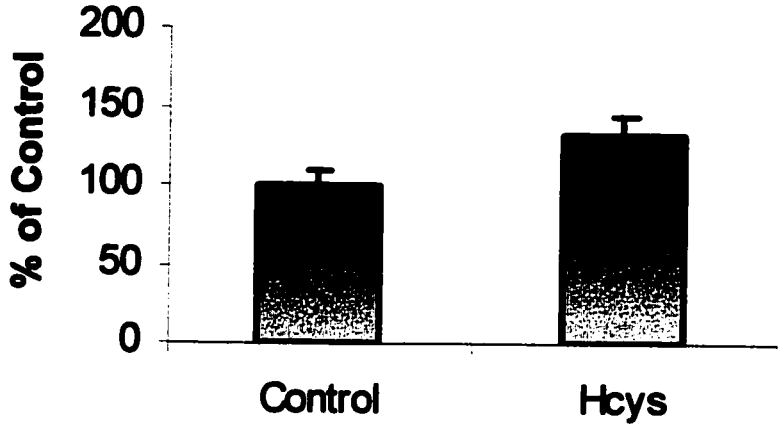

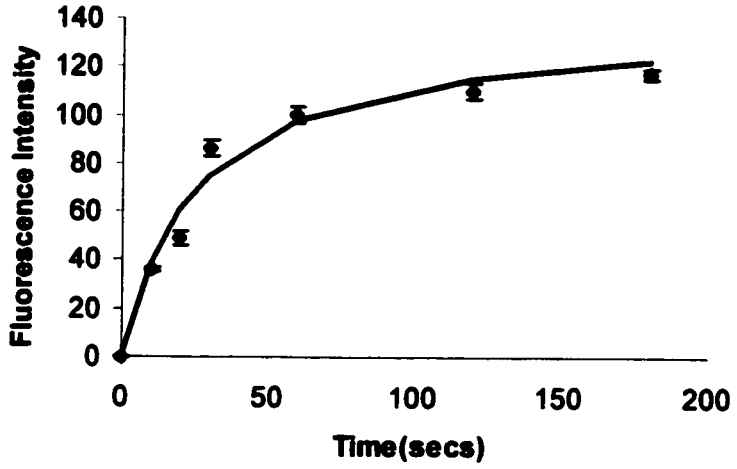

Fig 2.4.9:- (A) Total thiol levels in HUVECs treated with HCys. Cells incubated in 100μM HCys for 6hrs were lysed and incubated with monobromobimane (mBB). A fluorescence plate reader determined the fluorescence and corrected for background. (B) Time dependant saturation of mBB fluorescence. Intracellular mBB fluorescence was monitored over varying time intervals up to 3mins. The error bars represents standard deviation (n=5).

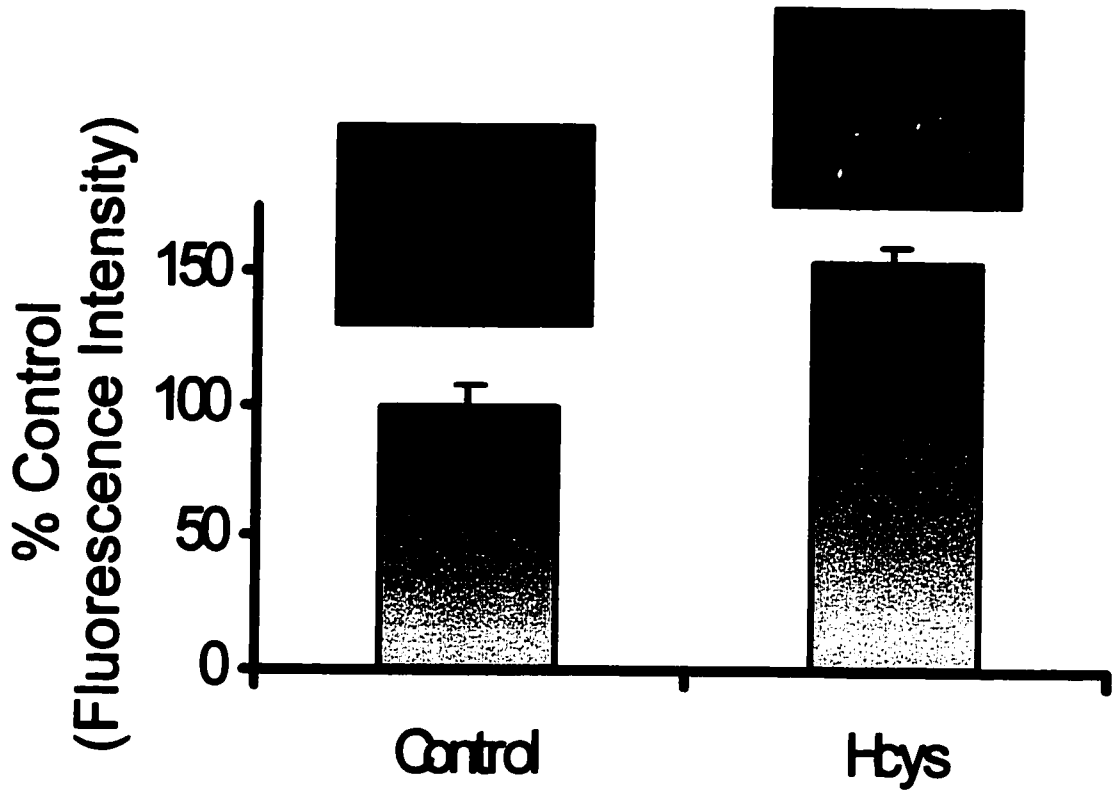

Fig 2.4.10:- Glutathione levels in HUVECs treated with HCys. Cells incubated in 100μM HCys for 6hrs were lysed and incubated with monochlorobimane (mCB) and glutathione-S-transferase. A fluorescence plate reader determined the fluorescence and corrected for background. The error bars represents standard deviation (n=5). Fluorescence microscopy images were also obtained of cells incubated with mCB.

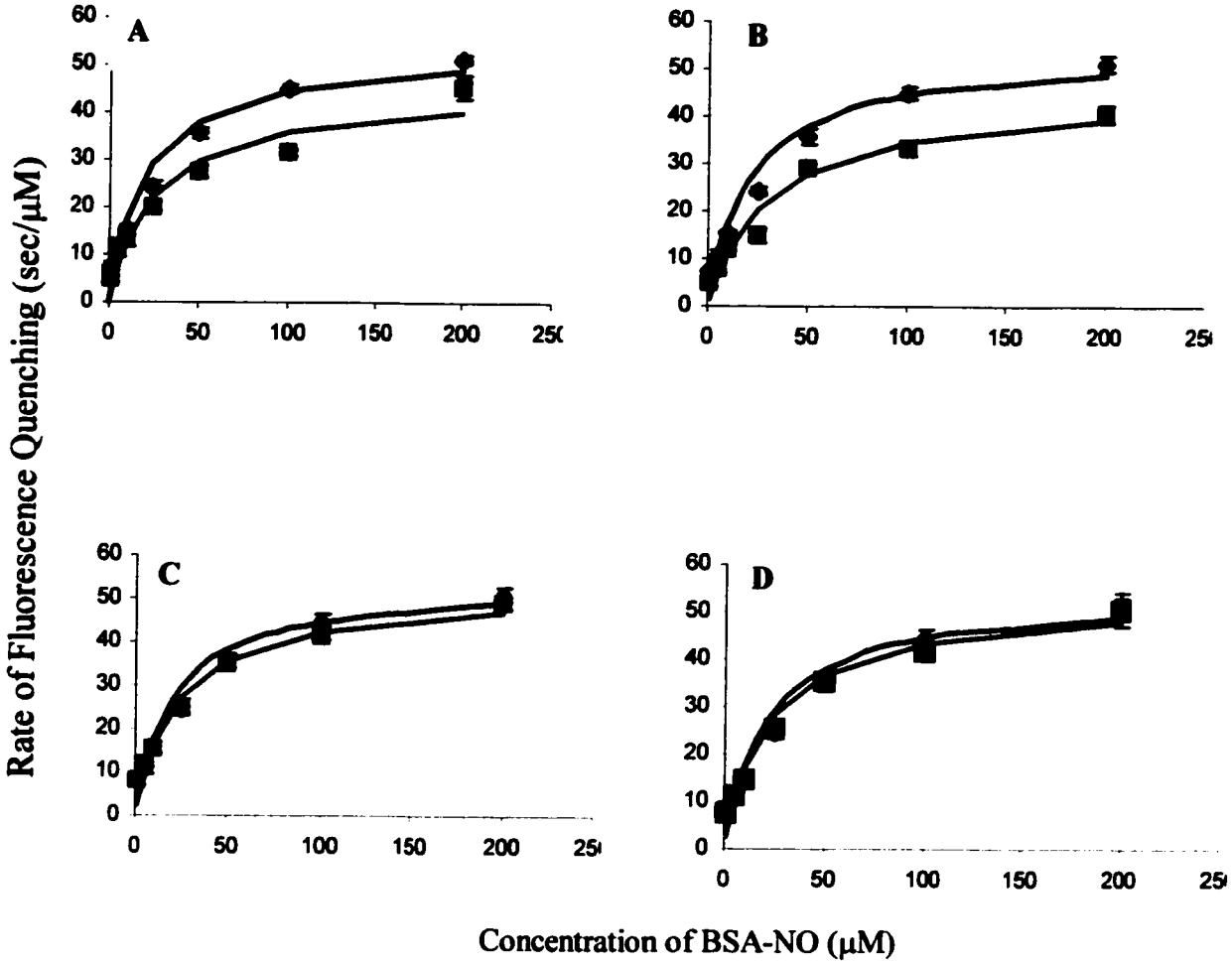

Fig 2.4.11:- BSA-NO uptake monitored using the N,N-didansylhomocystine fluorescent assay for S-nitrosothiols. HUVECs were treated with (A) HCys (100μM) for 6h (B) $HCys_2$(100μM) for 6h (C) $HCys_2$ (100μM) for 10min (D) GSSG (100μM) for 6h. Transport of BSA-NO (0-200μM) was monitored by fluorescence quenching. Change in fluorescence was determined using Leica Axiovert fluorescent microscope and image analysis software, Northern Eclipse 6.0. The data represents standard deviation (n=6).

2.4.6 PDI catalyzed in vitro denitrosation activity:- RSNO transport is mediated by csPDI. Therefore it is conceivable that the effects of $HCys_2$ on RSNO transport may stem from its effects on csPDI activity. In an attempt to understand the role of $HCys_2$ in PDI-catalyzed reactions, a novel substrate was utilized to probe the *in vitro* transnitrosation activity catalyzed by PDI. DnsHCysNO (200μM) was incubated with PDI in a sodium phosphate buffer supplemented with GSH (2mM)/GSSG (0.2mM). The removal of the NO moiety by PDI generates a highly fluorescent DnsHCys. The increase in fluorescence was monitored as a measure of PDI activity. A few precautions were taken to ensure accurate measurement of PDI activity. The photolysis of DnsHCysNO was minimized by reducing excitation slit width. The background transnitrosation activity of thiol buffer system was accounted for. As such, incubation with of 100μM $HCys_2$ inhibited the transnitrosation activity of PDI by 20±3% but not with GSSG, (Fig 12).

2.4.7 PDI catalyzed in vitro isomerization activity:- Since PDI catalyses reduction, oxidation and isomerization reactions, we assayed PDI isomerization activity with scrambled RNase A as substrate. PDI activity was determined by the rate of cGMP hydrolysis by recovered active RNase A, Fig 13. Precautions were taken to account for both the background activity of RNase A in the absence of PDI, and also the absorbance of PDI, itself. Isomerization activity observed in the presence of $HCys_2$ and GSSG was not significantly different from that of control.

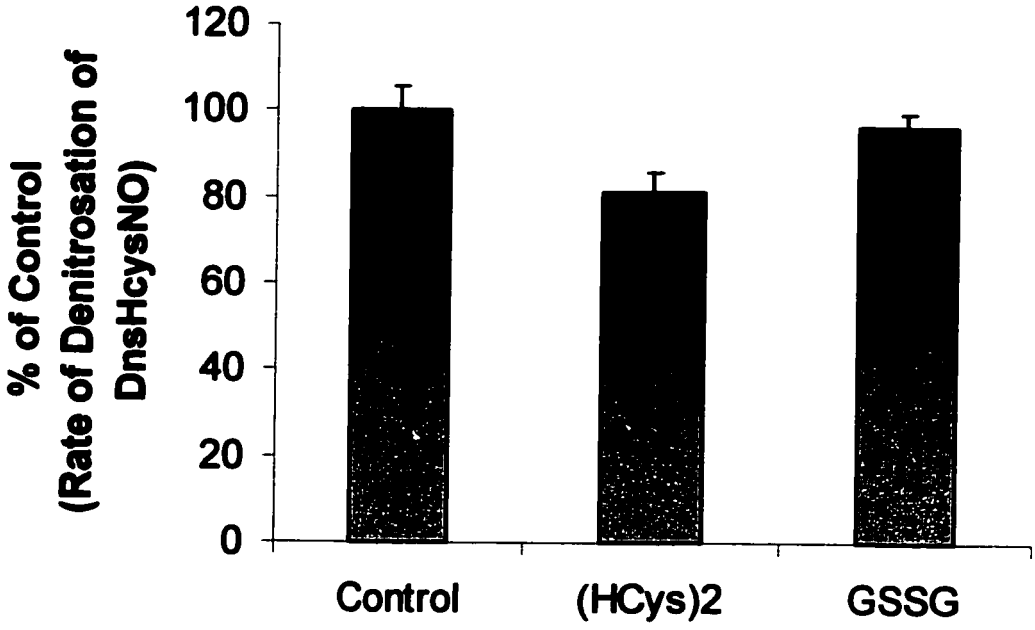

Fig 2.4.12:- Effects of $HCys_2$ and oxidized glutathione on the PDI catalyzed denitrosation of DnsHcysNO. PDI (1μM) was added to a reaction mixture containing 100μM DnsHCysNO, 2mM GSH, and 0.2mM GSSG. The Increase in fluorescence was monitored by Varian Fluorometer and the data was acquired by Eclipse. The data was corrected for background fluorescence, and minimal photodegradation of sample. The error bars represent standard deviation (n=3).

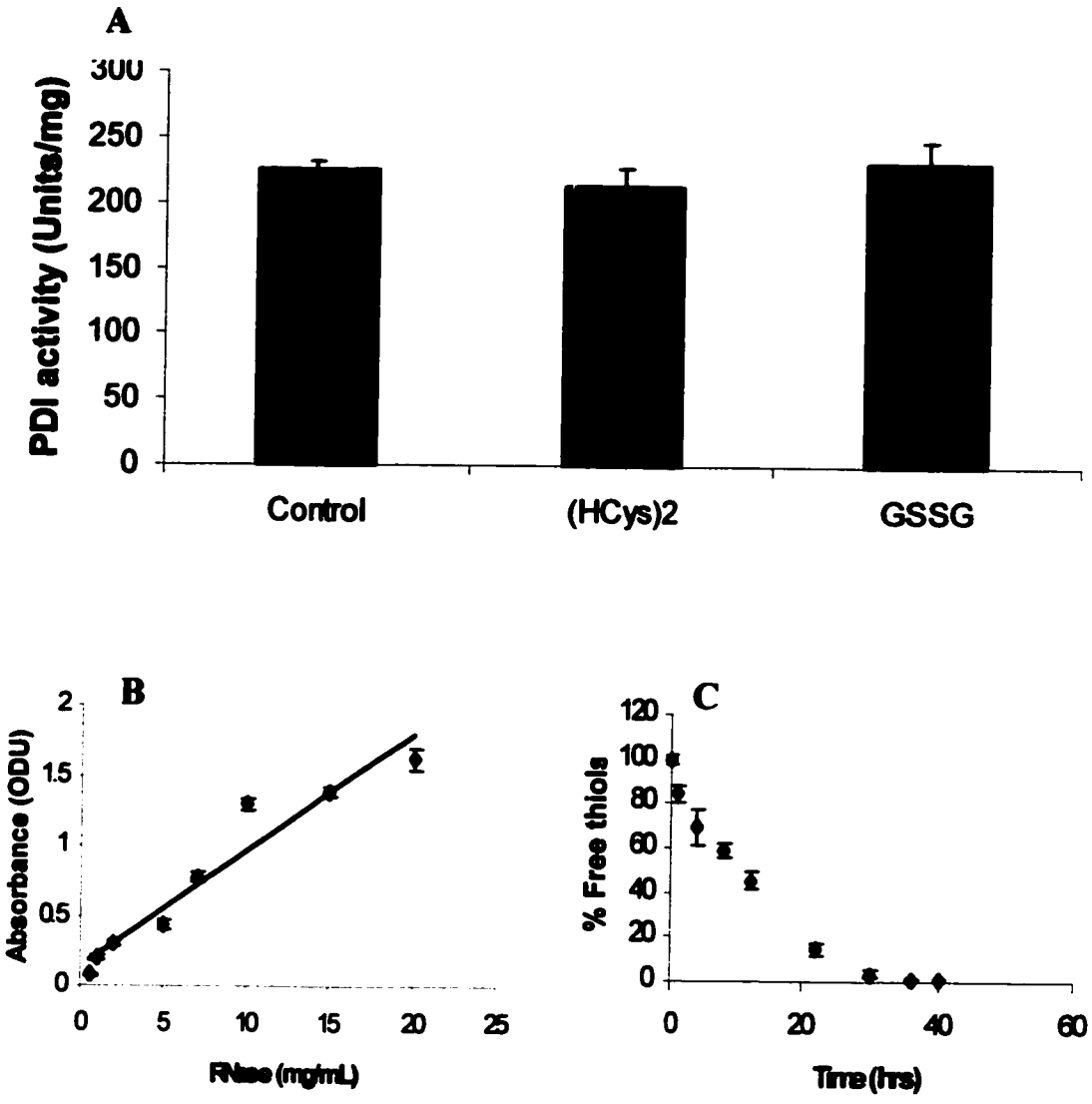

Fig 2.4.13:- Reactivation of Ribonuclease A by PDI in the presence of oxidized glutathione (100μM) and homocystine (100μM). (A) PDI activity is determined by the amount of RNase A activated which is monitored by amount of cGMP hydrolyzed. Hydrolysis was measured by A_{285nm} and background activity of PDI was accounted for. (B) RNase A standard curve was generated using varying concentrations of reduced RNase A at A_{280nm}. (C) Re-oxidation of RNase A was monitored by DTNB assay. Oxidation was monitored over a 40hr period.

2.5 Discussion

2.5.1 Effects of HCys/$HCys_2$ on L-Arg transport

There is a growing interest in the effects of HCys/$HCys_2$ on NO metabolism. It has been shown that the bioavailability of NO is decreased upon incubation with HCys (Upchurch *et al.*, 1997). This decrease is caused by the formation of HCysNO, which does not exhibit the similar toxic effects of HCys. Alternatively, lower NO levels may arise from changes in NOS expression and activity, studies related to these effects have been discussed in sections 1.1.1.1 to 1.1.1.6. Our study entails the effects of HCys/$HCys_2$ on other aspects of NO metabolism, such as L-Arg transport. L-Arg is a vital substrate for NOS, and is transported by the System y^+ transporter. This transport system affects the transmembrane traffic of positively charged amino acids such as L-Arg, lysine and ornithine (White *et al.*, 1981; Reviewed in Deves *et al.*, 1998 and Cheeseman *et al.*, 1991). System y^+ maintains a two fold greater intracellular [L-Arg] than that of extracellular (Preik-Steinhoff *et al.*, 1995). Initially it was thought that NO production by NOS might be independent of extracellular L-Arg. However, NO production can be stimulated by addition of extracellular L-Arg (Zhang *et al.*, 2000). Casey *et al.*, (2000) have suggested that compartmentalization of either NOS or L-Arg like Ca^{+2} may explain the observed phenomena.

Our results have indicated that longer incubation of endothelial cells with HCys/$HCys_2$ results in the attenuation of L-Arg uptake. Simultaneously the co-incubation of HCys with L-Arg also inhibited L-Arg transport. Since Cys/Cys_2 are minimally transported via System y^+, this inhibition could possibly be attributed to competitive uptake of HCys. L-Arg transport in HUVECs and fibroblasts were greatly inhibited upon pre-treatment with HCys/$HCys_2$ in a concentration dependent manner. For L-Arg transport in HUVECs the K_I values for co-incubation and pre-treatment with HCys were 168± 3μM and 101± 2μM, respectively, while in fibroblasts the K_I values for long term incubation was 90 ±1μM and 139± 4μM for co-incubation. Therefore, in HUVECs and fibroblasts, longer incubations with HCys resulted in ~35-40% reduction in the K_I values with respect to co-incubation. This implies that the inhibition of L-Arg transport is unlikely a simple competitive inhibition. In cases of hyperhomocysteinaemia where HCys concentrations range from 20-200μM, 16-66% inhibition of L-Arg uptake may be observed. One possible explanation is that the modification of sulfhydryl groups in System y^+ may affect L-Arg transport. Patel *et al.*, (1996) have reported that both Na^+ dependant and independent L-Arg transporters are inhibited upon incubation with sulfhydryl reactive compounds, N-ethylmaleimide (NEM) and acrolein, in a dose dependant manner.

The inhibition of L-Arg transport by HCys is expected to decrease NO production. Our findings show that HUVECs treated with HCys decreased NO secretion by ~35%. With limited L-Arg uptake and subsequent low production of NO, NOS is likely to transfer electrons to oxygen producing superoxide. It is established that NO and

superoxide react to form the highly oxidizing peroxynitrite anion which is the chief source of ROS species in the cell. To this end we monitored the levels of ROS as well as intracellular thiols as a function of HCys.

We were able to confirm the increase in ROS in the presence of HCys using DCF, a fluorescent probe for ROS. Endothelial cells subjected to longer incubation periods with HCys resulted in a 80% increase in ROS levels. Further studies probed the NO dependant effects on ROS levels in HCys treated endothelial cells. The production of NO stimulated by L-Arg (1mM) showed 30±1% decrease in ROS levels in HCys treated cells with respect to control. Increasing [L-Arg] to 10mM, continued to quench ROS generation by 40±2% with respect to control. Therefore, the oxidative stress induced by HCys has been suppressed by the regeneration of NO production. The role of NO as an anti-oxidant as been discussed in section 1.1.1.8. Specifically, in L-Arg deprived states NOS becomes a superoxide generating enzyme. The production of superoxide and other ROS species may cause damage to various functional proteins as well as plasma membrane. NO is involved in termination reactions of various radicals including lipid peroxides (Kelley *et al.*, 1999).

It is conceivable that an increase in ROS levels upon HCys incubation would affect the reducing thiol pool. We observed the changes in total thiols as well as glutathione levels in HCys treated cells. Following incubation with HCys the levels of total thiol and GSH increased. Given the fact that HCys induces oxidative stress, one might expect the GSH levels to be depleted. In our study, the increase in GSH levels

could be attributed to inhibition of GPx and/or a stimulation of the cellular compensatory mechanism, which responds to oxidative stress.

2.5.2 Effects of HCys/$HCys_2$ on RSNO transport

In addition to the endogenous production of NO by endothelial cells, the extracellular sources of NO play an integral role. NO is predominantly transported in the plasma as a S-nitroso adduct of albumin. Recent studies by Yamamoto *et al.*, have shown HCys reduces the binding of extracellular superoxide dismutase (EC-SOD) (Yamamoto *et al.*, 2000). We examined the effects of $HCys_2$ on the activity of another cell surface protein, protein disulfide isomerase, csPDI. CsPDI has been recently reported to be found on endothelial cells and to play an integral role in the transport of S-nitrosothiols (Zai *et al.*, 1999). Our studies showed significant changes in the affinity of csPDI to BSA-NO in HCys/$HCys_2$ treated cells. Endothelial cells treated with HCys showed an increase in K_M by 55%, while cells treated with $HCys_2$ showed a 75% increase in K_M. Furthermore, $HCys_2$ selectively inhibited the transnitrosation activity of PDI while leaving the isomerization activity intact. The selective effects of $HCys_2$ could be explained by the relative turnover rates of the isomerization and denitrosation activity of PDI. If the denitrosation reactions occur at higher rates than isomerization reactions, then the binding of an inhibitor will affect the denitrosation reaction over the isomerization activity. The binding of $HCys_2$ to PDI and the successive intramolecular PDI catalyzed cleavage of the mixed disulfide complex maybe rate limiting in its denitrosation activity without affecting its already slow isomerization activity. The csPDI competitively

catalyzes denitrosation and isomerization reactions, however in the presence of HCys/$HCys_2$, the isomerization reaction may prevail.

Under normal physiological conditions, csPDI catalyzes the denitrosation of RSNOs and the isomerization of various adhesion molecules involved in cell aggregation. In states of high NO/RSNO levels, denitrosation reactions are predominant hence promoting anti-aggregation. In conditions of low NO/RSNO levels, isomerization reactions prevail promoting cell aggregation. The much-studied effects of HCys as a pro-aggregatory agent can potentially be explained by its selective effects on csPDI observed here. The reduction in denitrosation activity catalyzed by csPDI without any loss to its isomerization activity may contribute to the pro-thrombotic and atherogenic effects of HCys.

Part III

The use of Raman Spectroscopy to probe thiols/S-nitrosothiols in live cells and model systems

3.0 Abstract

Raman spectroscopy is an invaluable tool for non-invasive studies of biological samples. In our study we made attempts to detect thiols in solution and monitor transnitrosation reactions. We also attempted to detect thiols in model systems such as liposomes and red blood cell ghosts, for the purposes of developing a dynamic assay in live cells. Using glutathione as our model substrate, we obtained a signature Raman spectrum of GSH including the SH stretch at 2580cm^{-1}. Upon nitrosation to S-nitrosoglutathione (GSNO), the SH peak disappeared and a new peak at 371cm^{-1} was attained. The SH peak was used to detect thiols in solution, however sensitivity was limited to 200mM. Similarly, the ability to detect S-nitrosothiols at 371cm^{-1} was also limited to 200mM. In order to increase sensitivity of Raman detection, Resonance Raman and Surface enhanced Raman spectroscopic techniques (SERS) were applied. The use of these techniques was hindered by the reactivity of thiols towards the SERS materials and the photolabile nature of GSNO. Derivatization of thiols with Ellman's reagent (DTNB, 5,5'-dithio-*bis*-3-nitrobenzoate) was successful in increasing the detection sensitivity. We were unable to obtain a Raman image of live cells because of [1] cellular auto fluorescence, [2] the need for higher numerical aperture and [3] laser power.

3.1 Introduction

3.1.1 Raman Spectroscopy

Raman spectroscopy is a valuable tool in investigating microenvironments of various molecules with great sensitivity. Detection using Raman is based on the light scattering phenomena, where a non-absorbing medium decreases the intensity of the incident light. The decrease in intensity is due to heat loss as well as the scattering of light into the surrounding space. The shift in wavelength from the incident and the scattered radiation corresponds to the chemical composition. Molecular vibrations provide information on structure, orientation and chemistry that allows us to define the characteristics of the molecule (Thomas *et al.*, 1999).

Many types of lasers are available for Raman detection, some in the visible range (Argon ion, 514nm, Krypton ion, 630nm, Helium/Neon, 633nm) and some in the near infra red (Diode laser, 830nm, Nd/YAG, 1064nm). Upon irradiation of sample, an electromagnetic field generates a positive and a negative pole; a molecule in this field is distorted by the pull of the electrons towards the positive pole and the nuclei to the negative pole. The distortion causes separation of charges and induces a dipole moment. The magnitude of the dipole moment with respect to volume is defined as polarizability of the molecule. Raman active compounds are classified according to their ability to distort or their polarizability.

Raman spectra of samples are obtained by irradiating with lasers ranging from visible to near infrared. The scattered light is measured at ~90°, with varying slit widths to capture scattered light at varying wavelengths. The downfall of Raman for most years has been that the intensity of signal detected is 0.001% of the incident intensity. Poor sensitivity of this instrument hinders the widespread use of this technique, however with the recent use of powerful lasers, which generate intense monochromatic light, has increased sensitivity and rekindled its use (Skoog *et al*, 1998).

Raman, in essence, is the bombardment of the sample with incident light ($h\nu$) resulting in the excitation of the ground state electron. The increase in energy of the electrons equals the energy of the incident photon. Since the electrons may assume any virtual state between the lowest excited state and ground state, the process is not necessarily quantized. The observed scattering is classified as Rayleigh scattering, anti-Stokes Scattering and Stokes scattering, which is the normal Raman effect. Raleigh scattering is caused by elastic collisions between the molecule and the photon. The energy of the scattered light and the photon are unchanged, this is the most probable type of scattering observed in the molecular environment. Inelastic scattering is less probable and results in scattering that is either higher or lower in energy of the incident photon. This is due to the exchange of energy between the molecule and incident photon. Since vibrational energies are defined, the energy lost or gained is quantized. This type of scattering produced two types Stokes and anti-Stokes. Stokes scattering is caused by a decrease in energy upon interacting with incident photon while anti-Stokes scattering loses quantum energy upon interaction with incident photon resulting with higher

scattering energy. Since anti-Stokes occurs from an excited vibrational or rotational state, the scattering is weak thus Stokes scattering is used as a measure of Raman effect. The amount of inelastic scattering (Stokes and anti-Stokes) is far less than that of elastic scattering (Rayleigh), which makes detection in Raman a problem (Skoog *et al.*, 1998; Thomas *et al.*, 1999).

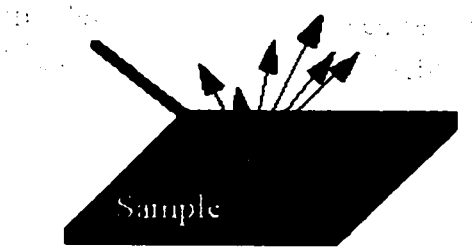

3.1.2 Resonance Raman Spectroscopy

Detection by Raman usually limits sensitivity to greater than 0.1M. Resonance Raman has increased the sensitivity dramatically to detect molecules as low as 10^{-8}M. In resonance Raman, the incident radiation is closely associated to that of the electronic absorption of the analyte. Under these conditions maximal vibrations are observed with peaks that correspond to the electronic absorption. Since only specific bands are targeted, dramatic increases in certain Raman peaks are observed over others for the same analyte. The increase in signal may be enhanced by a factor of 10^2-10^6. The major drawback in the use of Resonance Raman spectroscopy is that most electronic absorption maxima are in the UV range. This causes degradation of samples sometimes due to

localized heating. Interference by fluorescent properties of the compound has also caused some difficulty (Skoog *et al.*, 1998).

3.1.3 Surface Enhanced Raman spectroscopy (SERS)

Adsorption of sample of interest onto highly Raman active metals such as copper, gold or silver have enhanced Raman signals by 10^3-10^6. Lower detection limits of 10^{-9}-10^{-12}M have been observed with SERS. The mechanism by which signals are enhanced in SERS is still controversial. Nonetheless SERS could be used in conjunction with resonance Raman to increase the sensitivity of detection. Sample preparation is an important step in SERS, where a sample of interest may be bound to colloidal metal, deposited on thin film or a metal electrode (Skoog *et al.*, 1998).

3.1.4 Raman in Biological Setting

Many methods of detection have been developed for biological samples. Many have found the use of Raman to study biological samples to be beneficial. Over its counterpart, infra red spectroscopy, Raman offers the opportunity to study biological samples under aqueous conditions either in H_2O or D_2O. Raman has been largely used to probe changes in macromolecules such as secondary structures of proteins, determination of side chain configurations and interactions. The use of this technique lends itself to many advantages as well as disadvantages (Cotton et al., 1988).

3.1.5 Advantages and Disadvantages

Raman samples can be in different formats, such as in solution, precipitate, gels, crystals, fibers, films etc. Raman spectra of protein samples may be observed in crystalline form or in solution. As previously mentioned, H_2O (D_2O) generates weak signals and is an excellent medium for sample analysis including monitoring hydrogen isotope exchange/shifts. These analysis could be conducted in small sample sizes (1μL) which is smaller than that required for most spectroscopies. The use of Raman also negates the use of probes, which may alter the microenvironment of the sample. Since the sample remains intact following Raman analysis, it can be recovered and assayed. The short time scale in which Raman scattering occurs (10^{-15}sec) provides yet another advantage over fluorescence (10^{-9}sec) and nuclear magnetic resonance (10^{-6}sec) that allows us to study more temporarily resolved biological activities. Macro changes in proteins can be monitored by Raman by the various Raman active residues in protein such as peptide groups, aromatic side chains, sulfurs containing side chains, and carboxyl containing side chains. A number of proteins with relatively high UV/Vis absorbencies are good candidates for resonance Raman analysis (Cotton et al., 1988).

.

As always, every technique has its pitfalls, Raman does not provide a high resolution as compared to magnetic resonance. Since Raman deals with functional groups, proteins containing identical or similar functional groups may produce similar Raman spectra. Therefore some modification of the sample is necessary to generate

distinctive spectra. As mentioned, the level of measurable signal is only 0.001% of the incident light. When compared to signals generated by fluorescence and UV/Vis absorbance, measurable signal of Raman is considered weak and prone to contamination. However with the use of powerful lasers, the sensitivity of Raman can be increased to acceptable levels. Higher protein concentration is required within a small sample volume. Unfortunately, at high concentration, the protein might aggregate and complicate the Raman analysis (Cotton et al., 1988).

3.1.6 Thiols

Thiols play an important role in the biological system. The presence of thiols/disulphides is important in maintaining the structure and function of many proteins. For Raman analysis, thiols which are abundant in a protein are a valuable marker in protein spectra. The vibrational band stretching of sulfhydryl (SH) groups in proteins are detected in the 2500-2600cm^{-1} range. The absence of any other vibrational bands of functional groups in this range limits possible interferences (Thomas *et al.*, 1987). Ideally one should be able to detect the activity of one sulfhydryl group in a large macromolecule (Prevelige *et al.*, 1993). Raman peaks corresponding to SH stretches are expected to vary depending on their microenvironment. In addition, other interactions of thiols containing molecules can be analyzed by monitoring C-S stretching, for example in cysteinyl side chains C_{α}-C_{β}-S-H (Li *et al.*, 1992). For a Raman internal standard, Herzberg *et al.*, (1950) described a band at 2331cm^{-1}, which corresponds to the

vibrational-rotational band of N_2 gas. N_2 that is present in the air localized in the area of irradiation, can therefore serve as an internal standard for Raman Spectroscopy.

3.1.7 Cell surface thiols

The study of exofacial thiols has been of great interest because exofacial thiols are involved in proper functioning of transport proteins and targeted by various oxidants in the plasma (Bennett *et al.*, 1985). A common assay for thiols entails the use of fluorescence or UV/Vis absorbance. In this study we used Raman spectroscopy to observe surface thiols. In erythrocytes, exofacial thiols were difficult to measure, due to vulnerability of erythrocytes and the presence of hemoglobin contamination. An alternative approach is to observe Raman changes in the presence of a reporter molecule, such as the Ellman's reagent, 5,5'-dithio-bis-2-nitrobenzoic acid (DTNB) (O'Donnell *et al.*, 1995). Upon reacting with free thiols, DTNB forms a mixed disulphide and a thionitrobenzoic anion, TNB^-. The Raman spectrum of DTNB has a band at $1345cm^{-1}$ and in TNB^- the band shifts to $1325cm^{-1}$. These peaks are attributed to the symmetric NO_2 stretch. In order to develop a sensitive assay, a sufficient amount of DTNB must be added to achieve maximal conversion to TNB^-. The use of Ellman's reagent has also been used in Surface Enhanced Resonance Raman spectroscopy. Ellman's reagent was mixed with silver colloids following the incubation with erythrocytes. Resonance Raman spectroscopy was used to enhance the detection of signals (Rospendowski *et al.*, 1992).

3.1.8 Thioredoxin

Thioredoxin ($TRX(SH)_2$) is a small protein domain of a large family of proteins that contain active redox thiol groups (Katti *et al.*, 1990). Thioredoxin is also found as subunits in larger proteins such as protein disulphide isomerase. The active site of this enzyme contains two cystinyl residues, Cys 32 and Cys 35, which catalyze many redox reactions (Dyson *et al.*, 1990). The Raman fingerprint of thioredoxin was produced, which provided information with regards to its active site residues and conformation (Li *et al.*, 1993). The more prominent Raman peaks were generated by the presence of tryptophan ($756cm^{-1}$, $1339cm^{-1}$), phenylalanine ($1003cm^{-1}$), amide III ($1246cm^{-1}$), CH bend ($150cm^{-1}$), aliphatic CH stretch ($2937cm^{-1}$) and aromatic CH stretch ($3067cm^{-1}$). The active cysteinyl groups in the reduced form contributed to the SH stretch at $2569cm^{-1}$ with a closely associated N_2 ($2332cm^{-1}$) peak used as an internal standard. The oxidation of the thiols did not substantially change the secondary structure of $TRX(S)_2$ as observed by identical amide (I and III) peaks. The amide I peak can be resolved to determine the presence of β strands/turns or α helices. A shoulder on the higher frequency of amide I peak represents β turns and strands, while a shoulder on the weak frequency of amide I peak represents the α helix content. Minute changes observed in the spectra of the oxidized to the reduced TRX suggest a small decrease (<2%) in α helix content and a slight increase in β turns/sheets. A decrease at $754cm^{-1}$ indicates a more hydrophilic environment around the tryptophan group in $TRX(SH)_2$. The oxidation of the thiols can be monitored by the presence of the disulphide peak at $507cm^{-1}$. The activity of thioredoxin depends on the presence of the thiolate ion, which is poised to attack disulphides. The pKa of the cysteinyl thiol is 8.3. In order to form a thiolate ion at

physiological pH, the pKa of cysteinyl residues in TRX are expected to be lower. Raman was used to determine the pKa values of Cys 32 and Cys 35. An increase in pH was accompanied by an increase in thiolate ion formation, which was marked by the decrease in the intensity of the SH- peak. The increase in pH also caused a shift of the SH peak to a lower frequency. This suggested the presence of two cysteinyl residues, each with slightly different SH peak maxima. The pKa of Cys-32 was 7.1, and the pKa of Cys-35 was 7.5. No change in secondary structure was observed during pH transition.

3.1.9 Albumin

Albumin is the most abundant plasma protein. With respect to other proteins, albumin is highly stable and soluble. Physiologically, albumin is responsible for the transport of many metabolites, involved in detoxification mechanisms and the maintenance of blood colloidal pressure (Carter *et al.*, 1994). Thiol groups in albumin also play an integral role in its function. Albumin is capable of undergoing conformational changes under different pH conditions. As pH is decreased, the first conformational change occurs between pH 4.40-3.75 (N → F) and the second change occurs between pH 3.60-2.80 (F→E). This acid induced isomerization occurs in a two-step reversible process. Raman was used to monitor the changes in cystine disulphide bridges (Nakamura *et al.*, 1997). Albumin has one cysteine (Cys-34) and 17 cystine disulphide bridges located mainly in the α helices. Preliminary studies have shown the disulphide bonds of albumin to be in the gauche-gauche-gauche (*ggg*) conformation, while recently, the presence of gauche-gauche-trans (*ggt*) isomer has been found. A disulphide peak at 505cm^{-1} has been assigned the ggg conformation, while the peak at 520cm^{-1} is assigned to the *ggt* conformation. The ratio of $I_{505}/_{520}$ provides information on

the conformation of albumin in various pH conditions. The ratio increases with respect to decrease in pH, N ($I_{505}/_{520}$ =1.6), F ($I_{505}/_{520}$=2.1), and E ($I_{505}/_{520}$=6.1). Therefore acid induced isomerization results in the disulphide conformation change from *ggt* to the thermodynamically stable *ggg* conformation, which is detectable by Raman spectroscopy.

3.1.10 Human Skin

A novel use of Raman was to observe the molecular composition of human skin. The skin is made of a dermis (1.4mm) layer and an epidermis (1-0.4mm) underneath layer. Skin layers are primarily composed of type I and III collagen, lipids and water (Odland *et al.*, 1991; Jakubovic *et al.*, 1992). Confocal Raman analysis was carried out *in vitro* from skin samples obtained post mortem and *in vivo* (Caspers *et al.*, 1998; Caspers *et al.*, 2001). Using this technique, different spectra were obtained from different skin layers. Collagen itself produces two strong peaks at 855cm^{-1} and 936cm^{-1}, which correlate to the unusually high concentrations of proline and hydroxyproline found in collagen. Amide I bands at 1655cm^{-1} were also detected as representative of human keratin, providing information on the heavy α helical content. The confocal instrument allows light penetration below the surface layer to the dermis and epidermis. The laser focus was located ~85μm below the skin, therefore measurements were primarily from the dermis. Present studies aim to characterize skin surface and quantify molecules in skin by Raman.

3.1.11 Microorganisms in Culture

Confocal Raman spectroscopy has been introduced as a promising clinical diagnostic tool in microbiology. Generally the identification of pathogenic microorganisms is very lengthy and labour intensive. These microbes are generally grown for 16-24hrs to achieve a cell density that biochemical assays are carried out (Tang *et al.*, 1997). Preliminary attempts at using UV resonance Raman for detecting microbes in suspended samples as well as hydrated microbial smears were unsuccessful. Interferences by the media, heating of sample and photochemical contaminants were common problems (Nelson *et al.*, 1992). Raman signatures of microbes have recently been fruitful. Microcolonies grown on solid media were used as samples for Raman spectroscopy (Maquelin *et al.*, 2000). When spectra were corrected for water, and culture medium, the resulting spectra were analyzed and compared among various strains of the microbes. *Escherichia coli* (*E.coli*) provided a strong peak at 1004cm^{-1}, which was distinguishable from *Staphylococcus epidermidis* and *Enterococcus faecium*, which produced slightly different spectra. Two strains of *Staphylococcus aureus* did not provide significant differences in their spectra. Currently, the peaks corresponding to the changes in their spectra are unknown. Furthermore the difference in their thickness seems to be a limitation to this study.

3.2.1 Materials

Sigma-Aldrich (Oakville):- Glutathione (GSH, GSSG), Homocyst(e)ine, Cyst(e)ine, nitrite, 5,5'-dithio-*bis*-3-nitrobenzoate (DTNB), bovine serum albumin, silver shots, gold colloids, Phosphatidyl choline, cholesterol, dansyl chloride

Tilbury slaughter house (Tilbury, ON):- Sheep blood

University of Western Ontario:- Silicon chips

American Type Cell Culture (Manassas, VA):- Hamster Lung fibroblast (CCL-93),

3.2.2 Equipment

Extruder – Avestin Inc.

pH Meter -Orion 420A, Orion Research Inc. (Boston, MA)

Microcentrifuge tube centrifuge - Eppendorf Mixer 5423, VWR Scientific (Mississauga, ON)

Ultrasonicator – Transonic T420, Mandel Scientific (Toronto, ON)

Lyophilizer - Labconco Model 4451F, Labequip Limited (Markham, ON)

Weigh balance - Mettler AJ100, Mettler Instrumetn Corp. (Hightstown, NJ)

Stirrer – Stirrer 360, VWR Scientific (Mississauga, ON)

BioRad HPLC System (Hercules, CA)

BioRad Econo System (Hercules, CA)

Binomic Controller BC 100(20/20 Technology Inc)

Zeiss Axiovert 200 microscope, Empix (Mississauga, ON)

3.3 Methods

3.3.1 Raman

The Renishaw Research Raman microscope system RM 2000 was used in this study. It is equipped with different excitation sources 514nm Argon ion laser, 633nm He-Ne laser and 780nm diode laser. The laser commonly used in this study was the 633nm He/Ne laser with 100% power (2mW at the sample, 10mW at the source) and 514nm Argon ion laser with 100% power (0.7mW at the sample, 30mW at the source). Normal spectra are obtained in 100-3500cm^{-1} range with 1200grooves/mm grating. The Raman is also equipped with a Leica Microscope (DMLM series) with a motorized stage capable of 0.1μm minimum step. The spectra were captured by data acquisition software WiRE software for windows and Galactic industries Grams/32.

3.3.2 RSNO/RSH

GSH (500mM) and GSNO (500mM) were prepared in H_2O, the pH was adjusted to pH 2 with 2M HCl. The Raman spectra of these compounds in a NMR tube were obtained with 633nm He/Ne (2mW). Using a 50x long objective, the sample was exposed to 20sec and data was obtained over 10 accumulations. Similar protocol was also used to determine the Raman Spectra for HCys/HCysNO and Cys/CysNO.

3.3.2.1 GSH:- The spectra of varying concentrations of GSH (100mM – 500mM) were obtained using 633nm He/Ne (2mW). The sample was exposed for 20sec with 10 accumulations using a 50x long objective. The static spectrum focused at 1000cm^{-1} was obtained and analyzed using Grams 4.0.

3.3.2.2 GSNO:- The spectra of GSNO (100mM-500mM) were obtained using 633nm He/Ne (2mW). The sample was exposed for 20sec with 10 accumulations using a 50x long objective. The static spectrum focused at 1000cm^{-1} was obtained and analyzed using Grams 4.0.

3.3.2.3 Decomposition of GSH/GSNO:- GSH(1mM) was exposed to 514nm Argon ion laser for 15mins. At varying time intervals aliquots were assayed for free thiol content by incubating with DTNB (1mM). Absorbance at 412nm was used to monitor possible oxidation of GSH. GSNO (100mM) was also exposed to 514nm Argon ion laser and 633nm He/Ne laser. Absorbance of GSNO at 340nm was monitored over 15mins of exposure.

3.3.3 SERS

A solution of colloidal gold (~10nm diameter, 0.1mg) was incubated with 500mM GSH (pH 2). The Raman spectrum was obtained with 514nm Argon ion laser with 5 sec exposure and 30 accumulations. The data was standardized with the CH_3 stretch.

GSH solution was also placed on a silver coated slide and exposed to similar conditions as above. The areas under the peaks were calculated using WiRE software.

The spectrum of $nitrite_{(s)}$ was obtained using 514nm Argon laser (0.7mW). The sample was placed on a silicon plate and exposed for 10sec with 4 accumulations using a 50x long objective. The spectrum of 500mM $nitrite_{(aq)}$ in a NMR tube was obtained with 20sec exposure and 20 accumulations.

3.3.4 DTNB/TNB^-

DTNB assays were performed in varying concentrations to obtain maximal shifts in Raman peak. The static spectrum of DTNB (1mM) focused at 1700cm^{-1} was obtained using 514nm Argon laser (0.7mW). The DTNB (1mM) sample was exposed for 20sec with 10 accumulations using a 50x long objective. DTNB (1mM) was reacted with 20mM GSH and a spectrum of the resulting product was obtained, TNB^-. In order to show transition of DTNB-TNB^-, DTNB (5mM) was reacted with varying concentrations of GSH (0mM – 10mM). The following spectra were obtained with 10sec exposure over 5 accumulations. To quantitate the transition between DTNB-TNB^-, 1mM DTNB was incubated with increasing concentrations of GSH (0-5mM). The area of the peaks at 1326cm^{-1} (TNB^-) and 1345cm^{-1}(DTNB) was determined for each reaction sample. The spectra were obtained with 20sec exposure over 15 accumulations.

3.3.5 Liposomes

The liposomes were prepared by dissolving 10mM phosphatidylcholine in chloroform (MacDonald *et al.*, 1991). The compound of interest was added to the liposome mixture and chloroform was evaporated. To regulate the size of the liposomes, they were passed through an Avestin Extruder with polycarbonate membrane of 1000nm pore size. The sample was passed through 21 times to ensure uniform size. The liposomes were used to encapsulate various materials, N, N-didansylcystine(1mM), GSNO (500mM), and GSH (500mM). The liposomes were purified using Hi-Trap column on a Bio Rad HPLC. Formation of liposomes was confirmed using an inverted light microscope with 40x objective. Proper encapsulation of compounds was confirmed by the intra-liposomal fluorescence of N,N-didansylcystine.

Raman of liposomes on silicon was attempted using the 514nm Argon laser, with 30sec exposure over 25 accumulations.

3.3.6 Red blood cell ghosts

Sheep blood was collected in a container with the following anticoagulants, 0.2mM EDTA and 0.001% heparin. The blood was filtered through a cheesecloth and then centrifuged at 2000g for 5mins at 4°C. A buffy white coat of white blood cells were removed by aspiration. The packed reticulocytes and erythrocytes were washed 3times with salt solution (0.15M NaCl). Final pellet was lysed in the presence of cold milli-Q

water at 0°C. After 1min, the mixture was centrifuged to isolate the translucent pellets. Formation of RBC ghosts and encapsulation was carried out in a similar manner as for liposomes. Purification was done by centrifugation as opposed to HPLC (Fossel et al., 1979).

3.3.7 Hamster Lung Fibroblast (Confocal)

Hamster lung fibroblasts were grown on silicon. Cells were incubated in 100mM GSH for 10mins. Following incubation cells were washed and imaged on Raman. Raman spectra of live cells were performed using 514nm Argon laser with 5sec exposure and 10 times accumulation. The area sampled to obtain Raman image was 25nm x 25nm.

Detection of surface thiols was also performed on fibroblasts. Cells were grown to confluence on 35mm^2 petri dishes. Media was aspirated and cells were scraped onto silicon. A Raman spectrum of the sample was obtained before and after the addition of DTNB (100μM). A static spectrum was obtained with 20sec exposure and 25 accumulations.

3.4 Results

3.4.1 Thiols/S-Nitrosothiols Spectra:- We monitored transnitrosation reactions in solution among thiols such as GSH, HCys and Cys. Initially, a Raman spectrum of GSH (500mM) and GSNO (500mM) at pH 2 was obtained, Fig 1. As expected, upon nitrosation, the disappearance of the Raman band corresponding to the SH stretch at ~2580cm^{-1} was observed. Simultaneously, the appearance of a Raman band at 370cm^{-1} was observed in the GSNO spectrum. The dramatic changes that distinguish between the two spectra are indicated in Fig 2. Among the peaks, both spectra show aliphatic CH stretch of the backbone at 2940cm^{-1}, amide I and III peaks at 1660cm^{-1} and 1246cm^{-1}, respectively. Peaks corresponding to CC, CN, CO stretches (1038cm^{-1}), CCC bends (891cm^{-1}) and CS stretches (671cm^{-1}) were also found to exist in both spectra.

3.4.2 Thiols/S-Nitrosothiols Standard Curve:- The change in Raman signal upon nitrosation at 2580cm^{-1} was observed in other thiol/S-nitrosothiol pairs as well, Fig 3. Varying concentrations of GSH and GSNO was used to determine the sensitivity of Raman, Fig 3-6. A static spectrum of GSH (100mM-500mM) was obtained; the corresponding areas under the peaks were calculated from 4 independent experiments. The decrease in the Raman band at 2580cm^{-1}, with decreasing concentrations of GSH is shown in Fig 5. The corresponding standard curve is shown in Fig 6a. The decrease in peak area occurred in a GSH concentration dependant manner. Peak area for the 100mM GSH could not be determined with statistical significance.

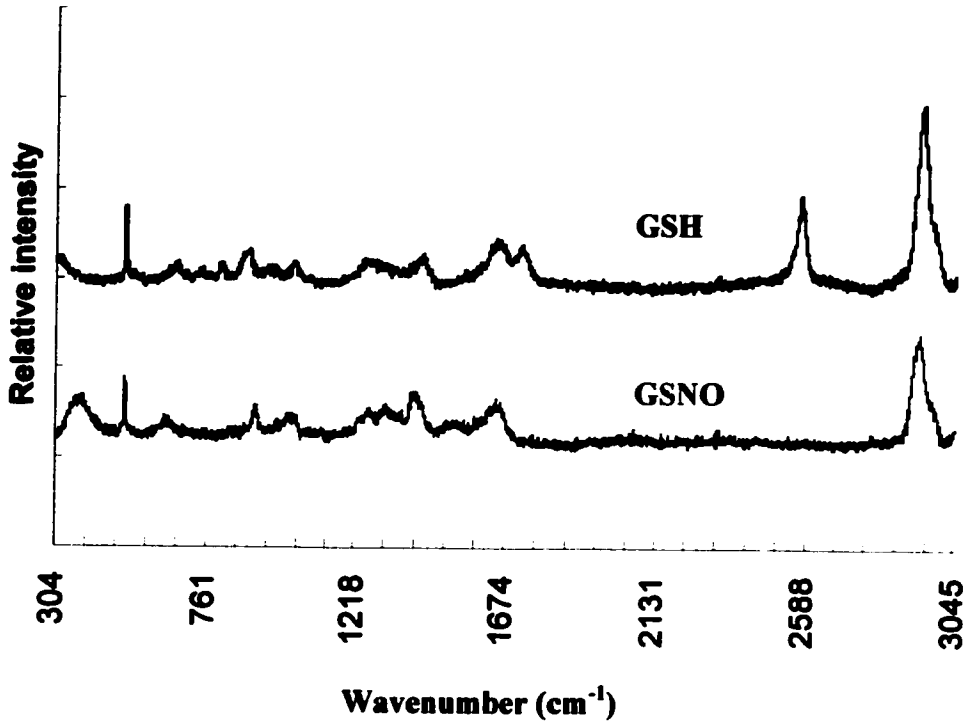

Fig 3.4.1:- Comparison of Raman spectra of GSH and GSNO. The spectra of GSH and GSNO (500mM) were obtained using 633nm He/Ne. The sample was exposed for 20sec with 10 accumulations using a 50x long objective. The data was analyzed using Grams 4.0.

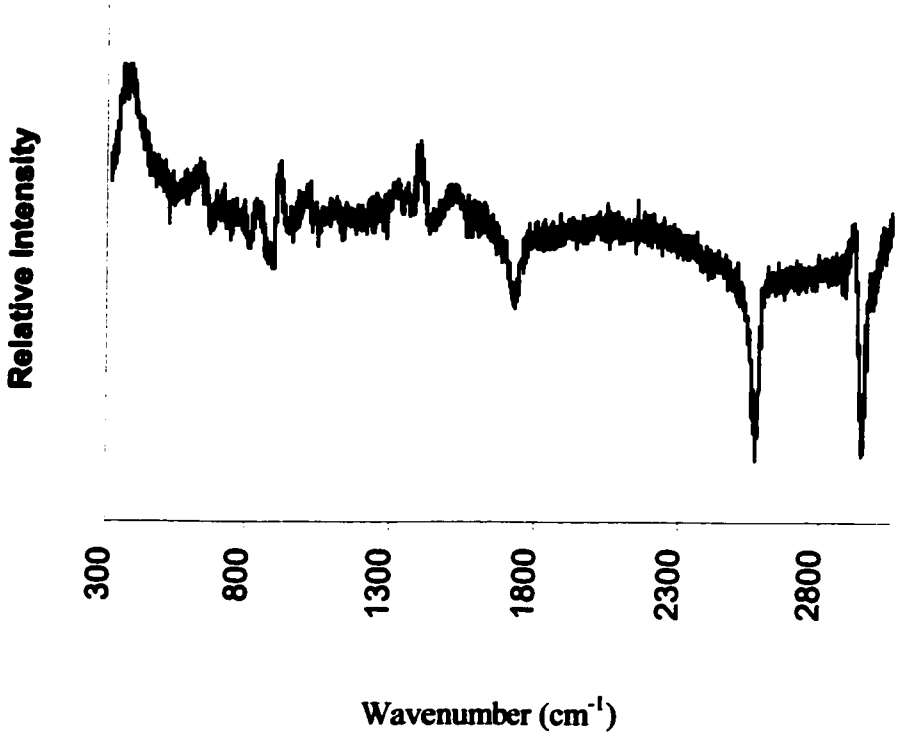

Fig 3.4.2:- Difference in Raman spectra between GSH and GSNO. The spectra of GSH and GSNO obtained in Fig 1 were subtracted by Grams 4.0. Peaks represent bands present in GSNO and absent in GSH while valleys represent bands in GSH and not in GSNO.

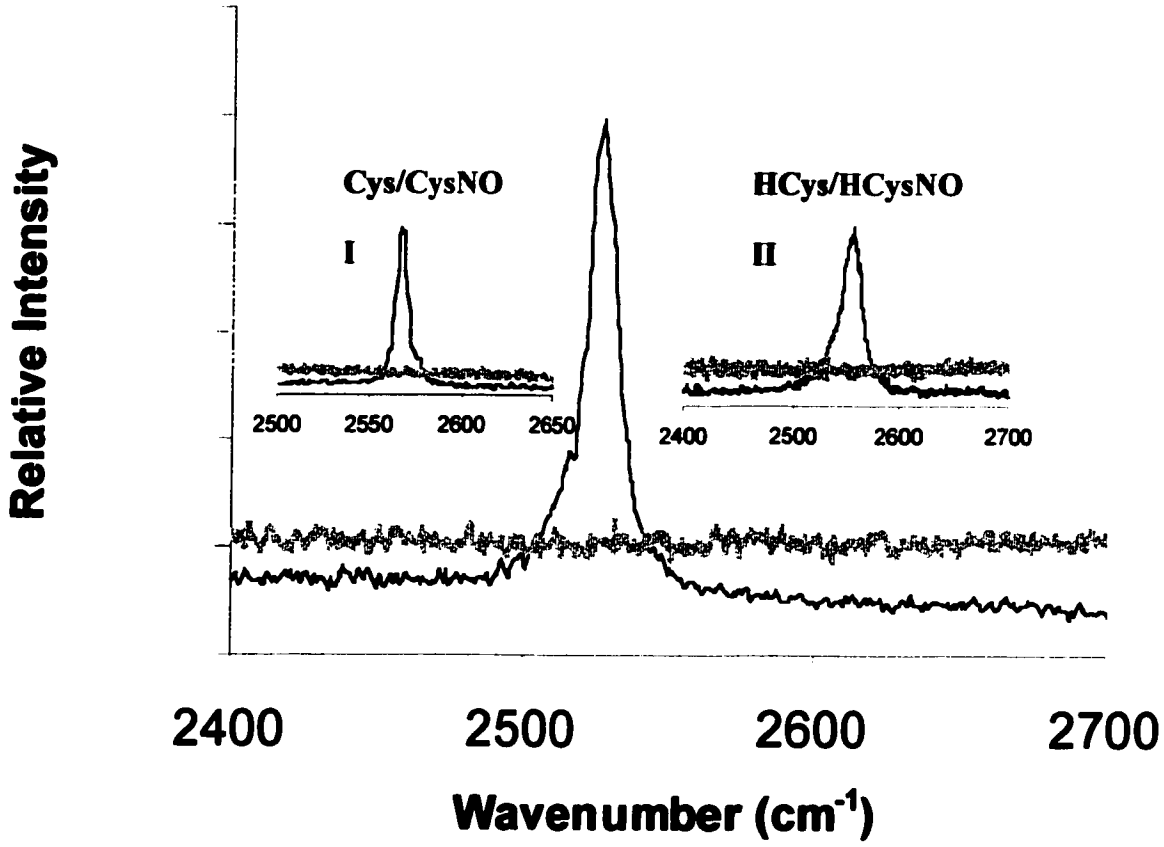

Fig 3.4.3:- Change in Raman Thiol signal upon nitrosation. GSH (500mM, solid) and GSNO (500mM, dotted) compared under 633nm He/Ne laser. Similar static spectra were obtained for HCys (500mM, solid) and HcysNO (500mM, dotted), inset I, and Cys (500mM, solid) and CysNO (500mM,dotted), inset II.

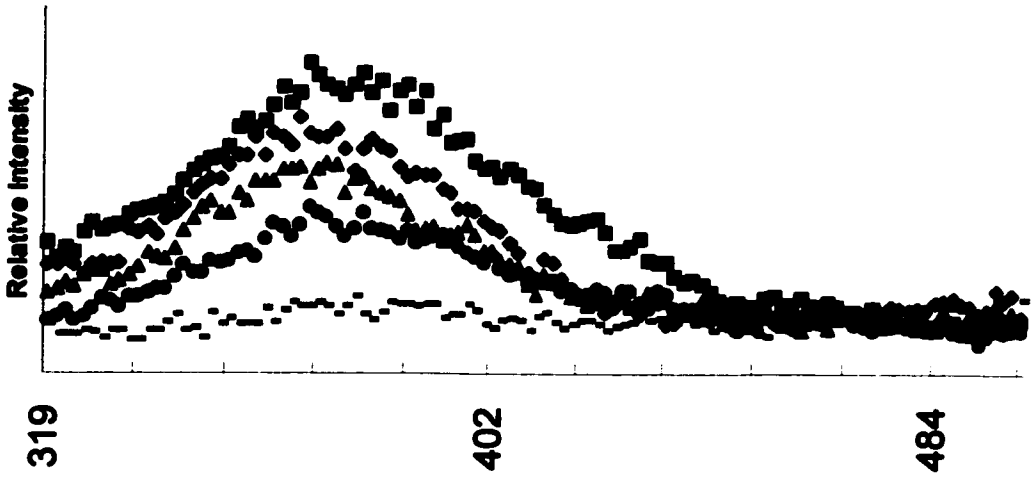

Fig 3.4.4:- Comparison of Raman spectra of varying concentrations of GSNO. The spectra of GSNO (500mM, Squares, 400mM, Diamonds, 300mM, Triangles, 200mM, Circles, 100mM, Dash) were obtained using 633nm He/Ne. The sample was exposed for 20sec with 10 accumulations using a 50x long objective. The static spectrum focused at $1000cm^{-1}$ was obtained and analyzed usng Grams 4.0.

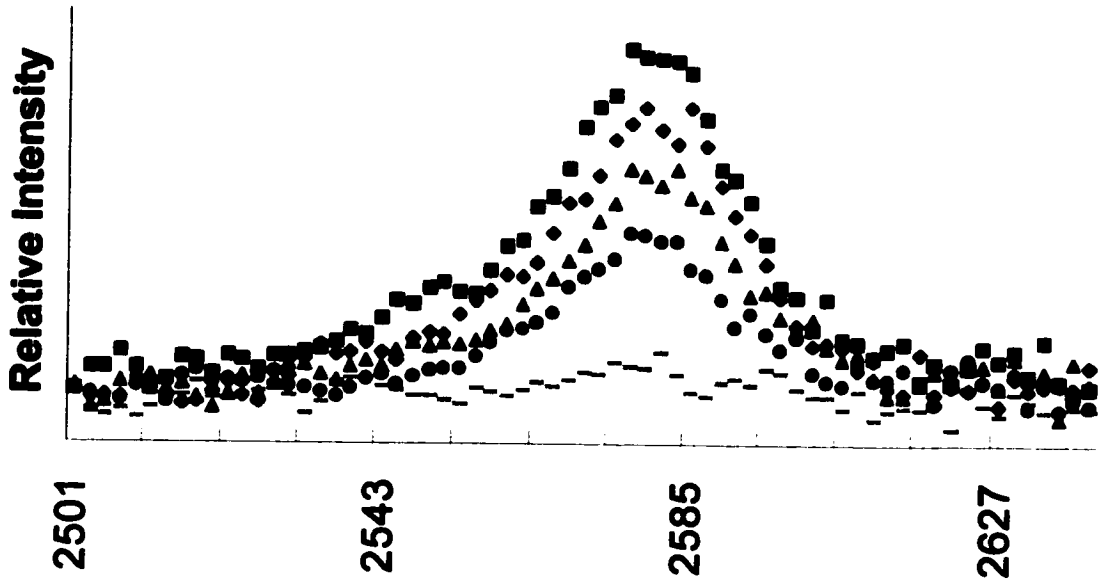

Fig 3.4.5:- Comparison of Raman spectra of varying concentrations of GSH. The spectra of GSH (500mM, Squares, 400mM, Diamonds, 300mM, Triangles, 200mM, Circles, 100mM, Dash) were obtained using 633nm He/Ne. The sample was exposed for 20sec with 10 accumulations using a 50x long objective. The static spectrum focused at 1000cm^{-1} was obtained and analyzed using Grams 4.0.

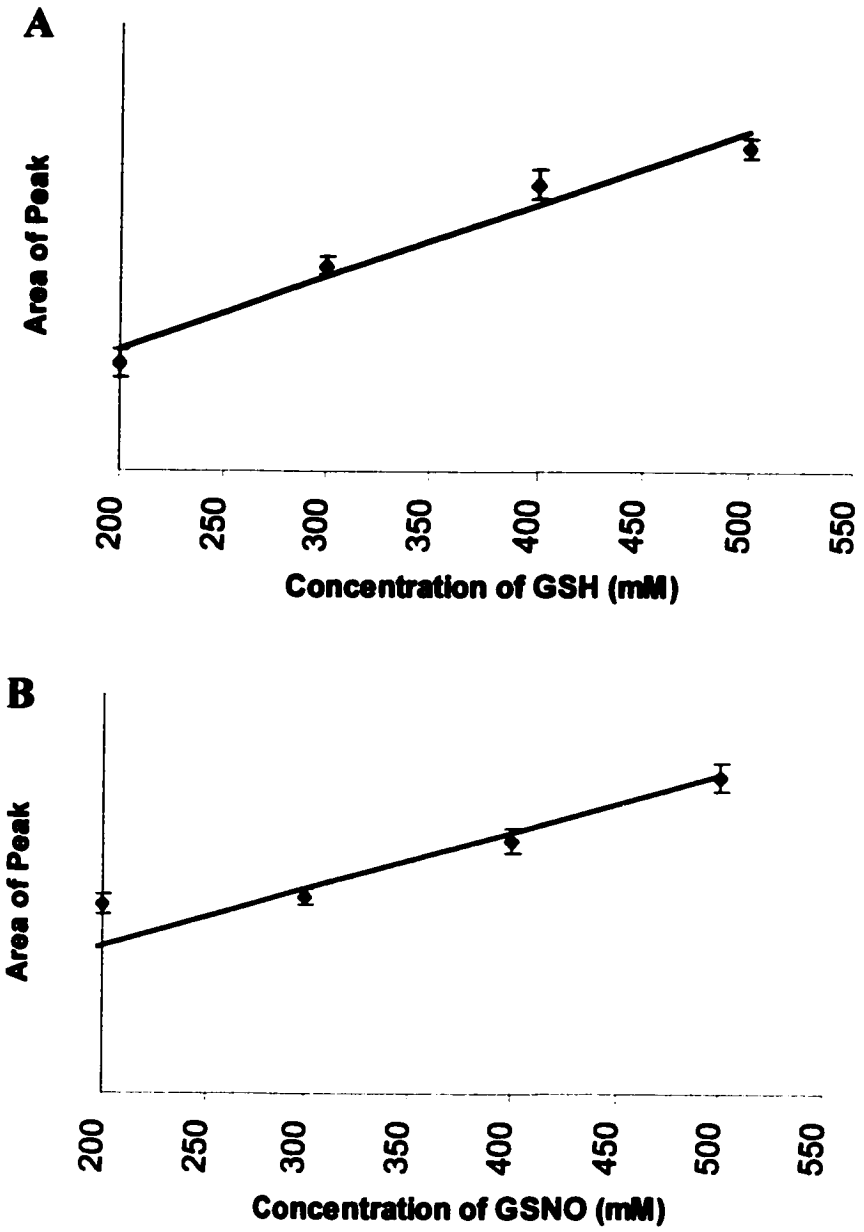

Fig 3.4.6:- Standard curve of GSH and GSNO. (A) Areas of peaks at 2580cm^{-1} were calculated over 4 trials to generate the GSH standard curve. (B)Areas of peaks at 371cm^{-1} were calculated over 4 trials to generate the GSNO standard curve.

A similar experiment was performed with varying concentrations of GSNO. Change in GSNO (100mM-500mM) was monitored by performing a static Raman spectra. From Fig 2, a change in Raman band at 371cm^{-1}was determined as the most sensitive indicator of GSNO due to the large change between the nitrosated and non-nitrosated species. Decreasing the GSNO concentrations was indicated by the corresponding change in peak area of the Raman band at 371cm^{-1}, Fig 4. A standard curve was then constructed using the peak areas obtained over 4 trials, Fig 6b. The sensitivity of Raman with the specified parameters was greater than 200mM. As in the case with GSH, 100mM GSNO did not produce statistically significant data.

3.4.3 DTNB Assay:- Intracellular concentrations of GSH are 5-10mM (Till *et al.*, 1998) while GSNO exists in low nanomolar concentrations. Therefore, direct probing of either metabolite under physiological conditions is not feasible. In an attempt to increase the sensitivity of the Raman for thiols and S-nitrosothiols, we used a 514nm Argon ion laser. Thiols are susceptible to oxidation in the presence of UV/Vis light; therefore a DTNB assay was utilized to determine free thiol content. Upon irradiation no significant changes were observed in thiol content, Fig 7I. Irradiation of GSNO (100mM) resulted in a 15% degradation of sample over 15min exposure, Fig 7 IIA, whereas irradiation with 633nm He/Ne laser resulted in ~4% degradation, Fig 7 IIB, as determined by its absorbance at 340nm. Detection of GSNO by Raman or Resonance Raman at 514nm was hindered by the increased photodegradation of GSNO with the 514nm Argon ion laser.

SERS has been known to increase Raman signals dramatically. We attempted to use gold colloids and silver coated slides to increase our sensitivity. Addition of GSH to gold colloids decreased the sensitivity of the assay by ~50%. The use of silver coated slides increased the sensitivity of GSH by 25%, Fig 8.

A reporter system was employed to increase sensitivity. Ideally, a reporter molecule should either be Raman active in the presence of the sample of interest or generate a new Raman band upon interaction. One such molecule that showed promise was the Ellman's Reagent (DTNB). DTNB reacts with free thiols to generate TNB^-, which has a strong absorbance at 412nm (ε =13 600$M^{-1}cm^{-1}$). DTNB in the presence of excess GSH was able to convert to TNB^-. Its corresponding peaks were observed at 1345cm^{-1} for DTNB and 1326cm^{-1} for TNB^-, Fig 9. The transition between DTNB and TNB^- was monitored by titration of DTNB by GSH, Fig 10. The peak area for DTNB and TNB^- Raman bands were determined over 3 trials and plotted with respect to increasing concentrations of GSH, Fig 11. The increase in TNB^- (1326cm^{-1}) and the corresponding decrease in DTNB (1345cm^{-1}) occur in a GSH concentration dependant manner.

The decomposition of various nitrosative species form nitrite in physiological conditions. Therefore, we attempted to obtain a Raman spectra of nitrite in the crystalline and aqueous (500mM) forms. A dominating band at 1325cm^{-1} was obtained for the NO_2 stretch in the solid sample. In the aqueous sample, a broad band corresponding to water was observed at ~1500cm^{-1}, Fig 12.

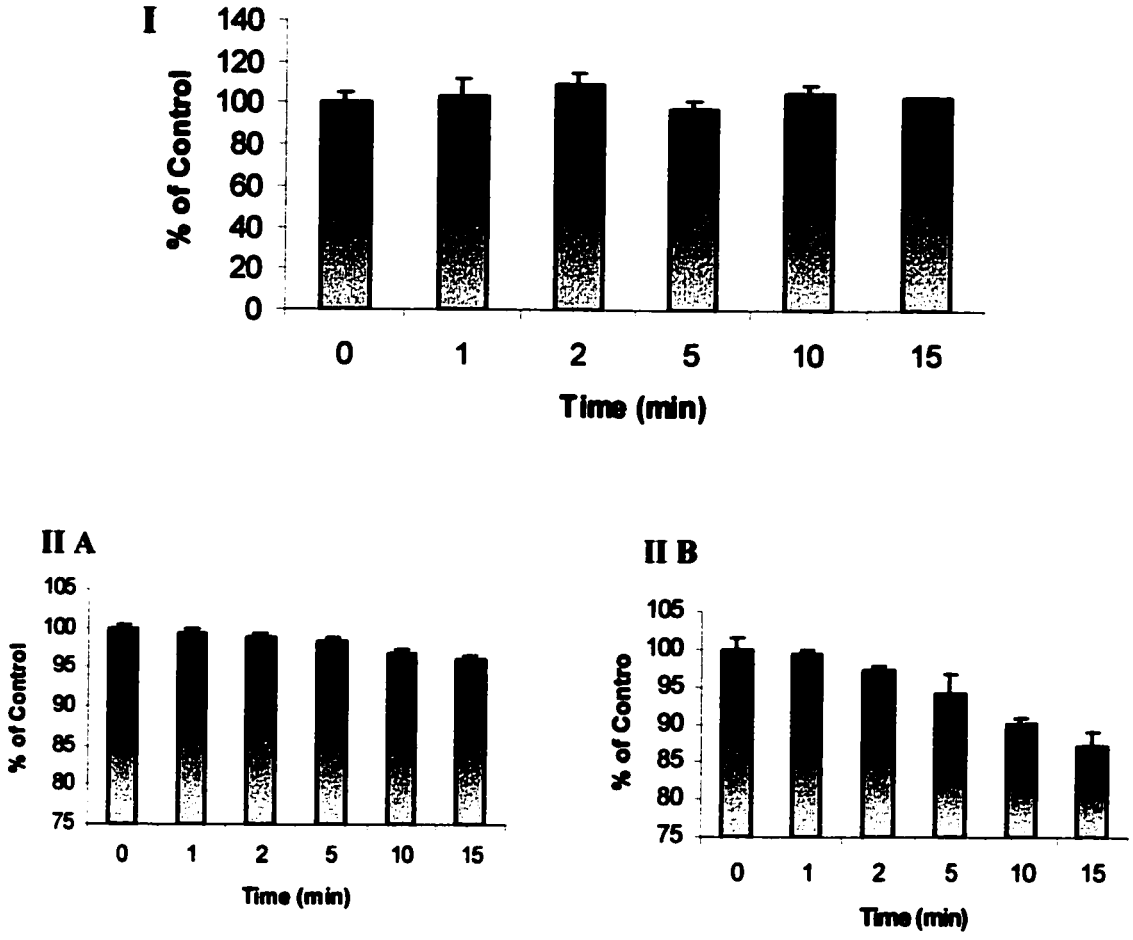

Fig 3.4.7:- Degradation of GSH/GSNO upon irradiation by 514nm or 633nm lasers. I) GSH (100mM) was exposed to 514nm Argon ion laser for 15mins. An aliquot of the sample was assayed periodically for free thiol content by the DTNB assay. GSNO (100mM) was exposed to 633nm He/Ne (II A) and 514 nm Argon ion laser (II B) aliquots were obtained over 15mins. The absorbances at 340nm were used to determine the integrity of GSNO. The error bars in all cases represent standard deviation (n=3).

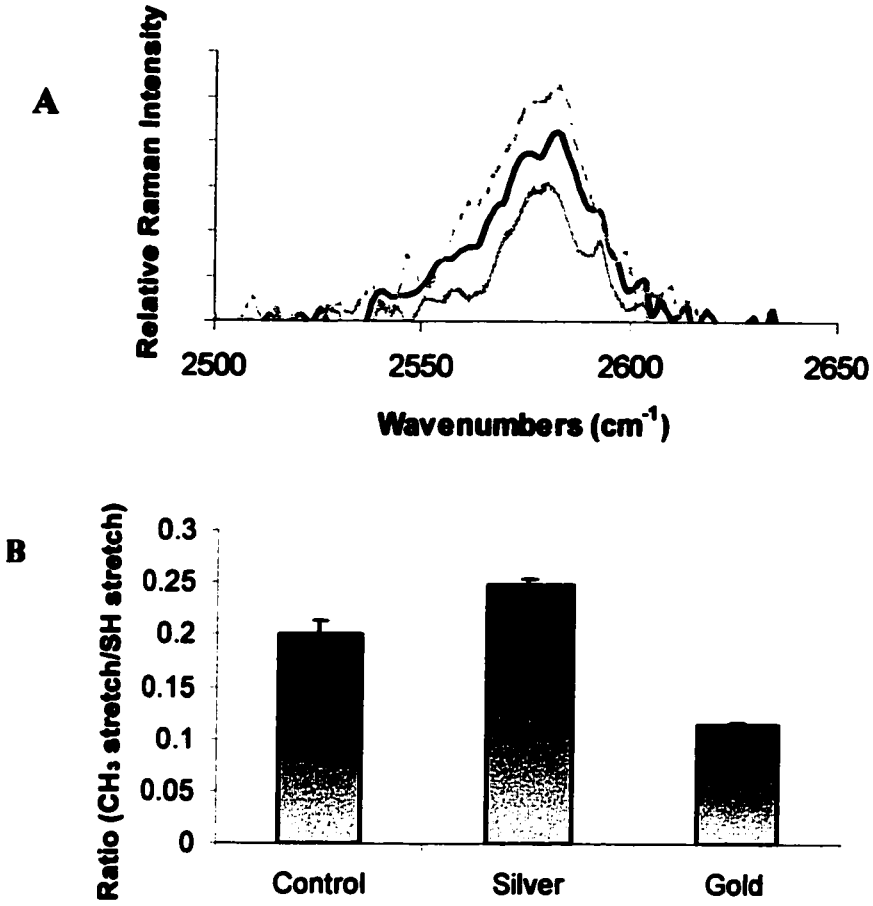

Fig 3.4.8:- SERS of GSH. (A) Raman spectra of GSH (500mM) on silicon (solid), on silver (dotted) and in gold colloids (shaded) were irradiated with 514nm laser. The data was obtained with 5sec exposure and 30 accumulations. (B) Change in intensity of SH stretch determined by the area of the SH peak (2580cm-1). The change is standardized with respect to CH_3 stretch. The error bars represent standard deviation over 6 trials.

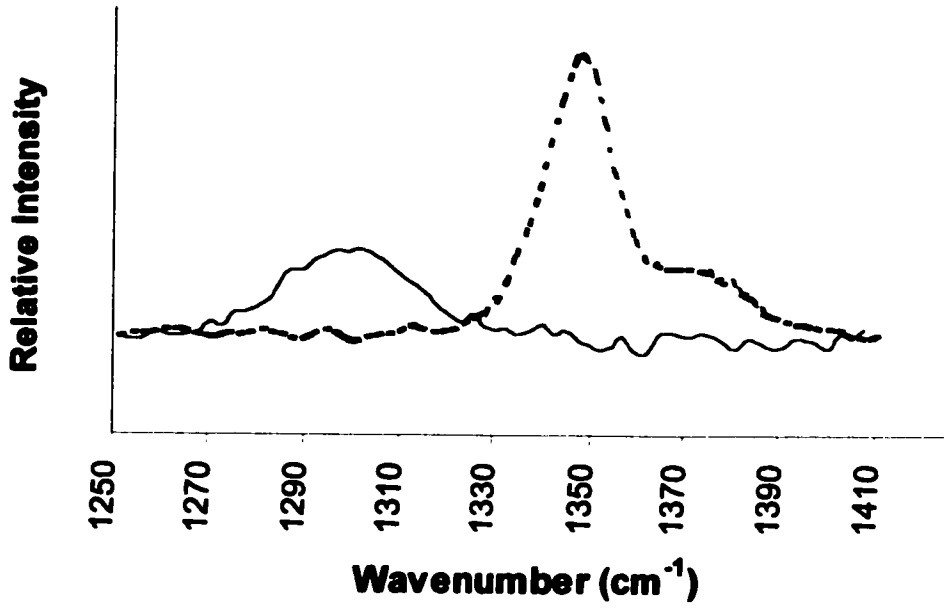

Fig 3.4.9:- Comparison of Raman spectra of DTNB and TNB^-. The static spectrum of DTNB (1mM) focused at 1700cm^{-1} was obtained using 514nm Argon laser (0.7mW). The DTNB sample (dotted lines) was exposed for 20sec with 10 accumulations using a 50x long objective. DTNB (1mM) was reacted with 20mM GSH and a spectrum of the resulting product was obtained, TNB^- (smooth line).

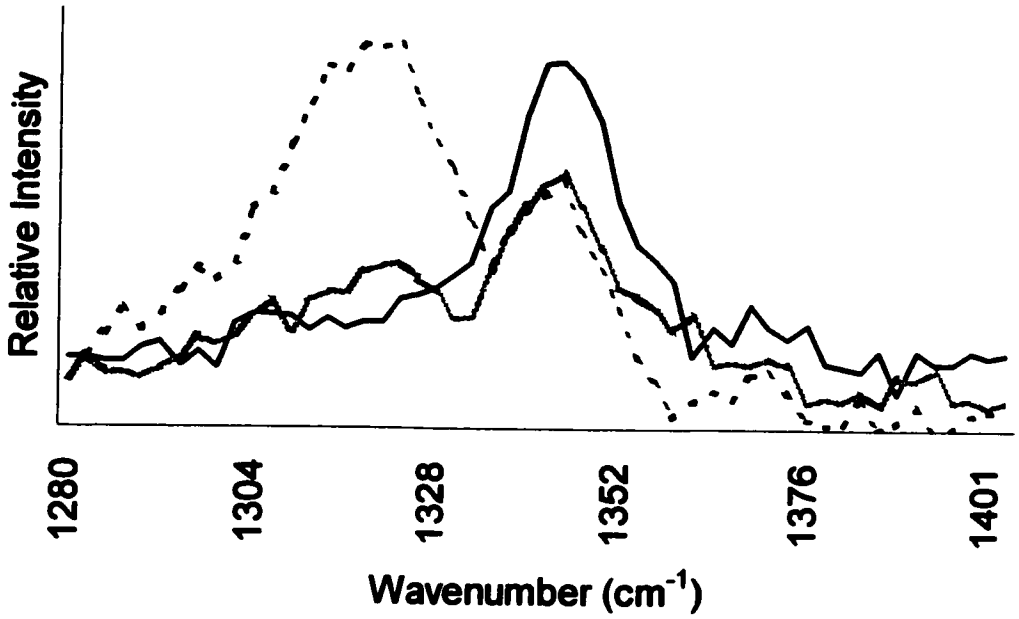

Fig 3.4.10:- Transition in Raman spectra from DTNB and TNB^-. The static spectra of DTNB/TNB- focused at 1700cm^{-1} were obtained using 514nm Argon laser (0.7mW). All samples were exposed for 10sec with 5 accumulations using a 50x long objective. DTNB (5mM) was reacted GSH (0mM, smooth line, 5mM, faded line, 10mM, dotted line) and the resulting spectra of the product was obtained.

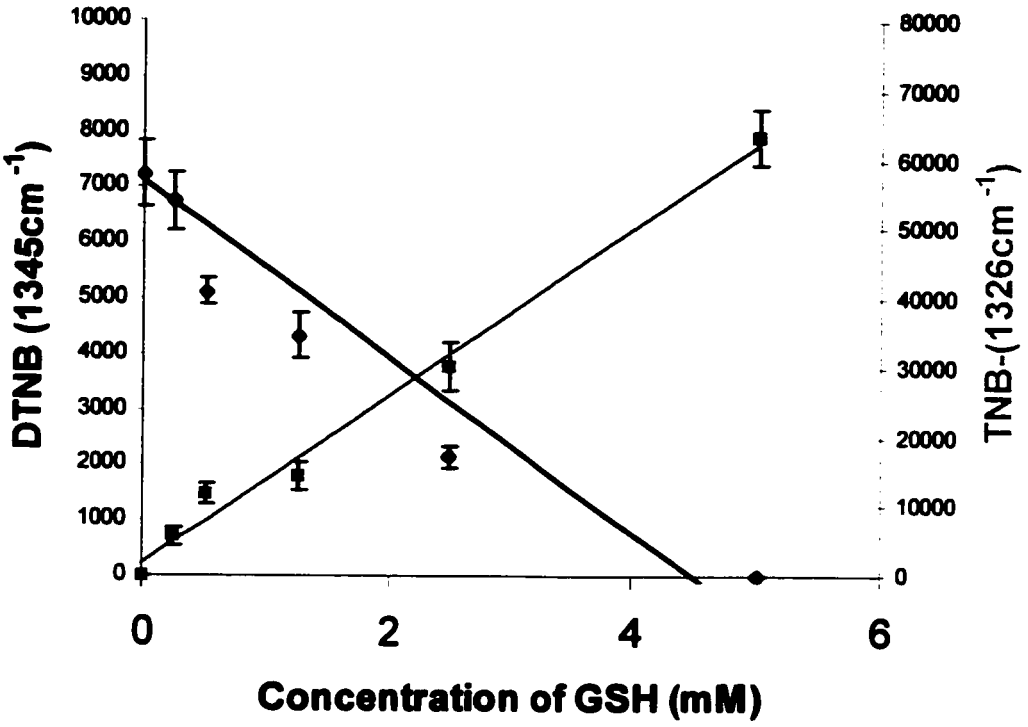

Fig 3.4.11:- Monitoring the appearance of TNB^- using Raman. DTNB (1mM) was incubated with increasing concentrations of GSH (0-5mM). The area of the peaks at $1326cm^{-1}$ (TNB^-) and $1345cm^{-1}$(DTNB) was determined for each reaction sample. The spectra were obtained with 514nm Argon laser, with 20sec exposure over 15 accumulations.

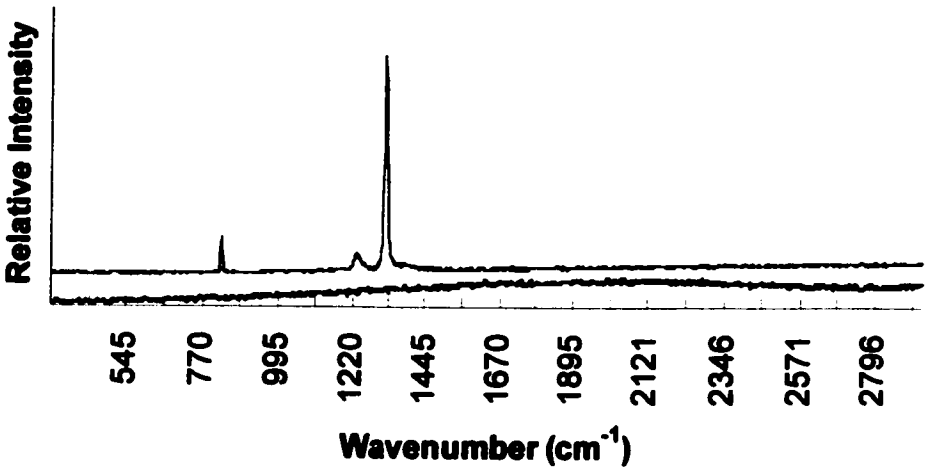

Fig 3.4.12:- Raman spectra of solid and aqueous samples of Sodium nitrite. The spectrum of Nitrite(s) was obtained using 514nm Argon laser (0.7mW). The sample was exposed for 10sec with 2 accumulations using a 50x long objective. The spectrum of 500mM nitrite(aq) in a NMR tube was obtained with 20sec exposure and 20 accumulations.

3.4.4 Biological Systems:- In the hopes that live cells or biological vesicles may prove Raman worthy, Raman spectra of liposomes, red blood cell ghosts, bacteria and live cells were measured. Liposomes were made with phosphatidyl choline and extruder to ensure uniform size. They were used as carriers of high concentrations of GSNO (500mM) and GSH (500mM). Formation of the liposomes was determined by light microscopy while proper encapsulation of sample of interest was attained by fluorescent study, Fig 13. Attempts were made to obtain Raman speaks of a single liposome containing 500mM GSH/GSNO, Fig 13. Increasing the exposure and the number of accumulations did not produce a significant peak at 2580cm^{-1}. We decided to use RBC ghosts as an alternative to liposomes since RBC ghosts were larger than liposomes. The increase in size did not increase the sensitivity since no Raman peak at 2580cm^{-1} was detected in RBC ghosts enclosed with GSH (500mM).

The final attempt was to probe live cells with Raman. Fibroblast cells grown on silicon were irradiated with 514 Argon ion laser. The subsequent Raman spectrum showed saturation by intracellular fluorescence, Fig 14. Furthermore, we attempted to Raman image the cell by monitoring the Raman scattering at 2580cm^{-1}. The live cell was highly Raman active with respect to its background. There was no peak observed at 2580cm^{-1} to correspond to the Raman image. Therefore it is reasonable to believe that the intracellular fluorescence or the presence of Raman active compounds may interfere with the thiol peak. Attempts to measure surface thiols proved to be successful using DTNB to enhance the sensitivity of the assay. An aliquot of cells was titrated with DTNB to

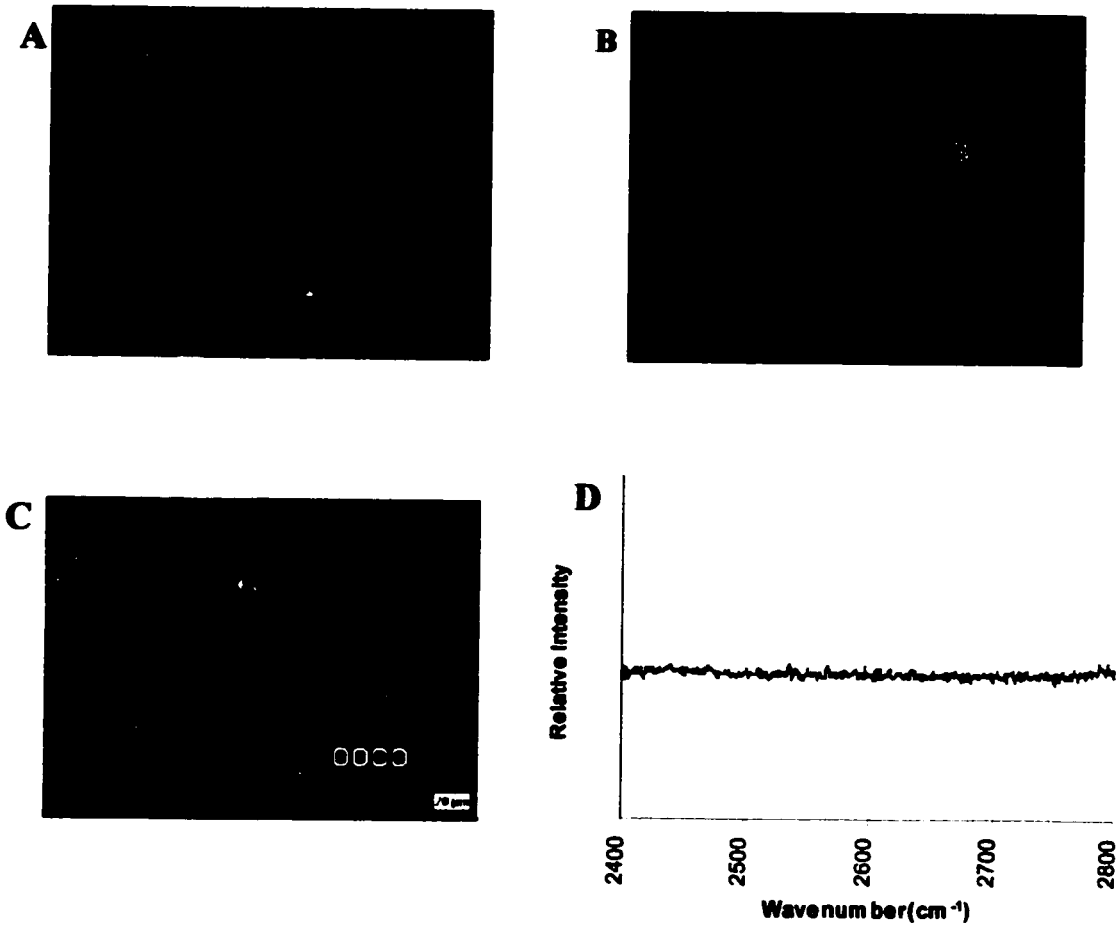

Fig 3.4.13:- (A) Formation of liposomes under light microscope (B) Encapsulation of N,N-didansylcystine by liposomes. (C)Images of liposome containing ~500mM GSH on Raman microscope. (D) Raman spectra of liposomes containing 500mM GSH. Liposomes were made with phosphatidylcholine and extruded to regulate the size of liposomes to 1000nm. Exposing the liposomes to 514nm Argon (0.7mW) laser for 30sec over 25 accumulations produced the above Raman spectra.

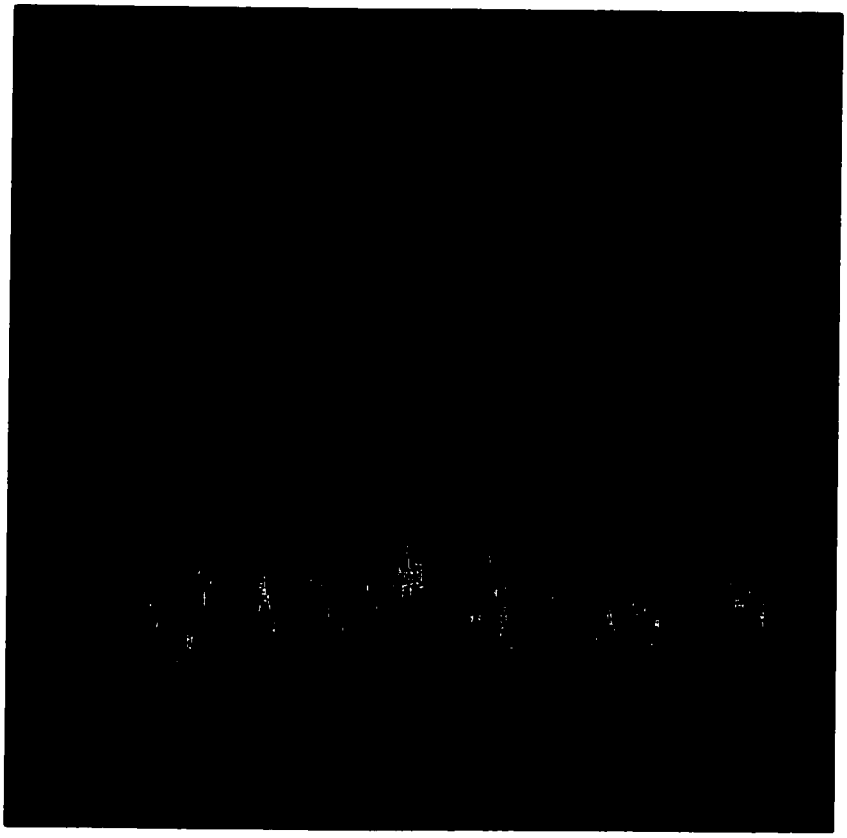

Fig 3.4.14:- Raman Image of Hamster lung fibroblast. The image was obtained using a 50x objective and a 514nm argon ion laser (0.7mW). The image area was adjusted to 25nm x 25nm.

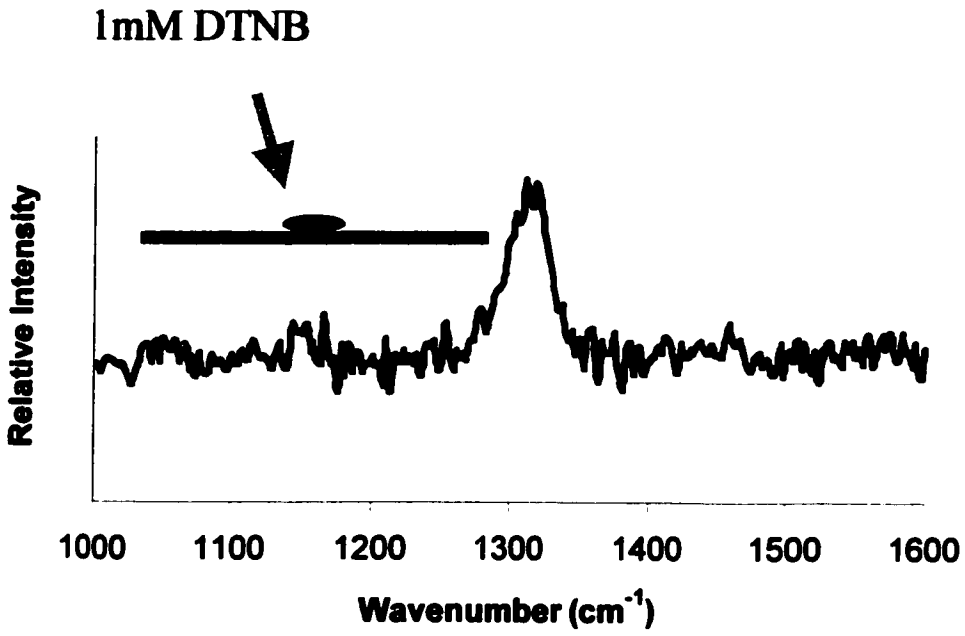

Fig 3.4.15:- Raman spectrum of cell surface thiol derived TNB^-. Hamster lung fibroblasts ($3x10^6$ cells) were scraped off confluent $35mm^2$ petri dishes and incubated with 50μL of DTNB (1mM). The static Raman spectrum of the mixture was obtained using Argon 514nm laser with 20sec exposure over 20 accumulations.

promote maximal formation of TNB^-. Raman band at $1326cm^{-1}$ is indicative of the surface thiols in fibroblasts, Fig 15.

Various media (silicon, silver, gelatin) were used to obtain spectra of liposomes, RBC ghosts, and live cells. *In vitro* attempts to increase sensitivity of thiols with Raman was not successful, possibly due to the reaction between silver and thiols. Using liposomes, red blood cells or live cells on silver, an increase in sensitivity was expected due to the presence of the membrane. The membrane provides a separation between the intravessicular GSH and the silver surface thereby minimizing the thiol-silver interactions and maximizing the SERS effect. However, there was no significant difference observed.

Raman spectroscopy was also used to probe bacterial cultures. *E. coli* grown and washed in buffer was smeared onto silicon to obtain its Raman signature. Irradiation of cell sample with 514nm laser did not evoke any Raman signals. Studies by Maquelin *et al.*, (2000) used a 514nm Argon ion laser with 100mW to obtain Raman signals from microorganisms such as *E.coli*. Furthermore, they were able to distinguish various microorganisms based on the signature Raman spectra. In our study, the 514nm Argon ion laser with 0.7mW did not evoke any spectra even with longer periods of irradiation.

3.5 Discussion

Many assays have been developed for monitoring thiols, nitric oxide and its metabolites. We aimed to develop a dynamic assay in live cells for monitoring the levels of thiols and S-nitrosothiols. Studies using non-invasive techniques would be invaluable. Using Raman spectroscopy, we observed spectral differences between thiols and S-nitrosothiols. As previously reported by Tuma *et al.*, (1993) the Raman band corresponding to the SH stretch at 2580cm^{-1} was observed in GSH. We also detected the disappearance of the band upon nitrosation. The sensitivity of Raman for GSH at this band was greater than 100mM. Nitrosation of GSH gave rise to a unique band at 371cm^{-1}. Yamamoto *et al.*,(1994) reported that sulfhydryl-mercury stretching occurs at 330cm^{-1} and proposed that most thiol containing complexes breathe in this range. Using the S-N stretch at 371cm^{-1}, the sensitivity of Raman for GSNO was also greater than 100mM. These Raman bands are not very sensitive to low concentrations of GSH/GSNO, thus physiologically insignificant. Previous studies have been able to successfully detect low mM (~6mM) levels of β-mercaptoethanol. The sensitivity in these studies was improved by using an argon ion laser (514nm) with 200mW of radiant power. Our data showed that the integrity of the GSH sample was maintained when exposed to either 633nm or 514nm laser. The oxidation of GSH was negligible within the observable time. On the other hand, Resonance Raman with GSNO samples (λ_{max} 340nm, λ_{max} 540nm) were more sensitive to photodecomposition, especially when exposed to 514nm laser.

We then used gold colloids and silver coated slides to increase the sensitivity of GSH. Gold colloids reduced the Raman sensitivity of GSH by 50% where as silver increased by 25%. The reduction in sensitivity is a result of the reaction between GSH and gold. This highly reactive nature between gold and thiols have been used as binding agents to bind gold to self assembled monolayers, and antibodies for the purposes of immunoassays (Karyakin *et al.*, 2000; Ulman *et al.*, 2000). Thiols are also reactive to silver as demonstrated by Lin *et al.* where alkanethiols were linked to silver by the SH group to bind LDL particles (Lin *et al.*, 2001). Both gold and silver have shown reactivity towards free thiols yet silver coated slides showed increase in thiol sensitivity. In consideration to the use of SERS, enhancements as high as 10^6 fold have been reported. Therefore our results may represent an equilibrium between the SERS mediated enhancement and thiol-metal reaction. In both instances, the SH stretch should be decreased as a result of S-metal bond formation. Thiol-metal vibrations are known to occur in the range 200-300cm^{-1}, no significant peaks were resolved in that region to indicate thiol-metal interaction. This observation is not attributed to the absence of thiol-metal interaction, but merely the lack of sensitivity.

Sulfhydryl reagents, such as DTNB have been used in Raman spectroscopic determination of surface thiols. DTNB reacts with thiols to produce an anionic species, TNB^-. The formation of TNB^- is marked by an increase in electronic absorbance at 412nm or a Raman shift in the NO_2 stretch. The symmetrical stretch of NO_2 in DTNB occurs at 1345cm^{-1} while in TNB^- the Raman band is at 1326cm^{-1}. The Raman shift is caused by the presence of the negative charge on the species. In our study, DTNB/TNB^-

was able to improve the sensitivity level of GSH (low mM levels). We were also able to detect thiols on the surface of fibroblasts using DTNB. However, DTNB is a better indicator of thiol levels using UV/vis spectrometric methods rather than Raman spectroscopy. Another observation is that the Raman shift between DTNB and TNB^- is small; therefore conditions must be optimized for maximal turnover of DTNB to TNB^-. Studies by Rospendowski *et al.*, (1992) have been very successful in detecting 10^{-6}M TNB^- using SERRS techniques. Lower detection limits were attained by using TNB^- adsorbed to silver colloids and irradiating with 457nm laser. The wavelength of laser line and the electronic adsorption of TNB^- (412nm) are close enough to exhibit resonance Raman effects. Using SERRS, TNB^- Raman band shifted from 1321cm^{-1} to 1329cm^{-1} and DTNB shifted from 1345cm^{-1} to 1337cm^{-1}. The overall shift in Raman spectra is attributed to the change in electron density due to adsorption to silver colloids. TNB^- Raman peaks are also sensitive to the surrounding microenvironment. The use of DTNB to detect thiols in albumin lead to a shift in TNB^-, possibly related to the behaviour of TNB^- in the crevice of albumin where Cys 34 is situated. The change in dielectric constants of the microenvironment within the protein and water may impose steric effects (Rospendowski *et al.*, 1992).

Large concentrations of GSNO and GSH were encapsulated in small vesicles such as RBC ghosts and liposomes to mimic live cells. We were unable to obtain Raman peaks corresponding to thiols in both instances. In addition, live cells loaded with GSH were also unable to generate Raman signals. Even though it was possible to obtain a Raman image for the cell, it was difficult to isolate the SH peak. Studies by Puppels *et*

al., (2001) were successful in obtaining Raman spectra of single cells using confocal Raman microspectroscopy. Using a 514nm Argon ion laser (15mW) equipped with a water immersion objective (x63, 1.2NA), Raman spectra of DNA-Protein complexes were obtained providing information on composition and structure. In our study, confocal mode was used with the same laser of lesser power (0.7mW) equipped with a water immersion objective (50x, 0.87 NA). With a lower powered laser and poor NA we were unable to achieve similar resolution as that of Puppels *et al.*, (2001).

Conclusion

This study deals with various aspects of NO and S-nitrosothiol (RSNO) metabolism with regards to its physiological and pathophysiological role. The initial study has put forth a plausible mechanism by which S-nitrosothiols are transported into live cells. This has been shown to occur via a cell surface protein disulfide isomerase (csPDI). The involvement of the enzyme in catalyzing high affinity, rapid kinetics of physiologically relevant S-nitrosothiols will immensely contribute to future work in this field.

NO/RSNO metabolism in the vascular system is critical in maintaining vascular tone. Perturbations in NO levels have been attributed to the induction of vascular damage. Our study focused on the effects of homocyst(e)ine on NO production and RSNO transport. Previous studies on the thrombotic effects observed in patients with hyperhomocysteinaemia have been ambiguous. We have shown the ability of homocyst(e)ine to inhibit NO production and RSNO transport without affecting the isomerization activity catalyzed by csPDI. This demonstrates the role of homocyst(e)ine as a pro-aggregatory molecule and thus an inducer of vascular damage.

Scientific research has always been hindered by the lack of sensitive analytical tools. We attempted to use Raman spectroscopy as a dynamic, non-invasive monitor of cell metabolites. This study has shown promise in its ability to monitor transnitrosation reactions as well as the associated conformational changes. The lack of sensitivity of Raman, which has plagued its use in the past largely, hindered the ability to detect physiologically relevant concentrations of various cell metabolites.

References

Abu-Soud, H.M., Wu, C., Ghosh, D.K., Stuehr, D.J., (1998) *Biochemistry* **37**(11), 3777-86

Abu-Soud, H.M., Yoho, L.L., Stuehr, D.J., (1994) *J Biol Chem.* **269**(51), 32047-50

Akagi, S., et al., (1988) *J. Histochem. Cytochem.* **36**, 1069-1074

Albritton, L.M., Tseng, L., Scadden, D., Cunningham, J.M., (1989) *Cell* **57**(4), 659-66

Al-Sa'Doni, H., Ferro, A., (2000) *Clin. Sci.* **98**, 507-520

Arnelle DR, Stamler JS., (1995) *Arch. Biochem. Biophys.* **318**(2), 279-85.

Asahi, M., Fujii, J., Suzuki, K., Seo, H.G., Kuzuya, T., Hori, M. Tada, M., Fujii, S., Taniguchi, N., (1995) *J. Biol. Chem.* **270**, 6689-6699

Askew, S.C., Butler, A.R., Flitney, F.W., Kemp, G.D., Megson, I., (1995) *Bioorg. Med. Chem.* **3**, 1-9

Azuma, J., Sawamura, A., Awata, N., (1992) *Jpn. Circ. J.* **56**, 95-99

Barbul, A., (1986) *J. Parenter. Enteral. Nutr.* **10**, 227-238

Barnett, D.J., Rios, A.M., Williams, D.L.H., (1995) *J. Chem. Soc. Perkin Trans.* **27**, 1279-1282

Barrett, J., Fitygibbones, L. J., Glauser. J., Still, R.H., Young, P.N.W. (1966) *Nature* **211**, 848

Baydoun, A.R., Emery, p.W., Pearson, J.D., Mann, G.E., (1990) *J. Physiol.* **41**.

Beckman, J.S., Beckman, T.W., Chen, J., Marshall, P.A., Freeman, B.A., (1990) *Proc. Natl. Acad. Sci.* **87**, 1620-1624

Bennett V., (1985) *Annu Rev Biochem.* **54**, 273-304

Bentz, B.G., Simmons, R.L., Haines, G.K. 3rd, Radosevich, J.A., (2000) *Head Neck* **22**(1), 71-83

Bogle, R.G., Coade, S.B., Moncada, S., Pearson, J.D., Mann, G.E., (1991) *Biochem. Biophys. Res. Commun.* **180**(2), 926-32

Boushey, C.J, Beresford, S.A., Omenn, G.S., Motulsky, A.G., (1995) *JAMA* **274**(13), 1049-57
Brattstrom, L.E., Hardebo, J.E., Hultberg, B.L., (1984) *Stroke.* **15**(6), 1012-6.

Bredt, D.S., (1999) *Free Rad. Res.* **31**, 577-596

Brune, B., Mohr, S., Messmer, U.K., (1996) *Rev. Physiol. Biochem. Pharmacol.***127**, 1-30

Burgess, J.K., Hotchkiss, K.A., Suter, C., Dudman ,N.P., Szollosi, J., Chesterman, C.N., Chong, B.H., Hogg, P.J, (2000) *J Biol Chem.* **275**(13), 9758-66.

Bussolati, O., Laris, P.C., Nucci, F.A., Dall'Asta, V., Franchi-Gazzola, R., Guidotti, G.G., Gazzola, G.C., (1989) *Am. J. Physiol.* **256**(4 Pt 1), C930-5

Butcher, E.C., (1991) *Cell* **67**, 1033-1036

Butler, A.R., Al-Sa' doni, H.H., Megson, J.L., Flitney, F.W., (1998) *Nitric Oxide Biol. Chem.* **2**, 193-202

Burton, B.K., (2000) *Clin. Liver. Dis.* **4**(4), 815-30

Canas, P.E., (1992) *Acta Physiol. Pharmacol. Ther. Latinoam* **42**, 133-137

Carter, D.C., Chang, B., Ho, J.X., Keeling, K., Krishnasami, Z., (1994) *Eur J Biochem.* **226**(3), 1049-52

Casey, T.E., Harrison, A.C., Zimmerman, J.K., Hilderman, R.H., (2000) *Arch. Biochem. Biophys.* **379**, 283-291

Caspers, P.J., Lucassen, G.W., Carter, E.A., Bruining, H.A., Puppels, G.J., (2001) *J Invest Dermatol.* **116**(3), 434-42.

Caspers, P.J., Lucassen, G.W., Wolthuis, R., Bruining, H.A., Puppels, G.J., (1998) *Biospectroscopy.* **4**(5 Suppl), S31-9.

Chen, K., Lin, Y., Detwiler, T., (1992) *Blood* **79**, 2226-2228

Chen, P.F., Tsai, A.L., Berka, V., Wu, K.K., (1996) *J Biol Chem.* **271**(24), 14631-5.

Chen, X., Medford, R,.M., (1999) Vascular Adhesion molecules and inflammation (Ed. Pearson, J.D.), Birkhauser Verlag, Boston

Chen, X., Wen, Z., Xian, M., Wang, K., Ramachandran, N., Tang, X., Schlegel, B., Mutus, B., Wang., P.g., (2001) *J. Org Chem.*, Accepted Aug 2001

Cheng, S., Gong, Q.H., Parkinson, C., Robinson, E.A., Apella, E., Merlino, G.T., Pastan, I., (1987) *J. Biol. Chem.* **262**, 11221-11227

Chillaron, J., Estevez, R., Mora, C., Wagner, C.A., Suessbrich, H., Lang, F., Gelpi, J.L.,Testar, X., Busch, A.E., Zorzano, A., Palacin, M., (1996) *J. Biol. Chem.* **271**(30), 17761-70

Chivers, P.T., Laboissiere, M.C.A., Raines, R.T., (1996) *EMBO J.* **15**, 2659-2667

Chivers, P.T., Raines, R.T., (1997) *Biochemistry* **36**, 15810-15816

Cho, H.J., Xie, Q.W., Calaycay, J., Mumford, R.A., Swiderek, K.M., Lee, T.D., Nathan, C., (1992) *J. Exp. Med.* **176**(2),599-604.

Christensen, H.F., (1984) *Biochem. Biophys. Acta* **779**, 255-269

Christensen, H. N., (1990) *Physiol. Rev.* **70**,43

Christensen, H. N., (1964) *PNAS* **51**, 337-344

Closs, E.I., Scheld, J.S., Sharafi, M., Forstermann, U., (2000) *Mol. Pharmacol.* **57**(1), 68-74.

Connor, M.J., Wheeler, L. A., (1987) *Photochem. Photobiol.* **46**, 239-245

Cotton, M.T., (1988) *Spectroscopy of surfaces* (Ed. Clark, R.J.H, Hester, R.E.), 91-153

Couet, J., et al., (1996) *Biochemistry* **35**, 14800-14805

Crane, B.R., Arvai, A.S., Ghosh, D.K., Wu, C., Getzoff, E.D., Stuehr, D.J., Tainer, J.A., (1998) *Science* **279**(5359), 2121-6.

Crieghton, T.E., Hillson, D.A., (1980) *J. Mol. Biol. 142*, 43-62

Dai, Y., Wnag, C., (1997) *J. Biol. Chem.* **272**, 27572-27576

Darby, N.J., Creighton, T.E., (1995) *Biochemistry* **34**, 11725-11735

Darby, N.J., Freedman R.B., Creighton, T.E., (1994) *Biochemistry* **33**, 7937-7947

Darby, N.J., Penka, E., Vincentilli, R., (1998) *J. Mol. Biol.* **276**, 239-247

Dardik, R., Varon, D., Tamarin, I., Zivelin, A., Salomon, O., Shenkman, B., Savion, N., (2000) *Thromb. Haemost.* **83**(2),338-44.

Deneke, S.M., Baxter, D.F., Phelphs, D.T., Fanburgh, B.L., (1989) *Am. J. Physiol.* **257**, L265-L-271

Deneke, S.M., Gershoff, S.N., Fanberg, B.L., (1983) *J. Appl. Physiol.* **4**, 147-151

Deneke, S.M., Lynch, B.A., Fanberg, B.L., (1985) *J. Nutr.* **115**, 726-732

Deneke, S.M., Lynch, B.A., Fanberg, B.L., (1985) *J. Appl. Physiol.* **58**, 571-574

Deneke, S.M., Steiger, V., Fanberg, B.L., (1987) *J. Appl. Physiol.* **63**, 1966-1971

Deves, R., Boyd, C.A., (1998) *Physiol. Rev.* **78**(2), 487-545

Deves, R., Chavez, P., Boyd, C.A., (1992) *J. Physiol.* **454**, 491-501

Donoghue, N., Yam, P.T.W., Jiang, X., Hogg, P.J., (2000) *Protein Science* **9**, 2436-2445

Dudman, N.P., Guo, X.W., Gordon, R.B., Dawson, P.A., Wilcken, D.E.J, (1996)Nutr. 126(4 Suppl), 1295S-300S

Dudman, N.P., Temple, S.E., Guo, X.W., Fu, W., Perry, M.A.,(1999) *Circ. Res.* **84**(4),409-16.

Dudman, N.P., Hicks, C., Wang, J., Wilcken, D.E., (1991) *Atherosclerosis* **91**(1-2),77-83.

Dyson H.J., Gippert G.P., Case D.A., Holmgren A., Wright P.E., (1990) *Biochemistry.* **29**(17), 4129-36

Dyson, H.J., Jeng, M.F., Tennant, L.L. Slaby, I., Lindell, M., Cui, D.S., Kuprin, S., Holmgren, A., (1997) *Biochemistry* **36**, 2622-2636

Eklund, H., Gleason, F.K., Holmgren, A., (1991) *Proteins* **11**, 13-28

Essex, D.W., & Li, M., (1999) *British Journal of Haematology* **104**, 448-454

Ewadh, M.J.A., Tudball, N., Rose, F.A., (1990) *Biochim Biophys. Acta* **1054**, 263-266

Fenouillet, E., Barbouche, R., Courageot, J., Miquelis, R., (2001) *J. Infect. Dis.* **183**(5), 744-52

Ferrari, D.M., Nguyen, P., Kratzin, H.D., Soling, H.D., (1998) *Eur. J. Biochem.* **255**, 570-579

Ferrari, D.M., Soling, H., (1999) *Biochem. J.* **339**, 1-10

Flagg, E.W., Coates, R.J., Jones, D.P., Eley, J.W., Gunter, E.W., Jackson, B., and Greenberg, R.S., (1993) *Brit. J. Nutr.* **70**, 797-808

Fossetta, J.D., Niu, X.D., Lunn, C.A., Zavodny, P.J., Narula, S.K., Lundell, D., (1996) *FEBS Lett.* **379**(2), 135-8

Fossel, E.T., Solomon, A.K., (1979) *BBA* **553**(1), 142-53

Frand, A.R., Kaiser, C.A., (1998) *Mol. Cell* **1**, 161-170

Freedman, R.B., (1984) *Trends Biochem. Sci.* **9**, 438-441

Freedman, R.B., Hawkins, H.C., McLaughlin, S.H., (1995) *Methods Enzymol.* **251**, 397-406

Freedman, R., Hirst, T.R., Tuile, M.F., (1994) *Trends in Biochem. Sci.* **19**, 331-336

Freshney, I. R., (2000) Culture of Animal Cells, pp314

Frixen, U.H., Behrens, J., Sachs, M., Eberle, G., Voss., B., Warda, A., Lochner, D., Birchmeier, W., (1991) *J. Cell. Biol.* **113**, 173-185

Gaston, B., (1999) *BBA* **1411**, 323-333

Geetha-Habib, M., Noiva, R., Kaplan, H.A., Lennarz, W., (1988) *Cell* **54**, 1053-1060

Gilbert, H.F., (1989)Biochemistry. 28(18), 7298-305

Goldberg, R.F., Epstein, C.J., Anfinsen, C.B., (1964) *J. Biol. Chem.* **239**, 1406-1410

Gorren, A.C., List, B.M., Schrammel, A., Pitters, E., Hemmens, B., Werner, E.R., Schmidt, K.,Mayer B., (1996) *Biochemistry* **35**(51), 16735-45

Goss, S.P.A, Singh, R.J., Hogg, N., Kalyanaraman, B., (1999) *Free Rad. Res.* **31**, 597-606

Griffith, O.W., Stuehr, D.J., (1995) *Annu Rev Physiol.* **57**, 707-36

Griffiths, G., Ericsson, M., Krijnse-Locker, J., Nilsson, T., Goud, B., Soling, H.D., Tang, B.L., Wong, S.H., Hong, W., (1994) *J. Cell. Biol.* **127**, 1557-1574

Guthapfel, R., Gueguen, P., Quemeneur, E., (1996) *J. Biol. Chem.* **271**, 2663-2666

Halliwell, B., Gutteridge, J.M., (1984) *Biochem. J.* **219**, 1-14

Harris, M.B., Ju, H., Venema, V.J., Liang, H., Zou, R., Michell, B.J., Chen, Z.P., Kemp, B.E., Venema, R.C., (2001) *J Biol Chem.* **276**(19), 16587-91

Harrison, D.G., (1999) *J Clin Invest.* **100**(9), 2153-7

Hawkins, H.C., Blackburn, E.C., Freedman, R.B., (1991) *Biochem. J.* **275**, 349-353

Hayes, K.C., Pronczuk, A., Addesa, A.E., Stephan, Z.F., (1989) *Am. J. Clin. Nutr.* **49**, 1211-1216

He, M.X., Carter, D.C., (1992) *Nature* **358**, 209-215

Heinecke, J.W., Rosen, H., Suzuki, L.A., Chait, A., (1987) *J. Biol. Chem.* **262**(21), 10098-103

Hemmens, B., Gorren, A.C., Schmidt, K., Werner, E.R., Mayer, B., (1998) *Biochem J.* **332** (Pt 2), 337-42

Hemmens, B., Mayer, B., (1998) *Methods Mol Biol.* **100**, 1-32

Herzberg, G, (1950), in Molecular Spectra and Molecular Structure, 658, Van Nostrand, Princeton, NJ

Hobbs, A.J., Higgs, A., Moncada, S., (1999) *Annu. Rev. Pharmacol. Toxicol.* **39**, 191-220

Hogg, N., Kalyanaraman, B., (1998) *Biochim. Biophys. Acta* **1411**, 378-384

Hogg, N., Kalyanaraman, B., Joseph, J., Struck, A., Parthasarathy, S., (1993) *FEBS Lett.* **334**(2), 170-4

Hogg, N., Singh J.R., Goss, P.A. S., Kalyanaraman, B., (1996) *Biochem. Biophys. Res. Comm.* **224**, 696-702

Hogg, N., Singh, R.J., Konorev, E., Joseph, J., Kalyanaraman, B., (1997) *Biochem. J.* **323** (Pt 2), 477-81

Holmgren, A., (1995) *Structure* **3**, 239-243

Hoog, J., O., Von Bahr Lindstrom, H., Josephson, S., Wallace, B. J., Kushner, S.R., Jornval, H., Holmgren, A., (1984) *Biosci Rep.* **4**, 917-923

Hotchkiss, K., Chesterman, C., Hogg, P., (1996) *Biochemistry*, **35**, 9761-9767

Huber-Wunderlich, M., Glockshuber, R., (1998) *Folding Design* **3**, 161-171

Huige, L., Forstermann, U., (2000) *J. Pathol.* **190**, 244-254

Hultberg, B., Andersson, A., Isaksson, A., (1998) *Biochim. Biophys. Acta* **1448**, 61-69

Humphries, M.J., (1990) *J. Cell. Sci* **97**, 585-92

Hurshman, A.R., Marletta, M.A., (1995) *Biochemistry.* **34**(16),5627-34.

Huxtable, R.J., (1992) *Physiol. Rev.* **72**, 101-163

Hwang, C., Sinskey, A.J. and Lodish H.F., (1992) *Science* **257**, 1496-1502

Hynes, R.O., Lander, A.D., (1992) *Cell* **68**, 302-322

Ignarro, L.J., Wood, K.S., Ballot, B., Wolin, M.S., (1984) *J. Biol. Chem.* **259**(9), 5923-31

Jakubovic, H.R., Ackerman, A.B., (1992) in Dermatology (ed Moschella, S.L., Hurley, H.J., Saunders, W.B.), 3-87, Philadelphia, Pennsylvania

Jeng, M.F., Holmgren, A., Dyson, H.J., (1995) *Biochemistry* **34**, 10101-10105

Jiang, Q., Elson-Schwab, I., Courtemanche, C., Ames, B.N., (2000) *Proc. Natl. Acad. Sci.* **97**(21), 11494-11499

Jiang, X., Fitzgerald, M., Grant, M.C., Hogg, P.J., (1999) *J. Biol. Chem.* **274**(4), 2416-2423

Jones, C., Vasquez-Vivary, J., Griscavage, J., Martasek, P., Master, B.S.S., Kalyanaraman, B., Gross, S.S., (1999) *Acta Physiol Scand* **167**, 645- 59

Josephy, P.D., Rehorek, D., Janzen, E.D., (1984) *Tetrahedron Letters* **25**, 1685-1688

Kanai, Y., Fukasawa, Y., Cha, S.H., Segawa, H., Chairoungdua, A., Kim, D.K., Matsuo, H., Kim, J.Y., Miyamoto, K., Takeda, E., Endou, H., (2000) *J. Biol. Chem.* **275**(27), 20787-93

Kanner, J., Harel, S., Granit, R., (1991) *Arch. Biophys. Biochim.* **289**, 130-136

Katti, S.K., LeMaster, D.M., Eklund, H., (1990) *J Mol Biol.* **212**(1), 167-84

Kaetzel, C.S., Rao, C.K., Lamm, M.E., (1987) *Biochem J.* **241**(1), 39-47

Kelly, E.E., Wagner, B.A., Buettner, G.R., Burns, C.P., (1999) *Arch Biochem Biophys.* **370**(1), 97-104

Kelm, H., (1999) *BBA* **1411**, 273-289

Kemmink, J., Darby, N.J., Dijistra, K., Nilges, M., Crieghton, T.E., (1997) *Curr. Biol.* **7**, 239-245

Kerwin, J.F. Jr., Lancaster, J.R. Jr., Feldman, P.L., (1995) *J Med Chem.* **38**(22), 4343-62

Khan, B.V., Parthasarathy, S.S., Alexander, R.W., Medford, R.M.., (1995) *J. Clin. Invest.* **95**(3), 1262-70

Khan, B.V., Harrison, D.G., Olbrych, M.T., Alexander, R.W., Medford, R.M., (1996) *Proc. Natl. Acad. Sci.* U S A. **93**(17), 9114-9

Kharitonov, V.G., Sundquist, A.R., Sharma, V.S., (1995) *J. Biol.Chem.* **270** (47), 28158-28164

Klappa, P., Hawkins, H.C., Zimmerman, R., (1997) *Eur. J. Biochem.* **248**, 37-42

Kortemme, T., Darby, N.J., Creighton, T.E., (1996) *Biochemistry* **35**, 14503-14511

Koivu, J., Myllyla, R., Helaakoski, T., Pilajanieme, T., Tasanen, K., Kivirikko, K.I., (1987) *J. Biol Chem.* **262**, 6447-6449

Kries, T., Vale, R., (1993) Extracellular Matrix and Adhesion Proteins, Oxford University Press, New York.

Kroning, H., Kahne, T., Ittenson, A., Franke, A., Ansorge, S., (1994) *Scand. J. Immunol.* **39**, 346-350

Kragh-Hansen, U., (1990) *Dan Med Bull.* **37**(1),57-84

Lahav, J., Gofer-Dadosh, N., Luboshitz, J., Hess, O., Shaklai, M., (2000) *Febs Letters* **475**(2), 89-92

Lambert, N., Freedman, R.B., (1983) *Biochem. J.*, **213**, 235-243

Lash, L.H., Hagen, T.M., Jones, D.P., (1986) *Proc. Natl. Acad. Sci.* **83**, 4641-4645

Li, H., Hanson, C., Fuchs, J.A., Woodward, C., Thomas, G.J. Jr., (1993) *Biochemistry.* **32**(22), 5800-8

Li, H., Thomas, G.J., (1991) *J. Am. Chem. Soc.* **113**, 1157-1175

Liu, L., Hausladen, A., Zeng, M., Que, L., Heitman, J., Stamler, J.S., (2001) *Nature.* **410**(6827), 490-4

[a]Liu, X., Miller, M.J., Joshi, M.S., Thomas, D.D., Lancaster, J.R., (1998) *Proc. Natl. Acad. Sci. U S A.* **95**(5), 2175-2179

[b]Liu, Z., Rudd, M.A., Freedman, J.E., Loscalzo, J., (1998) *J. Pharmacol. Exp. Ther.* **284**(2), 526-34

Lundstrom, J., Holmgren, A., (1990) *J. Biol. Chem.* **265**, 9114-20

Lundstrom, J., Krause, G., Holmgren, A., (1992) *J. Biol. Chem.* **267**, 9047-9052

MacDonald, R.B., MacDonald, R.I., Menco, B., Takeshita, K., Subbarao, N.K., Hu, L., (1991) *BBA* **1061**, 297-303

Malinski, T., (1998) *Pol. J. Pharmacol.* **50**, 387-191

Mandel, R., Ryser, H.J.P., Ghani, F., Wu, M., Peak, D., (1993) *Proc. Natl. Acad. Sci.* **90**, 4112-4119

Maquelin, K., Choo-Smith, L.P., van Vreeswijk, T., Endtz, H.P., Smith, B., Bennett, R., Bruining, H.A., Puppels, G.J., (2000) *Anal Chem.* **72**(1), 12-9

Marks, D.S., Vita, J.A., Folts, J.D., Keaney, J.F. Jr., Welch, G.N., Loscalzo, J., (1995) *J. Clin. Invest.* **96**(6), 2630-8

Martin, J.L., (1995) *Structure* **3**, 245-250

Masters, B.S., McMillan, K., Sheta, E.A., Nishimura, J.S., Roman, L.J., Martasek, P., (1996) *FASEB J.* **10**(5), 552-8

Mayer, B., Pfeiffer, S., Schrammel, A., Koesling, D., Schmidt, K., Brunner, F., (1998) *J. Biol. Chem.* **273**(6), 3264-3270

Mayer, B., Werner, E.R., (1995) *Adv Pharmacol.* **34**, 251-61

McCully, K.S., (1993) *Ann. Clin. Lab. Sci.* **23**(6), 477-93

Meister, A., (1991) *Pharmac. Ther.* **51**, 155-194

Meister, A., Tate, S.S., Griffith, O.W., (1981) *Methods in Enzymology* **77**, 237-253

Mendes Ribeiro, A.C., Brunini, T.M., Yaqoob, M., Aronson, J.K., Mann, G.E., Ellory, J.C., (1999) *Pflugers Arch.* **438**(4), 573-5

Mile, B., Rowlands, C.C., Sillaman, P.D., Fildes, M., (1992) *J. Chem. Soc. Chem. Commun.* **12**, 882-883

Mizushima, S., Nara, Y., Sawamura, M., Yamori, Y., (1996) *Adv. Exp. Med. Biol.* **403**, 615-622

Moghadasian, M.H., McManus, B.M., Frohlich, J.J., (1997) *Arch. Intern. Med.* **157**, 2299-2308

Mohney, K.B., Walker. G.C., (1997) *J. Am. Chem. Soc.* **119**, 9311-9312

Morjana, N.A., Gilbert, H.F., (1991) *Biochemistry* **30**, 4985-4990

Mudd, S.H., Levy, H.L., Skovby, F., (1989) The metabolic basis of inherited disease (Eds Scriver, a.L., Beaudet, W.S., Sly, Valle) 6ed., 693-734, McGraw Hill

Munro, S., and Pelham, H.R.B., (1987) *Cell* **48**, 899-907

Nakamura, K., Era, S., Ozaki, Y., Sogami, M., Hayashi, T., Murakami, M., (1997) *FEBS Lett.* **417**(3), 375-8

Nedospasov, A., Rafikov, R., Beda, N., Nudler, E., (2000) *Proc Natl Acad Sci* **97**(25), 13543-8

Nelson, W.H., Manoharan, R., Sperry, J.F., (1992) *Appl. Spectrosc. Rev.* **27**, 67-124

Niittynen, L., Nurminen, M., Korpela, R., Vapaatalo, H., (1999) *Ann. Med.* **31**, 318-326

Obata, T., Kitagawa, S., Gong, Q.H., Pastan, I., Chen, S.Y., (1988) *J. Biol. Chem.* **263**, 782-785

Odland, G.F., (1991) ed. L.A. Goldsmith, Oxford University Press, New York, pp 3-62

O'Donnell, M., Smith, W.E., MacCuish, A.C., Wilson, R., (1995) *Analyst.* **120**(9), 2357-60

Olszewski, A.J., McCully, K.S., (1993) *Free Rad. Biol. and Med.* **14**, 683-693

Paolocci, N., Biondi, R., Bettini, M., Lee, C.I., Berlowitz, C.O., Rossi, R., Xia, Y., Ambrosio, G., L'Abbate, A., Kass, D.A., Zweier, J.L., (2001) *J Mol Cell Cardiol.* **33**(4), 671-9

Park, J.W., Billman, G.E., Means, G.E., (1993) *Biochem. Mol. Biol. Int.* **30**(5), 885-91

Parthasarathy, S., (1987) *Biochim. Biophys. Acta.* **917**(2):337-40

Pietraforte, D., Mallozzi, C., Scorza, G., Minetti, M., (1995) *Biochemistry* **34**(21), 7177-85

Plow, E.F., McEver, R.P., Coller, B.S., Woods, V.L., Marguerie, G.A., (1985) *Blood* **66**, 724-727

Pollard, M.G., Travers, K.J., Weissman, J.S., (1998) *Mol. Cell* **1**, 171-182

Preik-Steinhoff, H., Zink, S., Rosen, P., Kelm, M., (1995) *Biochem Biophys Res Commun.* **213**(2), 447-53

Prevelige, P.E. Jr., Thomas, D., Aubrey, K.L., Towse, S.A., Thomas, G.J. Jr., (1993) *Biochemistry.* **32**(2), 537-43

Pruefer, D., Scalia, R., Lefer, A.M.,(1999) *Gen. Pharmacol.*, **33**(6), 487-98.

Quemeneur, E., Guthapfel, R., Gueguen, P., (1994) *J. Biol. Chem.* **269**, 5485-5488

Rodriguez-Crespo, I., Gerber, N.C., Ortiz de Montellano, P.R., (1996) *J. Biol. Chem.* **271**(19), 11462-7.

Rospendowski, B.N., Campbell, J.M., Reglinski, J., Smith, W.E., (1992) *Eur Biophys J.* **21**(4), 257-61

Ruoppolo, M., Freedman, R.B., Pucci, P. Marino, G., (1996) *Biochemistry* **35**, 13636-13646

Ryser, H.J., Levy, E.M., Mandel, R., DiSciullo. G.J., (1994) *Proc. Natl. Acad. Sci.* **91**, 4559-4563

Scanu, A.M., Fless, G.M., (1990) *J. Clin. Invest.* **85**(6), 1709-15

Scharfstein, J.S., Keaney, J.F. Jr., Slivka, A., Welch, G.N., Vita, J.A., Stamler, J.S., Loscalzo, J., (1994) *J. Clin. Invest.* **94**(4), 1432-9

Schrimer, R.H., Krauth-Siegel, R.L, Schulz, G.E., (1989) in Coenzymes and Cofactors (Dolphin, D.,Pouson, R., and Avromovic, A., eds) Vol 2, pp161-204, Wiley, New York

Simon, D.I., Mullins, M.E., Jia, L., Gaston, B., Singel, D.J., Stamler, J.S., (1996) *PNAS* **93**, 4736-4741

Singh, R.J., Hogg, N., Joseph, J., Kalyanaraman, B., (1996) *J. Biol. Chem.* **271**(31), 18596-603

Skoog, D.A., Holler, J.F., Nieman, T.A., (1998) Principles of Instrumental Analysis 5ed (ed Sherman M., Bortel, J.) 429-443, Harcourt Brace & Company, Orlando, FL

Soderberg, A., Sahaf, B. Rosen, A. (2000) *Cancer Res.* **60**, 2281-2289

Stamler, J.S., (1994) *Cell* **78**, 931-936

Stamler, J.S., Osborne, J.A., Jaraki, O., Rabbani, L.E., Mullins, M., Singel, D., Loscalzo, J., (1993) *J. Clin. Invest.* **91**(1), 308-18

Starkebaum, G., Harlan, J.M., (1986) *J. Clin. Invest.* **77**(4), 1370-6

Steven, P., Goss, A., Kalyanaraman, B., Hogg, N., (1999) *Methods in Enzymology* **301**, 444-453

Steudel, W., Hurford, W.E., Zapol, W.M., (1999) *Anesthesiology* **91**, 1090-121

Stuehr, D.J., (1997) *Annu Rev Pharmacol Toxicol.* **37**, 339-59

Stuehr, D.J., (1999) *BBA* **1411**, 217-230

Svardal, A.M., Mansoor, M.A., Ueland, P.M., (1990) *Anal. Biochem.* **184**, 338-346
Tang, Y.W., Procop, G.W., Persing, D.H., (1997) *Clin Chem.* **43**(11), 2021-38

Terada, K., Manchikalapudi, P., Noiva, R., Jauregui, H.O., Stockert, R.J., Schilsky, M.L., (1995) *J. Biol. Chem.* **265**, 15984-15990

Thomas, G.J., (1987) in Biological applications of Raman Spectroscopy (ed Spiro, T.G.),135-201, Wiley Interscience, New York

Thomas, G.J Jr., (1999) *Annu. Rev. Biophys. Biomol. Struct.***28**, 1-27

Till, U., Bosia, A., Losche, W., Spangenberg, P., Pescarmona, G.P., (1998) *Folia Haematol Int Mag Klin Morphol Blutforsch* **115**(4), 415-9

Tsikas, D., Sandmann, J., Gutzki, F.M., Stichtenoth, D.O., Frolich, J.C., (1999) *J. Chromatogr. B. Biomed. Sci. Appl.* **726**(1-2), 13-24

Tuma, R., Vohnik, S., Li, H., Thomas, G.J. Jr., (1993) *Biophys J.* **65**(3), 1066-72

Upchurch, G.R. Jr., Welch, G.N., Fabian, A.J., Freedman, J.E., Johnson, J.L., Keaney, J.F. Jr., Loscalzo, J., (1997) *J. Biol. Chem.* **272**(27), 17012-7

Upchurch, G.R. Jr., Welch, G.N., Fabian, A.J., Pigazzi, A., Keaney, J.F. Jr., Loscalzo, J., (1997) *Atherosclerosis* **132**(2), 177-85.

Upchurch, G.R. Jr., Welch, G.N., Loscalzo, J., (1996) *J. Nutr.* **126**(4 Suppl), 1290S-4S

Upchurch, G.R., Jr, Welch, G.N., Loscalzo, J., (1995) *Adv. Pharmacol.* **34**, 343-9

Violi, F., Marino, R., Milite, M.T., Loffredo, L., (1999) *Diabetes Metab Res Rev.* **15**(4), 283-8

Vetri, T., Maio, R.D., Bonafede, G., Passafiume, L., Postorino, A., (2000) *J Auton Pharmacol.* **20**(3), 133-7

Vleminckx, K., Vakaet Jr., L., Mareel, M., Fiers, W., Van Roy, J., (1991) Cell 66, 107-119

Walker, K.W., Gilbert, H.F., (1997) *J. Biol. Chem.* **272**, 8845-8848

Wall, R.T., Harlan, J.M., Harker, L.A., Striker, G.E., (1980) *Thromb. Res.* **18**(1-2),113-21

Wang, J., Rousseau, D.L., Abu-Soud, H.M., Stuehr, D.J., (1994) *Proc Natl Acad Sci U S A.* **91**(22), 10512-6

Wang, X.,(1999) *Med. Hypotheses.* **53**(5),386-94.

Weissman, J.S., Kim, P.S., (1993) *Nature* **365**, 185-188
Welch, G.N., Loscalzo, J., (1998) *N. Engl. J. Med.* **338**, 1042-50

White, M.F., Gazzola, G.C., Christensen, H.N., (1982) *J. Biol. Chem.* **257**(8), 4443-9

Wileman, S.M., Mann, G.E., Baydoun, A.R., (1995) *Br. J. Pharmacol.* **116**(8), 3243-50

Williams, C.H., (1995) Chemistry and Biochemistry of Flavoenzymes, (Mulle, F.,ed), pp.121-211, CRC press, Boca Raton

Williams, D., (1996) *Chem. Comm.* 1085-1091

Wink, D.A., Vodovotz, Y., Grisham, M.B., DeGraff, W., Cook, J.C., Roberto Pacelli, Krishna, M., Mitchell, J.B., (1999) *Methods in Enzymology* **301**, 413-424

Wolvetang, E.J., Larm, J.A., Moutsoulas, P., Lawen, A. (1996) *Cell Growth Differ.* **7**, 1315-1325

Woodard, M.H., Dunn, W.A., Laine, R.O., Malandro, M., McMahon, R., Simell, O., Block, E.R., Kilberg. M.S., (1994) *Am. J. Physiol.* **266**(5 Pt 1), E817-24

Yamamoto, R., Sumino, K., Nakamae, K., (1994) *Arch. Toxicol.***69**(2), 127-31

Yoshimoro, T., Semba, T., Takemoto, H., Akagi, S., Yamamoto, A., Tashiro, Y., (1990) *J. Biol. Chem.* **265**, 15984-15990

Zai, A., Rudd, A., Scribner, A.W., Loscalzo, J., (1999) *J. Clin. Invest.* **103**(3), 393-399

Zhang, X., Li, H., Jin, H., Ebin, Z., Brodsky, S., Goligorsky, M.S., (2000) *Am J Physiol Renal Physiol.* **279**(4), F671-8

Vita Auctoris

Niroshan Ramachandran

Education

1998-2001	Ph.D Biochemistry Department of Chemistry and Biochemistry University of Windsor, Windsor, ON
1993-1997	Hon. B.Sc. Biochemistry Department of Biochemistry University of Toronto, Toronto, ON

Awards

- Foreign NSERC Post Doctoral Scholarship, 2001
- NSERC Visiting Post Doctoral Fellowship, 2001
- University of Windsor Tuition Scholarship, 2001
- University of Windsor Summer Research Award, 2001
- Ontario Graduate Scholarship recipient, 2000
- Ontario Graduate Scholarship for Science and Technology, 2000
- University of Windsor Travel Award, 1999 & 2000
- American Society of Photochemistry and Photobiology Travel Award, 1999 & 2000

Publication

Ramachandran, N., Root, N., and Mutus, B., "Effect of Homocysti(e)ne on NO/RSNO metabolism", BBA, Manuscript in Preparation

Ukario, U., Root, N., Ramachandran, N., Cheung, R., and Mutus, B., "Effect of Omapatrilat on Endothelial cell Nitric Oxide Metabolism", Atherosclerosis, Manuscript in Preparation

Ramachandran, N., Root, P., Jiang, X., Hogg, P.J., and Mutus,B., "Mechanism of Transfer of NO from Extracellular S-Nitrosothiols Into the Cytosol by Cell-Surface Protein Disulfide Isomerase.", PNAS, Accepted for Publication July 2001

Chen, X., Wen, Z., Xian, M., Wang, K., Tang, X., Andreana, P.R., Schlegel, H.B., Ramachandran, N., Mutus, B., and Wang, P.G., "Fluorophore-labeled S-nitrosothiols: Experimental and Theoretical Investigation of Fluorescence enhancement mechanism, Application in kinetics study of SNO/SH transnitrosation and probing protein s-thiolation with s-nitrosothiols", Journal of American Chemical Society, Submitted for publication Dec 2000.

Hou, Y., Xie, W., Ramachandran, N., Mutus, B., Janczuk, and Wang, P. (2000) O-Alkylation chemistry of Neocupferron. Tetrahedron Letters, 41: 451-456

Ramachandran, N., Jacob, S., Zielinski, B., Curatola, G., Mazzanti, L., and Mutus, B., (1999) "N-dansyl-S-nitrosohomocysteine: A fluorescent probe for intracellular thiols and S-nitrosothiols", BBA, 1430(1) 149-54

Presentations

" Novel Mechanism of S-Nitrosothiol transport", Cardiovascular Arteriosclerosis Research Group, March 2001

"Probing Thiol/S-Nitrosothiol and Peroxynitrite levels in model systems and live cells with Fluorescence and Raman Imaging", 13th Annual American Society of Photochemistry and Photobiology held in San Francisco on July 1-6th, 2000.

"N,N-Didansylhomocystine: An intracellular probe Nitric Oxide probe for to demonstrate the involvement of protein disulphide isomerase in the influx of nitric oxide from extracellular s-nitrosothiols", 13th Annual American Society of Photochemistry and Photobiology held in San Francisco on July 1-6th, 2000.

"N,N-Didansylhomocystine as a probe for GSNO influx into live cells", 12th Annual American Society of Photochemistry and Photobiology held in Washington DC on July 10-14th, 1999.

"Development of thiol and S-nitrosothiol probes", 10th Annual American Association of Clinical Chemistry held at Detroit Medical center, Michigan, on September 10th, 1999.

"Enhanced Photolytic NO Release from S-Nitrosothiols Via intramolecular Energy Transfer", 12th Annual American Society of Photochemistry and Photobiology held in Washington DC on July 10-14th, 1999.